Dipl.-Ing. Sebastian Bernhard Schatz, BSc

Prediction of Lightning Discharges in Relation to Regional Thunderstorm Activity

DOCTORAL THESIS

to achieve the university degree of

Doktor der technischen Wissenschaften submitted to

Graz University of Technology

Supervisor

Ao.Univ.-Prof.i.R. Dipl.-Ing. Dr.techn. Stephan Pack

Institute of High Voltage Engineering and System Performance

Graz, July 2025

AFFIDAVIT

I declare that I have authored this thesis independently, that I have not used other than the declared sources/resources, and that I have explicitly indicated all material which has been quoted either literally or by content from the sources used. The text document uploaded to TUGRAZonline is identical to the present doctoral thesis.

Graz, 31 July 2025

Date

Signature

Dipl.-Ing. Sebastian Bernhard Schatz, BSc

Graz University of Technology

Institute of High Voltage Engineering and System Performance

Inffeldgasse 18

8010 Graz

Austria

Head of Institute

Univ.-Prof. Dr.-Ing. Uwe Schichler

Supervisor

Ao.Univ.-Prof.i.R. Dipl.-Ing. Dr.techn. Stephan Pack

Reviewer

Univ.-Prof. Dr.-Ing. habil. Michael Rock

July 2025

Danksagung – Acknowledgement

Mit dem Abschluss dieser Dissertation endet ein prägender Abschnitt meiner akademischen Laufbahn an der Technischen Universität Graz. Mein aufrichtiger Dank gilt all jenen, die mich auf diesem Weg mit ihrem Wissen, ihrem Engagement und ihrer Ermutigung unterstützt haben.

Allen voran möchte ich mich bei meinem Doktorvater Ao.Univ.-Prof.i.R. Dipl.-Ing. Dr.techn. Stephan Pack bedanken, der sich trotz seines wohlverdienten Ruhestands bereit erklärt hat, mich bis zum Abschluss dieser Arbeit zu begleiten. Vielen Dank für das entgegengebrachte Vertrauen und die wertvolle Unterstützung.

Für die Begleitung in der finalen Phase, vor allem für seine Bereitschaft zur Begutachtung, sowie die zahlreichen konstruktiven Anregungen zu dieser Arbeit, bedanke ich mich bei Univ.-Prof. Dr.-Ing. habil. Michael Rock.

Mein herzlicher Dank gilt meinem Projektkollegen, Freund und Vorbild Dr. Lukas Schwalt. Deine fortwährende Motivation, deine Geduld und deine fachliche, so wie freundschaftliche Begleitung haben mir während der gesamten Projektzeit und der Entstehung dieser Dissertation den Rücken gestärkt.

Ein besonderer Dank geht an das Team von ALDIS, Dr. Wolfgang Schulz, DI Hannes Kohlmann und DI Hannes Pichler. Während der produktiven und unkomplizierten Zusammenarbeit als Projektpartner im Forschungsprojekt RTLRA aber auch danach inspirierten viele fachliche und konstruktive Gespräche diese Arbeit.

Vielen Dank auch an Dr. Rudi Kaltenböck und Ing. Volker Marterer von der ACG. Neben der zur Verfügungstellung von unverzichtbaren Wetterradardaten (und deren Interpretation – danke Rudi!) war auch die unkomplizierte Zufahrt zu den Messstandorten auf dem Flughafengelände essentiell für meine Forschung.

Der größte Dank gilt schließlich meiner Familie. Meinen Eltern Astrid und Bernhard, die immer schon wussten, dass ich ein Blitzforscher werde. Ohne euch wäre dieser Weg für mich nicht möglich gewesen. Meiner scharfsinnigen Schwester Melinda danke ich herzlich für das gewissenhafte Durchlesen und Korrigieren dieser Arbeit. Von ganzem Herzen danke ich meiner Frau Jessica und unserem Hund Seppi. Ihr wart stets mein Rückhalt und meine größte Motivation.

Abstract

Cloud-to-ground lightning poses serious risks to persons and infrastructure, especially in outdoor settings like airports, construction sites, and public venues. It can cause operational disruptions, infrastructure damage, and in extreme cases fatalities. While modern weather models can forecast thunderstorm development, a prediction of the first and last cloud-to-ground (CG) lightning strike in a thunderstorm remains challenging. Airports have alert and shutdown protocols according to International Air Transport Association (IATA) regulations that restrict operations at the airport during thunderstorms. To target this uncertainty, this thesis focuses on the prediction of the first and last CG lightning strikes within thunderstorms to assess and reduce risks to personnel and infrastructure, using Graz Airport as a case study. An experimental system was developed, integrating data from an electric field meter (FM) network, a lightning location system (LLS) and a weather radar. The FM network operated from 2022 to 2024, with strategically placed sensors around the airport. The measurement period covered three thunderstorm seasons, with a focus on multiple observed areas, primarily a 5 km radius around the airport.

In total, 79 thunderstorm cases have been recorded during the convective thunderstorm seasons of 2022, 2023, and 2024. 51 thunderstorms producing CG lightning within 5 km and 28 without CG lightning in 5 km were analysed. Alert and shutdown initiation criteria are derived from thunderstorm data and by using logical combinations of predictive parameters from electric field, LLS and weather radar data. These combinations lead to a median shutdown Lead Time (LT) of 12.83 minutes for the first CG lightning strike within the 5 km radius. Within the optimal LT range of 2–30 minutes, 72.5% of cases were observed, with a further 15.7% falling within a range of 30–60 minutes. To clear alerts and shutdowns, two shutdown termination criteria are defined, and their effects are investigated. In this regard, alert and shutdown durations as well as the time to clear for thunderstorms are also analysed.

Additionally, Convolutional Neural Networks (CNN) were trained using radar data from 2020 to 2022 to explore image-based lightning detection. The best-performing model achieved an 89.84% accuracy, demonstrating the potential of radar data for pre-classifying lightning events and supporting future multimodal approaches.

Kurzfassung

Wolke-Erde-Blitze (CG) stellen ein erhebliches Risiko für Personen und Infrastruktur dar, insbesondere in Außenbereichen wie Flughäfen, Baustellen oder Open-Air-Veranstaltungsorten dar. Sie können zu Betriebsunterbrechungen, Sachschäden und im schlimmsten Fall zu Verletzungen oder Todesfällen führen. Während moderne Wettermodelle die Entwicklung von Gewittern vorhersagen können, bleibt die kurzfristige Prognose des ersten und letzten Wolke-Erde-Blitzes innerhalb eines Gewitters eine Herausforderung. Flughäfen haben dafür „Alert"- und „Shutdown"-Protokolle gemäß den Richtlinien der International Air Transport Association (IATA), die den Betrieb auf dem Flughafen während eines Gewitters einschränken.

Diese Arbeit konzentriert sich daher auf die Vorhersage des ersten und letzten Wolke-Erde-Blitzes zur Bewertung und Reduktion von Risiken für Personal und Infrastruktur am Beispiel des Flughafens Graz. Dazu wurde ein experimentelles System entwickelt, das Daten eines Netzwerks aus elektrischen Feldmetern (FM), eines Blitzortungssystems (LLS) und eines Wetterradarsystems kombiniert. Das FM-Netzwerk war von 2022 bis 2024 in Betrieb, mit Sensoren rund um den Flughafen. Der Messzeitraum umfasste drei Gewittersaisonen mit dem Fokus auf verschiedenen Beobachtungsradien, insbesondere eines 5 km Radius um den Flughafen.

Insgesamt wurden 79 Gewitterfälle erfasst, davon 51 mit CG-Blitzen im 5 km-Radius sowie 28 ohne CG-Blitze im 5 km-Radius. Alert- und Shutdown-Kriterien wurden durch logische Kombinationen von Vorhersageparametern aus den drei Datenquellen (elektrisches Feld, LLS und Wetterradar) definiert. Daraus ergab sich eine mediane Vorwarnzeit von 12,83 Minuten für den ersten CG-Blitz innerhalb von 5 km. 72,5 % der Fälle lagen im optimalen Bereich der Vorwarnzeit von 2–30 Minuten, 15,7 % zeigten eine Vorwarnzeit von 30–60 Minuten. Zur Beendigung von Alerts und Shutdowns wurden zwei Kriterien eingeführt und hinsichtlich ihrer Auswirkungen auf Dauer und Auflösezeit untersucht. Zusätzlich wurden Convolutional Neural Networks (CNNs) mit Radardaten der Jahre 2020 bis 2022 trainiert, um eine bildbasierte Erkennung von Blitzen zu ermöglichen. Das beste Modell erreichte eine Genauigkeit von 89.84% und zeigte das Potenzial von Wetterradardaten für die Vorabklassifizierung von Blitzen und zukünftige multimodale Ansätze.

Contents

1 Introduction

1.1 Motivation

Cloud-to-Ground (CG) lightning strikes produced in thunderstorms pose major risks for infrastructure and staff, particularly in exposed outdoor environments such as airports, construction sites, and public open-air venues. These lightning strikes can lead to infrastructure failures, operational delays, severe safety risks and fatality in the worst case. Despite accurate forecasts of thunderstorm development in terms of timing and location of modern weather prediction models, the precise short-term prediction of the first Cloud-to-Ground (CG) lightning strike remains uncertain.

For airports, the findings of this work are of particular importance, as operations at airports can be restricted or interrupted due to alerts and shutdowns. If there is thunderstorm activity within an 8 km radius of the airport, an alert is issued, leading to restricted operations on the apron. If thunderstorm activity and the presence of lightning strikes occur within a 5 km radius, all apron activities must be suspended (see Section 3.1). As the attractiveness of air travel and rising flight numbers go with safer flying but also personal safety on the ground[1]. The lightning risk for airports is increased by the rising number of remote air traffic management systems where on-site meteorologists are not present, making real-time decisions on safety measures during severe weather even more complex (IATA, 2006 [1]; EASA, 2023 [2]).

Airports are interested in optimising processes in the event of thunderstorm warnings. The aspect of personal safety and the protection of the infrastructure are the top priorities. There is an economic aspect as any interruption is expensive. Down times should therefore be as short as possible, but there should still be enough time to seek shelter so as not to be exposed to the risk of a lightning strike (Long and Miller, 2022 [3]; Liebold et al., 2021 [4]).

[1] https://de.statista.com/statistik/daten/studie/411620/umfrage/anzahl-der-weltweiten-fluege/, accessed on 14.07.2025; https://de.statista.com/statistik/daten/studie/374860/umfrage/flugverkehr-entwicklung-passagiere-weltweit/, accessed on 14.07.2025.

The research project Real-Time Lightning Risk Assessment (RTLRA) at Graz University of Technology was started to support the decisions of meteorologists (working remotely) and to reduce the associated risk for persons (e.g., ground staff and passengers), while also contributing to the optimisation of operational shutdown times. This work presents the research findings of RTLRA. The project employed a network of six electric Field Meters (FMs) installed in the vicinity of Graz Airport, Austria (see Figure 1), completed by Lightning Location System (LLS) data and weather radar data provided by the Austrian Lightning Detection and Information System (ALDIS) and the Austro Control GmbH (ACG), respectively.

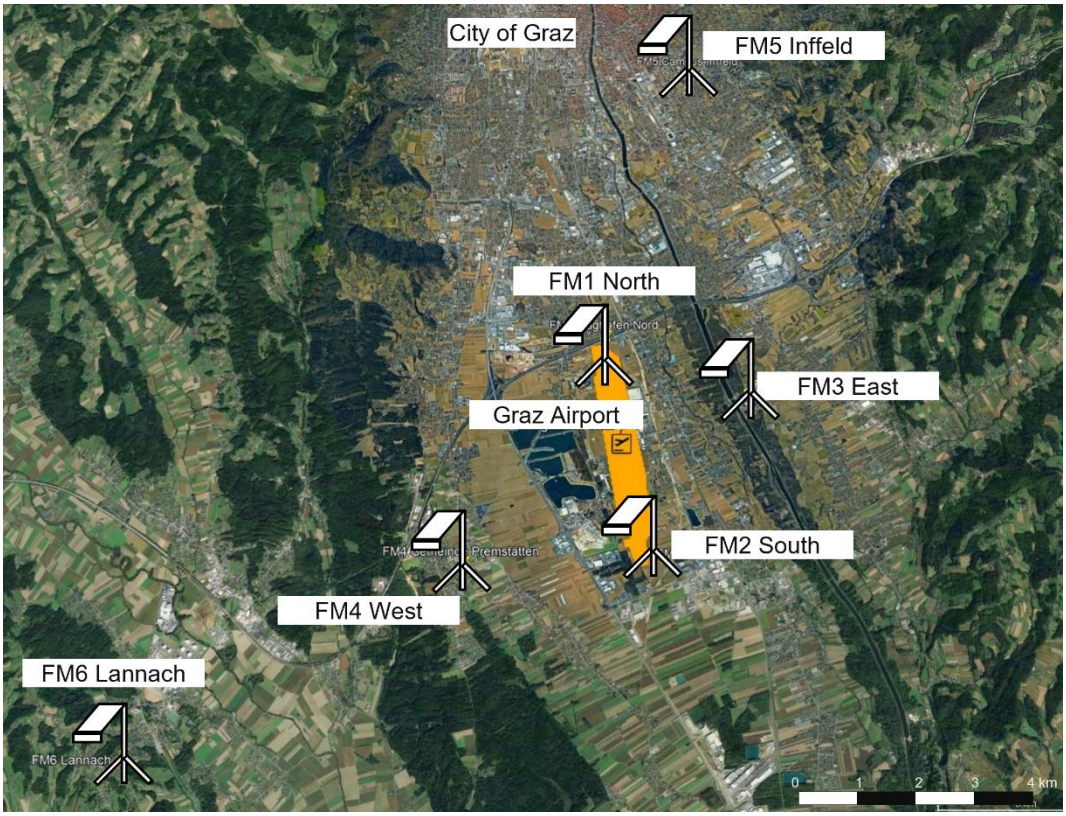

Figure 1: Map of sensor location in the vicinity of Graz Airport, Austria, Source: Google Earth, adapted by the author.

The analyses comprise data from these three data sources for the years 2022, 2023 and 2024 with special attention to convective thunderstorm seasons from May to September within a 5 km radius around Graz Airport. The integrating data from an FM network, LLS, and weather radar shall be used to predict the first and last CG lightning strikes of a thunderstorm around Graz Airport. To the best of the authors knowledge,

this is the first FM network of its kind in Europe and the first time such FM network data is combined with LLS and weather radar data for lightning prediction. The thunderstorm warning system (TWS) standard OVE EN IEC 62793 [5] provides a normative framework and technical recommendations on how TWS can be implemented and also defines characteristic values for assessing performance. This thesis shows how such a TWS can be implemented.

Electric field (E-field) measurements have long been recognised as a valuable tool for analysing and understanding thunderstorm behaviour. At the Kennedy Space Center (KSC) in Florida, initial experiments began in 1973 with a single electric Field Meter (FM) used to monitor the electrostatic field at the Earth's surface. This setup was expanded in 1974 into a network of 21 FMs. Today, KSC operates a network of 34 FMs, delivering high-resolution data on E-field variations to support detailed thunderstorm analysis (Jacobson and Krider, 1976 [6]; Lucas et al., 2017 [7]; Murphy et al., 2008 [8]; Wilson and Cummins, 2021 [9]).

Michimoto, 1993 [10] investigated ten cases of winter thunderstorms in Japan using a network of 27 FMs with a 10 km baseline, in combination with weather radars and VHF direction finders to monitor lightning activity. The FM data were used to classify three distinct types of thunderstorms based on the temporal evolution of their E-field signatures. Beasley et al., 2008 [11] analysed E-field measurements from the KSC and identified threshold levels that correlate increasing E-field with elevated lightning risk. Their findings showed that E-field values exceeding 1 kV/m within a 10 km radius served as reliable indicators of imminent lightning strikes, providing LTs of up to 10 minutes in 81.3% of cases. In the remaining 18.7%, however, the 1 kV/m threshold was not surpassed prior to the first observed CG lightning strike. Silva Ferro et al., 2011 [12] expanded upon previous research by analysing an FM network in Brazil, identifying a critical E-field threshold of 0.9 kV/m that yielded an average lead time of 13 minutes within a 10 km radius. Similarly, Pustovalov and Nagorskiy, 2018 [13] conducted studies in Siberia, classifying nine distinct types of E-field variations associated with different thunderstorm stages, thereby underscoring the dynamic nature of atmospheric E-fields during thunderstorm evolution. More recent developments have focused on integrating E-field data with other meteorological observations to improve the accuracy of lightning prediction. Rodrigues and Lacerda, 2022 [14] utilised a FM network in São Paulo, Brazil, to determine a mean lead time of

14 minutes and 41 seconds between the initial E-field pulse and the first CG lightning strike.

Montanya et al., 2008 [15] investigated 79 thunderstorm days at three different sites distributed over Catalonia, Spain. They applied a warning area of 20 km radius around the sites with different areas of concern (surrounding area) of 1 km, 5 km and 10 km. They used four different warning criteria: CG, intra cloud (IC) discharges, exceeding of a radar threshold in the warning area and a combination of those. They presented average LTs under 15 minutes with a more non-effective alarms than the effective alarms (no values provided). They also recorded and analysed electric field (E-field) measurements of FMs at some sites and showed the possibility of lightning warning with FMs. Nevertheless, they didn't use it for their presented warning system.

A deep neural network (DNN)-based approach for short-term forecasting of total lightning activity was introduced by Mansouri et al., 2023 [16]. Their method relied exclusively on satellite-derived lightning data and accounted for both IC discharges and CG lightning strikes. Focusing on a region that covered much of northern South America, the model demonstrated improved performance over traditional techniques, with gains of 4%, 12%, and 22% at LTs of 30, 45, and 60 minutes, respectively. In a separate study, Antonescu et al., 2013 [17] developed a forecasting technique for the onset of CG lightning strikes using weather radar data from Romania. Between 2003 and 2005, they observed thunderstorms with Doppler radar in combination with LLS data. Their most accurate predictor for CG lightning initiation in southern Romania resulted in a mean LT of 17 minutes. Studies conducted in Argentina (Antunes et al., 2020 [18]) and Japan (Yamashita et al., 2024 [19]) focus on the development of FMs and the deployment of FM arrays based on locally developed technology. While these works present initial results related to thunderstorm measurement, they have not yet been applied to forecasting. In a separate publication, Povcshenko and Bazhenov, 2023 [20] compare various atmospheric E-field measurement instruments and techniques, aiming to identify their respective advantages. Their findings conclude that the electric field meter is the most suitable device for this purpose.

1.2 Method

The measurement of the E-field using multiple FMs, complementing LLS data and weather radar data, has not yet been implemented in Austria nor in Europe and represents a unique aspect of this project. This innovative multi-source data combination aims for continuous analysis of rapidly evolving thunderstorm conditions and to enable more accurate assessments of short-term thunderstorm development at the research site Graz Airport.

The methods to achieve the described approach are summarised in this section. Measurement sites for the FMs are strategically selected to provide comprehensive coverage around Graz Airport, with installations to the north, south, east, and west of the airport within a radius of 5 km. Site selection is based on technical requirements, including a clear 7.62-meter (i.e., 300 inches) radius around the FM, minimal vegetation, proper sensor orientation, and stable power supply according to the specifications of the manufacturer[2]. Additional considerations include accessibility and compatibility with existing infrastructure. Two further locations for initial testing and for reference measurements are used for system validation but excluded from the main analyses (see Section 4).

The measurement period shall include the convective thunderstorm seasons from 2022, 2023 and 2024, during which FM data shall be recorded, supported by LLS and weather radar data. The conducted analyses focused on multiple observed areas around Graz Airport with radii of 5 km, 8 km, 10 km, 15 km and 30 km. The 5 km radius serves as the primary area of interest, while more distant lightning events are considered negligible. A buffer zone of ±0.5 km around the 5 km radius is defined to examine borderline lightning strikes and account for potential low quality LLS data, such events falling within this transitional area shall be analysed in detail. Cases without CG lightning strikes but with shutdowns triggered by the system shall also be included for a comprehensive evaluation (see Section 5).

As already described, the core feature of this work is the prediction of lightning strikes using a TWS that combines three subsystems and integrate data from an FM network,

[2]Campbell Scientific Inc., "CS110 Electric Field Meter: Product Manual", pp. 7-9, 2020.

LLS, and weather radar. This combined approach leverages the strengths of each individual system while increasing overall reliability through redundancy. If one subsystem fails, the system can continue to operate using the remaining components. In such cases, the prediction quality may be reduced, but functionality is maintained. For each subsystem predictive parameters shall be found. In accordance with terminology defined by the International Air Transport Association (IATA), alert and shutdown initiation criteria are derived from specific combinations of multiple parameters. Relying on a single parameter, for example, one being fulfilled well before the first CG lightning strike in the observed area, can result in non-effective alarms. To address this, E-field, LLS, and weather radar parameters are linked using logical operators to enhance reliability (see Figure 2). To clear the initiated alert and shutdown also termination criteria shall be defined (see Sections 6 and 7).

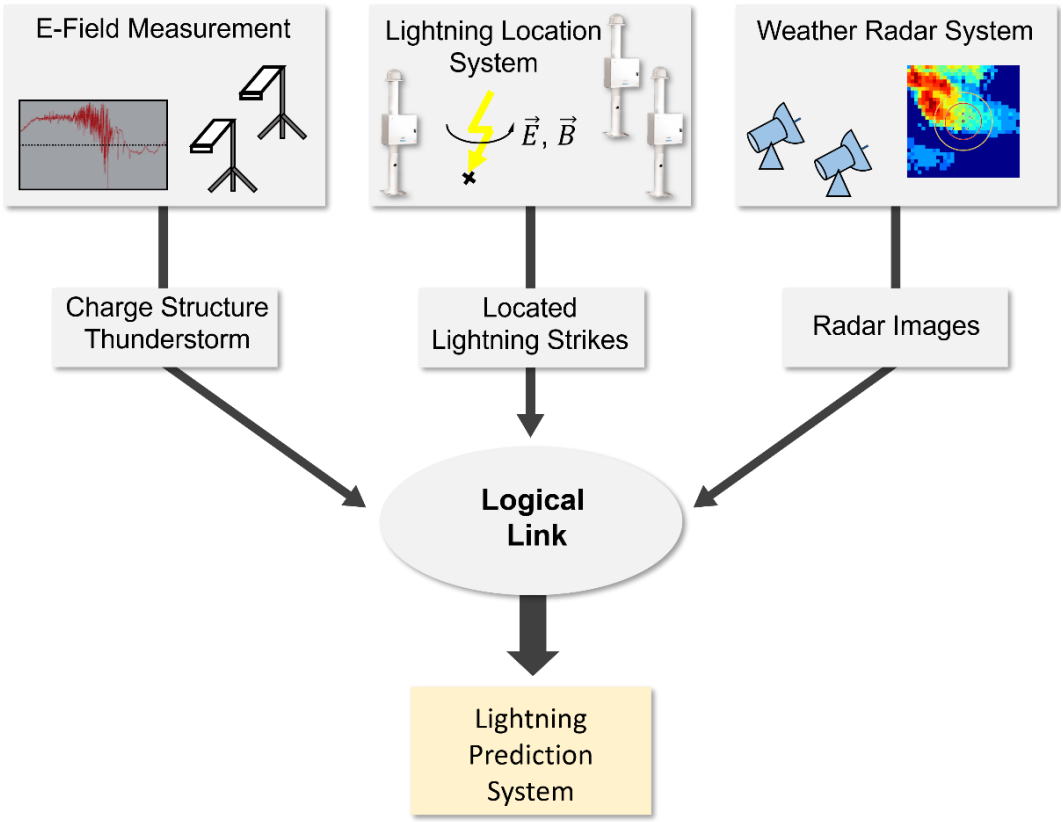

Figure 2: Combining of the different data sources, FM network, LLS and weather radar in one lightning predictive system by logically linking them.

As a complementary approach to the combined data analysis, the use of Convolutional Neural Networks (CNN) shall be explored for detecting lightning based solely on spatial

patterns in weather radar images. Using weather radar data provided by ACG, the CNN models shall aim to identify lightning occurrences without relying on additional data sources and explore their use in pre-classifying lightning producing thunderstorms. This image-based method shall offer an additional perspective within the presented lightning prediction framework. The results shall demonstrate that weather radar data can be used to pre-classify lightning strikes within the area covered by the radar image.

The recorded data will finally be evaluated as a combined data set by the developed algorithm. This shall result in different alert and shutdown LTs, durations and time to clear (TTC) for the various thunderstorm cases that will be investigated. The performance of the algorithm in combination with the various Shutdown Termination Criteria (STC) will then be evaluated on the basis of these parameters (see Section 8 and Section 9).

1.3 Aim of the Work

The following points shall outline the primary objectives of the present thesis:

1. Set up an electric FM network in the vicinity of Graz Airport for continuous recording of the E-field on the earth's surface during fair-weather and thunderstorm conditions. Install FM sites in each cardinal direction and two additional sites for reference measurements.
2. Analyse if standalone FM or FMs in a network without additional data sources are sufficient for lightning prediction or TWS.
3. Combine three different data sources, E-field meter network, LLS and weather radar data, to find common patterns and parameters for prediction and define suitable prediction parameters for this dataset.
4. Develop criteria for alert and shutdown initiation and termination from these predictive parameters and apply the criteria on thunderstorms in the vicinity of Graz Airport to analyse the performance in terms of LT before the first CG lightning strike of a thunderstorm and the time clear after the last lightning discharge of a thunderstorm.

5. Analyse the performance of the algorithm for alert and shutdown effective and non-effective alarms for two different STC and compare the annual shutdown duration for both STC.
6. Investigate the influence of different thunderstorm types on shutdown triggering. Analyse LTs and shutdown durations for single-cell, multicell, supercell and squall lines and the influence on the effective shutdown criteria.
7. Pre-classify LLS and weather radar data using CNNs. Train different CNN models with radar images with and without the occurrence of lightning.

2 Thunderstorm Development and Lightning Physics

2.1 Global Electric Circuit

History of Measurements of Atmospheric Electricity

The Global Electric Circuit (GEC) and atmospheric electricity are naturally occurring electric phenomena within the Earth's atmosphere, connecting the Earth's surface to the ionosphere. Scientific proof of atmospheric electricity was first provided by Benjamin Franklin with his kite experiment in the summer of 1752, in which he drew a spark from an electrically charged cloud structure (Franklin, 1752 [21]; McAdie, 1925 [22]). Shortly afterwards, John Canton and James Parsons conducted experiments that were able to detect atmospheric electricity even in fair weather. In the experiment by Canton, 1752 [23] it was shown how two freely suspended cork balls (dielectric) repel each other in the electric fair-weather field[3]. Parsons, 1753 [24] demonstrated the electric fair-weather field using an insulated iron wire, which becomes charged and thus repels a silk cloth.

Quantitative measurements of atmospheric electricity were first described by Lord Kelvin in 1860. He developed a “water dropper” in which an isolated suspended tank filled with neutral (uncharged) water generates two constant streams of water. When droplets form from the water streams, they are charged by the atmospheric E-field. The two streams of charged water droplets now charge a capacitor. The capacitor is charged until its E-field is equal to that of the environment. The potential and thus the E-field could then be measured on this capacitor using an electroscope. Kelvin was already aware that his measurement setup could have a geometric influence on the measurement of the E-field (Thomson[4], 1868 [25]; Harrison, 2013 [26]). Wilson, 1906 [27] provided a solution to this measurement influence with an insulated metal plate as a sensor electrode, which was installed flush with the ground and was therefore independent of geometric influences. This metal plate is charged by the surrounding

[3]Coulomb’s law
[4]William Thomson, 1st Baron Kelvin (1824 – 1907)

E-field and the potential difference between the sensor electrode and the ground potential can be measured. The “Wilson plate” was a forerunner of the electric FM, as used in the present work.

Model Description of the Global Electric Circuit

The GEC explains why electricity appears in the atmosphere even when there are fair-weather conditions. In this framework, Earth’s surface (ground level) and the ionosphere (about 80 km altitude) can be seen as the electrodes of a spherical capacitor: the ground carries a net negative charge, the ionosphere a positive charge. Between them there is a vertical E-field (Aplin et al, 2008 [28]). The air is the leaky dielectric medium (Rycroft et al., 2000 [29]). Near the surface, the fair-weather E-field is typically around 100 V/m (Burns et al., 1995 [30]) and assumed to vary between 0 V/m and 300 V/m (Minamoto and Kadokura, 2011 [31]). Note, that in some literature the fair-weather E-field has a negative sign due to the “physics sign convention”, where the downward directed E-field is negative because it is in the opposite direction to that of the radial normal vector of the spherical coordinate system of the Earth (in contrast to the “atmospheric electricity sign convention”). Because air is slightly conductive, a return current of about 1 kA (or 2–3 pA/m^2) flows continually to equalise those charges (Wilson, 1906 [27]; Rakov and Uman, 2003 [32]; Wilson, 1929 [33]; Burke and Few, 1978 [34]). The current in this circuit is continuously generated by the sum of thunderstorms around the globe. Thunderstorms refresh the charge separation and the that drives the global circuit, ensuring that fair-weather currents and the background E-field that can be measured on clear days persist around the globe.

Fair-weather conditions imply almost cloudless skies with no local electrification. Rakov and Uman, 2003 [32] describe it simply as bright sunshine and minimal cloud cover, while Harrison adds that there should be no significant convective clouds or other local charging or electrification processes (Harrison, 2013 [26]).

Figure 3 sketches a simplified model of the GEC. The right half illustrates the undisturbed fair-weather region, whereas the left depicts disturbed weather, such as during thunderstorms. Another factor that drives the current is precipitation, i.e., rain, which also transfers charge from the electrified cloud to the ground. Thunderstorms act as bipolar current sources in this model, where lightning and rain transfers negative charge from the lower part of the cloud to the ground, while the positively charged tops

of the clouds send charge upward into the ionosphere up to a potential of ~300 kV. Strong E-fields beneath the thunderstorm also trigger point or corona discharges that feed back into the overall circuit. The air in the atmosphere acts as leaky dielectric, where the conductivity increases with altitude (near surface ~$2 \cdot 10^{-14}$ S/m).

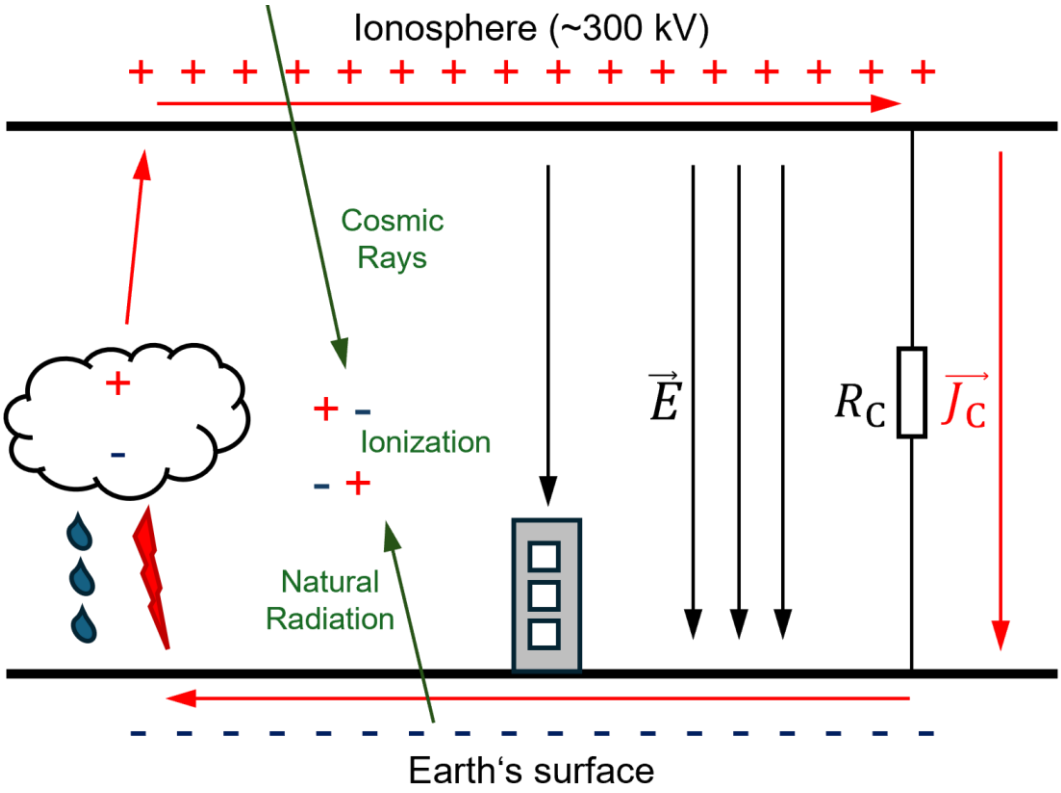

Figure 3: Simplified model of the GEC; a thunderstorm acts as current source and charges the GEC, while the atmosphere represents an ohmic resistance R_C, a currents flow through the model as current density $\vec{J_C}$, fair weather E-field $\vec{E}$ with shading effects presented by buildings; (Aplin et al., 2008 [28]), adapted.

The conductive properties of air result from ionisation by cosmic rays and natural radiation from the earth. The electric fair-weather field $\vec{E}$ also depends on the altitude due to the altitude-dependent conductivity through the relationship $\vec{J_C} = \sigma \cdot \vec{E}$. In addition, the E-field can be shaded by inhomogeneities of the earth's surface, i.e. trees, houses, hills and mountains. The vertical current component $\vec{J_C}$ via the equivalent resistance R_C is constant (Aplin et al., 2008 [28]; Rycroft et al., 2000 [29]; Rakov and Uman, 2003 [32]).

An additional phenomenon in regard to atmospheric electricity is the Carnegie Curve, which is named after the ship of the same name on which the atmospheres E-field over the seas was measured between years 1909 and 1929. The Carnegie Curve describes the diurnal cycle of the fair-weather E-field, which has a minimum between 00:00 UTC and 06:00 UTC and a maximum between 18:00 UTC and 00:00 UTC. The fluctuation range is about ±30% around the mean fair-weather E-field.

A similar curve was shown as part of project-related measurements[5]. Figure 4 shows the daily curves of the electric fair-weather field strength over a period from December 2022 to November 2023 (light green).

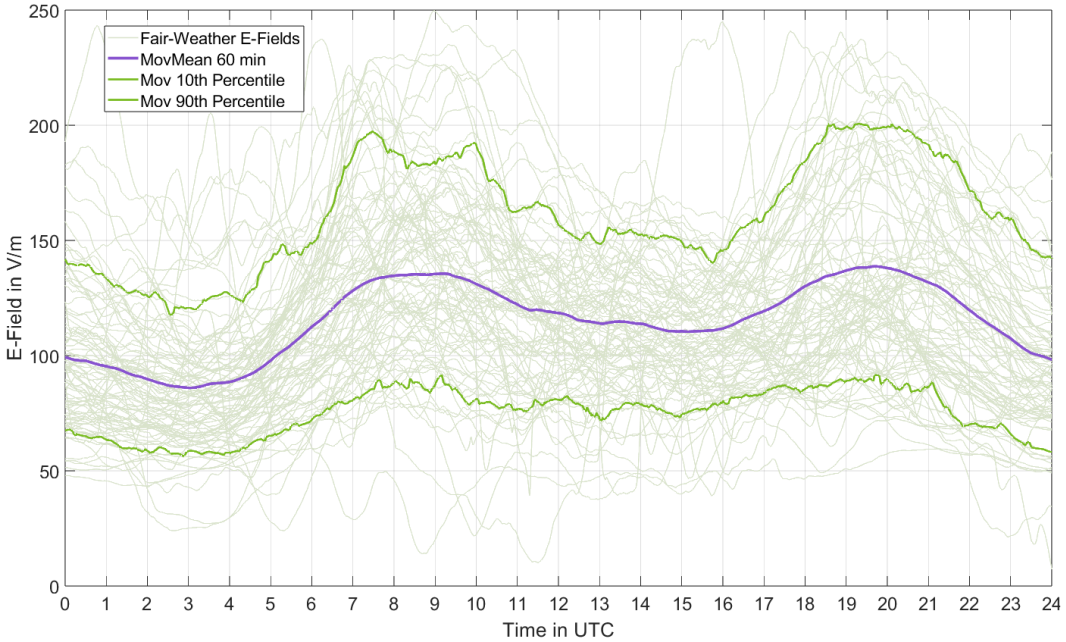

Figure 4: Diurnal cycles of the electric field measured by FM 5 Inffeld in Graz, Austria; presented by Maier[5].

The moving mean over 60 minutes (violet) and the moving 10th and 90th percentile (green) was calculated from these curves. In contrast to the Carnegie Curve (one maximum), the recorded diurnal cycles show two maxima. This could be related to the influence of aerosols in urban areas, which was also described by Yaniv et al, 2016 [35]. Due to the small fluctuations compared to the strong deviations of the E-field

[5]J. Maier, “Environmental Influences on Measurements with Electric Field Meters”, Master’s Thesis, TU Graz, 2023.

during thunderstorms, this influence was not considered in the present evaluations (Harrison, 2013 [26]). The described effects of the altitude-dependent fair-weather E-field can also be neglected in the present work due to the comparatively low altitudes (~500 amsl, meters above mean sea level).

2.2 Thunderstorm Development

Development and Types of Thunderstorms

For thunderstorms development, three atmospheric conditions must prevail: moist air, an unstable atmosphere, and a lifting mechanism. Warm and moist parcels of air are transported to higher air layers. The moisture in the lower to mid-levels of the atmosphere supplies the water vapor necessary for cloud formation and latent heat release, which fuels convective activity (Wallace & Hobbs, 2006 [36]). An unstable atmosphere exists when the environmental lapse rate is steeper than the adiabatic lapse rate, allowing rising air parcels to remain warmer than their surroundings and continue ascending, promoting the formation of deep, vertically developed cumulonimbus clouds (i.e., thunderstorm clouds) (Markowski and Richardson, 2010 [37]). However, even in the presence of moisture and instability, a lifting impulse is required to initiate upward motion. This lift can result from surface heating (convection), frontal boundaries, terrain (orographic lift), or low-level convergence zones (Doswell, 1987 [38]). When these three ingredients coincide, the atmosphere is primed for thunderstorm development. These processes are part of the first stage of a thunderstorm's life, the developing stage.

Thunderstorms can vary significantly in size, structure, and intensity, and are therefore classified into several distinct types like single-cell, multicell, supercell, and squall line thunderstorms. A single-cell thunderstorm is the smallest type, typically short-lived with a lifespan of about 30–60 minutes and with the lowest energy (see Figure 5). In contrast, a multicell thunderstorm consists of several single cells, again with a lifespan of 30–60 minutes, merging to form a more organised and longer-lasting system (lifespan up to several hours). Supercells are the most powerful type of thunderstorm, with a diameter of several 10 km, characterised by a large, rotating updraft with a lifespan of 1–4 hours and some up to 8 hours. Finally, squall lines are linear

arrangements of thunderstorms producing intense wind gusts and heavy rainfall along their leading edge. Each type of thunderstorm poses different hazards and forms under slightly different atmospheric conditions (Markowski and Richardson, 2010 [37]).

Figure 5: Developing single cell thunderstorm in the northeast of Graz, recorded from Campus Inffeldgasse at TU Graz on 09 June 2023.

Thunderstorms or cumulonimbus form in the troposphere and reach from the cloud base at about two kilometres up to twelve kilometres into the sky for midlatitudes. At the tropopause, the transition between troposphere and stratosphere, the upper area of the cumulonimbus cloud flattens out considerably, resulting in sharp, striped structures due to the freezing of the water droplets. The thunderstorm shows its characteristic anvil shape. This is called the mature stage, the most active phase of the thunderstorm. Both updrafts and downdrafts are present. Heavy rain, hail, and lightning are accompanying this stage. Charge separation within the cloud reaches a peak, leading to frequent lightning discharges. This stage can be intense but is often short-lived.

The last stage of a thunderstorm is called dissipating stage. The storm begins to weaken as downdrafts dominate and cut off the warm air supply. Without rising air to sustain it, the storm loses energy. Precipitation decreases, lightning activity fades, and the cloud structure begins to break apart. Eventually, the storm dissipates completely,

leaving cooler, more stable air in its place (Rakov and Uman, 2003 [32]; Kitagawa and Michimoto, 1994 [39]).

Charge Separation in the Atmosphere by Convection

Convection is the air circulation caused by solar radiation and is one mechanism behind thunderstorm formation. Two other mechanisms include frontal thunderstorms, where warm and cold air masses collide and the warm air is lifted, and orographic thunderstorms, where air is forced to rise over terrain such as mountains (Cooray, 2014 [40]).

In fair weather, positive space charges exist near the ground. Warm, moist air near the surface is lighter than surrounding air and rises, carrying these charges upward as so-called air parcel. As the air parcel ascends, it expands and cools due to adiabatic processes (i.e., no heat exchange). Because atmospheric instability causes the air parcel to cool slower than the surrounding air, it remains warmer and continues to rise until condensation forms a cumulus cloud.

Warm updrafts continue carrying positive charges upward. Negative charges, attracted by the cloud's positive regions, accumulate on the cloud's top and sides, forming a thin negative layer. Downdrafts from cooling processes circulate these negative charges to the cloud base, where they induce corona discharges at the surface, creating more positive charges and reinforcing charge separation. Cosmic rays contribute additional negative charges to the cloud top. This results in a dipole charge structure within the mature thundercloud (Rakov and Uman, 2013 [32]; Cooray, 2014 [40]).

Charge Separation in the Atmosphere by the Graupel-Ice Mechanism

The graupel-ice mechanism explains charge separation in thunderstorms through collisions between the hydrometeors graupel grains and ice crystals, producing both negative and positive charges. Thus, for a thunderstorm to produce lightning, it must reach altitudes at or above the freezing level, also known as the 0 °C isotherm. Graupel grains, being larger and heavier, fall due to gravity, while lighter ice crystals remain suspended or are carried upward by updrafts. These particles are surrounded by supercooled water droplets (below 0 °C), forming a suspension.

As graupel grains fall through this suspension, collisions with ice crystals generate electric charges on both hydrometeor types. The charge polarity depends on the

ambient temperature. A critical “reversal temperature”, between −10 °C and −20 °C, determines this polarity. In colder, higher regions of the cloud (below the reversal temperature), graupel becomes negatively charged and ice crystals positively. In warmer, lower regions, the charges are reversed, with graupel gaining a positive and ice crystals a negative charge (Rakov and Uman, 2003 [32]; Jayaratne et al., 1983 [41]). Several hypotheses have been proposed to explain the origin of the lower positive charge centre in a tripole structure thunderstorm. Jayaratne and Saunders, 1984 [42] suggested that graupel, which acquires a positive charge at temperatures warmer than the reversal temperature, is responsible for its formation.

2.3 Charge Distribution

The charge separation process in a thunderstorm formation results in a dipole structure, with a main positive charge region near the cloud top and a main negative region in the centre, each carrying up to several tens of coulombs. Additionally, a weaker positive charge region, typically below ten coulombs, forms near the cloud base, creating a vertical tripole structure (Krehbiel and Brooks, 1986 [43]). Several hypotheses exist regarding the origin of this lower positive charge centre (Rakov and Uman, 2003 [32]). The most widely accepted hypothesis, proposed by Bateman et al., 1999 [44], suggests that precipitation transports positive charges to the bottom of the cloud. The tripole structure of a thunderstorm is shown in Figure 6.

For the charge regions Rakov and Uman, 2003 [32] suggest that the top positive charge Q_{Pos}, mid negative charge Q_{Neg} and lower positive charge Q_{LowPos} are 40 C, −40 C and 3 C, respectively. Q_{Pos}, Q_{Neg} and Q_{LowPos} are arranged one above the other in heights of 12 km, 7 km and 2 km, respectively. With these values the resulting vertical component right beneath the thunderstorm’s tripole structure results in the E-field shown in Figure 7, according to the “atmospheric electricity sign convention”. The shape of the E-field can be described as W-shaped or inverted M-shaped. This shape could be observed in the objective measurements, e.g., on a thunderstorm recorded on the 12.08.2022 as described by Schatz et al., 2023 [45] (Appendix B).

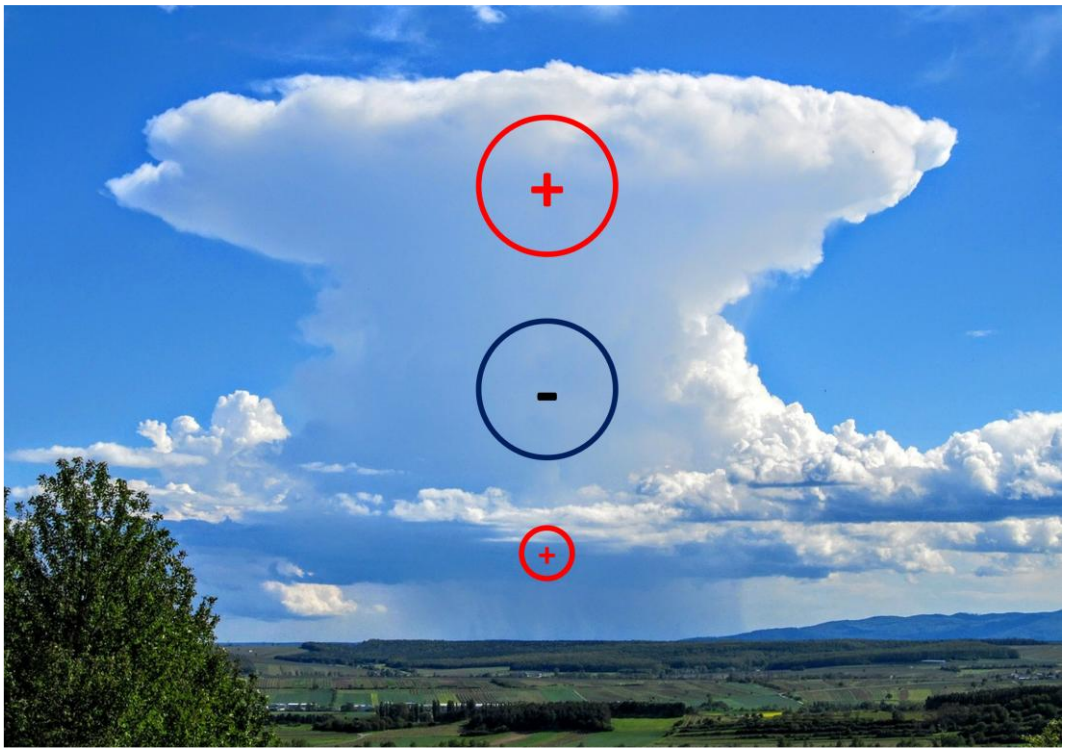

Figure 6: Tripole charge structure of a thunderstorm in midlatitudes, top positive charge Q_{Pos}, mid negative charge Q_{Neg} and lower positive charge Q_{LowPos}, Source: Pixabay.com/nyarytamas, adapted by the author.

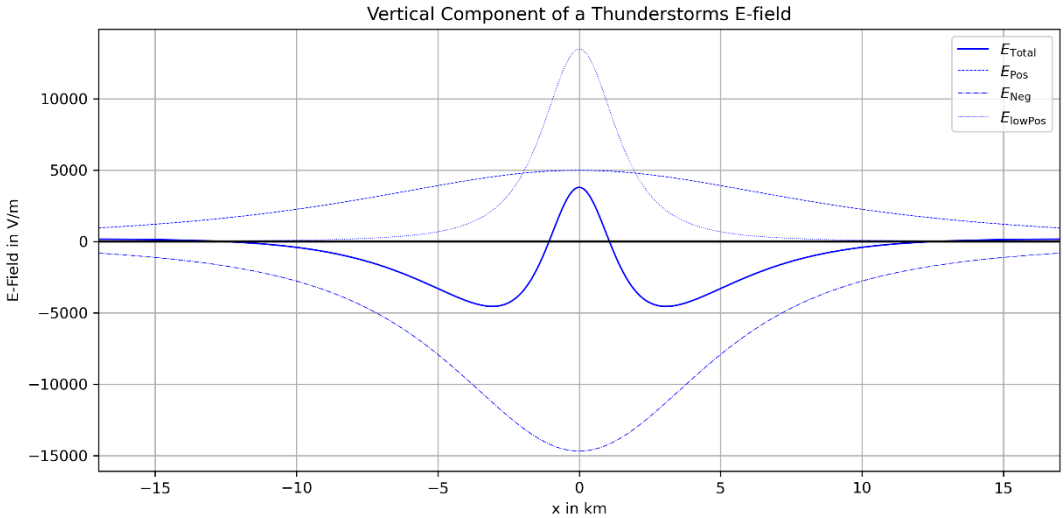

Figure 7: Vertical components of a thunderstorm's E-field, as observed right beneath the thunderstorm with a tripole charge structure, E_{Pos}, E_{Neg} and E_{LowPos} resulting from Q_{Pos}, Q_{Neg} and Q_{LowPos}, respectively, values and formulas for the plot from Rakov and Uman, 2003 [32].

Thunderstorm charge structures cannot always be represented by a simple vertically stacked model. In some cases, positive and negative charge regions are horizontally displaced, existing at similar altitudes within the cloud. This has been confirmed by aircraft measurements from Imyanitov et al.,1971 [46], who observed irregularly

distributed pockets of high charge density throughout the cloud. These observations revealed multiple localised regions of both positive and negative charge. Despite this complex distribution, the average vertical structure typically still resembles a classical dipole or tripole (Rakov, 2005 [47]).

Horizontally displaced or inclined vertical charge structures in thunderstorms have been described by Yamashita et al., 2022 [48]. Pustovalov et al., 2018 [13] also detail how the resulting E-fields vary in shape across different thunderstorm stages, developing, mature, and dissipating stage. Depending on the arrangement of charge regions, the resulting E-field can take on complex or irregular forms, differing significantly from the idealised vertically stacked charge model.

2.4 Lightning Physics

Cloud-to-Ground Lightning and Ground-to-Cloud Lightning

As the E-field strength within a thunderstorm increases, the likelihood of a lightning strike rises. While a lightning strike (i.e., stroke) refers to a single CG discharge, a lightning flash (or simply “flash”) typically consists of multiple strokes that occur as part of the same electric event. The sequence of a lightning flash starts with the occurrence of preliminary breakdowns, potentially triggering the lightning process and the formation of a stepped leader. During this phase, a stepping process generates one or more leader branches. In CG discharges, the stepped leader advances in segments of several tens of meters toward the ground at about 0.2 m/µs, leaving behind an ionised channel. Next, the attachment process begins when the stepped leader connects with a ground-reaching, oppositely charged connecting leader, which forms due to the enhanced E-field at ground level. Once connected, the first return stroke (i.e., CG lightning strike) is triggered, propagating from the ground upward along the ionised channel at roughly one-third the speed of light. This return stroke discharges the stored charge from the lightning channel to the ground. A return stroke can be followed by a low current in the same channel, known as continuing current, which ranges from several tens to hundreds of amperes and can last for several hundred milliseconds (Rakov and Uman, 2003 [32]).

Subsequent discharges may occur through the same pre-ionised channel. Unlike the initial stepped leader, these subsequent leaders, called dart leaders, travel smoothly without stepping. When a dart leader meets another connecting leader from the ground, it triggers a subsequent stroke. Multiple strokes can happen in the same or new channels, sometimes involving multiple Ground Strike Points (GSP, Dwyer and Uman, 2014 [49]).

Flashes can be classified into four main types, based on the direction of propagation (downward or upward) and the polarity of the leader (positive or negative). The four types are downward lightning with a negative leader, downward lightning with a positive leader, upward lightning with a negative leader and upward lightning with a positive leader. A fifth type, known as bipolar flash, involves a change in polarity during a single flash. This means both negative and positive charges are transferred from the cloud to the ground within the same CG flash (Rakov and Uman, 2003 [32]).

Inter- and Intracloud discharges

In addition to CG lightning strikes, there are three main types of cloud lightning, or cloud discharges, which do not extend to the Earth's surface. The first is intercloud discharge, occurring between charge regions of separate thunderclouds. The second is intracloud discharge, happening within the same cloud between different charge regions, such as the lower negative and upper positive zones. The third type is an air discharge, which extends out of the cloud but does not reach the ground or another cloud. The three types of cloud discharges are referred to hereafter as intracloud (IC) discharges. IC discharges account for approximately 75% of all lightning events (Rakov, 2013 [50]).

Each IC discharge and CG lightning strike emits an electromagnetic field, which then propagates radially from the lightning channel. This signal can be used, i.e., to locate lightning strikes with LLS, as described in Section 4.2.

2.5 Lightning in Austria

The highest lightning density in Austria can be found near the borders with Italy and Slovenia, extending into the foothill regions of Carinthia and Styria (Schulz et al., 2005

[51]; Schulz and Diendorfer, 2002 [52]). These regions experience an Illyrian climate, which represents a transition between the mediterranean climate of the upper Adriatic and the alpine climate of the Austrian alps. Even before the installation of the Austrian LLS, Cehak, 1980 [53] was able to show peaks in lightning activity of 30 to 40 thunderstorms per year in a 30-year average isocernauic[6] map of Austria, particularly in the regions around the cities of Graz in Styria and Klagenfurt in Carinthia. The convective thunderstorm season in Austria is between May to September (Schulz et al., 2005 [51]).

The highest lightning densities in southern and southeastern Austria exceed three CG flashes per km² per year, favoured by the prevailing meteorological and topographical conditions. In a Europe-wide comparison, only the upper Adriatic region shows a higher lightning density, with over six CG flashes per km² per year. In stark contrast, the main Alpine crests exhibit the lowest lightning density in Austria, with only zero to two CG flashes per km² per year. The glaciated and rocky areas, characterised by their high albedo and the lack of an appropriate moisture source, contribute to the dryness of the inner Alpine region (Frei and Schär, 1998 [54]) and thus the low lightning density (Schulz et al., 2005 [51]).

Figure 8 shows the 10-year ground flash density for the years 2015 to 2024, with a mean of 100,700 flashes per year. The flash density is displayed with a 1 × 1 km² grid size. Individual pixels or clusters of pixels occasionally show high lightning densities (up to eight CG flashes per km² per year), even in regions that are otherwise show sparse densities. These local maxima are typically caused by tall structures located at exposed sites, which tend to attract a higher number of upward lightning strikes. Meteorological and topographical conditions make the areas south of Carinthia along the northern border of Tyrol, and in southeastern Austria with Styria the primary hotspots for lightning activity in Austria.

[6]An isoceraunic line is a contour line on a map that connects points with the same number of thunderstorm days per year.

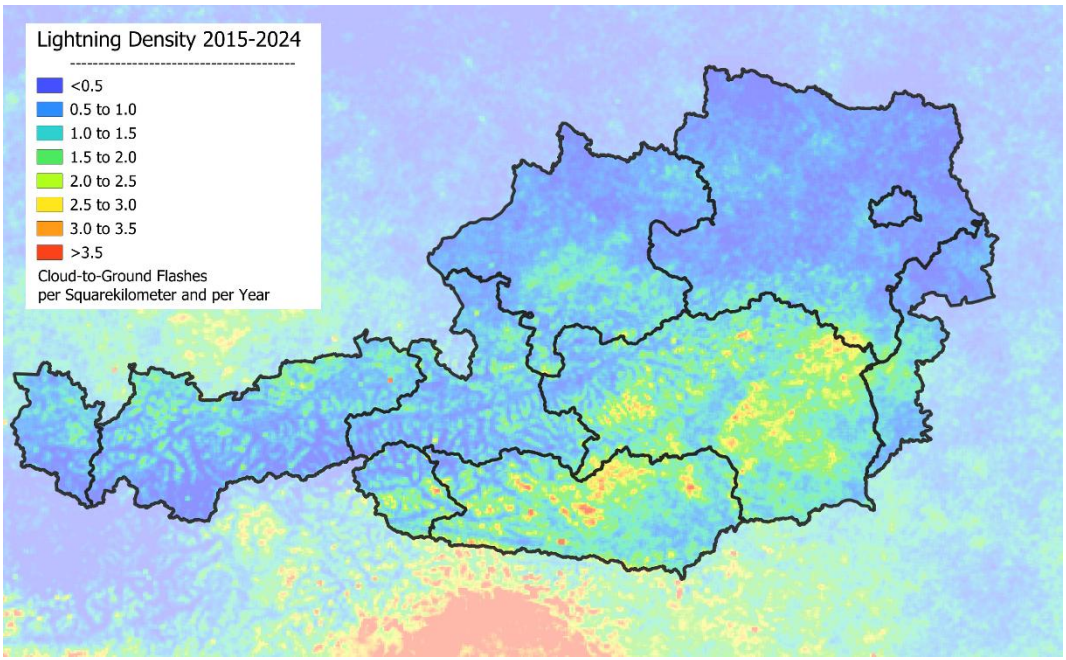

Figure 8: Lightning density map of Austria with its nine provinces for the years 2015 to 2024 for CG flashes per square kilometre and per year[7].

The importance of Graz as a location for lightning research has already been demonstrated by previous measurement campaigns (e.g., Vergeiner et al, 2013 [55]; Schwalt et al., 2020 [56]; Schwalt and Schulz, 2023 [57]; Schwalt et al., 2024 [58]; Schulz et al., 2013 [59] etc.).

[7]Data and graphic sourced by Hannes Kohlmann (ALDIS); design and layout adapted.

3 Thunderstorm Monitoring

3.1 Alerts and Shutdowns at Airports

This section addresses procedures at airports during severe weather. It also defines the terms alert and shutdown, which represent different stages of alarms according to the IATA (IATA, 2006 [1]). Among all the affected facilities mentioned, this thesis focuses specifically on LTs for initiating alerts and shutdowns at airports during thunderstorm activity but also to resolve them (see Figure 9, Phases 1, 2 and 3). A key objective is the optimisation of timing with regard to personnel safety. The centre of the installed FM network is Graz Airport (LOWG) in Austria. The observed areas in the performed analysis are based on the specifications of the IATA for airport operations. In this context, the 8 km and 5 km radii around an airport are particularly relevant for current alert and shutdown procedures during approaching thunderstorms. When an Alert is set by the airport, preparations for the Shutdown phase must be initiated. For example, non-essential outdoor activities have to be suspended, refuelling pressure reduced, and the use of highly conductive objects avoided (Figure 9, Phase 1).

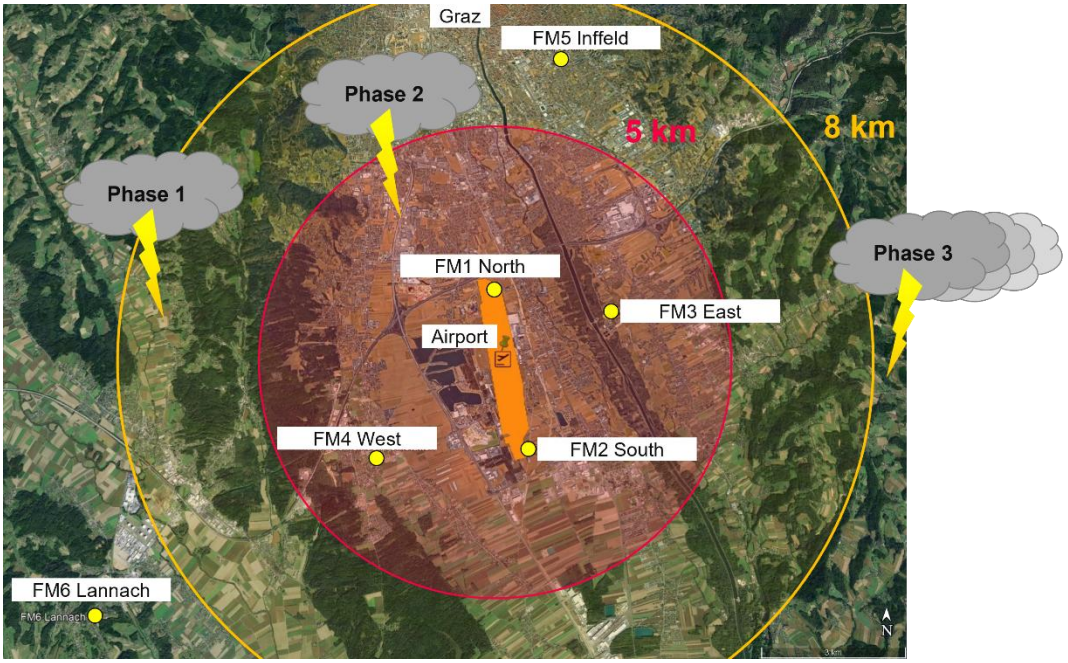

Figure 9: Satellite image of LOWG showing the locations of the electric field meter, a red circle with a 5 km radius and a yellow circle with an 8 km radius corresponding to IATA, 2006 [1] shutdown and alert zones. The three phases represent the alert phase (1), the shutdown phase (2), and the all-clear phase (3), Map source: Google Earth, adapted by the author.

Once a Shutdown is initiated, all personnel must seek shelter, and all ramp activities must cease, including refuelling and aircraft handling (Figure 9, Phase 2). Once lightning activity has subsided or the thunderstorm has moved beyond the 5 km and 8 km radius, alerts and shutdowns can be terminated and the all-clear can be given again (Figure 9, Phase 3) (IATA, 2006 [1]).

To compare the results of shutdown LTs in Section 8.2, four ranges are defined to structure the analyses in this work:

- LTs less than 2 minutes
- LTs from 2 to 30 minutes
- LTs from 30 to 60 minutes
- LTs over 60 minutes

LTs under 2 minutes are likely insufficient to safely interrupt work and seek protection, even though an alert phase precedes every shutdown. Thus, shutdown LTs of less than 2 minutes are considered a failure to warn, in accordance with TWS Standard (OVE, 2022 [5]), described in Section 3.3.1. As the optimal range, LTs from 2 to 30 minutes are defined, aligning with the LTs typically achievable by on-site meteorologists. When preceded by an alert, a two-minute LT is generally sufficient for personnel to seek shelter (e.g., in a building or vehicle). Lead timess from 30 to 60 minutes are considered acceptable, while LTs exceeding 60 minutes represent significant operational disruptions for airports and should be avoided.

While larger airports still have on-site meteorologists who can observe and assess weather conditions in real time, the trend, especially at smaller airports, is moving toward the use of remote towers. In such cases, the meteorologist is located elsewhere and no longer has direct visual access to local weather developments (EASA, 2023 [2]). A real-time lightning risk assessment system can support meteorological decision-making under these conditions.

3.2 Thunderstorm Forecasts

3.2.1 Meteorological Forecast Models

Weather is the spatial and temporal condition of the air and sky or what occurs naturally in the atmosphere at a given location p and time t. Some descriptive weather elements such as temperature, precipitation, wind, etc. can be measured quantitatively. Qian, 2017 [60] describes weather and its elements $W(p,t)$ by the climatic state $C_{\mathrm{S}}(p,t)$ and weather anomaly $W_{\mathrm{A}}(p,t)$:

$$W(p,t) = C_{\mathrm{S}}(p,t) + W_{\mathrm{A}}(p,t) \tag{1}$$

The climatic state is an equilibrium state estimated by an average over several years. In the case of temperature, for example, at least 30 years are taken into account, in some cases more than a hundred years of measurement data for a location. Weather anomalies can then be obtained by subtracting the climate state from the weather at a specific point in time, e.g., hours, days. While the climatic state can be estimated by its average, the future weather can be predicted by the application of scientific methods and the understanding of atmospheric processes.

Weather forecasting nowadays relies on numerical weather prediction models. Their reliability depends on the quality and resolution of the models but also on the quality of the input data. Weather forecasts can be distinguished in different time ranges, e.g., nowcast, short-term and long-term for forecasts within six hours, up to three days and several weeks. Nowcasts include the description and prediction of strong, small-scale phenomena like rain showers or convective storms. For example, in the case of deep moist convection, when moist air is lifted to saturation and reaches the point of positive buoyancy up to the level of free convection, this can lead to cloud formation and thunderstorms. These events can often be better predicted by experts than by computer models due to the many small details involved. Short-term forecasts can be performed by the observation of Rossby waves, large-scale waves in the troposphere. By the speed and direction of the waves for the last hours, the course of the next few hours and days can be extrapolated. Long-term forecasts rely mainly on the outputs of numerical weather models like the European Centre of Medium-Range Weather Forecasts (ECMWF) model. The basis for the numerical models is measurement data

from ground observations from weather station networks, like the Austrian TAWES[8] or from radiosondes. The models comprise mathematical models for different weather elements, which can simulate the development of air pressure, wind, surface temperature and so on. Different methods and resolutions are in use for modelling, but they all depend on the input data of climate state and weather anomalies (Markowski and Richardson, 2010 [37]; Qian, 2017 [60]; Meischner, 2004 [61]).

3.2.2 Weather Radar Systems and Satellite Meteorology

The electromagnetic principle of a radar (including weather radar) is equivalent to the echo of a sound wave in acoustics. A high-frequency electromagnetic pulse is emitted, with a propagation speed corresponding to the speed of light in air. When the radar pulse hits an object (e.g., raindrops, hailstones), it is reflected, and the reflected radar pulse can be received again by the radar station. The distance to the object can then be determined by measuring the transit time. Additionally, the size of the object can be determined based on the reflected power.[9]

The reflectivity Z of a target volume is estimated from the received power P_{R}. The received power can be described by a simplified meteorological radar equation (Doviak and Zrnic, 1984 [62]):

$$P_{\mathrm{R}}(r) = \frac{1}{C_{\mathrm{R}}} \cdot P_{\mathrm{T}} \cdot G_{\mathrm{A}}^2 \cdot \frac{G_{\mathrm{R}}}{L_{\mathrm{MF}}} \cdot \frac{1}{r^2} \cdot \frac{1}{L_{\mathrm{atm}}^2} \cdot Z \tag{2}$$

The equation includes a constant factor $\mathrm{C_R}$ depending on the type of precipitation (rain or snow), the transmitted power P_{T} of the radar pulse, the antenna gain G_{A} for both transmitting and receiving, the receiver gain G_{R} and the matched filter losses L_{MF}. These factors are technical specifications and are known for each radar system. The two-way distance r between the antenna and the target corresponds to the travel time of the radar pulse. The atmospheric attenuation L_{atm} between the antenna and the

[8]Teilautomatisches Wettererfassungssystem (Semi-automated weather recording system), https://www.blog.tawes.at/tawes/, accessed on 22.07.2025
[9]https://www.radartutorial.eu/01.basics/Das%20Prinzip%20von%20Radarger%C3%A4ten.de.html, accessed on 20.06.2025

target (two-way) must be determined through actual measurements (Meischner, 2004 [61]).

A relationship between reflectivity and raindrop size was established by Marshall and Palmer, 1948 [63], in which they compared the possible number of water droplets N per cubic meter to the droplet diameter D as Drop-size distribution. Since each hydrometeor (e.g., raindrop, snowflake, hailstone) has a different diameter, it is not possible to determine reflectivity by simply multiplying a value by the number of objects. Instead, reflectivity represents the combined contribution of all individual particles within one cubic meter of space, taking into account a model that describes the distribution of different droplet sizes:

$$Z = \int_{0}^{D_{\max}} N_0 \cdot e^{-\Lambda D} \cdot D^6 \cdot \mathrm{d}D \tag{3}$$

The constant parameter N_0 is describes the maximum droplets per cubic meter at the smallest possible droplet size $N_0 = 8000 \cdot \mathrm{m}^{-3}\mathrm{mm}^{-1}$, Λ is a slope parameter in mm^{-1} dependent on rainfall rate, $D_{\max}$ is the maximum droplet size within the volume with D in mm (Rogers and Yau, 1989 [64]).

The Radar reflectivity Z measures the intensity of precipitation by the power backscattered from hydrometeors. Due to the large dynamic range of reflectivity values, a logarithmic scale is used (Markowski and Richardson, 2010 [37]; Meischner, 2004 [61]:

$$\mathrm{dB}Z = 10 \cdot \log_{10}\left(\frac{Z}{1\ \mathrm{mm}^6/\mathrm{m}^3}\right) \tag{4}$$

For the use in this work, the radar data provided by the ACG are already in logarithmic form and stored as portable grey maps. The 256 greyscale levels of the images are linearly mapped onto a scale ranging from 0 to 60 dBZ. Further details on this linear relationship are provided in Section 4.3.

Satellite Meteorology

Another method of observing the weather and the formation of thunderstorms is satellite meteorology. The idea of studying weather from extreme altitudes emerged long before the first satellite reached space. In 1929, Robert H. Goddard launched a

small rocket equipped with a barometer, a thermometer, and a camera[10]. With advances in rocket technology during World War II, the first photographs of clouds from high altitudes were taken in the late 1940s. The first weather satellite, TIROS-1, was launched in April 1960. Early polar-orbiting satellites evolved from simple cameras to advanced multispectral radiometers, expanding their use from meteorology to oceanography. As new applications emerged, the focus shifted from cloud imagery to atmospheric sounders that provided quantitative data for weather models. In the 1970s, the transition began from polar-orbiting satellites to Geostationary Operational Environmental Satellites (GOES), in 36,000 km above the Earth. The ability to capture satellite imagery at short intervals from geosynchronous orbit allowed meteorologists to observe continuous image sequences of weather developments. This advancement significantly improved the forecasting of local severe weather (Ostby, 1985 [65]). Satellite imagery is used for the identification of cloud patterns, thunderstorm centres, frontal bands, jet streams, vorticity, fog, thunderstorm development and dissipation, as well as areas of rain and snow. It can also be used to detect snow cover, dust storms, and estimate ground temperature (Smith et al. 1986 [66]).

According to Dr. Kaltenböck, satellite-based data is also used operationally by ACG for severe weather detection. Although fine structures cannot be identified as clearly as in radar data, infrared temperature measurements of cloud tops allow for the estimation of thunderstorm cloud-top heights. However, lightning production is associated with charge transport by hydrometeors, which is much more clearly detectable in radar data and can be tracked with higher vertical accuracy. Even tough satellite-based data represents a significant component of atmospheric science, it is not used in the present thesis. Nevertheless, it is included here to provide a complete overview of commonly used observational systems in meteorology.

[10] https://www.nasa.gov/dr-robert-h-goddard-american-rocketry-pioneer/, accessed on 20.06.2025

3.3 Thunderstorm Warning Systems

3.3.1 General Description and Standard

A TWS is a technical system designed to detect lightning activity or impending electric storms within a defined geographical area and to issue early warnings. It relies on various sensor technologies, such as those for detecting electromagnetic or electrostatic fields, as well as LLS. The goal is to provide early warnings to risk areas in order to enable the implementation of preventive measures. According to OVE EN IEC 62793:2022 (OVE, 2022 [5]), a TWS consists of one or more thunderstorm detection devices that monitor electric activity and provide information in the form of alerts. These alerts help mitigate risks associated with so-called lightning events (i.e., CG lightning strike or IC discharge), such as direct lightning strikes or strong E-fields.

Thunderstorms and lightning pose significant risks both to human life and to property. The standard outlines hazards that may arise from factors such as:

- **Injuries and fatalities** caused by direct or indirect lightning strikes.
- **Failures and disruptions in industry** due to power outages or electronic malfunctions.
- **Interruptions to transportation systems** or communication networks.
- **Explosions or fires** in hazardous industrial processes or sensitive environments.
- **Risks to events** involving large gatherings of people like concerts and sporting events.

An effective warning system can make the difference between a harmless incident and a disaster. It provides LT to implement preventive measures such as evacuations or shutdowns of sensitive areas. Typical areas of application are:

- **Airports and airfields**, where protecting passengers and ground personnel is essential.
- **Industrial facilities**, especially in the chemical, energy, or petroleum sectors.
- **Wind and solar power plants**, which are particularly exposed.

- **Critical infrastructure**, such as power grids, data centres, and communication systems.
- **Mining operations and large construction sites**, particularly where cranes or elevated machinery are in use.

Various systems can be used for thunderstorm warning (e.g., FMs, LLS, weather radar), as described in Sections 3.3.2 and 3.3.3, or combinations of these systems, as implemented and discussed in the present thesis.

To ensure the analyses and results presented in this work are normatively comparable, this section relates the terminology used in the thesis to definitions from the relevant standard. The terms Target Area, Surrounding Area, Monitored Area, and Coverage Area are used to describe areas at risk. Different conditions and measures apply to each of these areas:

- Target Area (TA): The area in which people or infrastructure are directly at risk and must be protected from or prepared for a lightning strike (e.g., the grounds of an airport, such as Graz Airport in the context of this work)
- Surrounding Area (SA): The immediate vicinity of the TA, where the occurrence of a lightning strike already poses a risk or where there is a possibility of a lightning strike affecting the TA. In reference to IATA regulations (IATA, 2006 [1]) and this work, this corresponds to the shutdown zone within the 5 km radius.
- Monitored Area (MA): The outer observed area. If lightning strikes occur in this area, or lightning conditions are met, an alarm is triggered. This area corresponds to the IATA Alert Zone between the 5 km and 8 km radius. In the context of this work, it refers to all areas outside the 5 km radius.
- Coverage Area: A broader region representing the entire observed area in which thunderstorm activity could potentially impact the TA. No specific actions are defined for this area.

The alarm activation is based on lightning strikes or fulfilled lightning conditions within the MA. However, this area can be subdivided into multiple zones with different alarm criteria. Alarm criteria may include various thresholds (not further specified) or lightning detections within the MA. The standard also refers to distinguishing between IC

discharges and CG lightning strikes, as well as the possible combination of multiple criteria.

The alarm process begins once the alarm has been activated. This is followed by the LT the interval between alarm activation and the first CG lightning strike occurring in the SA. The alarm remains active until a decision is made that the danger has passed, and the alarm can be cleared. This decision may be based on thresholds falling below defined limits or the absence of lightning activity for a specified period. The time from this decision until the end of the alarm is referred to as the time to clear (TTC).

To evaluate the performance of a Thunderstorm Warning System (TWS), several performance parameters are defined:

- Total Number of Alarms (TNA), The total number of alarms triggered over a specific period.
- Effective Alarms (EA), Alarms that were successfully issued prior to a lightning strike in the SA and Effective Alarm Ratio (EAR), the proportion of EAs relative to the total number of alarms:

$$\mathrm{EAR} = \frac{\mathrm{EA}}{\mathrm{TNA}} \tag{5}$$

- Non-Effective Alarms (Non-EA) or False Alarms (FA), Alarms that were issued but no lightning strike was detected in the SA and the false alarm rate (FAR):

$$\mathrm{FAR} = \frac{\mathrm{FA}}{\mathrm{TNA}} \tag{6}$$

- Failure to Warn (FTW) and Failure to Warn Ratio (FTWR), when a lightning strike occurred in the SA, but no alarm was triggered:

$$\mathrm{FTWR} = \frac{\mathrm{FTW}}{\mathrm{FTW} + \mathrm{EA}} \tag{7}$$

- Probability of Detection (POD), as the opposite of FTWR is the proportion of EA relative to all lightning strikes that could trigger an alarm

$$\mathrm{POD} = \frac{\mathrm{EA}}{\mathrm{FTW} + \mathrm{EA}} = 1 - FTWR \tag{8}$$

The standard does not specify values for LTs, TTC, or threshold values for performance parameters. It only provides an example in the annex, which lists various values for the radius of the MA (10, 15 and 20 km) and for the TTC (10, 20, and 30 minutes), measured from the last CG lightning strike within the MA.

3.3.2 Lightning Location Systems

In thunderstorm warning applications, an LLS can function as a TWS. The ground-based sensor network detects and locates lightning by capturing the electromagnetic signals emitted during an IC discharge or a CG lightning strike (see Section 4.2). Thunderstorm warnings based on LLS data, different warning zones (i.e., MA) are defined around an object to be protected (i.e., TA like Graz Airport), as described in Section 3.2.3. If a lightning event is detected within this area, distinguishing between IC discharges and CG lightning strikes for alarm triggering, an alarm is activated for the TA. In addition to the description provided in the standard (OVE, 2022 [5]), there is only a limited number of studies addressing this topic. The methods used vary widely, making direct comparisons difficult.

Holle et al., 2014 [67] used data from the United States National Lightning Detection Network (NLDN) in North America. CG lightning strikes combined with IC discharges were used within a MA of 15 km radius. Their analysis covered 47 days in August and September 2013 across 10 locations throughout the United States. For an inner warning zone (what they refer to as the SA) with a 4.8 km radius and using only CG lightning data for warning purposes, they achieved a probability of detection (POD) of 76% and 69% non-EAs. The TTC was set to 15 minutes.

Schmitt, 2016 [68] analysed EUCLID data from 2010 to 2015 for 105 randomly selected locations across Europe. He considered a MA with a 20 km radius and a dwell time of 60 minutes. For a 5 km SA, his analysis resulted in a POD of 91% and 77% non-EAs.

Schmitt, 2023 [69] analysed LLS data of the global LLS (GLD360) for six different countries in Africa and Asia. He analysed 668 lightning events (see Section 3.3.1) in total using the occurrence of IC discharges as warning criterion. He considered a MA

with a 25 km radius and a dwell time of 60 minutes. Only a SA of 2 km were considered. The results showed a POD of 98% but no non-EAs.

3.3.3 Electric Field Meters

The use of electric FMs for thunderstorm warning is typically limited to a single sensor at smaller airfields. The first documented implementation of an FM network was in 1973 at Kennedy Space Center (KSC) in Florida (Jacobson and Krider, 1976 [6]), following a lightning strike to the Saturn V rocket during the Apollo 12[11] mission in November 1969, which caused system malfunctions. Another FM network is operated in São José dos Campos, Brazil (Rodrigues and Lacerda, 2022 [14]).

The applied E-field thresholds for the Space Program of the United States of America changed for different missions and were defined as Lightning Launch Commit Criteria (LLCC). In the first years after establishing the FM Network at KSC a lightning warning would be issued if the magnitude 3000 V/m within 9 km was exceeded (no details about filtering of the FM recordings given). Later a threshold of 1000 V/m was added for disturbed weather conditions and thunderstorms in the vicinity. Another threshold of 1500 V/m magnitude was added if clouds in an 18 km radius are transparent or if they have tops warmer than +5 °C. So also, meteorological parameters are included for lightning warning (Merceret et al, 2010 [70]).

Studies using a single FM for warning mostly show low POD below 40% and Non-EA above 70% (e.g., Aranguren, 2009 [71]; Murphy et al, 2008 [8]). A Study of Silva Ferro, 2011 [12] show for a threshold of 0.9 kV/m and a MA with a 10 km radius a more efficient configuration with a POD and Non-EA of 60% and 41%, respectively. The sole use of E-field data for lightning warning or lightning forecast shows limitations (see Section 4.4). Additional analyses conducted in this work have shown that high E-field values also occur on days without lightning strikes (according to LLS data). Values of 3000 V/m and higher have been observed during the three observed thunderstorm seasons. A comparison of E-fields on days with and without lightning strikes is presented in Appendix E.

[11] https://www.nasa.gov/missions/apollo/apollo-12-the-pinpoint-mission, accessed on 24.06.2025

4 Measurement System

4.1 Electric Field Meter

4.1.1 Measurement Principle

The FMs utilised in this work are used to measure slowly varying E-fields with low frequencies in the sub-hertz range (i.e., <1 Hz). To describe the measurement principle, the sensor unit of the FM (see Figure 10) can be regarded as a capacitor. However, since static and very slowly changing electromagnetic fields do not couple displacement currents into electric conductors or induce voltages in loops, the temporal change must be generated mechanically (Küchler, 2005 [72]). FMs therefore use a reciprocating aperture that alternately exposes the measuring surface (sensor electrode) to the E-field $\vec{E}$ and shields it from it again. This changes the effective area $A(t)$ trapezoidally[12].

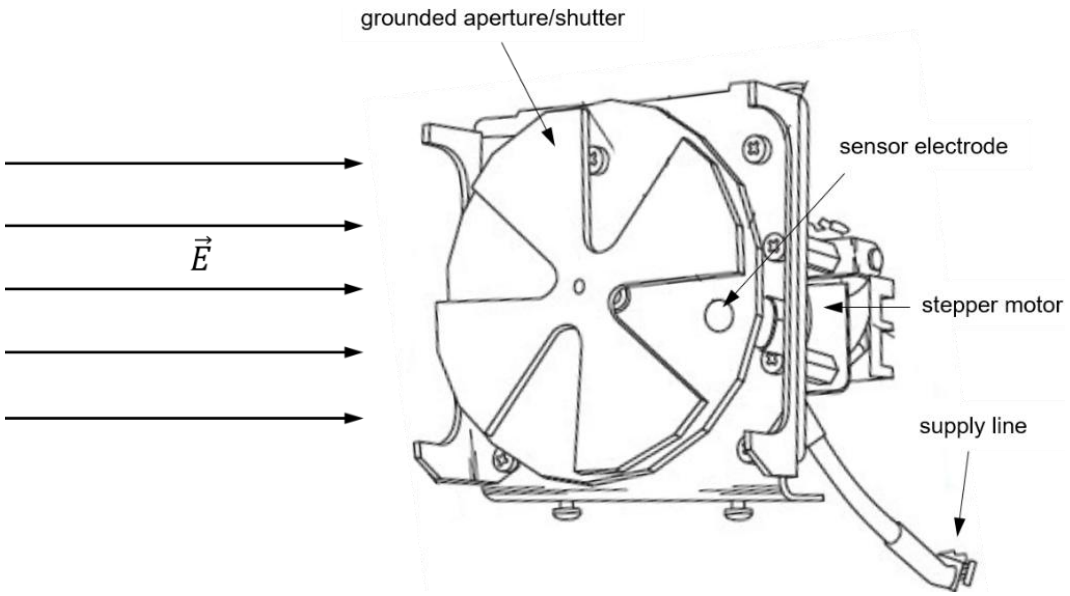

Figure 10: Measuring principle of an electric field meter using the example of the CS110[13] in an E-field $\vec{E}$, the main components are the sensor electrode, the grounded reciprocating aperture (i.e., shutter), the stepper motor and the supply line.

[12]Campbell Scientific Inc., "CS110 Electric Field Meter: Product Manual", p. 13, 2020.
[13]Campbell Scientific Inc., "CS110 Electric Field Meter: Product Manual", p. 29, 2020.

The displacement current is thus derived as follows (Küchler, 2005 [72]; Plaßmann and Schulz, 2012 [73]):

The charge Q accumulates on the sensor electrode until the potential of the sensor electrode corresponds to the equipotential of the environment. The following applies to the capacitance of the plate capacitor $C = \varepsilon_0 \cdot \varepsilon_\mathrm{r} \cdot \frac{A}{d}$ with the vacuum permittivity ε_0, the relative permittivity ε_r, the area of the capacitor A and the distance between the electrodes d. The E-field in the capacitor is described by $\left|\vec{E}\right| = \frac{Q}{\varepsilon_0 \cdot \varepsilon_r \cdot A}$. This results in:

$$Q = \varepsilon_0 \cdot \varepsilon_\mathrm{r} \cdot A(t) \cdot \left|\vec{E}\right| \tag{9}$$

If one had a time-varying E-field $\left|\vec{E}\right|$, the charge Q would also change and a current $i(t)$ would flow. Since it is an electrostatic field, this change is achieved by the alternating shading of the sensor electrode, i.e., a change of the capacitors area $\frac{\mathrm{d}A}{\mathrm{d}t}$; as soon as the sensor electrode is shielded, the charge Q flows towards ground:

$$i(t) = \frac{\mathrm{d}Q(t)}{\mathrm{dt}} = \varepsilon_0 \cdot \varepsilon_\mathrm{r} \cdot \frac{\mathrm{d}A(t)}{\mathrm{d}t} \cdot \left|\vec{E}\right| \tag{10}$$

A shunt resistor at the sensor electrode can be used to measure a trapezoidal alternating voltage, the amplitude of which is proportional to the E-field.

4.1.2 Field Meter Setup

The FM sensors of the type CS110 from Campbell Scientific (see Figure 11, left) are provided with a metal housing, a sensor electrode, an aperture (i.e., shutter), a charge measurement circuit and a leakage current compensation circuit. The main task of the sensor is the permanent recording of the atmospheric E-field on the earth's surface, in fair-weather as well as during thunderstorms. In addition to precipitation, outdoor use also involves exposure to dust and dirt and strong UV radiation. The requirement for the FM sensors is therefore to prevent the ingress of water and dirt, to be resistant to solar radiation while the measurement drift is as small as possible.

Ideally, the FM sensor is installed looking upwards and flush with the earth's surface. In this case, the sensor would measure the E-field directly at the earth's surface and the recording would be unaffected by the housing and mounting position. In practice, the sensor is mounted on a tripod looking downwards due to the environmental influences mentioned (e.g., precipitation, dust, etc.). The manufacturer specifies a mounting height of two meters between the surface of the earth and the lower edge of the FM sensor. To take into account, the influence of the tripod, the inverted FM sensor and the distance to the surface, the manufacturer references each individual FM sensor with a flush and upward-facing FM sensor. The result of this referencing is a characteristic $M_{parallel\_plate}$ factor for each FM sensor, which is implemented in the configuration file of each FM sensor[14].

Compared to conventional FM sensors, which use a rotating aperture to ground the sensor electrode, the FM sensor used here has a grounded reciprocating aperture. This alternatingly shields and exposes the sensor electrode (see Fig.1, right) from the prevalent atmospheric E-field, which yields to a defined open and closed position.

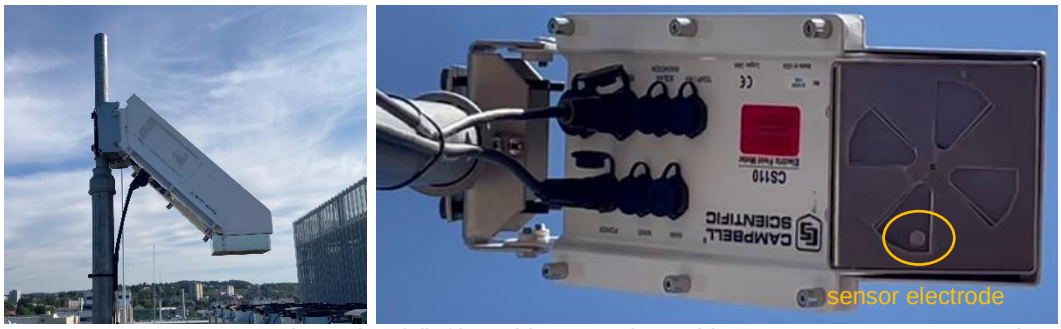

Figure 11: FM-Sensor mounted on tripod (left) and bottom view with open aperture, sensor electrode is visible (right).

One measurement cycle is set to one second (sample rate is 5 Hz), with an open period of about 140 ms (validated with high-speed video measurement). The significantly longer closed period (860 ms) ensures, that the sensor electrode is fully grounded and thus the last measurement cycle does not affect the current one. The measuring range

[14]Campbell Scientific Inc., "CS110 Electric Field Meter: Product Manual", pp. 19-21, 2020.

of the CS110 is divided into two intervals: 0 to ±2,200 V/m and ±2,200 to ±22,300 V/m. The device automatically switches between these ranges as required.

On the underside of the FM-sensor are seven sealed connectors (Power, I/O, RS232, Temperature/Rel. Humidity, Rain, Wind, Solar Radiation). For the conducted measurements, the Power and the I/O connector were used, for power supply and data transfer, respectively.

The matching tripod is also supplied by Campbell Scientific. The CM106B is made of galvanised steel tubes and can be adjusted to different heights and surfaces. The base plates can be anchored in the ground with ground spikes. The FM sensor is firmly connected to the tripod with a clamping plate. For low-resistance, low-inductance earthing of the tripod and the sensor, a copper-plated earthing spike (length: 1200 mm) is driven into the ground and connected to the tripod with stranded copper earthing cable (cross-section: 30 mm^2). The circular area of the tripod in its assembled state has a diameter of approximately three meters.

Control boxes for mounting on the tripods were designed to integrate the peripheral devices. They contain an uninterruptible power supply (UPS), a circuit breaker, a surge arrester, two earthing terminals, a 12 V AC/DC converter, an industrial Mini-PC, a Network Link Interface (NLI) from Campbell Scientific and an LTE module with external antenna (mobile data connection). All components were mounted on a mounting plate. In addition, an anti-condensation bag was installed in each control box to regulate the humidity. The control boxes are insulated and heated to regulate the temperature.

The UPS is used to bridge power failures. In UPS mode, a time of over 20 minutes was determined during which the industrial Mini-PC, the NLI and the FM sensor can be operated. The AC/DC converter is a 12 V switching power supply with an output of 60 W. The requirement for the device is a low voltage ripple to keep interference low. The industrial Mini-PC with a complete Windows 10 version is used to control the FM sensor, store data locally and transfer data. The PC has the necessary serial RS232 interfaces, USB 3.0 interfaces, Ethernet interfaces, VGA and HDMI connections for the measurement setup. Power is supplied via the AC/DC converter. To avoid connection interruptions, additional aluminium brackets were built and installed to fix the LTE modules and the antenna connections in the slots. The Network Link Interface NL 201 from Campbell Scientific is used to transfer the data from the FM sensor to the Mini-

PC. The NL 201 acts as a virtual COM port for the conversion of the serial signal to an Ethernet standard.

The temperature is regulated by two PTC heating elements, each with 20 W, which are riveted directly to the mounting plate in the switch cabinet. These are controlled by a thermostat. If the temperature in the upper area of the switch cabinet rises to 40 °C, the heating elements switch off. In addition, the enclosure doors and ceiling panel are insulated with EPS insulation material. For temperatures below 15 °C and without the influence of solar radiation, this results in a stable temperature difference of +17 K in the enclosure relative to the outside temperature.

Figure 12: Tripod with mounted FM-sensor and control box (left), equipped control box with peripheral devices (right).

4.1.3 Field Meter Network

To monitor the area around Graz Airport, locations were selected in the north, south, west and east of the airport, where one FM was installed at each location. Two further locations were installed further away from the airport for reference and test measurements. The decision on the choice of measurement sites is also supported by preliminary tests and simulations. The manufacturer does not provide any specifications or instructions for use in a network. As guidance for the average distances applied between FM sensors, networks in Brazil (about 2 km, Rodrigues and

Lacerda, 2022 [14]) and at Cape Canaveral in Florida, USA (about 2 km to 4 km, Handel et al., 2022 [74]) were used as reference.

The first experimental location where an FM was installed was an accessible measuring platform on the Inffeldgasse campus of Graz University of Technology. The field meter FM 5 Inffeld at this test location was installed in May 2022. All software and hardware were tested on this FM before it was used in the other FMs. The recordings of FM 5 Inffeld were not used for the analyses described in the Sections 7 and 8.

The choice of location is dependent on technical specifications, which can be found in the operating manual[15] of the electric FMs (no obstacles within a radius of 7.62 meters of the FM, no or little vegetation in the area of the FM, sensor facing ground and no tripod leg). In addition, there must be a permanent connection to the electric power supply. These conditions are met at the Graz Airport site. This resulted in two locations to the north and south of the Graz Airport site. The first field meter FM 1 North in the area of a wind measuring station, the second FM 2 South in the area of the southern shelter of the instrument landing systems, both of which are operated by Austro Control GmbH. The distance between the two FMs is approx. 4 km and at a distance of approx. 2 km from the centre of Graz Airport. The site of a sewage treatment plant in Gössendorf was chosen as the eastern location for the third field meter FM 3 East. This site also meets the necessary conditions and is located 2.4 km from the centre of Graz Airport. An available site for the fourth field meter FM 4 West in the west was found on the roof of an administrative building in Premstätten. The available free space on the roof deviates from the manufacturer’s specifications (free space in a radius of 7.62 meters around the FM). In order to compensate for structural conditions, correction factors were determined on fair weather days (see Appendix A). The western location is 3.7 km away from the centre of Graz Airport. A private site for the sixth field meter at a distance of 10.7 km to the southwest of Graz Airport was selected as the reference site. This FM 6 Lannach reference field meter is located close to a tall broadleaf tree, due to site-specific conditions (approx. 5 meters from the edge of the tree canopy). The recordings of the Reference FM in Lannach were not used for the evaluations described in Sections 7 and 8.

[15]Campbell Scientific Inc., "CS110 Electric Field Meter: Product Manual", p. 8, 2020.

The FM stations are synchronised by using windows time sync options. The used time server is the ptbtime1.ptb.de by the “Physikalisch-Technische Bundesanstalt (PTB)” in Braunschweig, Germany. The PTB operates four atomic clocks, two caesium clocks and two caesium fountain clocks[16].

4.2 Austrian Lightning Location System

The Austrian Lightning Detection and Information System (ALDIS) operates a network consisting of eight Vaisala LS7002 sensors, strategically placed across Austria with a maximum distance of 150 km between sensors (Diendorfer, 2016 [75]). In 2023, ALDIS expanded significantly by integrating the LLS lightning information service (Blitz-Informationsdienst, BLIDS) network, increasing its sensor count to 50 distributed across 11 European countries. Additionally, ALDIS has been a member of the European Cooperation for Lightning Detection (EUCLID) since 2000, a collaborative network currently comprising 173 sensors (Schatz et al., 2024 [76]; Schatz et al., 2025 [77]).

The calculations by the LLS are based on measurements of the radiated electromagnetic fields propagating as ground waves (VLF and LF range) from CG lightning strikes. After two or more sensors have detected the electromagnetic pulse of a lightning strike, the data is calculated in a central processor. In order to decide which lightning strike detected by the LLS belongs to which flash, a grouping algorithm is stored in a central processor. Strokes within a specified clustering radius (usually 10 km) and a time interval of one second are grouped into a flash. The interstroke interval, i.e., the time between two strokes, must not exceed 500 ms (Diendorfer, 2007 [78]).

Recent studies by Graz University of Technology have shown that the Austrian LLS achieves a flash detection efficiency (DE) of over 96% and a location accuracy (LA) of around 100 m for negative cloud-to-ground (CG) lightning (Schwalt et al., 2020 [56]). Despite this high performance, the detectability of individual strokes can still vary depending on the number of sensors reporting the signals (Diendorfer, 2010 [79]). An

[16] https://www.ptb.de/cms/ptb/fachabteilungen/abt4/fb-44/fragenzurzeit/fragenzurzeit11.html, accessed on 10 June 2025

overview of the limitations of the ALDIS LLS is given in Section 4.4. The performance of the LLS in relation to individual CG strokes (Lightning strike DE over 80%) depends, e.g., on the signal strength, ground conductivity, the shape of the lightning channel, site errors and the number of sensor reports (Schulz et al., 2005 [51]; Nag et al., 2015 [80]; Cooray, 1987 [81]). Overall, the robust sensor infrastructure of ALDIS and EUCLID provides comprehensive and reliable lightning monitoring throughout Europe.

The localisation of lightning discharges or specific ground strike points is based on the Time Difference of Arrival (TDoA) method and the Magnetic Direction Finding (MDF) method. When a CG lightning strikes the ground, an electromagnetic pulse is emitted radially. At this time, the impact time is unknown. The TDoA uses the difference in the arrival time at two receivers (LLS sensors), which defines a hyperbola, while several sensor reportings lead to several hyperbolas. The intersection of those hyperbolas represents the ground strike point of the CG lightning strike. It requires at least three GPS synchronised sensors to get the location of the ground strike point, the source of the electromagnetic pulse. Some conditions, i.e., a ground strike point outside the triangle formed by the sensors, can result in an ambiguous localisation, due to another intersection. To get unambiguous results, four or more LLS sensors must be used (Diendorfer, 2007 [78]; Cummins and Murphy, 2009 [82]).

The MDF method utilises crossed loop antennas to determine the direction of a return stroke’s emitted signal. In a multi-sensor network, the best-case scenario is for three or more sensors to detect a return stroke. From the received magnetic field, a direction vector, pointing in the direction of the lightning channel, can be calculated for each LLS-sensor. The estimated coordinates of a Ground Strike Point (GSP) are located in the centre of the polygon created by the direction vectors. To increase the accuracy of locating the GSP, the algorithm must correct electromagnetic signal interference caused by various nearby objects (Diendorfer, 2007 [78]).

The LS7002 sensors utilise both, the TDoA and the MDF method with the IMPACT (Improved Accuracy from Combined Technology) algorithm. The IMPACT algorithm was developed by Global Atmospherics Inc. in 1992. The development was initiated with the objective of enhancing the location accuracy of the United States NLDN in North America. Compared to conventional methodologies that depend exclusively on angle or time data, the IMPACT algorithm performs a simultaneous estimation of the lightning strike location (latitude and longitude) and the discharge time. The IMPACT

method combines azimuth vectors and range circles to enhance the precision of ground strike point. As stated by Cummins et al., 1993 [83], the precision of location of a lightning strike that occurs between two sensors, at their baseline, is higher with the intersection of two azimuth vectors and two range circles than only by the azimuth vector intersection (Diendorfer, 2007 [78]; Cummins et al., 1998 [84]).

The estimation of the return stroke peak current I_{Peak} is based on a linear relationship between the peak current in a CG lightning strike and the peak E-field E_{Peak} from the emitted signal. This relationship is described by the Transmission Line Model (TLM) by Uman et al., 1975 [85] with the following equation:

$$I_{\mathrm{Peak}} = \frac{2\pi \cdot \varepsilon_0 \cdot c^2 \cdot D}{v} \cdot E_{\mathrm{Peak}} \tag{11}$$

with the abbreviations D for the horizontal distance between the lightning channel and the LLS-sensor, v as the return stroke velocity, ε_0 as the permittivity in vaccum and c as the speed of light. The TLM is valid under the assumption of a perfectly conducting ground, a constant return stroke velocity and a return stroke front that has not reached the top of the channel. Until today, due to the lack of ground truth data, the TLM is only validated for negative CG flashes up to a return stroke peak current of 60 kA (Cummins et al., 1998 [84]; Diendorfer, 2007 [78]; Diendorfer et al., 2009 [86]).

4.3 Weather Radar System

The weather radar data for this work are supplied by Austro Control GmbH (ACG) (Schatz et al., 2023 [45]). The ACG operates a network of four radar stations. These stations are Patscherkofel in Tyrol, Feldkirchen in Salzburg, Wien-Rauchenwarth in Vienna, and Zirbitzkogel in Carinthia. A fifth radar station in Valluga (Vorarlberg) has been inactive since 2017 and did not provide any data for this work.

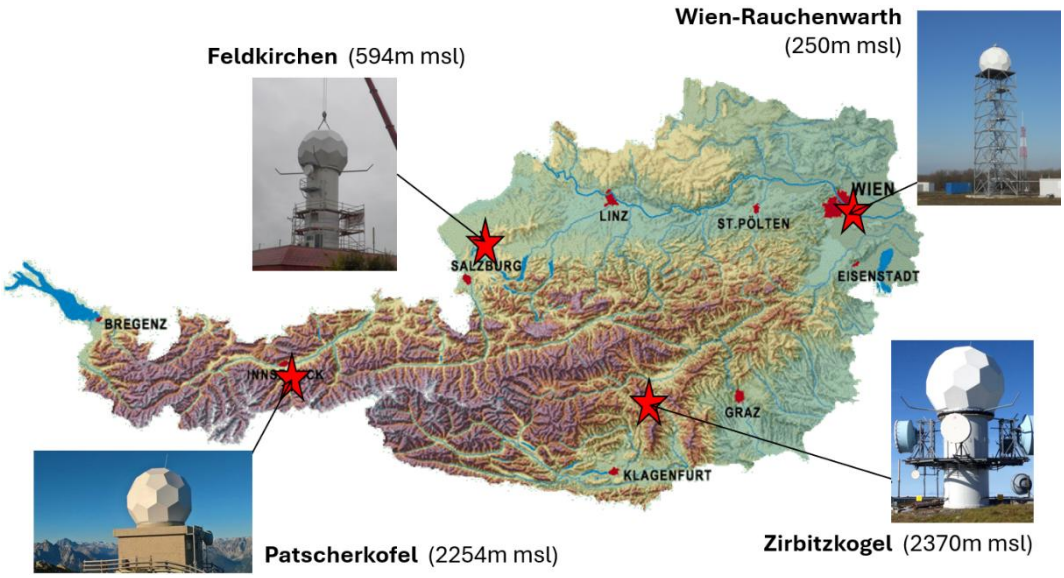

Figure 13: The Austrian weather radar system of the ACG (Kaltenböck, 2012 [87]), adapted.

The stations Feldkirchen and Wien-Rauchenwarth are located at lower altitudes close to international airports, at 571 m msl and 250 m msl respectively. The stations Patscherkofel and Zirbitzkogel are located at 2246 m msl and 2371 m msl, respectively, in mountainous sites. All four stations are C-Band (5600–5650 MHz) dual-polarisation weather radars of the type DWSR-5001C from Enterprise Electronics Corporation with a pulse peak power of 500 kW. These stations employ an interleave scan strategy, wherein the radar antenna's elevation angle changes with each rotation to cover the entire atmospheric volume. Elevation angles and range of the radar beams (up two 224 km for lower elevation angles) of the different stations are overlapping and selected to cover the entire Austrian air space. This process is divided into two half-scans, each consisting of eight distinct elevation angles scanning from top to bottom in about 2.5 minutes (Kaltenböck, 2012 [87]). Over a five-minute period, all sixteen elevation layers are scanned, and the data of the radar stations are provided as Constant Altitude Plan Position Indicator (CAPPI) images. The CAPPI combines measurements from all four radar stations and provides a spatial resolution of 1×1 km² per pixel and a vertical resolution of 1 km (0–16 km altitude) (Kaltenböck, 2016 [88]).

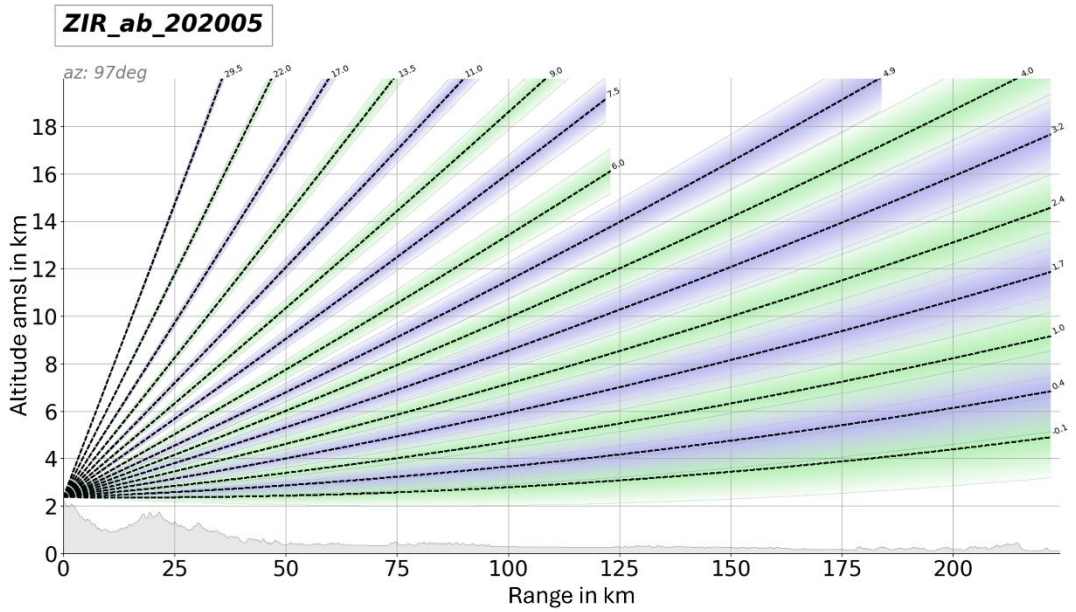

Figure 14: Interleave scan strategy on the example of the Zirbitzkogel radar station, full volume scan consists of two half scans (green and blue), provided by ACG.

These sixteen elevation CAPPI layers, are provided as portable grey map (pgm) files (see Section 5.3, Figure 18 and Figure 19). Each pixel represents the reflectivity as a value between zero (no reflectivity) and 255 (highest reflectivity), while areas outside the range of the radar are also displayed in white. The CAPPI layers 0 to 7 (e.g., layer 0 = 0–1 km amsl) are shown in Figure 18 for the thunderstorm on 12 August 2022 at 14:40:00 UTC where layer zero represents the scan at the lowest elevation. Due to the scanning strategy, the radar stations from the south-eastern part of Austria can only provide radar data from layer 2 and above. The reason for this is the topography, which can be seen at the Zirbitzkogel radar station in Figure 14. The lowest elevation for Zirbitzkogel is above 2 km, areas below this are not visible for this radar station. The layers 8 to 15 are shown in Figure 19, where layer 15 represents the scan at the highest elevation (layer 15 = 15–16 amsl). The CAPPI therefore corresponds to cross-sections of the clouds in Austrian airspace at different altitudes. A three-dimensional cloud image can therefore be created from all 16 layers. Section 5.3 describes in detail the further processing of the weather radar data for combination with E-field and LLS data.

4.4 Limitations of the Measurement Systems

Electric Field Meter Network

As any other remote sensing system (e.g., LLS), a single FM but also FMs operated in a network are strongly depending on calibration and site correction. In the case of the CS110, the calibration is performed by the manufacturer and confirmed by a certificate. A site correction is important, if E-field measurement of several FMs shall be compared. Different sites provide different influences on measurements, while the installation on a building or another tall structure increases the E-field due to the inhomogeneity, while the E-field decreases, when installed in the vicinity of a tall structure (trees, buildings, towers) due to shading effects. To target these site effects, measurements from a fair-weather day (similar E-field at the different sites with distances of up to 10 km between, see Section 4.1.3) were used to calculate correction factors relative to the site least affected by external influences (see Appendix A and Maier et al., 2024 [89]).

Animals, people or vehicles in the vicinity of an FM can significantly alter the measurements. The presence of aerosols, dust, and polluted air can also affect the local E-field[17]

Another important factor for FMs is the temporal resolution. The recorded E-field show low frequencies with changes over several seconds or minute. At a sampling frequency of 1 Hz, the sensor aperture is open for a few milliseconds during each measurement cycle. If the electromagnetic field from a lightning discharge reaches the sensor while the aperture is open, the discharge will appear in the recorded data as spike (see Section 6.1). Since the objective is to measure the E-field generated by a charged cloud, such disturbances must be filtered out. The disturbed signal is smoothed (e.g., using moving median or moving mean), nevertheless, influences from lightning discharges on the measurement of a thunderstorms E-field remain unavoidable.

Using FMs as TWS without additional data sources has limitations, particularly when relying on threshold-based triggering. Analyses conducted for the years 2022, 2023,

[17]J. Maier, “Environmental Influences on Measurements with Electric Field Meters”, Master’s Thesis, TU Graz, 2023.

and 2024 show that high E-field values, exceeding 1000 V/m and reaching up to 10 kV/m, can occur even on days without lightning activity, according to LLS data. The results of these analyses are presented in Appendix E.

Lightning Location System

When validating the results with LLS data, it must be considered that the LLS is subject to a certain degree of inaccuracy. One reason is that a CG lightning strike does not have to have a perfectly vertical lightning channel, but can be skewed and curved, with branches also occurring. The emitted electromagnetic field has not only horizontal but also vertical components. It propagates over mountains and valleys, where the ground has a wide range of conductivities and attenuations. All these factors make it difficult to precisely locate lightning strikes. IC discharges and CG lightning strikes are classified automatically by a stored algorithm that is continuously updated. Classification is based on various waveform discrimination criteria, e.g., ratio of electric to magnetic field, pulse rise time, and pulse width (Krider et al., 1980 [90]; Diendorfer et al., 1998 [91]). An additional parameter, the peak to zero time (PTZ), was introduced in 1998 (Schulz, 2005 [51]). Measurement campaigns from the United States showed that about 90% of the detected positive strokes of less than 10 kA are actually ICs (Cummins et al., 2006 [92]; Cummins and Murphy, 2009 [82]) and thus classified all positive strokes with an amplitude below 15 kA as IC, from 2006 onwards (Murphy et al., 2021 [93]). For negative CG lightning strikes lower than 10 kA a classification accuracy between 50% and 87% is reported by Biagi et al., 2007 [94]. Schulz 2005, [51], stated that this approach is a compromise because misclassification of ICs occurs over a wide range of amplitudes and the amplitude threshold is arbitrary and related to network configurations, regional dependencies, and climate. Nevertheless, ALDIS employed a lower threshold of 5 kA for the classification of positive ICs. The latest algorithms still rely on the same waveform criteria and thresholds, but a linear discriminant analysis, a statistical method for finding features that characterise different classes, supports classification (Kohlmann et al. 2017 [95]). The small baselines between the sensors (<150 km) also positively affect the percentage of misclassified lightning strikes in the Austrian LLS. Due to the small baselines, ALDIS is able to detect lightning strikes with amplitudes as low as 2 to 3 kA (Diendorfer et al., 2022 [96]). An

overall Classification Accuracy (CA) of 89% was evaluated in 2017 for the Austrian LLS. Positive lightning strikes with a CA of 95% were significantly better classified than negative lightning strikes with a CA of 85% (Kohlmann et al. 2017 [95]). Further, Schwalt and Schulz, 2023 [57] revealed a median distance between two ground strike points of the same lightning strike of 1.4 km and a maximum distance of 6.9 km for CG lightning in the alpine region.

Weather Radar System

Radar beams are reflected by most surfaces, so signals from weather radar are often influenced by unwanted echoes. These unwanted signals are classified as clutter. Clutter includes reflections from terrain, planes and buildings as well as birds and insects. Also jamming by a high-power electromagnetic source can lead to unwanted echoes. Since the radar position is fixed and the topography is known, clutter from terrain and buildings can be eliminated. Due to different velocities, also moving objects can be distinct from cloud formations. Signal attenuation during thunderstorms, particularly due to heavy rain and hail, can result in ambiguities or misinterpretations Radar stations located in mountainous areas have limited visibility at low altitudes due to shielding effects. The lowest elevation angle of radars is restricted downward, as illustrated in Figure 14. This and further information on weather radar systems is provided in Meischner, 2004 [61].

5 Data Sources

5.1 Electric Field Meter Network

Data Generation

The FM network described in Section 4.1 has been continuously recording the E-field at the Earth's surface since 05 August 2022. One measurement cycle per FM is one second. The recorded data are saved in a log file in DAT-format. The settings of the individual FMs are set via a command file in CR1-format which contains special instructions for the Campbell Scientific datalogger and is supplied with the CS110 FM. A correction factor ($M_{parallel\_plate}$) determined specifically for each FM by the manufacturer is set in the command file. This correction factor is used to correct all measured values before they are saved. The file then contains a list of all measured values that are saved for each measuring point and are to be saved in the log file ("CR1000_FMName_Tab1sec.dat"), e.g., timestamp, consecutive record number, E-field, status flags, leakage current, panel temperature, battery voltage, relative humidity, etc. It is also defined that average values with a time resolution of 60 seconds are also saved in parallel in a different log file ("CR1000_FMName_Tab60sec.dat"). This option is used for data backup if an original log file with a resolution of one second is defective or incomplete. At the end of the command file there is an error check loop which checks whether the status flag indicates an error before the measuring point with the corresponding E-field measured value is written to the log file. With continuous recording, the log file contains 86,400 new measuring points per day (1,440 measuring points for "CR1000_FMName_Tab60sec.dat").

For backup reasons, the data was continuously sent to a server PC on the Inffeldgasse campus at Graz University of Technology and to InfluxDB[18] for further visualisation in Grafana[19]. In order to have a manageable file size for this, the data was additionally split into files with 10 measuring points each ("CR1000_FMName_Tab1sec_

[18] https://www.influxdata.com/, accessed on 15 May 2025.
[19] https://grafana.com/, accessed on 15: May 2025.

YYYYMMDD_hhmmss.dat") using a batch script. The batch script runs in an endless loop.

Data transfer

The industrial Mini PCs were equipped with an LTE USB modem, described in Section 4.1.2 to enable remote maintenance of the FM software at all locations. The data volume was limited to 10 GB for economic reasons, the bandwidth for download and upload is highly location-dependent (maximum bandwidth download 40 Mbit/s, upload 10 Mbit/s).

The online database InfluxDB from the software company InfluxData, a time series database, is used in the free version for continuous data transfer. This offers the option of encrypted data storage and data access for 30 days. The data is stored in tabular form in so-called buckets.

The data is transferred automatically via a python script "SendData_FMName.py", which uses the python library "influx_client" provided by InfluxData. This was executed as an executable file directly on the respective industrial Mini-PCs. The python scripts directly access the files "CR1000_FMName_Tab1sec_YYYYMMDD_hhmmss.dat" and read out the date, the time stamp and the E-field value for each of the 10 measuring points. The E-field values are then multiplied by the respective location-dependent correction factor (see Appendix A), which is stored directly in the python script. This is followed by the initialisation of the InfluxDB, whereby a security token, the organisation and the URL of the InfluxDB are specified. After initialisation, the data is written to a bucket in the InfluxDB (only one bucket for the data of all six stations). Since errors can occur when visualising the data if all 10 measuring points of a FM are written to the InfluxDB at the same time, a time delay of one second was included to simulate the measuring process and ensure that a single E-field value is written per time stamp. A "try-except" structure was used for errors in data transmission, whereby the script continues to run even after unsuccessful data transmission and writes the error messages to a separate log file until the error is rectified. This has the advantage that data can be transferred again immediately after the error has been rectified without any further delay.

Data backup

For data backup, another Python script “Receive_FM_Data.py” is executed simultaneously on the server PC at the Inffeldgasse campus of Graz University of Technology. The python script automatically accesses the measurement data from the various measurement stations stored in InfluxDB. The InfluxDB is accessed by specifying the security token, the organisation and the URL, as with data transfer. The program runs in an endless loop and checks the current system time with each query cycle. If the system time reaches a predefined time (set to 00:05:00 UTC), a database query is started. To allow for system delays (between 10 seconds and 30 seconds elapse between the storage of the data at the measurement location and the transfer to InfluxDB), the system waits 5 minutes after the day change to ensure that the previous day's data is complete. During the query, the data from all six stations in the bucket were queried. Errors during the database query are also written to a log file, but do not lead to an interruption of the query. Should one or more stations fail and no longer send data, this ensures that the data from the remaining measuring stations continues to be saved.

In addition to the automatic data backup from the InfluxDB, the raw data of the six individual measurement locations (splitted files “CR1000_FMName_Tab1sec _YYYYMMDD_hhmmss.dat”), which are stored in the folder of the same name (“CR1000_Tab1sec”), were backed up manually in a monthly cycle. The number of files per month was over 250,000, which corresponds to a folder size of about 0.9 GB. The corresponding folder was compressed (ZIP-format) and provided with the date of the backup (“YYYYMMDD _CR1000_Tab1sec.zip”). The size of the compressed folder was reduced to about 130 MB. This is in favour of the limited data volume but also the transfer time. AnyDesk's file transfer function was used for the transfer, which enables direct copying between the remote PC (Mini-PC) and the server PC. The compressed folders were unpacked again for further processing on the server PC. The unpacked DAT-files were summarised in folders for each FM on a daily basis and combined again into a daily file with 86400 measuring points (“CR1000_FMName_Tab1sec_ YYYYMMDD.dat”) for further data processing in Section 6.1.

Data visualisation

The web application Grafana from the software company Grafana Labs was used to visualise the data in real time (delay due to transmission of approx. one minute). Grafana enables the monitoring of time series data by creating a dashboard that contains charts and graphs and directly accesses data sources such as InfluxDB[20].

Once Grafana was connected to InfluxDB, a new dashboard could be created (see Figure 15). Two graphs, one with the unfiltered E-field data (Figure 15 bottom) and one as moving average over 60 seconds (Figure 9 top) were then inserted in the dashboard. At this point, the time delay of one second, which was built into the data transmission, takes effect. Without this, all E-field values of a transmission cycle (10 measurement points) would be plotted on the x-axis at the same time. In order to highlight the deviation from the fair-weather field strength, a gauge visualisation of the E-field for all six locations was inserted (deflection to the left – negative E-field values, deflection to the right – positive E-field values, Figure 15 right).

Figure 15: Grafana Dashboard on 04. June 2023 from 04:00 UTC to 10:00 UTC, fair weather values.

[20] https://grafana.com/docs/grafana/latest/getting-started/get-started-grafana-influxdb/#get-started-with-grafana-and-influxdb, accessed on 28 April 2025.

In addition to immediate feedback through changes in the E-field in different weather conditions, this real-time view also has the advantage that a failure of a location can be recognised immediately and countermeasures can be taken. Grafana's alert function is used as an additional warning, where an e-mail is sent in the event of an error (location not transmitting data) containing information on which measurement location is not transmitting. For the duration of the interruption, NaNs are written to the InfluxDB instead of the measurement data.

5.2 Lightning Location System

The data of the Austrian LLS is provided by ALDIS, which is stored in a PostgreSQL database (PostgreSQL35W) on a daily basis. The LLS data in the database is accessed using Open Database Connectivity (ODBC), a Windows interface designed for accessing databases. The name of the database, the IP address of the host server and the port are specified in the ODBC driver setup. In addition, a username and password are requested which are stored with the IP address of the client PC in the PostgreSQL database.

The query is then carried out using DataViewer (Version 1.5.1), an application developed by ALDIS specifically for querying LLS data in the PostgreSQL database. The DataViewer user interface shows the sub-item “Request” for LLS data queries. A time period and the circular area, for which the query shall be performed, are specified. Figure 16 shows the input for a query from 12 August 2022 from 00:00:00 UTC to 23:59:59 UTC.

The circular area queried is defined by the coordinates of a centre and the radius in km. For the analyses in this thesis, a radius of 30 km around the centre of LOWG (latitude: 46.99 °N, longitude: 15.44 °E) was queried. The result of the query from 12 August 2022 is shown in Figure 17. The LLS received from the server show all lightning strikes that were located in the queried time period and circular area. The red number at the bottom left of the image shows that 313 lightning events were found.

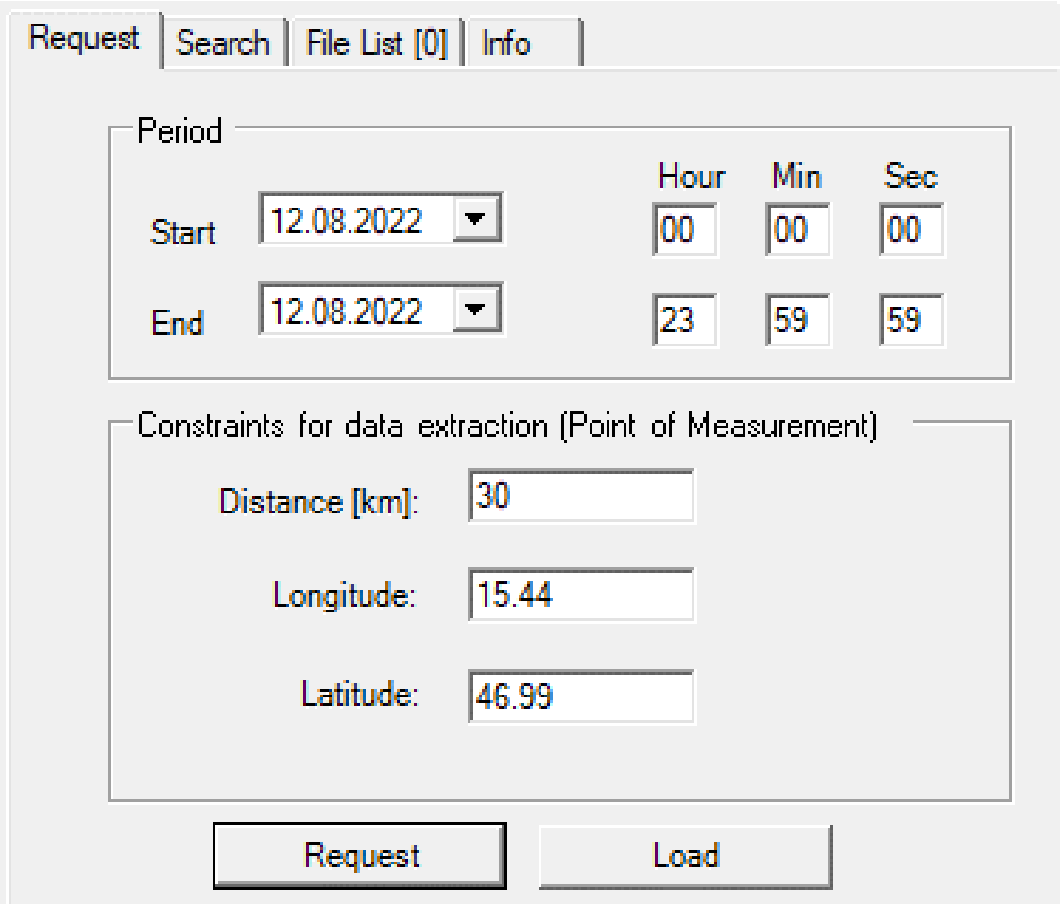

Figure 16: ALDIS DataViewer v1.5.1 user interface for LLS requests, time period for the request exemplary for 12 August 2022 00:00:00 UTC to 23:59:59 UTC, request area with LOWG coordinates and the radius in km.

date	nano	latitude	longitude	amplitude	distance	nbloc	numloc	calcul	nbdf	nbdfit	icloud	maxis	ki2
20220812_111050	133056512	47.0728	15.1386	-5.4	24.6	1	1	114	11	6	1	0.1	1.4
20220812_111258	048015360	47.0698	15.1457	-6.0	24.0	3	1	114	14	10	1	0.1	0.9
20220812_111258	230435328	47.0852	15.1392	2.0	25.1	3	2	114	3	3	1	0.2	0.5
20220812_111258	230896128	47.0376	15.2432	-3.2	15.8	3	3	114	3	2	1	2.2	0.4
20220812_111530	682348544	47.0707	15.1428	-6.1	24.2	4	1	114	15	13	1	0.1	0.6
20220812_111530	896574464	47.0842	15.1390	2.0	25.1	4	2	114	3	3	1	0.3	0.2
20220812_111530	944222720	47.0878	15.1367	2.8	25.4	4	3	114	4	4	1	0.1	0.7
20220812_111530	965056000	47.0765	15.1369	2.3	24.9	4	4	114	4	4	1	0.1	0.5
20220812_121125	584395776	46.7785	15.5709	-3.5	25.5	1	1	114	6	5	1	0.1	0.7
20220812_121631	256328448	46.7879	15.5705	-10.7	24.5	1	1	114	10	9	1	0.1	0.7
20220812_123945	707600896	46.7444	15.4146	119.9	27.4	2	2	114	65	39	0	0.1	1.3
20220812_124047	197043968	46.7705	15.4871	-5.8	24.7	1	1	114	14	8	1	0.2	1.9
20220812_124218	877027840	46.7504	15.4521	-2.3	26.6	1	1	114	4	3	1	0.2	0.3
20220812_124342	856741120	46.7689	15.3951	-2.5	24.8	1	1	114	3	3	1	0.4	1.0
20220812_124410	022599168	46.7660	15.3874	-2.7	25.2	2	2	114	2	2	1	2.0	0.8
20220812_124444	354597376	46.8225	15.4208	-6.6	18.7	1	1	114	8	6	1	0.1	0.7
20220812_124558	370767872	46.7724	15.3785	3.0	24.6	1	1	114	7	3	1	0.4	1.3
20220812_124733	404677120	46.8154	15.4128	-4.5	19.5	3	1	114	7	4	1	0.3	1.0
20220812_124733	405040640	46.8158	15.4195	-4.4	19.4	3	2	114	3	3	1	0.2	0.5

313 Save

Figure 17 Received LLS data for the request with the DataViewer v1.5.1, exemplary for the 12 August 2022.

Table 1 lists and explains the parameters that describe the LLS detection of a lightning strike. The parameters “date”, “amplitude”, “distance” and “icloud” were particularly

important for further analyses. These were used for the comparison with FM data and weather radar data.

Table 1: Descriptions of parameters, provided by the LLS request with DataViewer v1.5.1.

Parameter	Description
date	Date and timestamp in UTC as YYYYMMDD_hhmmss
nano	Nanosecond precision for timestamp
latitude and longitude	Calculated coordinates of each lightning strike
amplitude	Calculated peak current of each lightning strike in kA
distance	Distance between located GSP and selected centre
nbloc	Number of lightning strikes grouped to one Flash
numloc	Numeration of lightning strikes of the respective group
calcul	Status flag
nbdf	Number of sensors which located the lightning strike
nbdfit	Number of sensors used for the calculation
icloud	Classification as IC (1) discharge or CG (0) lightning strike
maxis	Major axis of the error ellipse of the located GSP in km
ki2	Chi-squared test, quality criterion

Other quality parameters such as “nbdf”, “nbdfit”, “maxis” and “ki2” were used to decide if the detection quality of a lightning strike was sufficient for use in the analyses. In practice, the LLS data was queried on an annual basis, i.e. for 2022, 2023 and 2024 for 30 km around LOWG. The query is then saved in DAV-format, a text format. For further evaluation, the LLS data per year was then split into daily files “LLS_LOWG _30km_YYYYYMMDD.dav”.

5.3 Weather Radar System

The weather radar data, provided by Austro Control GmbH, was shared daily on an FTP server using a cron job (a job scheduler on Unix-like operating systems). To save data when storing it on the server and during transmission, the combined archive

format “tar.bz” was used. This compresses the radar data for an entire day (approx. 2.3 GB) to less than 50 MB.

As described in Section 4.3, the folders contain CAPPI images in PGM-format (greyscale images with grey values of 0–255, see Figure 18 and Figure 19 in false colours) with a resolution of 824 × 648 pixels. Since a full volume scan takes five minutes, resulting in 288 scans per day, and each scan consists of 16 vertical layers (0–15 km amsl) for different altitudes, each folder contains 4608 CAPPI images. The image filenames follow the pattern “wxr3d_at4_YYYYMMDDhh mm.00.pgm”, where “wxr3d” refers to the 3D weather radar data, “at4” indicates Austria with data from four radar stations, “YYYYMMDDhhmm” represents the date and time of the scan, and the final two digits denote the layer index (ranging from 00 to 15).

A 2D projection was created from the 16 CAPPI layers for further evaluation. This so-called maximum CAPPI (MaxCAPPI) image projects the maximum reflectivity values at each pixel across the 16 superimposed layers.

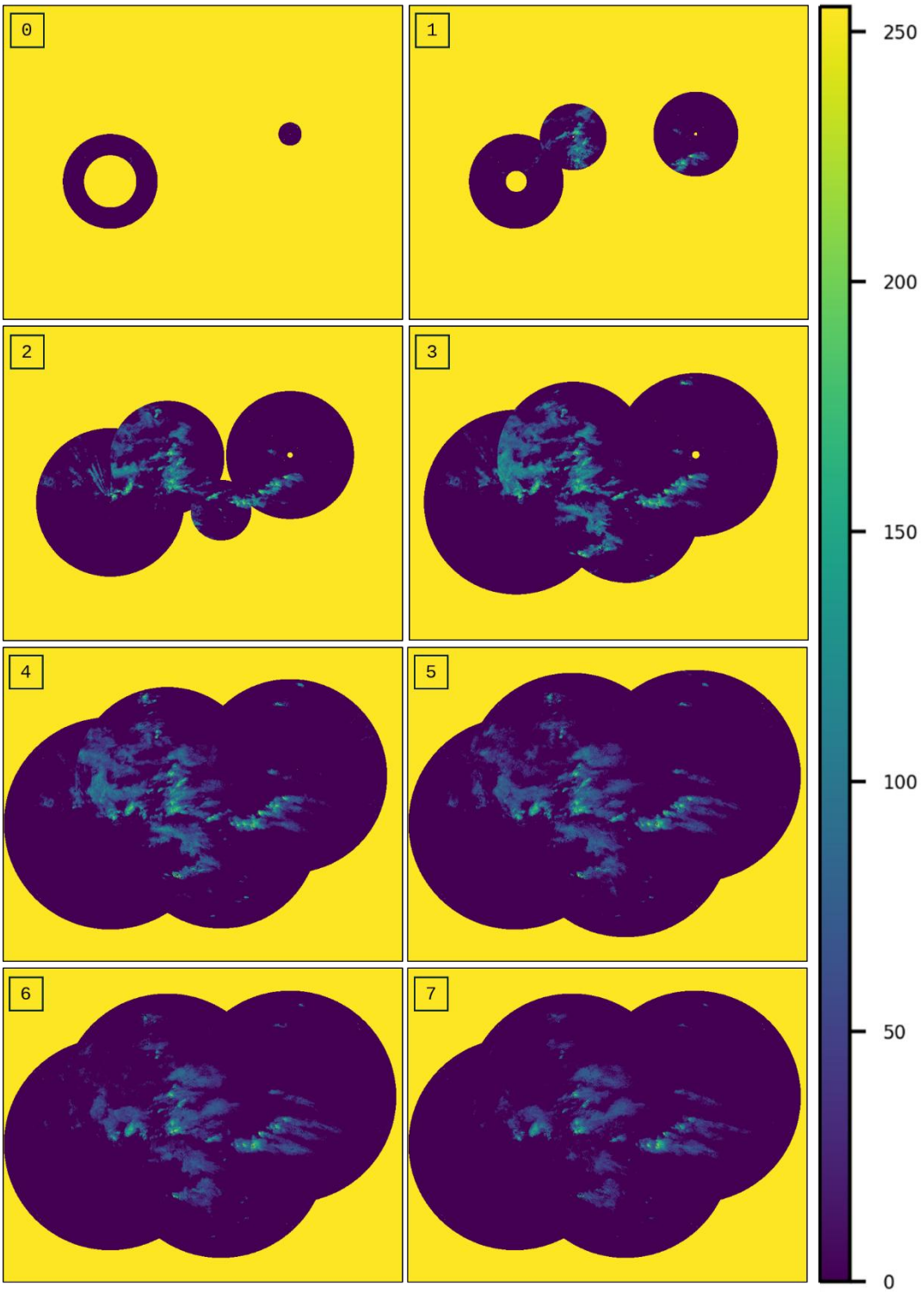

Figure 18: Combined radar images of the four ACG weather radar stations as pgm-files (false colours), CAPPI layer 0 (lowest elevation angle; 0–1 km amsl) to CAPPI layer 7 (7–8 km amsl) for the thunderstorm on 12 August 2022 at 14:40:00 UTC.

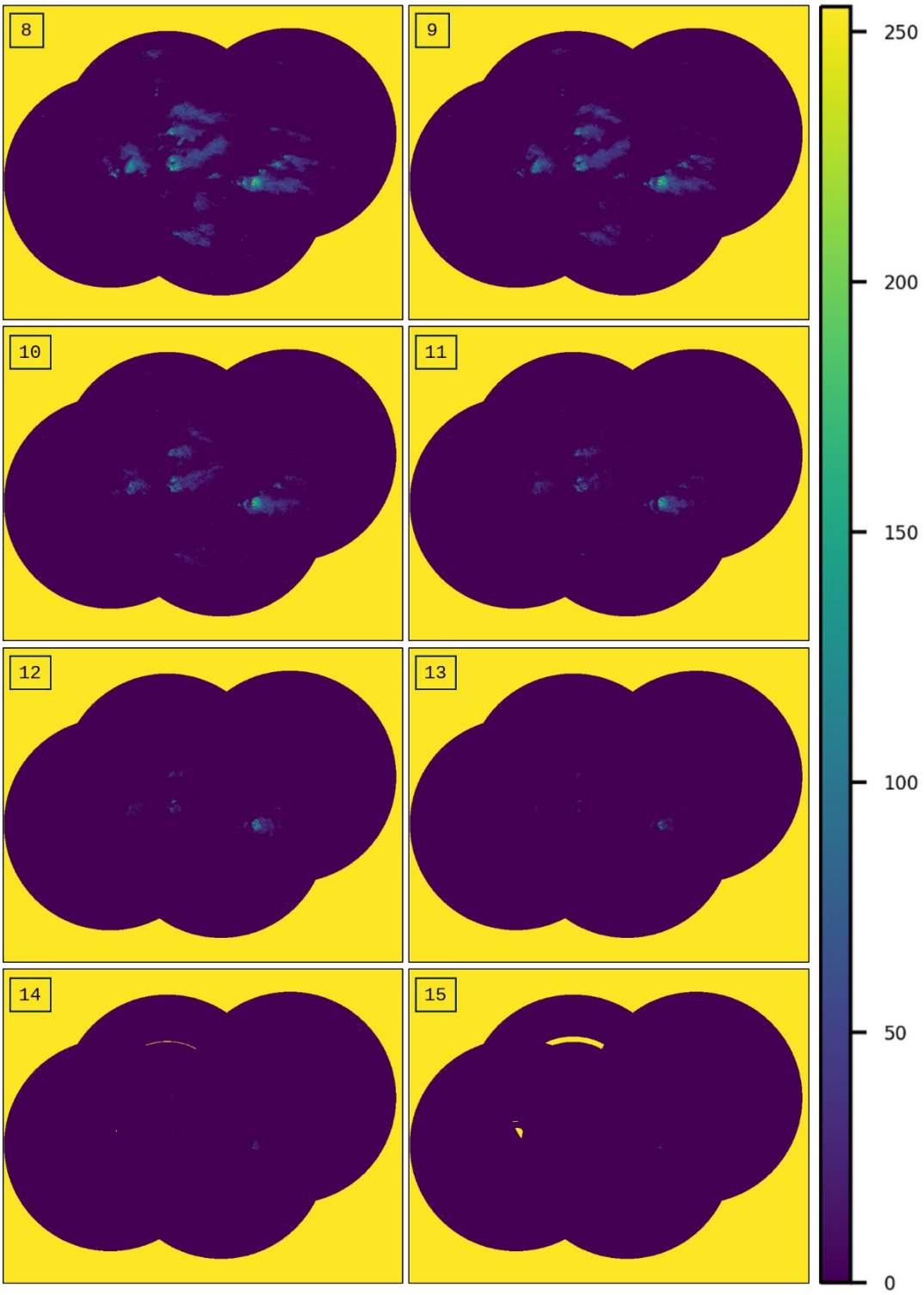

Figure 19: Combined radar images of the four ACG weather radar stations as pgm-files (false colours), CAPPI layer 8 (8–9 km amsl) to CAPPI layer 15 (highest elevation angle; 15–16 km) for the thunderstorm on 12 August 2022 at 14:40:00 UTC.

The process is shown in Figure 20 and Figure 21. For better visibility, the black and white images in PGM-format were displayed in false colours. Black was represented in blue and corresponds to zero reflectivity or a pixel value of zero, and white was represented in yellow and corresponds to the maximum reflectivity or a pixel value of 255. Figure 20, left, shows layer 6 (6–7 km amsl) of the radar image from 12 August 2022, at 14:30 UTC; the large yellow areas have no coverage by the weather radar. Figure 20, right, also shows layer 6, but the areas without coverage have been corrected to zero reflectivity (blue). The reflectivities of a thunderstorm structure for an altitude between 6–7 km amsl can be seen in this radar image.

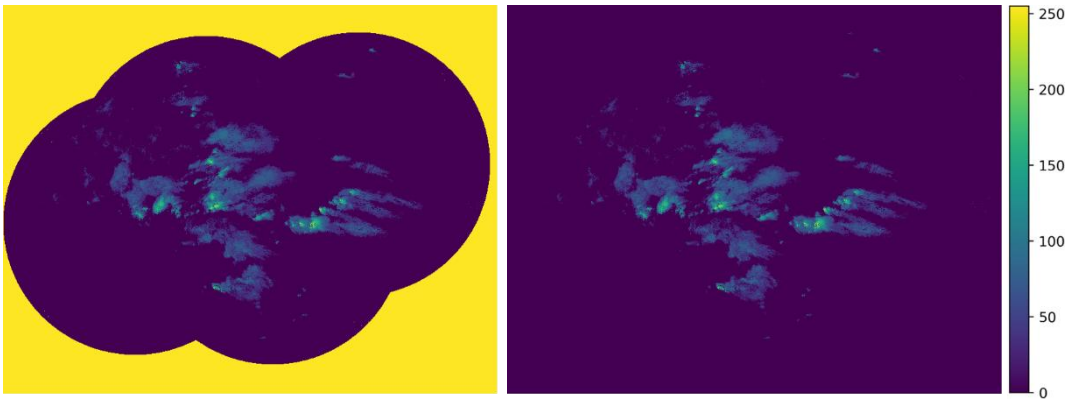

Figure 20: CAPPI Layer 6 (6–7 km) of radar CAPPI image from 12 August 2022 at 14:30 UTC, representation of pgm format with grey values of 0–255 in false colours (black to blue: zero reflectivity, white to yellow: maximum reflectivity), left: original image (raw data), right: blind spots (large yellow areas) corrected to zero reflectivity.

The MaxCAPPI image (Figure 21) was calculated using a matrix operation in a numeric computing software. To do this, the 16 layers of a scan were read in as an $824 \times 648 \times 16$ matrix, after which the maximum value was calculated pixel by pixel across all 16 layers.

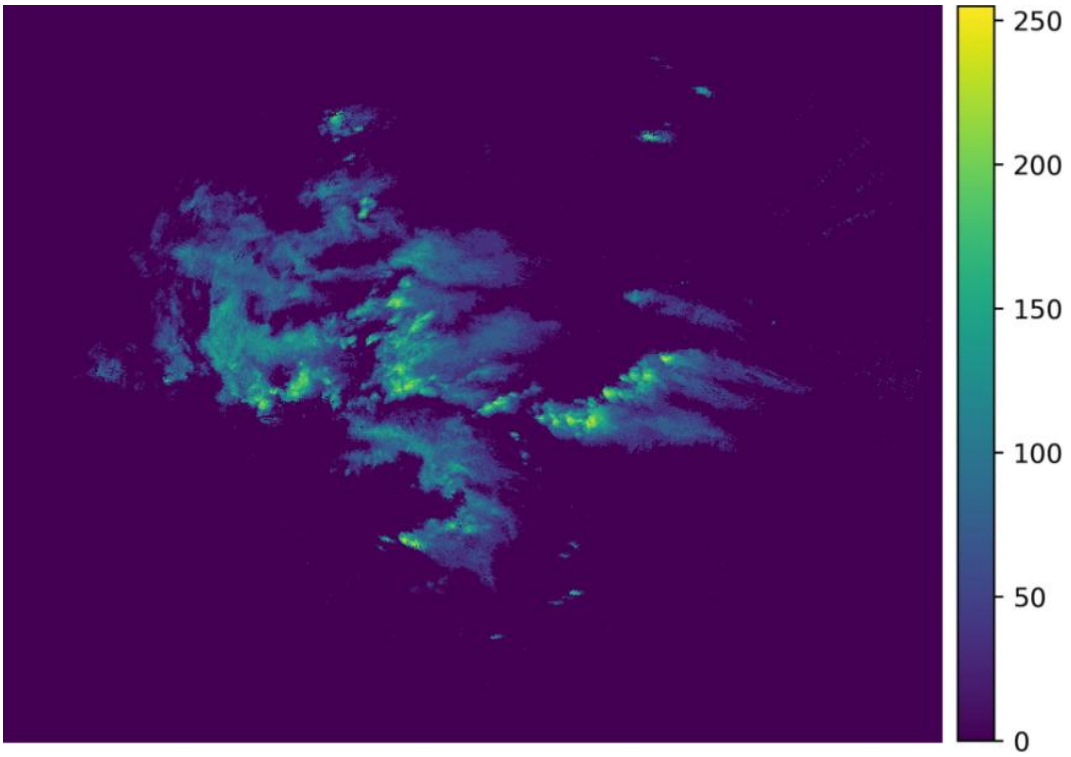

Figure 21: MaxCAPPI radar image from 12 August 2022 at 14:30 UTC in false colours (blue: zero reflectivity, yellow: maximum reflectivity).

Finally, the pixel values are converted into dBZ values. A linear relationship applies here, as shown in Equation (12). The linear conversion function was calculated from conversion factors provided by the ACG. The parameters are $\mathrm{k} = 0.207$ and $\mathrm{d} = 8.908$. For a value range of the PGM-files from zero to 255, this results in a reflectivity range of zero to 61.7 dBZ.

$$\begin{aligned} \mathrm{dBZ} &= \text{pixel values} \cdot \mathrm{k} + \mathrm{d} \text{ for pixel values} > 0 \\ \mathrm{dBZ} &= 0 \text{ for pixel values} = 0 \end{aligned} \tag{12}$$

The result of the conversion, i.e. the representation of the MaxCAPPI in dBZ, can be seen in Figure 22. Blue represents a low reflectivity around 0 dBZ, red corresponds to a high reflectivity around 60 dBZ.

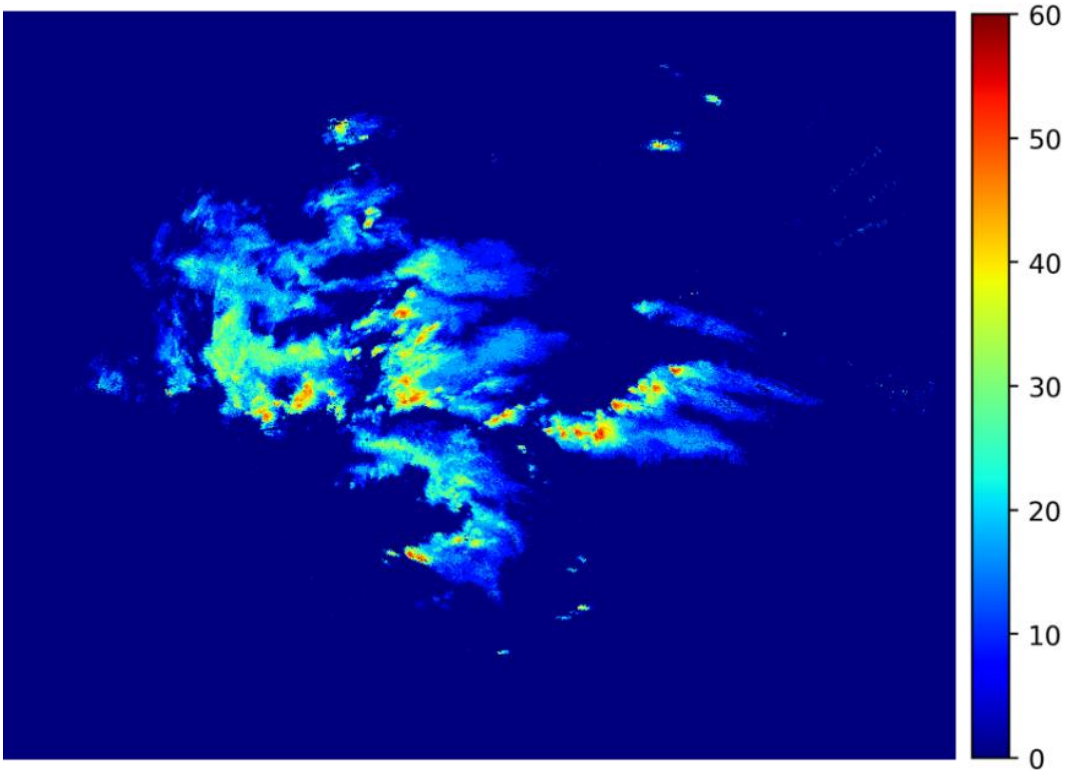

Figure 22: MaxCAPPI Radar image from 12 August 2022 at 14:30 UTC in dBZ values (blue: zero dBZ, red: up to 60 dBZ).

5.4 Selected Thunderstorm Days

The E-field measurements for the present research project began on 05 August 2022 following the installation of the complete FM network. Data were continuously recorded until the network was dismantled on 26 September 2024, except for a few isolated cases of brief power outages at individual location. In addition, ALDIS LLS data and ACG weather radar data were available for this period. Based on the LLS data, 89 days with lightning activity in the Graz Airport area were identified during the measurement period. On 65 of those days, with a total of 79 thunderstorms, the algorithm described in Section 7.2 triggered a shutdown. The evaluations in this thesis are based on these 79 thunderstorms. Two cases occurred outside the defined thunderstorm season (May to September) and are examined in more detail.

For initial analyses, according to (Schatz et al., 2025 [77]), 45 thunderstorms producing CG lightning strikes within 5 km radius around Graz Airport on 44 thunderstorm days are investigated. One of those thunderstorms occurred before the main thunderstorm season in Austria and thus, was excluded when developing alert and shutdown criteria

for lightning prediction (see Section 7.1). This yields 44 thunderstorms on 43 thunderstorm days used for defining universal predictive parameters for lightning onset in E-field, LLS and weather radar data in the surroundings of Graz Airport.

The extended analyses were divided into different observed areas with radii of 5 km, 8 km, 10 km, and 15 km, within which CG lightning strikes were filtered using the LLS data. For an observed area outside the 15 km radius and up to 30 km radius all thunderstorms with CG lightning strikes or IC discharges were considered. In this area of 15–30 km radius, three additional cases without CG lightning strikes are included, in which the algorithm still triggered a shutdown. When these cases are also considered, the area is referred to as “Total Area”. The observed area is limited in any case by an area of 30 km radius for which the LLS data for the analysis was requested. The observed area with a 5 km radius is of key interest and the system and the algorithm were optimised specifically for this area. Thunderstorms with CG lightning strikes outside the 15 km radius or without CG lightning strikes were assumed to have no influence on Graz Airport.

Table 2 shows the analysed thunderstorms for 2022, 2023, 2024 and in total, as well as the thunderstorms with CG lightning strikes in the different observed areas. These are divided into areas with a radius of <5 km, 5–8 km, 8–10 km, and 10–15 km, as well as the 15–30 km radius, which includes cases without CG lightning strikes (“No CG”) but with a shutdown triggered by the algorithm.

Table 2: Analysed thunderstorms, Thunderstorms within the observed area of 5 km, 5–8 km, 8–10 km, 10–15 km, 15–30 km radius, for the years 2022, 2023 and 2024 and in total.

Year	Total Thunder-storms	Thunderstorms within the observed areas				
		<5 km	**5–8 km**	**8–10 km**	**10–15 km**	**15–30 km**
2022*	7	6	1	0	0	0
2023	36	22	10	2	1	1
2024	36	23	7	2	2	2
Total	79	51	18	4	3	3

*The earliest FM recordings started in August 2022, for 2023 and 2024 the full thunderstorm season was recorded.

A buffer zone was defined to investigate borderline cases of lightning strikes occurring in the transitional area between the inner 5 km radius and an extended area up to 8 km radius. A tolerance of ±0.5 km was applied, and 20 out of 79 cases showing CG lightning strikes located within this buffer zone were analysed in detail. This also aimed to account for potential limitations in the location accuracy of the LLS (see Section 4.2).

A total of 14 cases were marked in the results due to poorly located CG lightning strikes with low-quality LLS data, which was defined by a low absolute peak current (<3 kA), a small number of contributing sensors (≤3 sensors), or a large error ellipse (major axis >0.5 km). Some of these cases overlap with the previously defined borderline cases. However, they are not treated or analysed separately.

For 2022, 2023 and 2024, 47 thunderstorms producing CG lightning within a 5 km radius around Graz Airport were recorded on 44 thunderstorm days and classified into four types by ACG meteorologist Dr. Rudolf Kaltenböck. The time reference for each event was the first CG lightning strike. Thunderstorms were categorised as single cell, multicell, supercell, or squall line.

Weather radar data from 2020, 2021, and 2022 were provided by the ACG and used to train, validate and test CNN models. While 2021 and 2022 data served for training and validation, the 2020 data set was reserved for testing prediction accuracy. Around 45,000 radar images per year have been used for training, evaluation, and validation purposes. LLS data were requested for the same time period to combine it with the radar data for CNN training.

6 Data Processing

6.1 Combination of All Datasets

For the prediction of CG lightning strikes within a 5 km radius described in Section 7 and the determination of parameters from which an alert or shutdown at the airport is subsequently derived, all three data sets, FM data, LLS data, and weather radar data, were combined. To compare these data sets, it is essential that all three data sources are referred to the same time axis in the analyses.

The four FMs closest to the airport, FM 1 North, FM 2 South, FM 3 East, and FM 4 West, were used for the analyses and combination with the other data sets. For each of these, the corresponding “CR1000_FMName_Tab1sec_YYYYMMDD.dat” file was read out, using the date as the time and the E-field value. Due to the electromagnetic field emitted by individual IC discharges and CG lightning strikes (see Section 2.4), spikes occur in the FM measurement if the FM’s aperture is open. These E-field spikes, overlap with the actual E-field resulting from the charge accumulation in the thunderstorm (see Figure 23). The effect is also listed under Limitation of the measurement systems in Section 4.4.

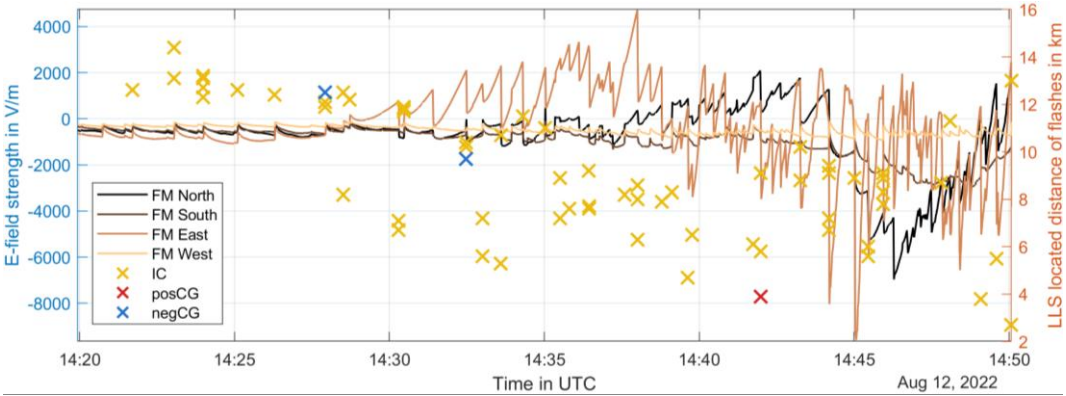

Figure 23: Spikes in the E-field on each FM measurement, caused by CG lightning strikes and IC discharges.

Thus, all E-field measurements are filtered using a moving median with a five-minute time window (see Figure 24). The E-field is inverted to convert it from the “physics sign convention” to the “atmospheric electricity sign convention” based on the

measurement, so that a positive charge leads to a positive deflection and a negative charge leads to a negative deflection in the E-field. Finally, the site-specific correction factors (see Appendix A) are applied.

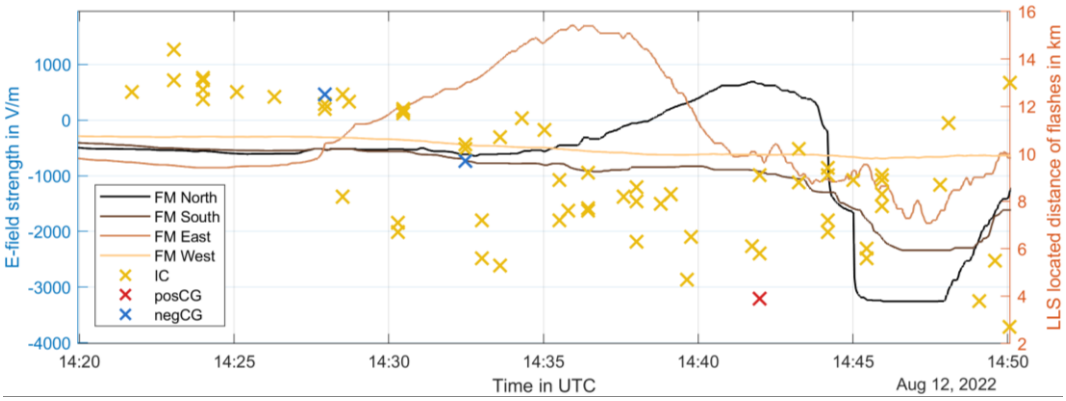

Figure 24: Filtered E-field with a moving median over five minutes of a thunderstorm on 12 August 2022. The E-field crosses zero V/m several times between 14:20 and 14:50 UTC.

The LLS data was divided into three categories for comparison: IC discharge, negative and positive CG lightning strike. These were coloured yellow, blue and red, respectively, for visual differentiation (see Figure 23 and Figure 24). For the presentation and comparison of the data, the LLS data were selected according to distances of less than 15 km to clearly show the interesting areas of the 5 km radius and the 5–8 km radius, but also to partially depict the lightning events outside these areas. The IC discharges are filtered via the “icloud” flag (IC = 1) in the LLS data (see Figure 17), the remaining negative and positive CG lightning strikes are classified by the sign of the amplitude. The LLS data are displayed in the three categories as a distance over the time axis.

From the radar data six variables were calculated, which graphically represent the temporal radar progression within the 5 km radius and the 5–8 km radius. To define these two areas in the MaxCAPPI radar images, they were multiplied by binary masks, whereby the corresponding pixels are retained and all those outside the areas are set to zero. These weather radar variables are as follows (Schatz et al., 2025 [77]):

- Max dBZ 8 km: Maximum reflectivity within the 5–8 km radius in dBZ
- Max dBZ 5 km: Maximum reflectivity within the 5 km radius in dBZ

- 90thpctl dBZ 8 km: 90th percentile of the reflectivity within the 5–8 km radius in dBZ
- 90thpctl dBZ 5 km: 90th percentile of the reflectivity within the 5 km radius in dBZ
- Median dBZ 8 km: Median reflectivity within the 5–8 km radius in dBZ
- Median dBZ 5 km: Median reflectivity within the 5 km radius in dBZ

LLS data was used to select days with thunderstorm activity. All days were selected on which CG lightning strikes were detected within areas with radius of 5 km, 5–8 km, 8–10 km, 10–15 km and 15–30 km. Locations outside 15 km radius were assumed to have no influence on the Graz Airport as described in Section 5.4.

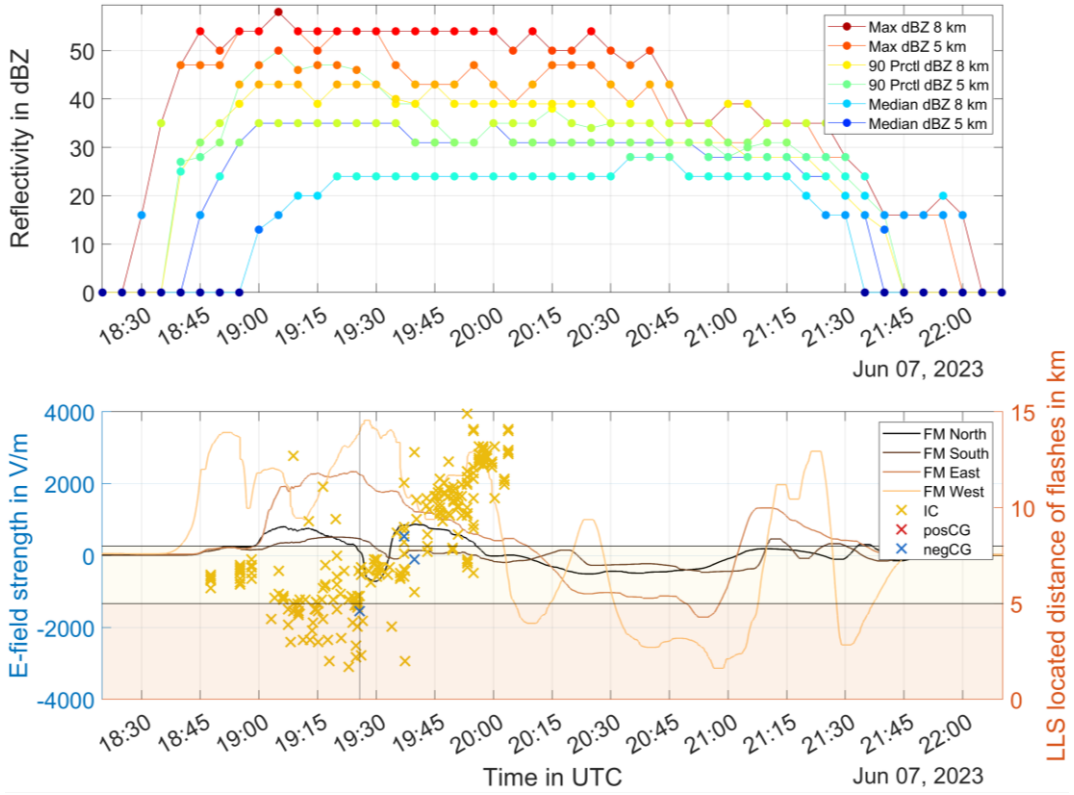

Figure 25: Combined data set of weather radar data (top) and LLS and FM network data (bottom), exemplary for a thunderstorm on 07 June 2023 from 18:15 to 22:15 UTC.

6.2 Classification of Thunderstorm Types

Between 2022 and 2024, 47 thunderstorms on 44 thunderstorm days that produced CG lightning within the 5 km radius around Graz Airport were classified by thunderstorm types. For each thunderstorm, the first lightning strike between cloud and

ground was taken as time reference. The classification into four main types was carried out by ACG meteorologist Dr. Rudolf Kaltenböck. Those thunderstorm types are single cell, multicell, supercell, and squall lines (Markowski and Richardson, 2010 [37]).

Figure 26 shows weather radar images of the four different thunderstorm types for the 12 August 2022, 23 May 2023, 25 August 2023 and 08 August 2024.

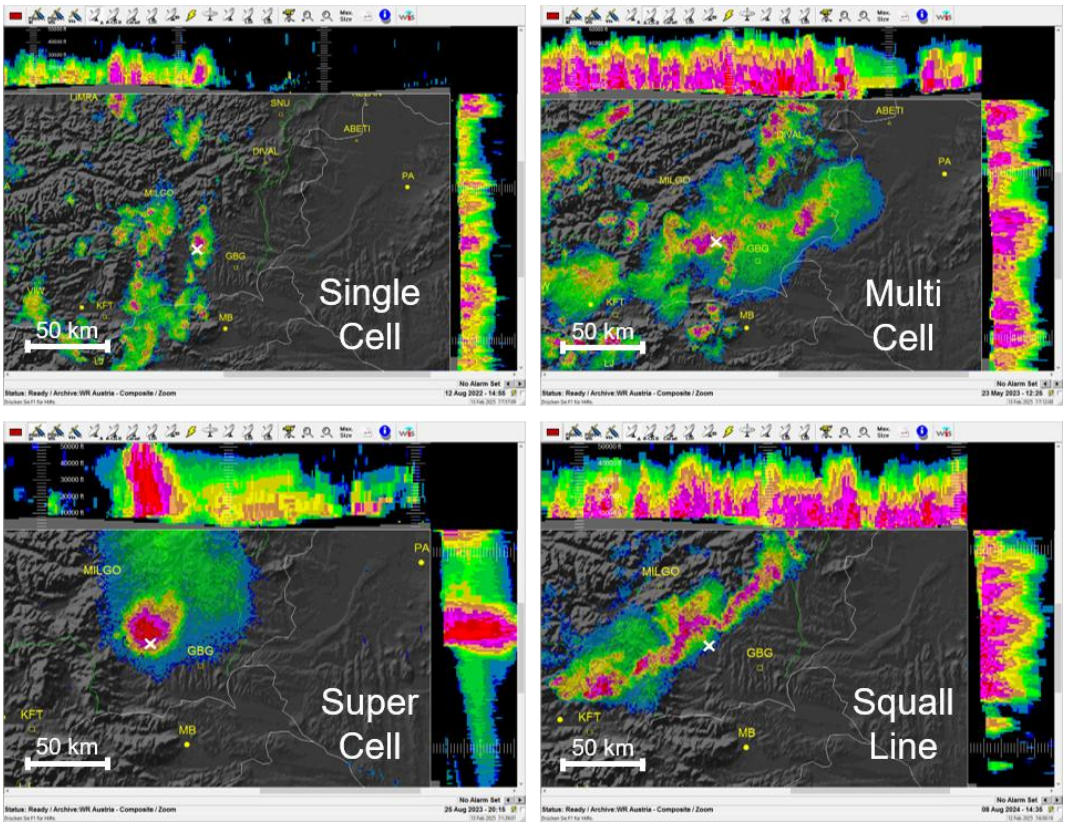

Figure 26: Weather radar images showing the four different thunderstorm types, single cell, multi cell, super cell and squall line for the 12 August 2022, 23 May 2023, 25 August 2023 and 08 August 2024, respectively.

For the classification only 2D MaxCAPPI radar images were evaluated by the expert meteorologist. Additional meteorological data like wind and temperature or soundings were not considered. As described in Section 2.2, single cells can be defined as short-lived, isolated updrafts of the smallest scale, multicells have a longer lifetime described as small clusters in which new cells were triggered along the outflow; supercells are defined by a rotating core and the greatest longevity, squall line thunderstorms are line orientated mesoscale convective systems that are sometimes curved or shaped into line echo wave patterns (Doswell and Markowski, 2004 [97]). The type of thunderstorm

that develops depends, among other factors, on the lapse rate, the lifted condensation level, and the vertical wind shear (Craven and Brooks, 2004 [98]). Hybrid or transitional forms such as single cells that grew into multicell clusters, multicell systems that met the criteria for supercells or mesoscale convective systems, etc., were counted toward the predominant thunderstorm type by the expert. Bright band signatures (transition between snow and rain), bow echo, and other radar features were also used to determine the thunderstorm type but are not presented in the results in Section 8.5.

6.3 Training of Convolutional Neural Networks using Lightning Location System and Weather Radar Data

As a complementary approach to the analyses of the combined dataset, the use of convolutional neural networks (CNN) for the detection of lightning in weather radar images was also explored. Utilising radar data from the ACG, the CNN models aim to detect lightning occurrences based solely on spatial patterns in the radar imagery. This image-based method shall provide an additional perspective within the presented lightning prediction concepts (Schwalt et al., 2024 [58]).

For the classification of images, an image is represented by a three-dimensional matrix (red, green and blue pixels). After the input of the image, it is filtered by a convolution layer, where the convolution extracts certain features in the image like edges, textures, colour-transitions and shapes. The convolution layer is followed by an activation layer, is a nonlinear function that decides which features are used in the next layer. Usually, a rectified linear unit, which outputs the input directly if it is positive or outputs zero if the input is negative. Then there is also a pooling layer that simplifies the output of the convolution layer by nonlinear down sampling. The result is a matrix with a smaller dimension. The resulting matrix is then flattened to a vector. This vector is then connected to the output layer by the fully connected layer, where features of the flattened vector are weighted. The result of the fully connected layer is an output of probabilities for the different classes in percent (Goodfellow et al., 2016 [99]).

The number of convolution, activation and pooling layers differ depending on the used CNN model AlexNet consists of a total of eight trainable layers, five convolutional layers followed by three fully connected layers (Krizhevsky et al., 2017 [100]). In

addition, the DenseNet-121 model was employed, where 121 indicates the model's depth, i.e., the total number of convolutional layers. DenseNet-121 includes five convolutional layers outside of its dense blocks. The dense blocks themselves are composed of 6, 12, 24, and 16 dense layers, respectively, each containing two convolutional layers. A dense block is made up of several convolution blocks, all of which use the same number of output channels. During forward propagation, the input and output of each convolution block are concatenated along the channel dimension, rather than simply passed forward (Huang et al., 2017 [101]). Similarly, the ResNet model also utilises blocks but differs in structure. Each block includes two convolutional layers with batch normalisation, along with a residual connection that adds the input to the output, unlike DenseNet, which links them. This addition operation is enabled by a preceding convolutional layer. Before the first residual block, the input passes through a convolutional layer, batch normalisation, and a max pooling layer. The final part of the model uses average pooling to convert the feature map into a vector, which is then passed through a fully connected layer for output. The variant used in this work was ResNet-18, consisting of 18 convolutional layers (He et al., 2016 [102]). The SqueezeNet model was selected for its efficiency in memory usage, achieved with minimal compromise in prediction accuracy. This is primarily accomplished by replacing most convolutional filters with 1×1 kernels, reducing the number of parameters to be stored to roughly one-ninth of typical CNNs. The core component of SqueezeNet is the fire module, which includes a squeeze layer with 1×1 filters and an expand layer composed of both 1×1 and 3×3 filters. Unlike the other models, SqueezeNet concludes with an average pooling layer (Iandola et al., 2017 [103]). The VGG11-BN model (referred to as VGG), used in this work, comprises eight convolutional and three fully connected layers. The “BN” suffix denotes the use of batch normalisation layers. This model relies exclusively on max pooling layers, and the three fully connected layers are positioned at the end of the network structure (Simonyan et al., 2015 [104]).

All models were implemented using PyTorch (Paszke et al., 2019 [105]) and were either initialised pre-trained weights on the ImageNet[21] dataset, or left untrained for baseline comparison. In the case of pre-training, the convolutional kernels were loaded

[21] https://image-net.org/, accessed on 20.03.2025

from ImageNet-trained models. Depending on the experimental configuration, feature extraction may or may not be applied. Feature extraction (FE) defines which layers are updated during further training on weather radar images. If FE is set to “True”, only the final layer of the CNN is trained, keeping the rest of the network fixed. If FE is set to “False”, the entire model, including all trainable parameters, is updated during training. Consequently, training duration varies based on the number of parameters involved.

As described in Section 5.4, weather radar data for the years 2021 and 2022 were used for the training and validation of five different CNN models. For further processing, a 100 km × 100 km (100 pixel × 100 pixel) section centred around Graz Airport was used. To determine and compare the prediction accuracy, the trained CNN models are tested with radar images from 2020. The distribution between the radar images with and without lightning differs significantly in terms of the proportion of blue pixels (see Figure 27) in the radar image. For an initial attempt all images were sorted and used for training the CNN models. Approximately 5,000 images in the “Flash” class over two years, while there were over 80,000 images in the “No Flash” class during the same period. This is also referred to as the unbalanced data set and the first data set to train the CNN.

Since an unbalanced dataset can bias a CNN toward the majority class, reducing accuracy for the minority class and the overall performance, the distribution of the radar images was examined more closely in a second step. The radar images were divided according to the proportion of blue pixels they contain. This is shown in Figure 27, where in the “No Flash” class, the number of images with 95 to 99.9% blue content makes the majority of the total class.

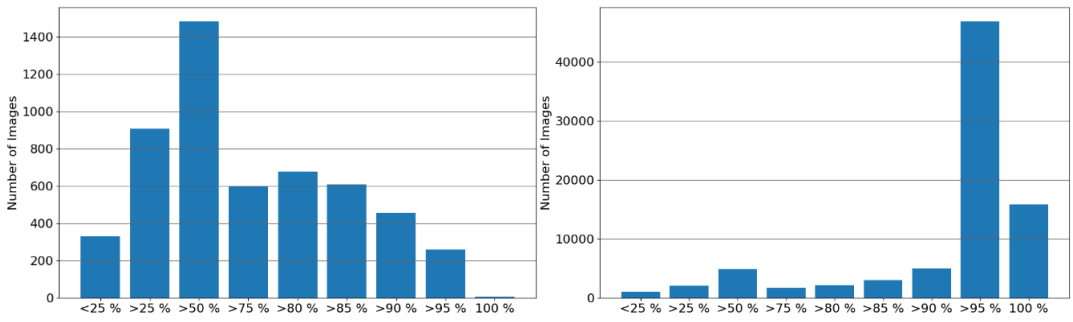

Figure 27: Distribution of images and their proportion of blue pixels in % (no reflectivity) for “Flash” class (left), distribution of images and their proportion of blue pixels in % (no reflectivity) for “No Flash” class (right).

For this reason, only these images were reduced to achieve a better balance between the two classes. This down sampled data set is also referred to as “<95% Blue” in the following and it is the second to train the CNN.

The third dataset was balanced by further down sampling the “No Flash” images based on the distribution of the blue component. This means that there are approximately the same number of images in both classes (approximately 4,500 for training and approximately 1,100 for validation). This dataset is labelled “balanced” and it is the third data set to train the CNN. The “balanced” dataset with the blue background pixels converted to white pixels were used as the fourth and final dataset for training. This fourth data set is not presented in the results of this thesis.

7 Methodology

7.1 Alert and Shutdown Parameters

For the present algorithm, twelve predictive parameters for lightning onset are defined and described in this section. These parameters were developed from E-field, LLS, and weather radar data. Nine parameters, originally developed using data from 2022 and 2023, were reassessed using data from 2024. One E-field and two weather radar parameters were added. To identify thunderstorm days which include at least one CG lightning strike within the 5 km radius around Graz Airport, the LLS data from the thunderstorm seasons of 2022, 2023, and 2024 were filtered accordingly. A pre-season thunderstorm was excluded (see Section 5.4). This refines existing parameters and extends the findings of Schatz et al., 2023 [45] and 2024 [76] by three additional parameters.

To enable comparisons and cross-calculations between the FM, LLS and weather-radar data, the datasets were aligned with respect to array length and time axis, as explained in Section 6.1. To develop an initial approach for lightning-warning criteria, specific parameters were derived from these datasets, as listed subsequently. Due to the algorithm used to sort the data and distinguish thunderstorms, the observation period before the first CG lightning strike within the 5 km radius was limited to 90 minutes, referred to as 90-minute limit. For the extended analyses and results presented from Section 8.2.2 to Section 8.5, this 90-minute limit was removed as it is not possible to define an onset time for thunderstorm during continuous monitoring of the data. The examined parameters, based on Schatz et al., 2025 [77], describe the time that elapses between the fulfilment of the following criteria and the occurrence of the first CG lightning strike within the 5 km radius:

E-field parameters

- Zero crossing E-field: The first E-field of one of the FMs crossing zero V/m, considering all four FMs. A zero-crossing in the E-field can only occur in the vicinity of a charged cloud.
- |E-field| >1 kV/m: The first absolute value of the E-field exceeds the threshold of 1 kV/m, considering all four FMs.

- ∑|E-field| >2 kV/m: The sum of the absolute E-field values of all four FMs exceeds a threshold of 2 kV/m.
- |E-field| >2 kV/m: The first absolute value of the E-field exceeds the threshold of 2 kV/m, considering all four FMs.

The “Zero crossing E-field” parameter (see Figure 24) is based on observations in all analysed thunderstorms with a CG lightning strike in 5 km radius and provides a LT for all cases (see Figure 37 and Appendix B). Such characteristics were also described as M-shape (W-shape) of the E-field of a passing thunderstorm by Schatz et al, 2023 [45].

LLS Parameters

- IC in 5 km: The first IC discharge of the thunderstorm that occurs within the 5 km radius (IC discharges usually occur before a CG discharge).
- IC/CG in 8 km: The first occurrence of an IC discharge or CG lightning strike within the 5–8 km radius. A CG lightning strike in this area is not yet so critical for the airport and can therefore be used as an additional (forecasting) warning parameter.

Weather radar parameters

- ∑(Max dBZ) >78 dBZ: The maximum reflectivity value in dBZ is evaluated within the 5 km radius and within the 5–8 km radius, resulting in two values for different areas. The sum of these two values must exceed a threshold of 78 dBZ. By using the two separate areas, the size of the thunderstorm is also considered in this parameter.
- ∑(90thpctl) >63 dBZ: The Sum of 90th percentile (pctl) of the reflectivity value dBZ within the 5 km radius and within the 5–8 km radius is evaluated and must exceed a threshold of 63 dBZ (see “∑(Max dBZ) > 78 dBZ”).
- Max dBZ 5km>50 dBZ: The maximum reflectivity value in dBZ within the 5 km radius exceeds 50 dBZ.
- 90thpctl 5km >40 dBZ: The 90th percentile of the reflectivity value in dBZ within the 5 km radius exceeds 40 dBZ.
- 90thpctl >25 dBZ: The 90th percentile of the reflectivity value exceeds 25 dBZ for either the 5 km radius or the 5–8 km radius.
- Median >20 dBZ: The median reflectivity value exceeds 20 dBZ for either the 5 km radius or the 8 km radius.

To determine the optimal radar reflectivity threshold for the parameters "∑(Max dBZ) >78 dBZ" and "∑(90thpctl) >63 dBZ" across all thunderstorms, the sum of Max dBZ or 90thpctl reflectivity values was calculated at every time step, separately for the 5 km radius and the 5–8 km radius. For each of the investigated thunderstorms, appeared in the 5 km radius and showing at least one CG lightning strike in the area, the highest sum value was identified. From these maximum values, the lowest one was chosen as the threshold, to also detect thunderstorms showing weather radar images in the lower reflectivity range. Selecting a higher threshold would risk overlooking thunderstorms with lower maximum sum values. To address this, the alert and shutdown initiation criteria were developed based on combinations of multiple parameters. Relying on a single parameter, for instance, one that is triggered long before the first CG lightning strike in the observed area, can lead to non-EAs. To enhance reliability, E-field, LLS, and weather radar parameters are combined using logical operators within the alert and shutdown algorithm. This algorithm is described in detail in the Sections 7.2 and 7.3.

7.2 Alert and Shutdown Initiation Criteria

7.2.1 Alert Criterion

As already mentioned in Section 7.1, a single parameter may be fulfilled long before CG lightning strikes occur, but also in cases where no lightning strikes occur at all. Therefore, the alert and shutdown algorithm has been designed so that various parameters must be fulfilled in combination before an alert or shutdown criterion is triggered.

As described in Section 3.3, an alert should be triggered before a shutdown occurs so that precautions can be taken, and the duration of the shutdown is as long as needed and as short as possible. Figure 28 illustrates the alert criterion sequence. Parameters were selected to trigger the alert that result in a median LT before the first CG lightning strike within 5 km radius of between 30 minutes and 40 minutes. These include the E-field parameters "|E-field| >1 kV/m" and "∑|E-field| >2 kV/m" and the weather radar parameters "90thpctl >25 dBZ" and "Median >20 dBZ" in a 5 km or 8 km radius. To trigger an alert, one of the two weather radar parameters must be met in a first condition (Figure 28, top) (logical OR) and the amount of the E-field must exceed a

threshold of 1 kV/m and the sum of the amounts of all E-fields must exceed 2 kV/m (logical AND). There is also a second condition that triggers the alert independently, i.e., it is linked to the first alert condition with OR. The second condition (Figure 28, bottom) immediately triggers an alert when a CG lightning strike is detected within the 5–8 km radius. Since the first condition is not met, E-field values and weather radar reflectivity indicate low values, a single CG lightning strike in the 5–8 km radius does not trigger a shutdown despite its proximity.

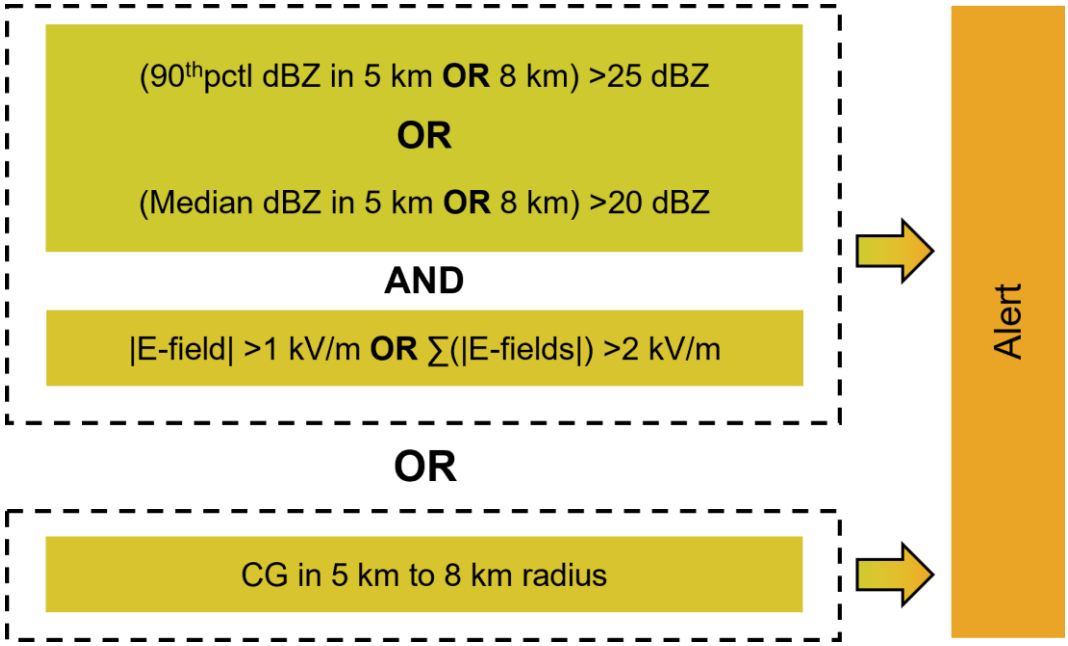

Figure 28: Alert criterion combining different predictive parameters for CG lightning strikes.

7.2.2 Shutdown Criteria

To initiate shutdowns with an algorithm, five different Shutdown Initiation Criteria (SIC) were used for the initial analyses shown in Section 8.2.1 combined with the 90-minute limit. For the extended analyses from Section 8.2.2 onwards, the fifth Shutdown Initiation Criterion (SIC5) and the 90-minute limit were removed. The conditions and parameters (e.g., threshold values for E-field, LLS and weather radar) are based on empirical values, statements by ACG meteorologists, as well as information from the literature.

The first Shutdown Initiation Criterion (SIC1) is shown in Figure 29. It is based on the observation that the forecast parameter “IC in 5 km” provides a median LT of less than

10 minutes, which would be in the optimal range (see Section 3.1) of shutdown LTs. Therefore, an attempt was made to use this parameter as an override criterion (i.e., an IC discharge in 5 km radius always leads to a shutdown). However, it has been shown that some cases would result in long LTs (see outliers in box plot, Figure 37), and removing the 90-minute limit further worsens this approach. Therefore, the weather radar conditions were added, whereby the maximum reflectivity exceeds a threshold value of 28 dBZ in the 5 km radius or in the 5–8 km radius (not shown in the box plot, see Figure 37) and the E-field conditions "|E-field| >1 kV/m" or "∑|E-field| >2 kV/m" were linked with "IC in 5 km" using logical AND. If all these conditions are met, the SIC1 triggers a shutdown.

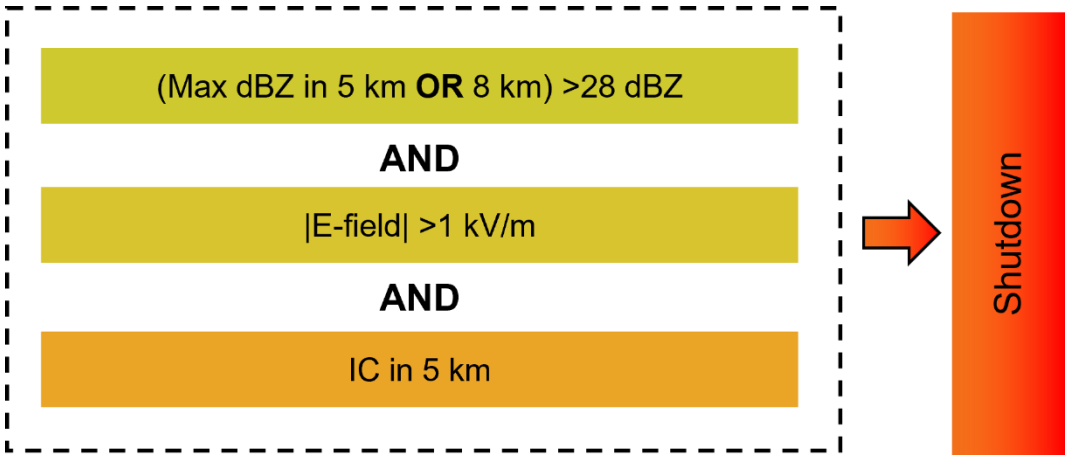

Figure 29: First shutdown initiation criterion combining different predictive parameters for CG lightning strikes.

The second Shutdown Initiation Criterion (SIC2) is shown in Figure 30. For the SIC2, the first indicator used is the LLS detection of an IC discharge or CG lightning strike in the 5–8 km radius, i.e., fulfilment of the parameter "IC/CG in 8 km." If there is an IC discharge or CG lightning strike in the corresponding area, a counter is set for 5 minutes. If the criteria "∑(Max dBZ) >78 dBZ", "∑(90^{th}pctl) >63 dBZ", "|E-field| >1 kV/m" and "Zero crossing E-field" are met within 5 minutes (linked with logical AND, Figure 30, top centre), the SIC2 triggers a shutdown. If more than 5 minutes elapse after "IC/CG in 8 km" is fulfilled (Figure 30, bottom centre), no shutdown is triggered despite the other parameters being fulfilled. If "IC/CG in 8 km" is fulfilled again within the 5-minute counter, the counter is reset and starts from the beginning.

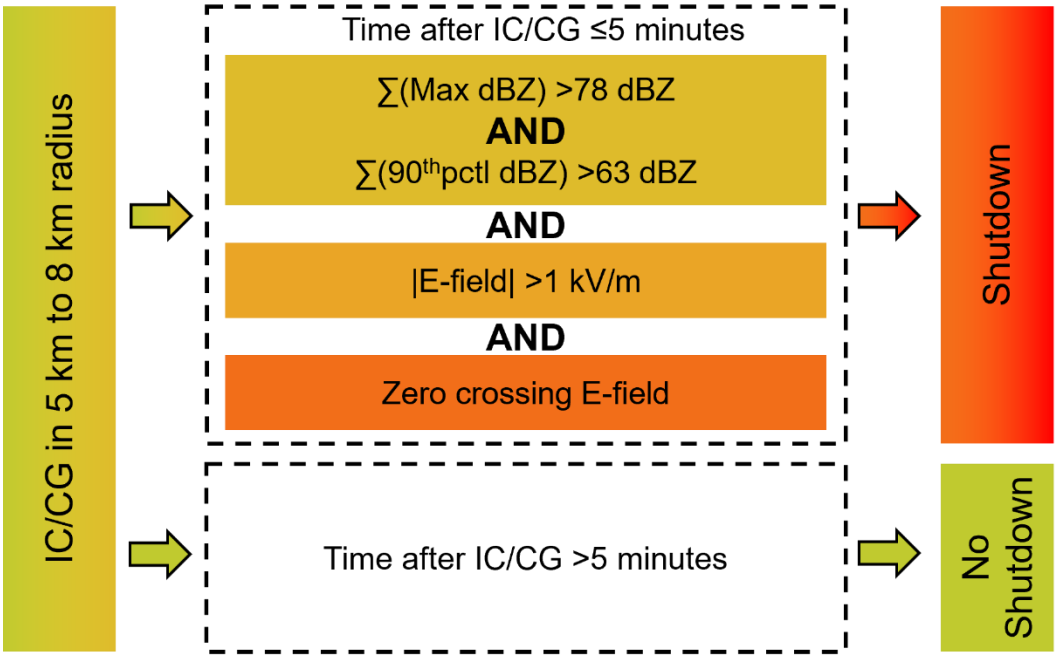

Figure 30: Second shutdown initiation criterion combining different predictive parameters for CG lightning strikes.

The third Shutdown Initiation Criterion (SIC3) is shown in Figure 31. For the SIC3, the first indicator used is a zero crossing in the E-field at one of the four FMs, i.e., fulfilment of the parameter "Zero crossing E-field." If there is a zero crossing in the E-field, a counter is set for 5 minutes. If the parameters "∑(Max dBZ) >78 dBZ", "∑(90thpctl) >63 dBZ", "|E-field| >1 kV/m" and " IC/CG in 8 km" are met within the 5 minutes (linked with logical AND, Figure 20, top centre), the SIC3 triggers a shutdown. If more than 5 minutes elapse after the "Zero crossing E-field" parameter is met (Figure 31, bottom centre), no shutdown is triggered despite the other parameters being met. If the "Zero crossing E-field" parameter is met again within the 5-minute counter, the counter is reset and starts from the beginning.

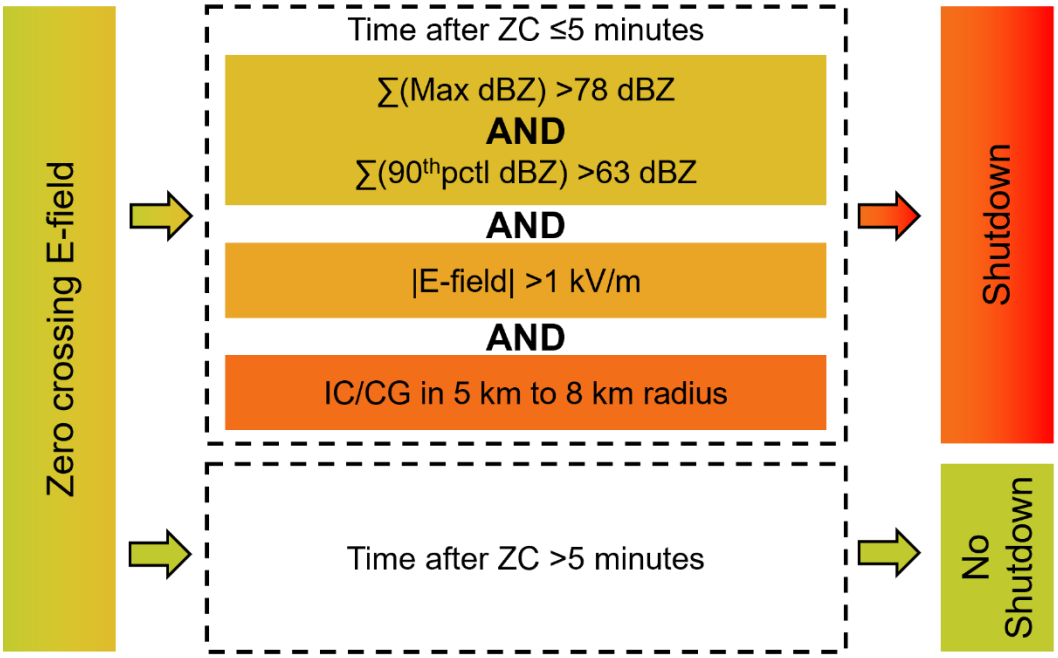

Figure 31: Third shutdown initiation criterion combining different predictive parameters for CG lightning strikes.

The fourth Shutdown Initiation Criterion (SIC4) takes into account cases in which the first IC discharge or CG lightning strike in the 5–8 km radius occurs immediately before the first CG lightning strike within the 5 km radius. The shutdown criteria SIC1, SIC2 and SIC3 would provide very short shutdown LTs here. The SIC4 is shown in Figure 32. The weather radar parameters are limited here to the 5 km radius. The parameters "Max dBZ 5km >50 dBZ" and "90thpctl 5km >40 dBZ" must therefore be fulfilled, in combination with the condition that the median reflectivity in the 5 km radius exceeds a threshold value of 28 dBZ (also used in SIC1). The threshold value of the E-field parameter has been doubled; the parameter is "|E-field| >2 kV/m". These four parameters are linked with logical AND, i.e. they must occur simultaneously to trigger a shutdown.

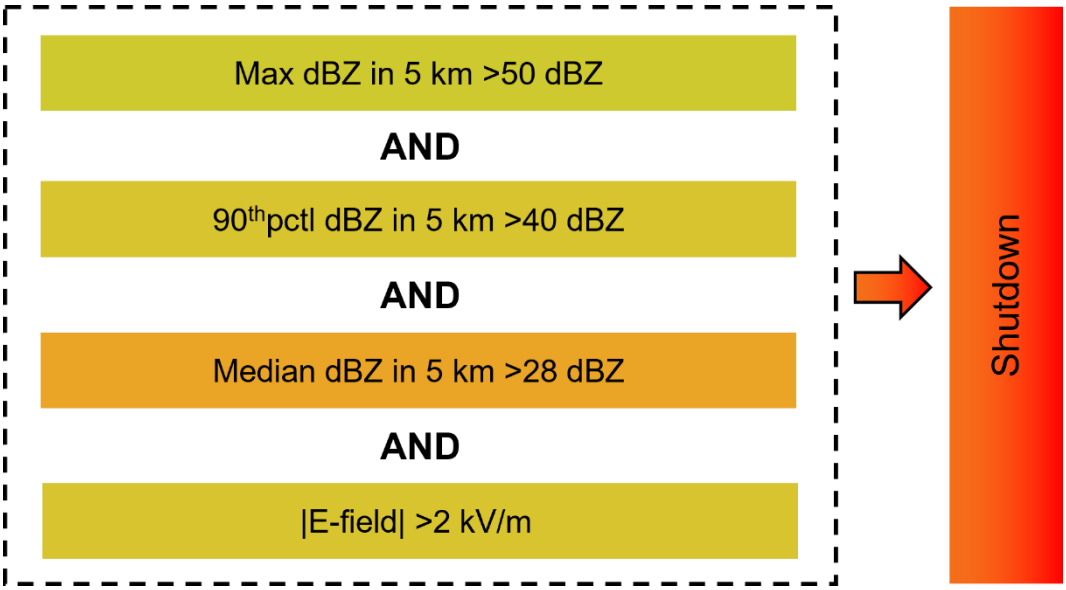

Figure 32: Fourth shutdown initiation criterion combining different predictive parameters for CG lightning strikes.

The fifth shutdown initiation criterion (visualised in Figure 33) is intended for thunderstorms that show only low radar reflectivity in the observed 5 km (maximum reflectivity in 5 km radius around 30 dBZ). The first indicator is “IC/CG in 8 km” which, in combination with the parameter “|E-field| >1 kV/m”, leads to the start of a 5-minute counter. If “IC/CG in 8 km” is fulfilled within this time, another 10-minute counter is triggered. If there is a zero crossing in the E-field within these 10 minutes, a final 5-minute counter starts. Within the last counter, the maximum reflectivity, the 90th percentile of the reflectivity and the median reflectivity in 5 km in the weather radar must exceed 30, 25 and 20 dBZ, respectively. If all parameters are fulfilled in the corresponding time, the SIC5 is triggered. This criterion was only used for the results of initial analyses shown in Section 8.2.1, but was discarded for an extended analyses as it leads to a high number of non-EAs.

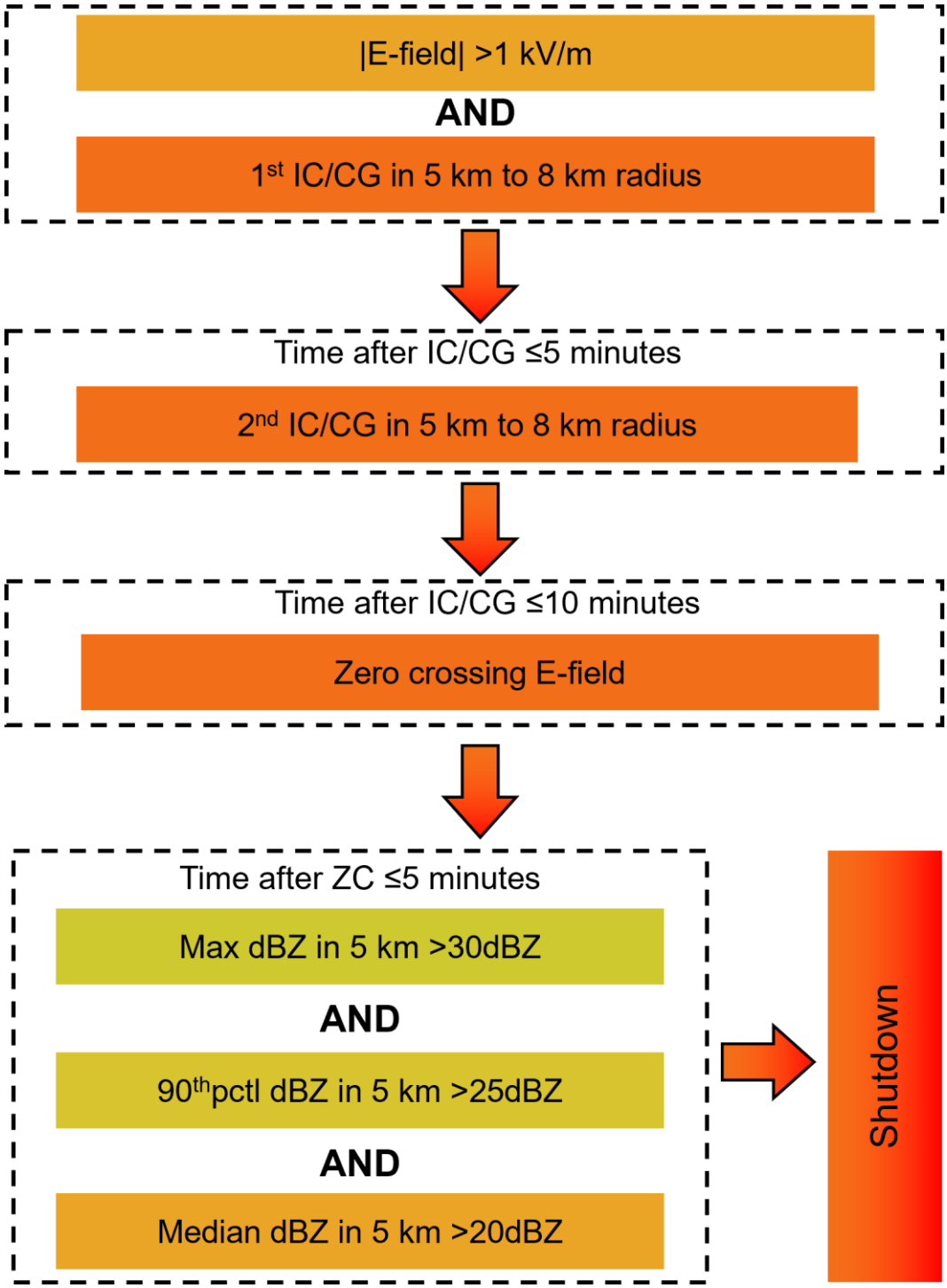

Figure 33: Fifth shutdown initiation criterion combining different predictive parameters for CG lightning strikes.

After the removal of the initially set 90-minute limit (originally defined to distinguish thunderstorms, see Section 7.1), an additional criterion was introduced. For this criterion there must be at least two ICs in the 5 km radius or in the 5–8 km radius for a shutdown to be triggered, this additional criterion does not change the shutdown LTs for the thunderstorms with CGs in the 5 km radius, but leads to a lower number of non-

EA alerts when the observed area is extended. Extending the areas under investigation serves the performance analysis of the algorithm and the four shutdown criteria.

Besides the thunderstorm days that bring CG lightning strikes within the 5 km radius, the observed area was extended to the areas of the 5–8 km radius, 8–10 km and 10–15 km radius, as well as the 15–30 km radius the final analysis. Thunderstorm days that do not produce CG lightning strikes within 30 km but do produce IC discharges were also considered (see Section 5.1).

7.3 Alert and Shutdown Termination Criteria

7.3.1 Shutdown Termination Criterion 1

The first approach for the selection of a Shutdown Termination Criterion (STC) to clear a shutdown is based on the measures of the standard for TWS in Austria (OVE, 2022 [5]). The standard specifies a TTC of 30 minutes after the last CG lightning strike in an observed area of 10 km radius around a TA. This interval of 30 minutes was adopted for the Shutdown Termination Criterion 1 (STC1) and adapted to the conditions of the present investigations. The observed area was reduced from 10 km radius to a 5 km radius, in accordance with the defined shutdown zone (see Sections 3.1 and 5.4). The last lightning can either be an IC discharge or a CG lightning strike. The interval of 30 minutes represents the minimum here, as there are also cases in which the shutdown criteria are still fulfilled, i.e., weather radar shows high reflectivities, FM network shows high E-field values and frequent zero crossings. In these cases, fulfilled criteria indicate that CG lightning strikes could appear at any time within the 5 km radius.

The STC1 is shown graphically in Figure 34. At least 30 minutes must elapse after the last IC discharge or CG lightning strike in a 5 km radius, after which it is verified if the reflectivity values of all weather radar variables fall monotonically or whether the radar variables “Max dBZ”, “90pctl dBZ” and “Median dBZ” in the 5 km radius or the 5–8 km radius fall below the thresholds 30 dBZ, 25 dBZ and 20 dBZ, respectively. For the E-field, it is verified whether the magnitude of the E-field has fallen below 1 kV/m for all FMs or whether there has been no zero crossing (if these termination parameters are fulfilled in combination, a shutdown is terminated, see Figure 34). Each shutdown is

terminated 60 minutes after the last IC discharge or CG lightning strike within 5 km, even if the previously mentioned parameters are still met.

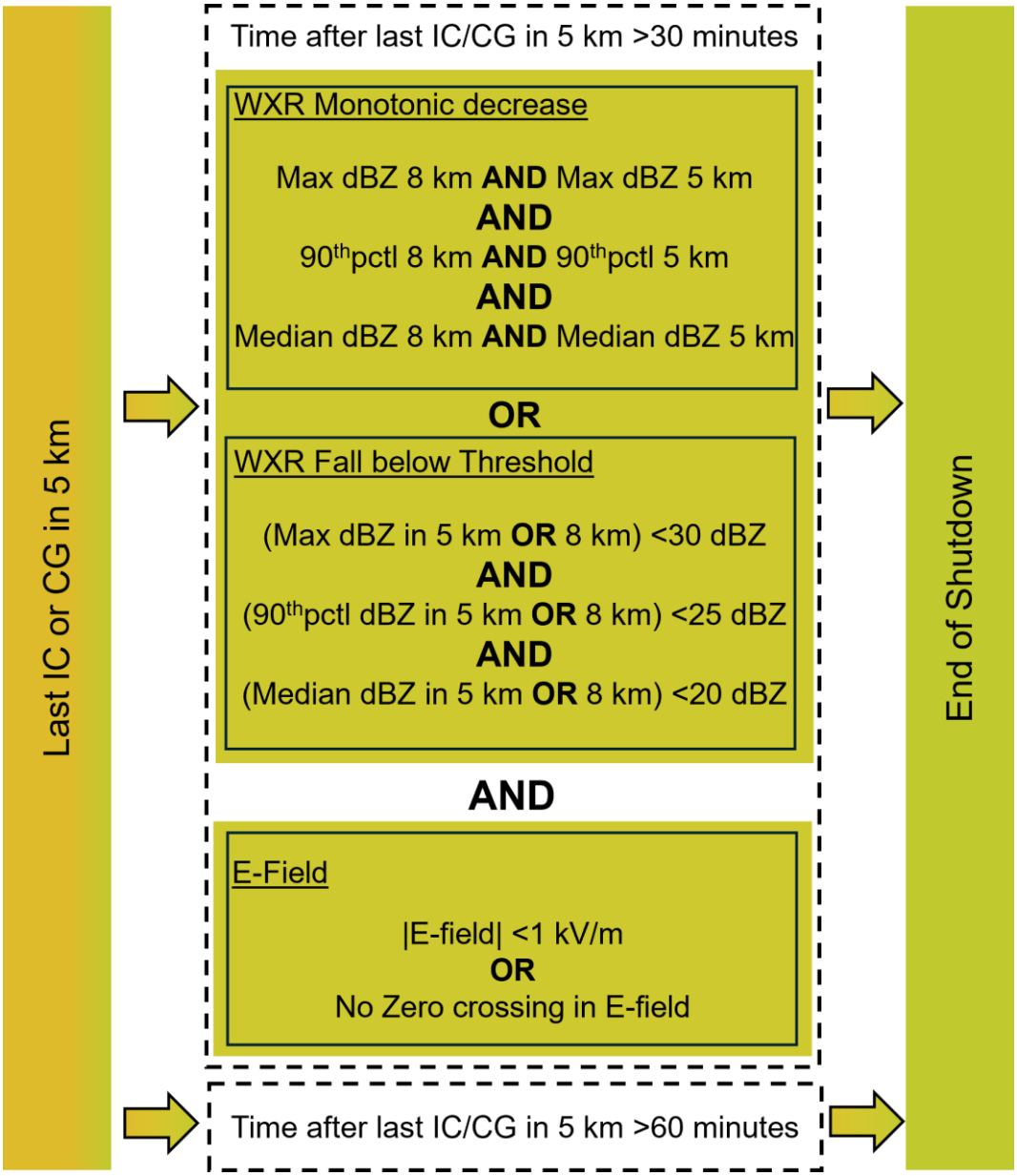

Figure 34: Shutdown termination criterion 1, termination of shutdown after 30 to 60 minutes.

7.3.2 Shutdown Termination Criterion 2

In addition to the first approach for shutdown termination in Section 7.3.1, a second approach was selected in which the focus is on resolving a shutdown as quickly as possible. This Shutdown Termination Criterion 2 (STC2) is shown in Figure 35. In this approach, a counter is set to 10 minutes after the last IC discharge or CG lightning

strike within the 5 km radius. If there is no further IC discharge or CG lightning strike within 10 minutes, the shutdown is terminated.

To prevent the algorithm from running indefinitely in cases where no IC discharges or CG lightning strikes occur within 5 km after a shutdown is triggered, an additional condition was introduced. If the last IC discharge or CG lightning strike is located within the 5–8 km radius (no further IC discharges or CG lightning strikes within 8 km radius), the shutdown is also terminated after 10 minutes. This ensures that there is a condition which will eventually resolve the shutdown.

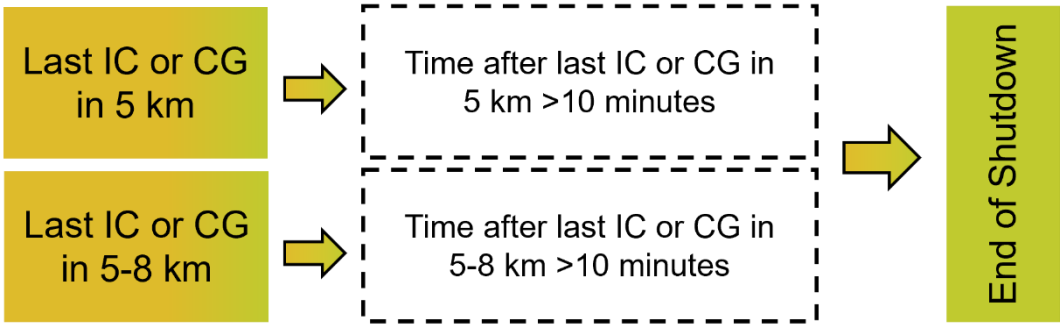

Figure 35: Shutdown termination criterion 2, termination of shutdown after 10 minutes.

7.3.3 End of Alert

The alert criterion has to be negated for the termination of an alert. This means that an alert is resolved once the alert criterion is no longer fulfilled. The criterion for resolving the alert is shown in Figure 36. An alert is ended, if the radar variables "90thpctl dBZ" and "Median dBZ" in 5 km radius and the 5–8 km radius fall below a threshold of 25 dBZ or 20 dBZ, respectively, or the magnitude of the E-field decreases and the parameters "|E-field| >1 kV/m" and "∑|E-field| >2 kV/m" are no longer fulfilled. Additionally, there must be no further CG lightning strikes within the 5–8 km radius, which is already accounted for by STC1 and STC2. In addition, it has been specified that the alert criterion according to Section 7.2.1, Figure 28 must not be met again within 10 minutes in order for an alert to actually be cleared. If the criterion for ending an alert is fulfilled but the shutdown remains active, because the TTC of STC1 is at least 30 minutes, the alert will not be resolved until the shutdown is cleared.

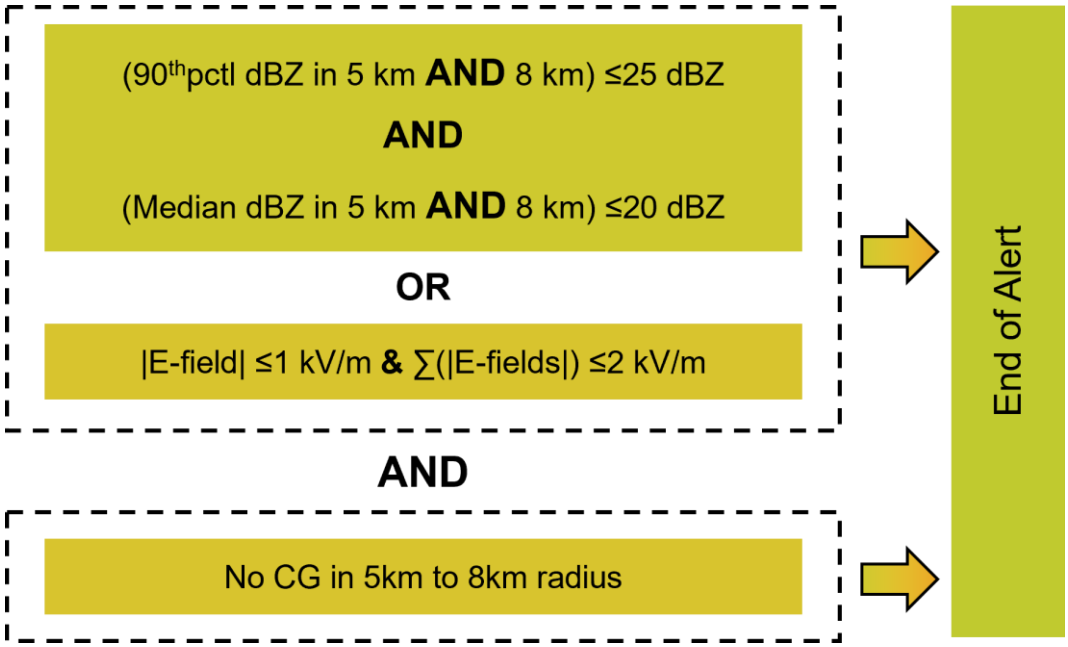

Figure 36: Criterion for ending an alert

8 Results

8.1 Lead Times of Alert and Shutdown Parameters

The median LTs observed in this work range from 8.4 minutes to 64.9 minutes for the parameters described in Section 7.1. Analysed data include 44 thunderstorms showing CG lightning strikes within the 5 km radius. Box plots with median, the 25th and 75th percentiles as well as the minimum and maximum LTs in minutes for all described parameters are depicted in Figure 37. The upper bound represents the initially used 90-minute limit (see Section 7.1).

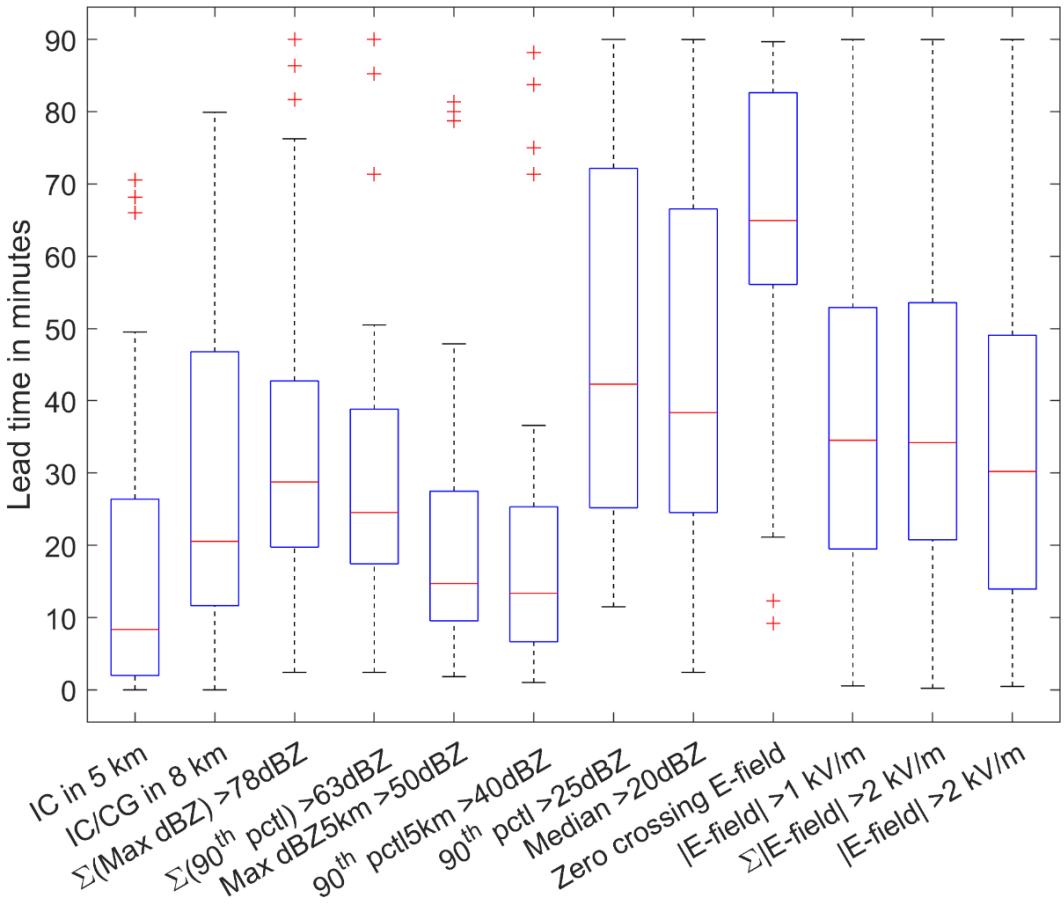

Figure 37: Predictive alert and shutdown parameters for CG lightning strikes within a 5km radius around LOWG, box plots showing the elapsed time (y-axis) between the fulfilment of various parameters (x-axis) – derived from LLS, weather radar, and FM data – and the first CG lightning strike within a 5 km radius, the red line indicates the median, the upper and lower box boundaries represent the 75th and 25th percentiles, the whiskers denote the minimum and maximum values, and the red crosses indicate outliers (Schatz et al., 2025 [77]), adapted.

The shortest median LT is provided by “IC in 5km” at 8.4 minutes. Slightly longer times are observed for “90thpctl 5 km >40 dBZ” (13.4 minutes) and “Max dBZ >50 dBZ” (14.7 minutes), followed by “IC/CG in 8 km” at 20.5 minutes.

A set of parameters exhibits intermediate median LTs: “∑(90thpctl) >63 dBZ” at 24.5 minutes, “∑(Max dBZ) >78 dBZ” at 28.8 minutes, and “|E-field| >2 kV/m” at 30.2 minutes. Comparable times are found for “∑|E-field| >2 kV/m” at 34.2 minutes and “|E-field| >1 kV/m” at 34.5 minutes. Longer LTs are observed for “Median >20 dBZ” at 38.4 minutes and “90thpctl >25 dBZ” at 42.3 minutes, while “Zero Crossing E-field” has the longest median LT, at 64.9 minutes. Although not examined in this work, choosing parameters that lead to very long LTs typically results in a much higher number non-EAs. A similar statement was also made by Beasley et al., 2008 [11].

Note that some parameters may not apply to all thunderstorms, and others may only be met if the first CG lightning strike has already struck within the 5 km radius. Despite the low median values, outliers with LTs of more than 70 minutes should also be mentioned at this point. To overcome such issues, combined prediction parameters as described as alert and shutdown initiation criteria in Section 7.2 are used to determine alert and shutdown LTs for the results presented in Sections 8.2, 8.3 and 8.4.

8.2 Lead Time Analyses for Alerts and Shutdowns

8.2.1 Lightning Strikes within 5 km radius and 90-minute limit

The following Sections 8.2.1 and 8.2.2 provide an overview of the resulting alert and shutdown LTs based on the criteria described in Section 7.2. Section 8.2.1 presents results of the initial analyses (Schatz et al., 2025 [77]) for comparison with the extended analyses. An overview of the alert and shutdown LTs is provided in Table 3. The case numbering follows the increasing shutdown LTs and is therefore in ascending order, which facilitates comparison with other results. For this analysis 45 cases are analysed and the 90-minute limit and the SIC5 were applied.

Table 3: Analysed thunderstorm cases for initial analyses are shown with the date and time of the first CG lightning strike within 5 km in UTC and the corresponding alert and shutdown lead times. Numbering of cases according to initial analyses, shutdown lead times are color-coded from shortest (green) to longest (orange), pre-season Case 1 is greyed out.

Case	**First CG in 5 km radius**		**Lead Time in Minutes**	
No.	Date	Time in UTC	Alert	Shutdown
1	16.04.2024	08:39:09	90.00	0.00
2	15.09.2022	11:21:40	15.53	2.02
3	30.05.2024	12:34:12	29.40	2.25
4	28.07.2023	17:12:25	2.42	2.42
5	22.07.2024	17:43:48	6.22	3.8
6*	08.08.2024	14:59:51	23.80	3.87
7	01.08.2023	14:04:36	63.35	3.97
8	19.07.2023	13:31:21	21.10	3.97
9*	18.08.2024	13:16:13	5.38	4.05
10	14.07.2024	18:58:22	23.22	4.53
11*	11.07.2024	19:56:30	46.50	6.5
12*	08.06.2024	17:29:34	10.38	7.58
13	22.07.2023	13:56:01	51.02	7.67
14	05.07.2023	20:10:06	20.07	7.93
15*	12.08.2022	14:41:58	16.97	8.38
16*	19.07.2024	16:45:32	21.40	9.22
17	06.06.2024	18:31:39	20.87	10.07
18	13.07.2023	01:48:32	49.97	10.25
19	10.06.2024	04:01:15	61.48	10.72
20	04.06.2024	16:44:26	11.75	10.93
21	09.06.2023	13:47:10	12.67	11.2
22*	21.07.2023	14:23:12	58.20	11.92
23	10.07.2023	14:54:28	14.80	12.35
24	27.06.2024	01:12:43	22.72	12.83
25	04.06.2023	13:53:04	53.57	14.08
26	02.08.2024	15:23:59	76.03	14.17
27	18.07.2023	16:16:50	51.83	14.52
28	12.07.2024	15:22:03	32.05	18.65
29	06.09.2022	18:28:21	38.12	18.78
30	21.05.2024	14:47:57	20.58	19.37
31	07.05.2023	13:53:27	36.48	20.45
32*	20.08.2022	10:26:07	23.88	21.12
33*	07.06.2023	19:25:46	40.77	22.62
34	25.08.2023	19:56:58	31.97	23.77
35	05.07.2023	14:41:35	32.35	24.98
36	25.05.2024	20:54:56	27.27	27.27
37	25.07.2023	06:11:31	41.52	28.67
38	11.06.2023	13:37:53	46.28	37.93
39	28.07.2024	11:47:25	50.72	39.2
40*	23.05.2023	12:20:16	73.47	46.33
41	01.08.2024	19:05:29	70.48	49.23
42	06.06.2023	15:31:20	90.00	51.77
43	01.07.2024	11:38:13	90.00	73.02
44	04.07.2023	12:53:43	78.55	74.87
45	23.06.2023	14:40:02	90.00	83.98

*Low-quality LLS data for the first CG lightning strikes within 5 km radius.

Some poorly located CG lightning strikes with low-quality LLS data were manually reclassified by Wolfgang Schulz (ALDIS) at the author's request. During this process, it was determined that for Cases 11, 46, 61, and 77 the "First CG" was misclassified as CG lightning strike when they were actually IC discharges. These cases showed low-quality LLS data like low absolute signal amplitude (<3 kA), a small number of sensors used for localisation (≤3 sensors), or a very large error ellipse (major axis >0.5 km). These cases with low detection quality are still used for analyses because they reflect real-world conditions. For completeness, these cases are marked with an asterisk (*).

This analysis comprises 45 thunderstorm cases, each including at least one CG lightning strike within a 5 km radius of Graz Airport, and is sorted by shutdown LTs in ascending order. The column "First CG 5 km" indicates the time of the first CG lightning strike occurrence within that radius. The shutdown LTs range from 2.02 to 83.98 minutes, with a median of 12.35 minutes and a mean of 19.85 minutes.

Case 1 (greyed out) corresponds to a thunderstorm recorded on the 16 April 2024, which occurred prior to the main thunderstorm season in Austria (May to September, see Section 2.5). For this case, the algorithm could not predict the first CG lightning strike within 5 km for this case, resulting in a LT of 0.00 minutes.

The minimum, maximum, median and mean alert LTs are 2.42, 90, 32.35, and 39.89 minutes, respectively. Note that the maximum LT of 90 minutes for Cases 1, 42, 43, and 45 is constrained by the 90-minute limit described in Section 7.1. In two cases (Case 4 and Case 36), the alert and shutdown were initiated simultaneously, as their associated parameters were fulfilled at the same time.

Overall, the results of shutdown LTs can be divided in four groups:

- LTs less than 2 minutes: 2.2%
- LTs from 2 to 30 minutes: 80.0%
- LTs from 30 to 60 minutes: 11.1%
- LTs over 60 minutes: 6.7%

Cases 39 through 42 exhibit a particular characteristic: A CG lightning strike was detected near the 5 km boundary, with distances from Graz Airport ranging between 5.3 km and 7.5 km. If these CG lightning strikes would have been used to calculate the

shutdown LT, the LTs for Cases 39 to 41 would improve to less than 30 minutes. Although Case 42 would also show a potential improvement, its LT would still be 47.08 minutes, which remains outside the optimal range (see Section 3.1).

Cases 43, 44, and 45 all exhibit high radar reflectivity values (greater than 50 dBZ), large absolute E-field magnitudes (up to 4000 V/m), a high frequency of zero-crossings in the E-field signals, and a high IC discharge rate within the 5 km radius. In all three cases, at least one of the five shutdown criteria remained met throughout the entire period between shutdown initiation and the first CG lightning strike within the 5 km radius, resulting in LTs ranging from 73.02 to 83.98 minutes.

Figure 38 shows the respective criterion described in Section 7.2.2, that triggered each shutdown of the 45 cases. Most shutdowns were initiated by the SIC3, accounting for 21 out of 45 cases (46.7%), followed by the SIC1 with 31.1%. The SIC2 triggered 13.3% of shutdowns, and the SIC4 was responsible for 6.7%. Although the SIC5 was met on several days, it resulted in only one EA shutdown (2.2%) and was therefore excluded from extended analyses.

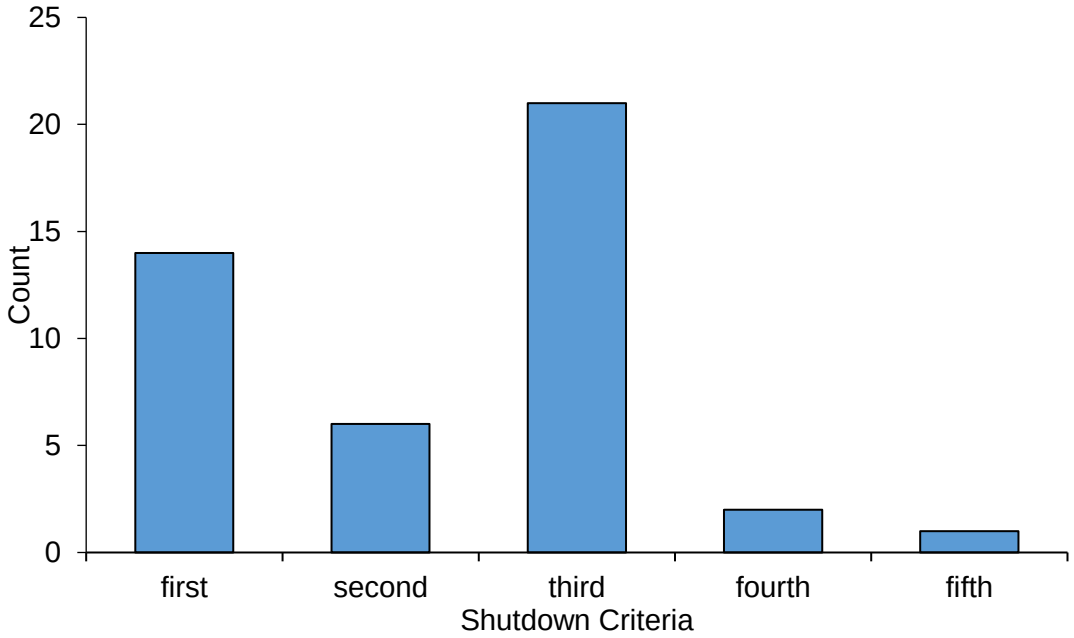

Figure 38 Distribution of shutdown criteria, including the SIC5, for the 45 cases of the initial analyses.

8.2.2 Lightning Strikes within 5 km without time limitation

For the extended analyses in this section, six additional cases were included compared to Section 8.2.1. The analysis follows the same methodology; however, the 90-minute limit was removed, and the SIC5 was also excluded. This brings the total to 51 thunderstorm cases, each containing at least one CG lightning strike within a 5 km radius around Graz Airport. The applied criteria and limits are changed for this analysis, the case numbering remains the same as for the analysis in Section 8.2.1, which facilitates comparison with other results. For additional cases, the numbering continues in ascending order[22].

With the STC described in Section 7.3 specifically STC1, further thunderstorms occurring on days with already existing thunderstorm activity could be identified. As a result, additional Cases 47, 48, and 51 for the dates 11.07.2024, 18.08.2024 and 22.07.2023, respectively, were included.

Since the influence of misclassified LLS data cannot be avoided, it was decided to include all cases, also those with low amplitude, low location accuracy, large error ellipses, and a small number of sensor reports. It is possible that a weak CG stroke with low detection quality, or even a misclassified IC discharge could result in personal injury. Based on this assumption, Case 46 from 07.08.2024 and Case 49 from 27.08.2022, were included in this analysis.

Within the 5 km radius but in a buffer zone of 5 ±0.5 km near edge, 18 borderline cases were found (Table 4) with their first CG lightning strike in this zone, as described in Section 5.4. For 14 of the 18 borderline cases, the analysis shows no change in the shutdown LTs, as CG lightning strikes occurred simultaneously or shortly after the first CG lightning strike used. For the remaining six borderline cases, the shutdown LTs are shortened by 0.55 to 17.07 minutes. There is an improvement in two cases, which are shifted from the LT range of 30–60 minutes to the optimal range of 2–30 minutes.

[22]Note: The numbering of the six additional cases continues sequentially from the numbering used in Table 3. As a result, the numbering in Table 4 (which is sorted by shutdown LTs) is not consecutive.

Case 50 from 04.09.2022 had a modified LLS data format due to changes by the operator, which the algorithm couldn't process. After manual processing of the LLS data, the case was included.

For Case 2 on 15.09.2022, the shutdown LT changes for this analysis from 2.02 to 4.83 minutes. The reason for this adjustment is a time shift error in the E-field data recorded by FM 1 North on that day. The E-field signal was offset by two hours, causing the triggering criterion to be missed. After correcting this error, the shutdown LT increases by 2.81 minutes.

The shutdown LTs for the extended dataset range from 2.25 to 83.98 minutes, with a median of 12.83 minutes and a mean of 19.10 minutes. Removing the time limit had no effect on the maximum shutdown LT. For Cases 1, 11, 46, and 47 a shutdown could not be predicted (Case 1 is described in Section 8.2.1). Although Case 46 shows high radar reflectivity values with maximum values ≥39 dBZ and 90th percentile values ≥35 dBZ and absolute E-field values between 1000 V/m and 2500 V/m, there was no zero crossing in the E-field. As a result, for Case 46, the SIC1 was not fulfilled until the time of the first CG lightning strike within 5 km.

The removal of the SIC5 (intended for low-reflectivity thunderstorms within 5 km radius) leads to a change in the shutdown LT for Case 11 on 11.07.2024. During the occurrence of CG lightning strikes within the 5 km radius, radar reflectivity remains low, with maximum values below 35 dBZ and 90th percentile values below 30 dBZ, increasing only after 22:45 UTC. The E-field data show that FM 2 South, FM 3 East, and FM 4 West reach −2000 V/m as early as 19:00 UTC, while FM 1 North records values around −1000 V/m. Due to the absence of IC discharges within the 5 km radius, the algorithm triggers the shutdown only at the moment of the first CG lightning strike within 5 km, fulfilling the SIC1, resulting in a shutdown LT of 0 minutes (previously 6.5 minutes with the SIC5). Case 47 on the same day also cannot be predicted due to low radar reflectivity and the absence of CG lightning strike within the 5 km radius. Cases 11 and 47 still remain within the same alert period and have alert LTs of 46.50 minutes and 176.38 minutes, respectively.

The minimum, maximum, median, and mean alert LTs are 2.42, 176.38, 31.97, and 43.63 minutes, respectively. The increase in the maximum alert LT by 86.38 minutes is due to the removal of the 90-minute limit. Cases 11 and 47, as well as Cases 13 and

51, fall within the same alert period, resulting in longer alert LTs for the latter case on each respective day. The maximum alert LT increases to 176.38 minutes.

For this extended analysis, the shutdown LTs are distributed among the four groups as follows:

- LTs less than 2 minutes: 7.8%
- LTs from 2 to 30 minutes: 72.5%
- LTs from 30 to 60 minutes: 15.7%
- LTs over 60 minutes: 3.9%

Table 4: Analysed thunderstorm cases including all CG lightning strikes within 5 km, without 90-minute limit and without the SIC5, date and time of the first CG lightning strike within 5 km (in UTC), corresponding alert and shutdown LTs color-coded from shortest (green) to longest (orange) and zero LTs greyed out.

Case	**First CG in 5 km radius**		**Lead Times in Minutes**	
No.	Date	Time in UTC	Alert	Shutdown
1†	16.04.2024	08:39:09	114.90	0.00
46*	07.08.2024	21:03:50	149.07	0.00
11*	11.07.2024	19:56:30	46.50	0.00
47*†	11.07.2024	22:06:23	176.38	0.00
3	30.05.2024	12:34:12	29.40	2.25
4	28.07.2023	17:12:25	2.42	2.42
5	22.07.2024	17:43:48	6.22	3.80
6*	08.08.2024	14:59:51	23.80	3.87
7	01.08.2023	14:04:36	14.83	3.97
8	19.07.2023	13:31:21	21.10	3.97
9*	18.08.2024	13:16:13	5.38	4.05
10	14.07.2024	18:58:22	23.22	4.53
2	15.09.2022	11:21:40	6.28	4.83
12*	08.06.2024	17:29:34	10.38	7.58
13	22.07.2023	13:56:01	51.02	7.67
14	05.07.2023	20:10:06	16.83	7.93
15*	12.08.2022	14:41:58	16.97	8.38
16*	19.07.2024	16:45:32	21.40	9.22
17†	06.06.2024	18:31:39	20.87	10.07
18	13.07.2023	01:48:32	49.97	10.25
19	10.06.2024	04:01:15	61.48	10.72
20	04.06.2024	16:44:26	11.75	10.93
21†	09.06.2023	13:47:10	12.67	11.20
22*	21.07.2023	14:23:12	14.52	11.92
23	10.07.2023	14:54:28	14.80	12.35
24	27.06.2024	01:12:43	22.72	12.83
48*	18.08.2024	14:43:23	18.17	12.87
25	04.06.2023	13:53:04	53.57	14.08

26†	02.08.2024	15:23:59	19.02	14.17
27†	18.07.2023	16:16:50	51.83	14.52
28†	12.07.2024	15:22:03	32.05	18.65
29	06.09.2022	18:28:21	38.12	18.78
30	21.05.2024	14:47:57	20.58	19.37
31†	07.05.2023	13:53:27	36.48	20.45
49*†	27.08.2022	14:33:55	22.77	20.57
32*†	20.08.2022	10:26:07	23.88	21.12
33*†	07.06.2023	19:25:46	42.37	22.62
34	25.08.2023	19:56:58	31.97	23.77
35†	05.07.2023	14:41:35	32.35	24.98
36	25.05.2024	20:54:56	27.27	27.27
37	25.07.2023	06:11:31	41.52	28.67
50†	04.09.2022	13:14:48	41.10	33.02
51	22.07.2023	15:43:49	158.82	35.45
38†	11.06.2023	13:37:53	46.28	37.93
39†	28.07.2024	11:47:25	50.72	39.20
40*†	23.05.2023	12:20:16	56.78	46.33
41†	01.08.2024	19:05:29	70.48	49.23
42†	06.06.2023	15:31:20	96.33	51.77
43	01.07.2024	11:38:13	90.00	55.47
44	04.07.2023	12:53:43	78.55	74.87
45	23.06.2023	14:40:02	99.47	83.98

*Low-quality LLS data for the first CG lightning strikes within 5 km radius;
†borderline case with first CG lightning strike in a distance of 5±0.5 km.

The distribution of criteria that initiated the respective shutdown is shown in Figure 39. Most shutdowns were triggered by the SIC3, accounting for 22 out of 51 cases (43.1%), followed by the SIC1 with 35.3%. The SIC2 triggered 13.7% of the shutdowns, and the SIC4 for 7.9%.

8.2.3 Lightning Strikes outside 5 km

For a comprehensive analysis of the systems sensitivity, not only cases with lightning discharges within the 5 km radius were examined, but all cases that showed thunderstorm activity during the measurement period and triggered the alert and shutdown algorithm. As described in Section 5.4, the area was divided into several observed areas between 5–8 km, 8–10 km, and 10–15 km radius as well as 15–30 km. In addition, three cases without any CG lightning strikes still triggered a shutdown and are for that reason also included in the analysis.

As described in Section 4.4, the ground strike points (GSPs) of different lightning strikes within a single flash can be up to 6.9 km apart (maximum LA distance and maximum distance between GSPs, see Schwalt and Schulz, 2023 [57]). From this perspective, a shutdown zone of 5 km radius is rather limited. Therefore, for the following analyses alert and shutdown LTs were also calculated for cases that did not include any CG lightning strikes within 5 km. In each of these cases, the nearest CG lightning strike was used as a reference.

In Case 52, IC discharges occurred at distances of 8 km and 5 km at 14:59:23 UTC and 15:06:55 UTC, respectively. This would have resulted in a shutdown LT of at least 6.78 minutes. However, due to low E-field values, none of which exceeded the 1 kV/m threshold at any FM, no shutdown was triggered. Case 53 occurred on the same day as Case 29 and followed it directly. The first CG lightning strike in the 5–8 km radius at 20:45:18 UTC still fell within the shutdown period initiated by Case 29. As a result, it could not be captured as part of Case 53 and is associated with a negative LT. Assuming a strict separation between the 5 km radius and the 5–8 km area, the shutdowns of Cases 52 to 69 must be classified as non-EA. If this is considered in comparison with Cases 1 to 51 from the 5 km radius, it can be observed, that the performance of the algorithm influenced accordingly.

For an observed area within 8 km radius and CG lightning strikes within the 5–8 km radius, there were 21 cases, 18 of them led to a shutdown. These cases are listed in Table 5, from Case 52 to Case 69, sorted in ascending order by shutdown LT. The shutdown LTs refer to the first CG lightning strike within the 5–8 km radius. These cases therefore lie outside the critical surrounding area (area of high risk that a lightning strike affects the airport, see Section 3.3.1) of 5 km radius. There are two cases in a transitional zone near this area (5 ±0.5 km) that are considered borderline cases. These cases, Case 53 and Case 54, are marked with a dagger symbol (†).

The distribution of criteria that initiated the respective shutdown is shown in Figure 39. Most shutdowns were triggered by SIC3 accounting for 10 out of 18 cases (55.6%), followed by the SIC1 with 27.7%. The SIC2 triggered 11.1% of the shutdowns, and the SIC4 for 5.6%.

Table 5: Analysed thunderstorm cases with CG lightning strikes within the 5–8 km radius, date and time of the first CG lightning strike within the 5–8 km radius (in UTC), corresponding alert and shutdown lead times color-coded from shortest (green) to longest (orange) and zero or negative lead times greyed out.

Case	First CG in 5–8 km		Lead Time in Minutes	
No.	Date	Time in UTC	Alert	Shutdown
52	30.07.2023	15:13:42	6.43	-20.32
53†	06.09.2022	20:45:18	175.07	-3.58
54†	09.08.2023	19:36:54	11.43	0.00
55	01.07.2024	09:37:08	14.15	0.00
56*	24.07.2023	20:55:16	12.72	0.00
57	28.05.2024	10:09:16	3.30	0.00
58	12.07.2023	03:53:46	9.28	2.12
59	21.05.2024	04:11:39	25.93	4.65
60	03.06.2024	18:52:27	16.67	4.87
61	21.05.2024	09:05:14	20.12	7.13
62	08.06.2023	14:06:31	9.75	8.22
63	29.08.2023	14:49:18	53.00	13.18
64	13.07.2023	15:48:24	28.40	13.4
65	02.06.2024	21:02:53	23.17	16.73
66*	17.07.2023	12:00:18	35.30	19.92
67	18.08.2023	16:03:05	26.08	21.42
68	29.07.2023	20:14:14	54.23	22.63
69	28.06.2024	11:28:55	34.07	24.3

*Low-quality LLS data for the first CG lightning strikes within 5–8 km radius;
†borderline case with first CG lightning strike in a distance of 5 ±0.5 km.

For an observed area within 10 km radius and CG lightning strikes within the 8–10 km radius, there were 8 cases, 4 of them led to a shutdown. These cases are listed in Table 6, from Case 70 to Case 73, sorted in ascending order by shutdown LT. The shutdown LTs refer to the first CG lightning strike within the 8–10 km radius. These cases therefore lie outside the critical surrounding area of 5 km radius. Cases 70 and 71 have no LT to the First CG lightning strike in the 8–10 km radius, Case 72 a LT of 1.90 minutes and Case 73 has a LT of 17.63 minutes.

Assuming a strict separation between the 5 km radius and the outer areas, the shutdowns of Cases 70 to 73 must be classified as non-EA. If this is taken into account in comparison with Cases 1 to 51 from the 5 km radius and Cases 52 to 69 in the 5–8 km radius, has again an influence on the performance.

The distribution of criteria that initiated the respective shutdown is shown in Figure 39. Two of four (50%) shutdowns were triggered by the SIC3, followed by the SIC1 with 25%. The SIC2 triggered the residual 25% of the shutdowns.

Table 6: Analysed thunderstorm cases with CG lightning strikes within 8–10 km radius, date and time of the first CG lightning strike within 8–10 km radius (in UTC), corresponding alert and shutdown lead times color-coded from shortest (green) to longest (orange) and zero or less than 2 minutes lead times greyed out.

Case	**First CG in 8–10 km radius**		**Lead Time in Minutes**	
No.	Date	Time in UTC	Alert	Shutdown
70	25.07.2023	12:17:20	31.63	0.00
71*	04.06.2024	18:55:11	142.50	0.00
72*	23.04.2023	16:51:05	4.80	1.90
73	07.08.2024	19:02:01	27.25	17.63

*Low-quality LLS data for the first CG lightning strikes within 8–10 km radius.

For an observed area within 15 km radius and CG lightning strike within the 10–15 km radius, there were 20 cases, three of them led to a shutdown. These cases are listed in Table 7, from Case 74 to Case 76, sorted in ascending order by shutdown LT. The shutdown LTs refer to the first CG lightning strike within the 10–15 km radius. These cases therefore lie outside the critical surrounding area of 5 km radius. The Cases 74, 75 and 76 have LTs of 4.73, 11.62 and 52.30 minutes, respectively.

Assuming a strict separation between the 5 km radius and the outer areas, the shutdowns of Cases 74 to 76 must be classified as non-EA. If this is taken into account in comparison with Cases 1 to 51 from the 5 km radius, the Cases 52 to 69 in the 5–8 km radius and the Cases 70 to 73 in the 8–10 km radius, again influences the performance.

The distribution of criteria that initiated the respective shutdown is shown in Figure 39. Each of the three cases were triggered by another criterion, the SIC1, SIC2 and SIC3, each account for 33.3%.

Table 7: Analysed thunderstorm cases with CG lightning strikes within 10–15 km radius, date and time of the first CG lightning strike within 10–15 km radius (in UTC), corresponding alert and shutdown lead times in the last columns.

Case	First CG in 10–15 km		Lead Time in Minutes	
No.	Date	Time in UTC	Alert	Shutdown
74	23.06.2023	12:17:20	6.13	4.73
75	07.07.2024	18:55:11	28.58	11.62
76	17.05.2024	16:51:05	65.08	52.30

Three additional Cases 77, 78, and 79 corresponding to thunderstorms on 1 August 2024, 29 April 2023, and 24 May 2024, respectively, exhibited thunderstorm activity but no CG lightning strikes within the total observed area (up to 30 km radius). Although no CG lightning strikes occurred, the shutdown criteria (SIC1 for Case 77, SIC3 for Case 78, and SIC3 for Case 79) were met, and the algorithm was consequently triggered. However, due to the absence of CG lightning strikes, no alert or shutdown LTs could be determined.

Figure 39 shows the total frequency with which the individual shutdown criteria occur. The number of cases was shown via the individual criteria.

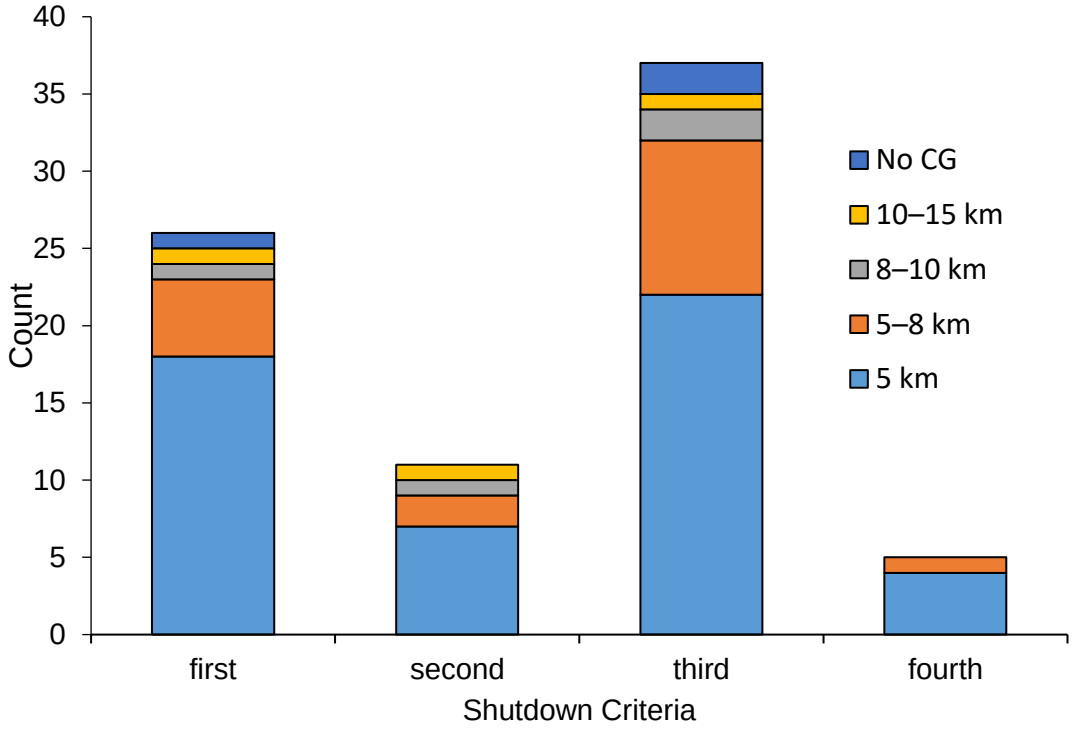

Figure 39: Distribution of shutdown criteria over the different observed areas and cases without CG.

The individual columns were divided into the various observed areas and the “No CG” category. Across all 79 cases examined, the SIC3 led to 37 triggers (46.8%) and thus most frequently led to a shutdown. The SIC1 with 26 triggers (32.9%) led to the second most frequent shutdown. The SIC2 and SIC4 were triggered eleven times (14.5%) and five times (6.3%), respectively.

8.3 Shutdown Termination Criterion 1

8.3.1 Lead Time Performance

The following Sections 8.3.1 to 8.3.5, show results for 79 shutdowns for the 79 analysed thunderstorm cases. For the termination of shutdowns, STC1 is applied with a minimum TTC of 30 minutes and a maximum TTC of 60 minutes after the last IC discharge or CG lightning strike within 5 km radius (see Section 7.3.1).

This section compares the LT performance of the alert and shutdown algorithms to show how they behave across the various observed areas and the total area, i.e., taking all cases into account. The shutdown zone within a 5 km radius for which the algorithm was optimised, applies again. Shutdowns triggered for CG lightning strikes within 5 km radius are classified as EA. Shutdown triggers without CG lightning strikes within 5 km are classified as non-EA.

Figure 40 shows the distribution of alert LTs for the various observed areas. For each observed area, the percentages are distributed across the respective alert LT ranges, i.e., the distribution for the 15 km radius totals 100%, of which 0% is within 0–2 minutes, 32.9% is within 2–30 minutes, 21.0% within 30–60 minutes, 13.2% for >60 minutes, and 32.9% categorised as non-EA alerts (also applies to Figure 37). None of the 79 cases had a LT of less than 2 minutes. For the 51 cases within the 5 km radius, 49.0%, 31.4% and 19.6% were in the time ranges of 2–30 minutes, 30–60 minutes and >60 minutes, respectively. The ratio between the time ranges remains the same for the consideration of further cases and the extension of the observation radius. The proportion of non-EA alerts increases accordingly from the 8 km radius with 26.1% and rises to 35.4% when all cases in the total area are considered.

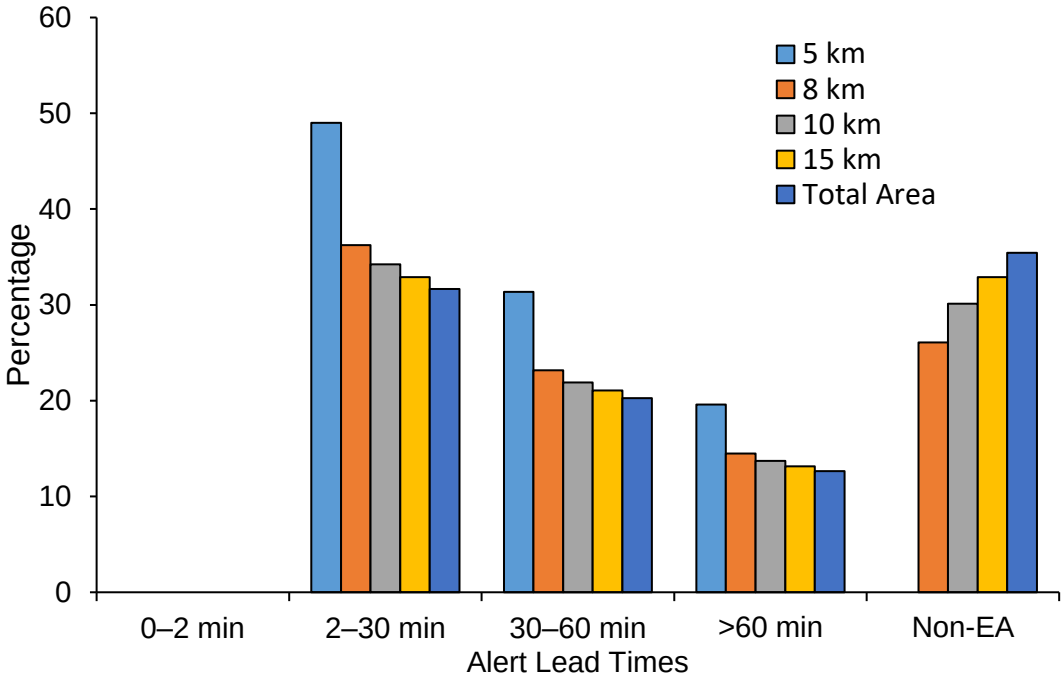

Figure 40: Distribution of alert LTs for the different observed areas with a radius of 5 km, 8 km, 10 km and 15 km, the last column includes the total area (30 km) and cases without CG.

Figure 41 shows the distribution of shutdown LTs for the different observed areas. For an observation radius of 5 km and Cases 1 to 51, 92.2% of cases result in an EA, and 72.5% of cases are within the optimal shutdown LT range of 2–30 minutes. Four cases, or 7.8%, have a LT that is too short, in the range of 0–2 minutes. There are no non-EA shutdowns for the 5 km radius. When the observed area is expanded, the number of EAs remains the same, but the number of non-EAs shutdowns increases with each expansion of the area. In the 8 km radius, including Cases 52 to 69, 68.1% of cases result in an EA. A proportion of 53.6% is within the optimal range. Non-EA shutdowns already account for 26.1% in this area. As more and larger areas are taken into account, the proportion of non-EAs continues to rise and the proportion of EAs decreases accordingly. For the 10–15 km radius (including Cases 70 to 76), this represents 64.6% and 61.8% EA shutdowns. Considering all cases that triggered a shutdown in the total area, i.e., including also Cases 77 to 79 without CG lightning strikes, results in 59.5% EAs (46.8% in the optimal range of 2–30 minutes) and 35.4% non-EAs.

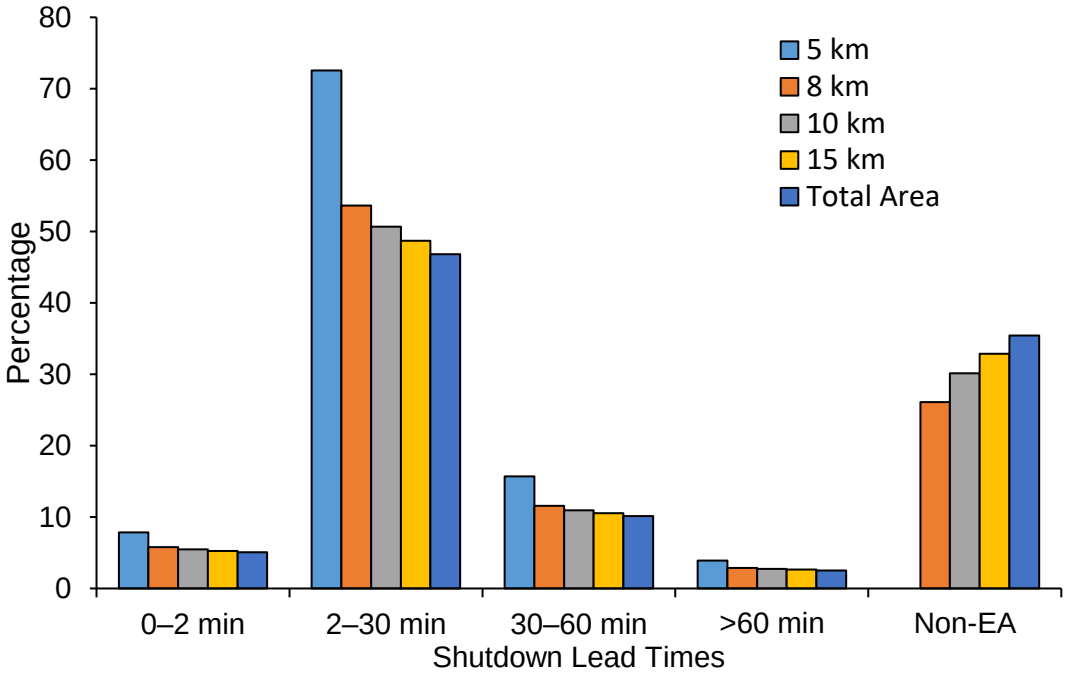

Figure 41: Distribution of shutdown LTs for the different observed areas with a radius of 5 km, 8 km, 10 km and 15 km, the last column includes the total area (30 km) and cases without CG.

Table 8 summarises all results for the distribution of shutdown LTs. The percentages and counts for each time range and non-EA shutdowns are presented for the individual areas and the total area.

Table 8: Shutdown lead time range, non-effective alarms and total cases per observed area and total area in percent; Case count in parenthesis.

Shutdown Lead Time	**5 km**	**8 km**	**10 km**	**15 km**	**Total Area**
Minutes	% (Count)	% (Count)	% (Count)	% (Count)	% (Count)
0–2	7.8 (4)	5.8 (4)	5.5 (4)	5.3 (4)	5.1 (4)
2–30	72.5 (37)	53.6 (37)	50.7 (37)	48.7 (37)	46.8 (37)
30–60	15.7 (8)	11.6 (8)	11.0 (8)	10.5 (8)	10.1 (8)
>60	3.9 (2)	2.9 (2)	2.7 (2)	2.6 (2)	2.5 (2)
Non-EA	0 (0)	26.1 (18)	30.1 (22)	32.9 (25)	35.4 (28)
Total	100 (51)	100 (69)	100 (73)	100 (76)	100 (79)

8.3.2 Alert and Shutdown Duration for Different Areas

8.3.2.1 Lightning Strikes within 5 km

To illustrate how the different observed areas affect alert and shutdown durations, statistical values and distributions were calculated. Again, Cases 1 to 51 were used for the 5 km radius.

Table 9 shows the statistical values for alert and shutdown durations in minutes and for an observed area of 5 km radius. The duration of an alert ranges from 46.35 to 339.42 minutes, with a median of 157.75 minutes and a mean of 158.44 minutes. The duration of a shutdown ranges from 33.48 to 204.37 minutes, with a median of 82.23 minutes and a mean of 93.75 minutes. For medians, an alert triggered by a CG lightning strike within a 5 km radius lasts 1.92 times longer than a shutdown. The 10th and 90th percentiles of the alert and shutdown durations are also given.

Table 9: Statistical values of alert and shutdown duration in minutes, observed area 5 km radius.

Measure	**Duration in Minutes**					
	Min	10th	Median	Mean	90th	Max
Alert	46.35	71.12	157.75	158.44	289.98	339.42
Shutdown	33.48	56.75	82.23	93.75	150.13	204.37

Figure 42 displays these results as a distribution representing the duration of alerts and shutdowns in 15-minute intervals. The intervals include the lower value and exclude the upper value (e.g., the interval of 0–15 minutes represents durations where 0 minutes ≤ duration < 15 minutes). The alerts show two clusters, one around the interval of 75–90 minutes with 15.7% and another around the interval of 180–195 minutes interval, also with 15.7%. The median and mean alert durations lie between the two clusters. 17.7% have an alert duration of over 225 minutes. The shutdowns show only one cluster around the interval of 60–75 minutes with 25.5%. The interval of 75–90 minutes has the second highest number of values at 13.7%, and the median is also in this interval.

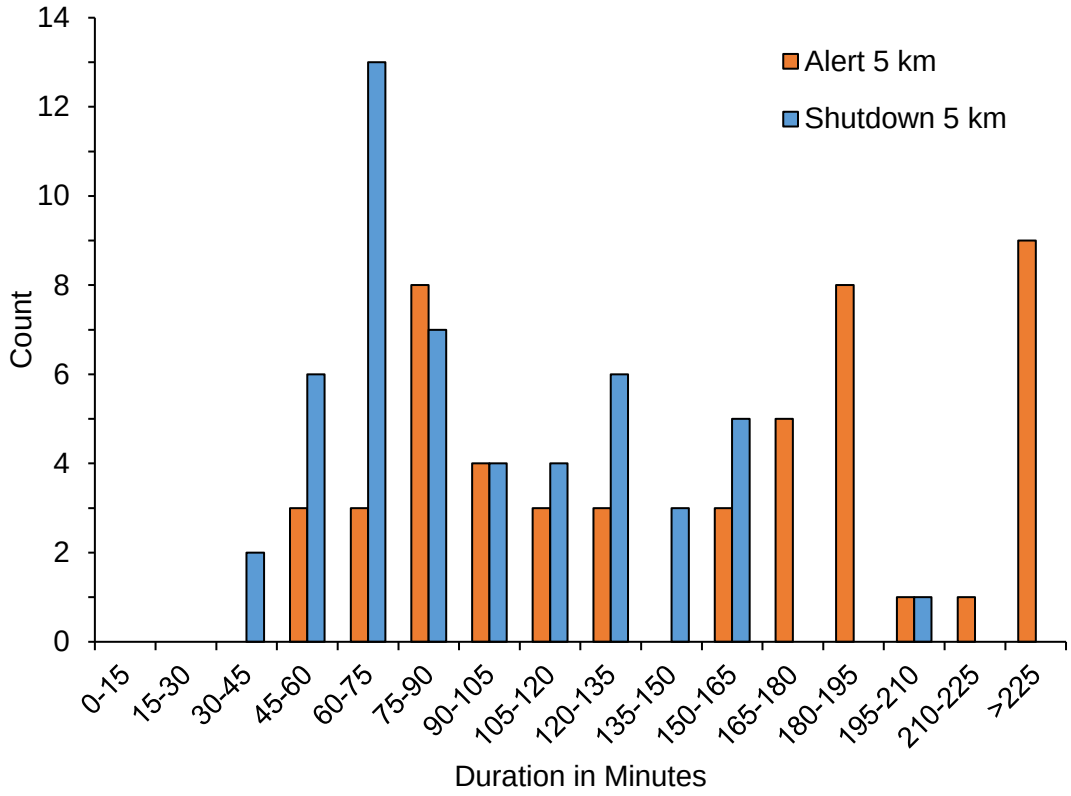

Figure 42: Distribution of alert and shutdown durations in minutes for an observed area of 5 km radius.

8.3.2.2 Lightning Strikes within 8 km

This section considers a radius of 8 km, so the cases between the 5–8 km radius with the cases of the 5 km radius included. For thunderstorm Cases 1 to 69, statistical values and distributions were calculated to make these results comparable across different observed areas.

Table 10 shows the statistical values for alert and shutdown durations in minutes and for an observed area of 8 km radius. The duration of an alert ranges from 39.97 to 339.42 minutes, with a median of 129.20 minutes and a mean of 146.65 minutes. The duration of a shutdown ranges from 13.22 to 204.37 minutes, with a median of 79.40 minutes and a mean of 86.75 minutes. Median alert duration triggered by a CG lightning strike within an 8 km radius are 1.63 times longer than for shutdown durations. In addition, the 10th and 90th percentiles of alert and shutdown durations are also given.

Figure 43 displays these results as a distribution representing the duration of alerts and shutdowns in 15-minute intervals. The intervals include the lower value and exclude the upper value. The alerts show two clusters, one around the interval of 75–90 minutes with 13.0% and another around the 180–195 minutes, also with 13.0%.

Table 10: Statistical values of alert and shutdown duration in minutes, observed area 8 km radius.

Measure	Duration in Minutes					
	Min	10th	Median	Mean	90th	Max
Alert	39.97	59.08	129.20	146.65	268.81	339.42
Shutdown	13.22	48.47	79.40	86.75	140.74	204.37

The median and mean alert duration lie between these two clusters, 14.5% have an alert duration of over 225 minutes. The shutdowns show only one cluster around the interval of 60–75 minutes with 26.1%. The interval of 75–90 minutes interval has the second highest number of values at 14.5%, and the median is also in this interval.

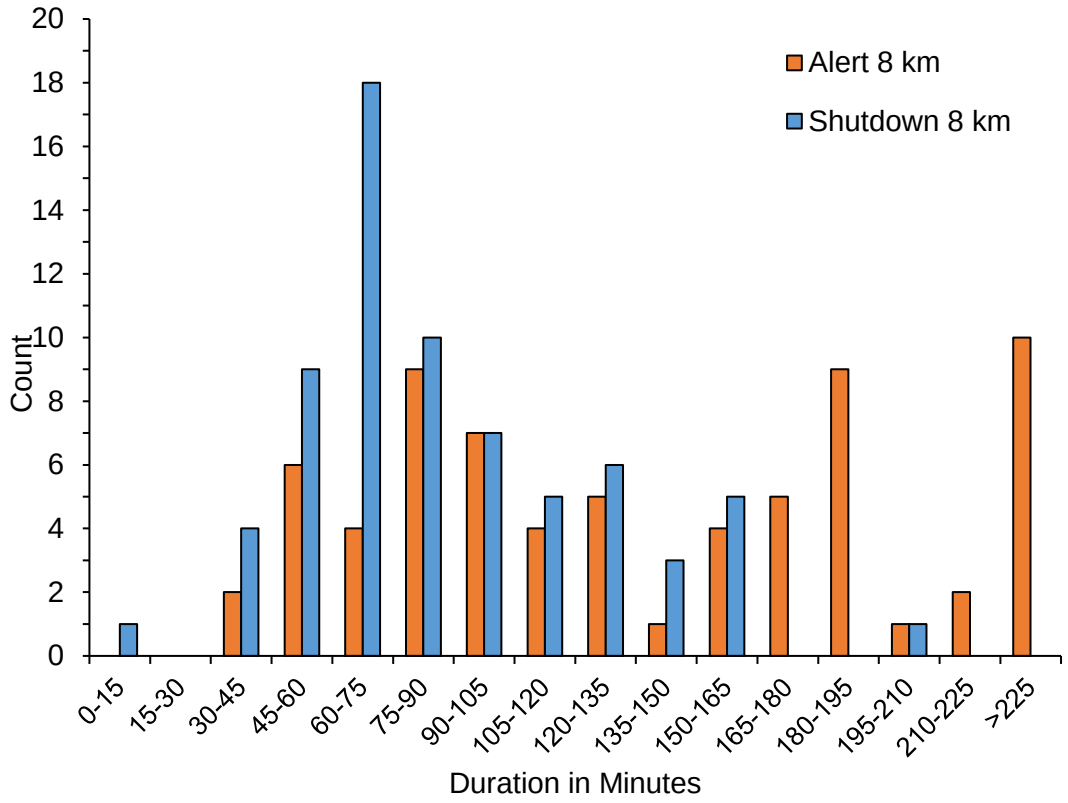

Figure 43: Distribution of alert and shutdown durations in minutes for an observed area of 8 km radius.

Compared to the results for the 5 km radius, the median value within an 8 km radius for alert and shutdown is 18.1% and 3.4% lower, respectively.

8.3.2.3 Lightning Strikes outside 8 km

CG lightning strikes within 10 km

This section considers a radius of 10 km, so the cases within the 8–10 km radius with the cases of the 8 km radius included. For the thunderstorm Cases 1 to 73, statistical values and distributions were worked out in order to make these results comparable across different observed areas.

Table 11 shows the statistical values for the alert and shutdown durations in minutes and for an observed area of 10 km radius. The duration of an alert is in the range of 39.97 and 339.42 minutes, with a median of 129.20 minutes and a mean of 147.45 minutes. The duration of a shutdown is in the range of 13.22 and 204.37 minutes, with a median of 76.85 minutes and a mean of 84.21 minutes. The median duration of an alert triggered by a CG lightning strike within a 10 km radius is 1.68 times longer than a shutdown. The 10^{th} and 90^{th} percentiles of the alert and shutdown durations are also shown.

Table 11: Statistical values of alert and shutdown duration in minutes, observed area 10 km radius.

Measure	Duration in Minutes					
	Min	10^{th}	Median	Mean	90^{th}	Max
Alert	39.97	59.88	129.20	147.45	284.69	339.42
Shutdown	13.22	45.50	76.85	84.21	140.50	204.37

Figure 44 visualises these results as a distribution of alert and shutdown durations in 15-minute intervals. These intervals include the lower value and exclude the upper value. The alerts show two clusters, one around the interval of 75–90 minutes with 12.3% and another around 180–195 minutes with 13.7%. The median and mean durations lie between the two clusters. 15.0% have an alert duration over 225 minutes. Shutdowns show only one peak at the interval of 60–75 minutes with 26.0%. The interval of 75–90 minute has the second most values, 13.7%, and the median also lies in this interval. Compared to the results for the 5 km radius, the median value within a 10 km radius for alert and shutdown is 18.1% and 6.5% lower, respectively.

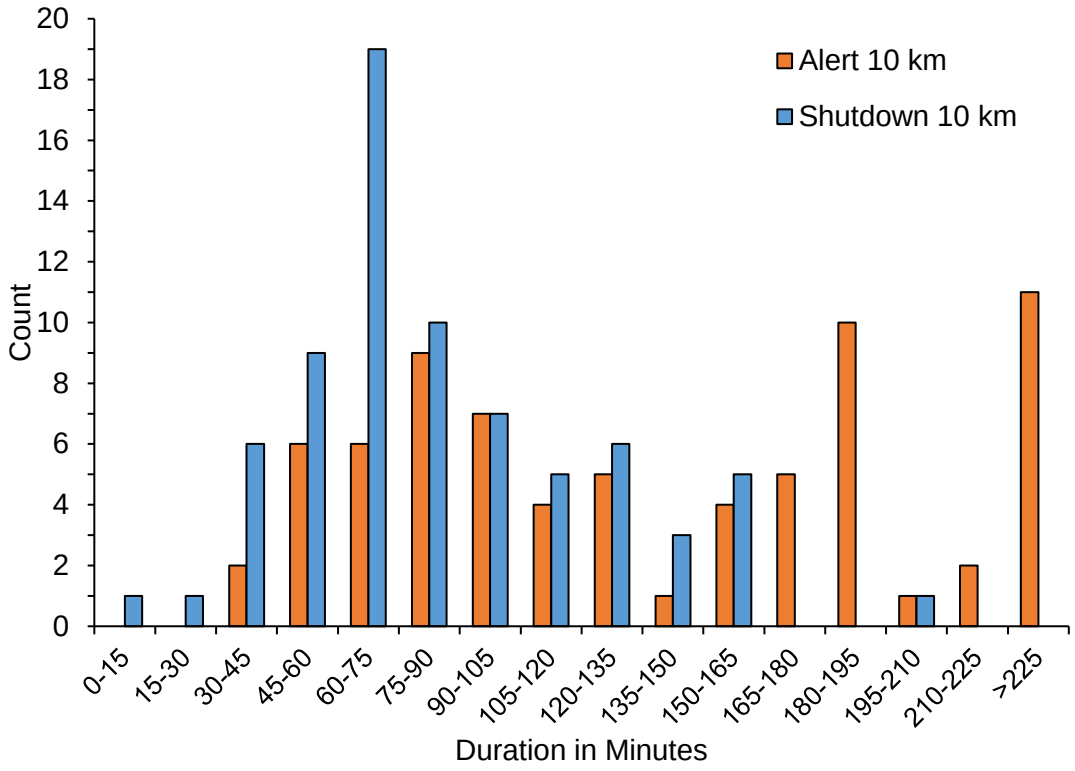

Figure 44: Distribution of alert and shutdown durations in minutes for an observed area of 10 km radius.

CG lightning strikes within 15 km

This section considers a radius of 15 km, so the cases within the 10–15 km radius with the cases of the 10 km radius included. For the thunderstorm Cases 1 to 76, statistical values and distributions were worked out in order to make these results comparable across different observed areas.

Table 12 shows the statistical values for the alert and shutdown durations in minutes and for an observed area of 15 km radius. The duration of an alert is in the range of 32.35 and 339.42 minutes, with a median of 121.58 minutes and a mean of 143.90 minutes. The duration of a shutdown is in the range of 13.22 and 204.37 minutes, with a median of 75.64 minutes and a mean of 82.75 minutes. The median duration of an alert triggered by a CG lightning strike within a 15 km radius is 1.61 times longer than a shutdown. The 10^{th} and 90^{th} percentiles of the alert and shutdown durations are also shown.

Figure 45 visualises these results as a distribution of alert and shutdown durations in 15-minute intervals. These intervals include the lower value and exclude the upper value. The alerts show two clusters, one around the interval of 75–90 minutes with

11.8%, and another around 180–195 minutes with 13.2%. The median and mean durations lie between the two clusters, 14.5% have an alert duration over 225 minutes. Shutdowns show only one peak at the interval of 60–75 minutes with 25.0%. The interval of 75–90 minutes has the second most values, 14.5%, and the median also lies in this interval.

Table 12: Statistical values of alert and shutdown duration in minutes, observed area 15 km radius.

Measure	Duration in Minutes					
	Min	10th	Median	Mean	90th	Max
Alert	32.35	54.02	121.58	143.90	276.75	339.42
Shutdown	13.22	36.71	75.64	82.75	140.33	204.37

Compared to the results for the 5 km radius, the median value within a 15 km radius for alert and shutdown is 22.9% and 8.0% lower, respectively.

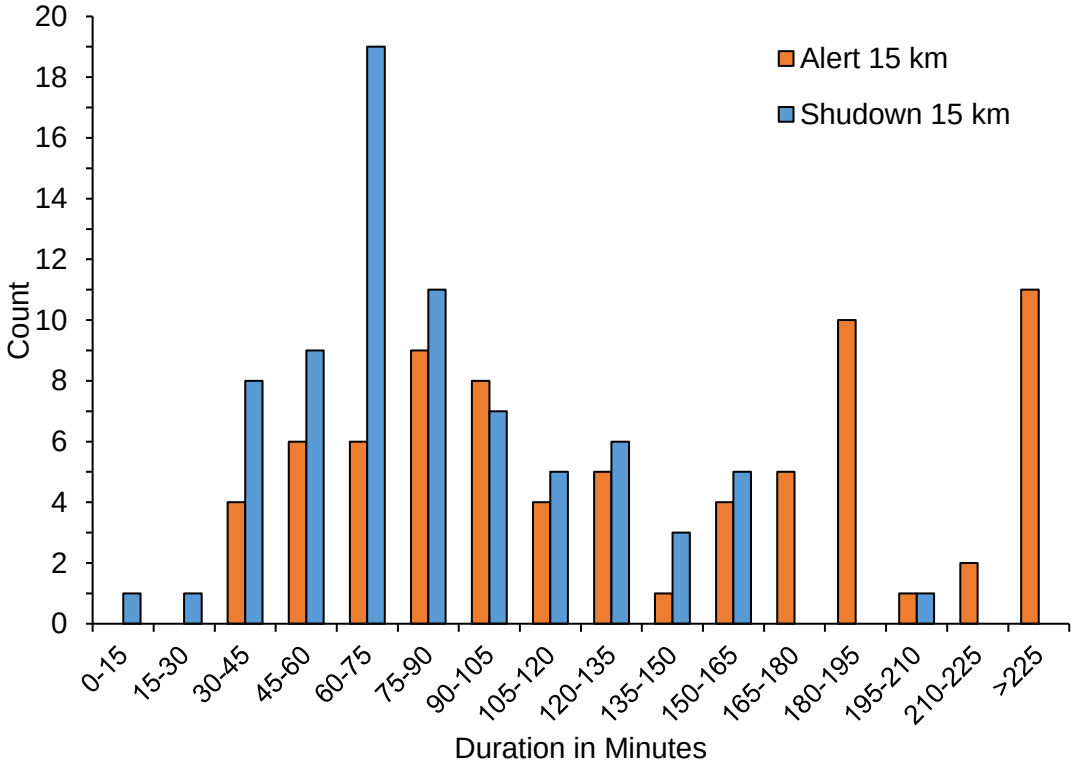

Figure 45: Distribution of alert and shutdown durations in minutes for an observed area of 15 km radius.

8.3.2.4 All Shutdown triggering Thunderstorms

This section considers the total area of 30 km radius all thunderstorm cases that led to a shutdown. Statistical values and distributions were developed for thunderstorm Cases 1 to 79 in order to make these results comparable across different observed areas.

Table 13 shows the statistical values for the alert and shutdown durations in minutes and for all thunderstorm cases investigated. The duration of an alert is in the range of 32.35 and 339.42 minutes, with a median of 118.12 minutes and a mean 140.96 minutes. The duration of a shutdown is in the range of 13.22 and 204.37 minutes, with a median of 73.88 minutes and a mean of 81.09 minutes. Taking all cases into account, the median duration of an alert is 1.60 times longer than a shutdown. The 10th and 90th percentiles of the alert and shutdown durations are also shown.

Table 13: Statistical values of alert and shutdown duration in minutes, all thunderstorm cases

Measure	**Duration in Minutes**					
	Min	10th	Median	Mean	90th	Max
Alert	32.35	50.22	118.12	140.96	268.81	339.42
Shutdown	13.22	33.72	73.88	81.09	140.16	204.37

Figure 46 visualises these results as a distribution showing the alert and shutdown durations in 15-minute intervals. These intervals include the lower value and exclude the upper value. The alerts show two clusters, one around an interval of 75–90 minutes with 12.7% and another around 180–195 minutes, also with 12.7%. The median and mean durations lie between the two clusters, 13.9% have an alert duration of over 225 minutes. The shutdowns only show an accumulation around the interval of 60–75 minutes with 24.1%. At 13.9%, the interval of 75–90 minutes has the second most values, and the median is also in this interval.

Compared to the results for the 5 km radius, the median value for all thunderstorm cases for alert and shutdown is 25.1% and 10.2% lower, respectively. The distribution shows no significant deviations.

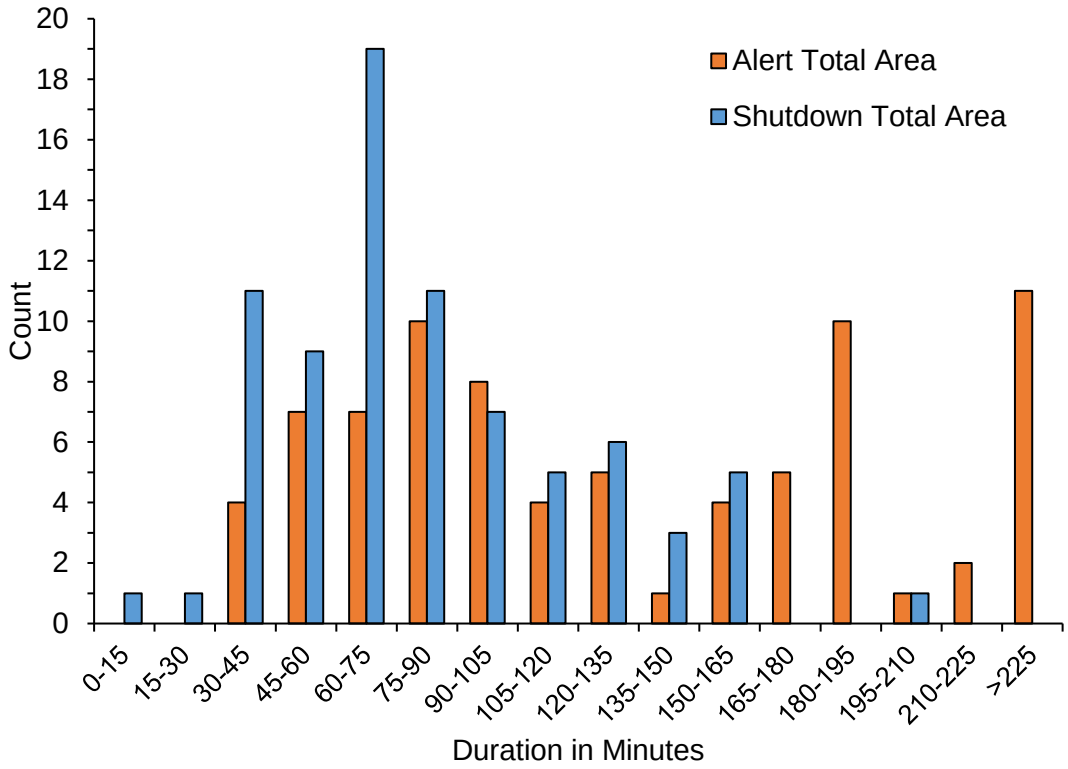

Figure 46: Distribution of alert and shutdown durations in minutes for the total area (30 km) and all thunderstorm cases.

8.3.3 Effective and Non-Effective Alarm Durations

The following comparisons show the differences for alert and shutdown duration in the case of an EA but also for a non-EA. The EAs correspond to Cases 1 to 51 (51 EAs) with CG lightning strikes in 5 km, the non-EAs are Cases 52 to 79 (28 Non-EAs) without CG lightning strikes in 5 km.

Figure 47 illustrates the distribution of alert durations for EA and non-EA in 15-minute intervals (see Section 8.3.1). The alert EAs show a clustering of 15.7% around 75–90 minutes and another 15.7% around 180–195 minutes. 17.6% of all EAs have a duration of over 225 minutes. There are no EAs in the intervals between 0 and 45 minutes. The non-EAs show an equal distribution in the lower intervals of 30–45 minutes, 45–60 minutes and 60–75 minutes with 14.3% each. There are also 14.3% in the interval of 90–105 minutes. With 7.1% per interval or less, durations over 105 minutes occur less frequently. There are no non-EA alerts in the intervals between 0 and 30 minutes.

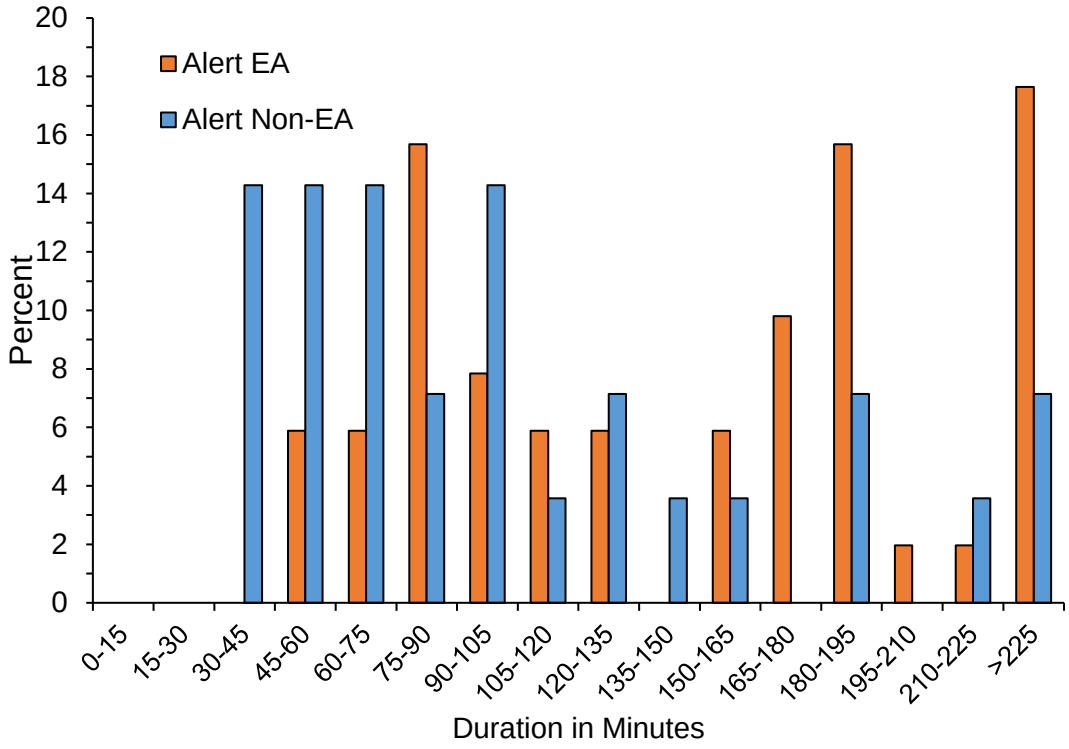

Figure 47: Distribution of alert durations in minutes for effective and non-effective alarms.

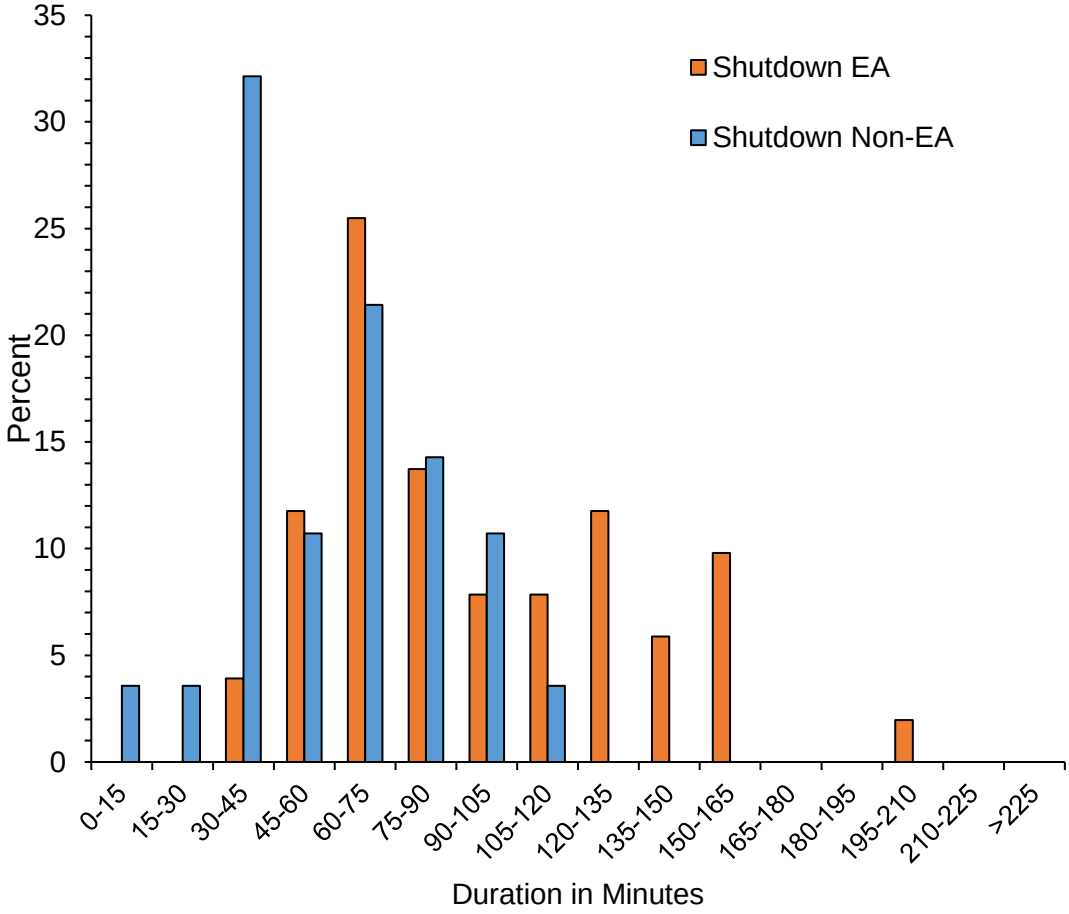

Figure 48: Distribution of shutdown durations in minutes for effective and non-effective alarms.

Figure 48 illustrates the distribution of shutdown durations for EAs and non-EAs in 15-minute intervals. The EAs show a clustering of 25.5% around 60–75 minutes, the second most frequent interval with 13.7% is 75–90 minutes.

The percentage of all other intervals is below this. The maximum shutdown duration for EAs is 204.4 minutes. There are no non-EA shutdowns in the intervals between 0 and 30 minutes. At 32.1%, most non-EA shutdowns are in the interval of 30–45 minutes, while 21.4% of non-EAs are in the interval of 60–75 minutes. The maximum shutdown duration for non-EA is in the interval of 105–120 minutes, so there are no non-EAs over 120 minutes.

8.3.4 Annual Alert and Shutdown Durations

An overview of the shutdown durations per year is shown in Table 14 and Figure 49. 2022 shows the lowest total duration with 1,173.1 minutes for the TNA[23] of alerts and 658.2 minutes for the TNA of shutdowns. Less than 25% compared to the years 2023 and 2024. The reason for this is the start of measurements in August 2022, whereby only part of the entire thunderstorm season could be recorded. The proportion of EA shutdown durations is 92.6% for 2022. The entire thunderstorm season was recorded for the years 2023 and 2024, resulting in similar alert and shutdown durations for those two years.

Table 14: Alert and Shutdown duration per year and in total for EA, Non-EA and TNA.

Year	Alert Duration per Year	Shutdown Duration per Year		
	TNA	EA	Non-EA	TNA
	Minutes		Minutes	
2022*	1173.1	609.6	48.5	658.2
2023	4745.8	2163.7	878.2	3041.9
2024	5217.2	2007.7	698.7	2706.4
Total	11136.1	4781.1	1625.4	6406.5

*The earliest FM recordings started in August 2022, for 2023 and 2024 the full thunderstorm season was recorded.

[23]Total Number of Alarms, described in Section 3.3.1

The average duration for the two years is 4,981.5 minutes and 2,874 minutes for alerts and shutdowns, respectively. The proportion of shutdown durations for EAs is 71.1% and 74.2% for 2023 and 2024, respectively. In total, an active alert was set by the algorithm for 11,136 minutes and a shutdown was triggered for 6,406 minutes during the entire recording period. The proportion of EA shutdown durations is 74.6% overall. If we now compare alerts with shutdowns, we can see that an alert lasts 1.7 times longer than a shutdown.

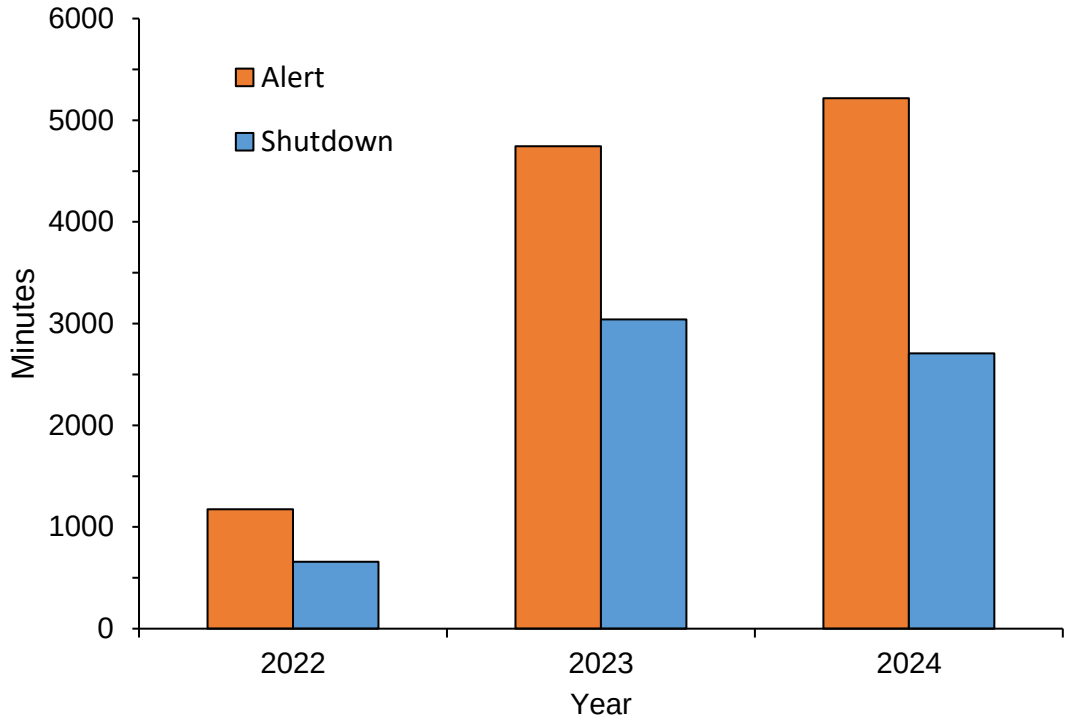

Figure 49: Alert and shutdown durations for 2022, 2023 and 2024 in minutes.

8.3.5 Time to Clear for Effective and Non-Effective Alarms

The distributions in Figure 50 and Figure 51 show the TTC for EAs and non-EAs for alerts and shutdowns, respectively. This is based on 51 cases for EAs and 28 cases for non-EAs. For alerts, most EAs and non-EAs have a TTC in the interval of 30–45 minutes. In this interval lie 41.2% and 57.1% of EAs and non-EAs, respectively. The remaining alert EAs and non-EAs are distributed across the time ranges with a TTC of over 45 minutes. The second most common time interval is 105–120 minutes (11.8%)

for EAs and 75–90 minutes (14.3%) for non-EA alerts. Due to the condition that an alert cannot be longer than a shutdown (see Section 7.3.3), the shortest TTC is 30 minutes.

The TTC for shutdowns is limited for EAs and non-EAs to the intervals of 30–45 minutes, 45–60 minutes, and 60–75 minutes. Most shutdowns, EAs as well as non-EAs, have a TTC in the interval of 30–45 minutes. In this range are 60.8% and 71.4% of shutdown EAs and non-EAs, respectively. There is no discernible difference in the TTC for EAs and non-EAs. Due to the STC1, the minimum TTC for a shutdown is 30 minutes, the maximum is 60 minutes.

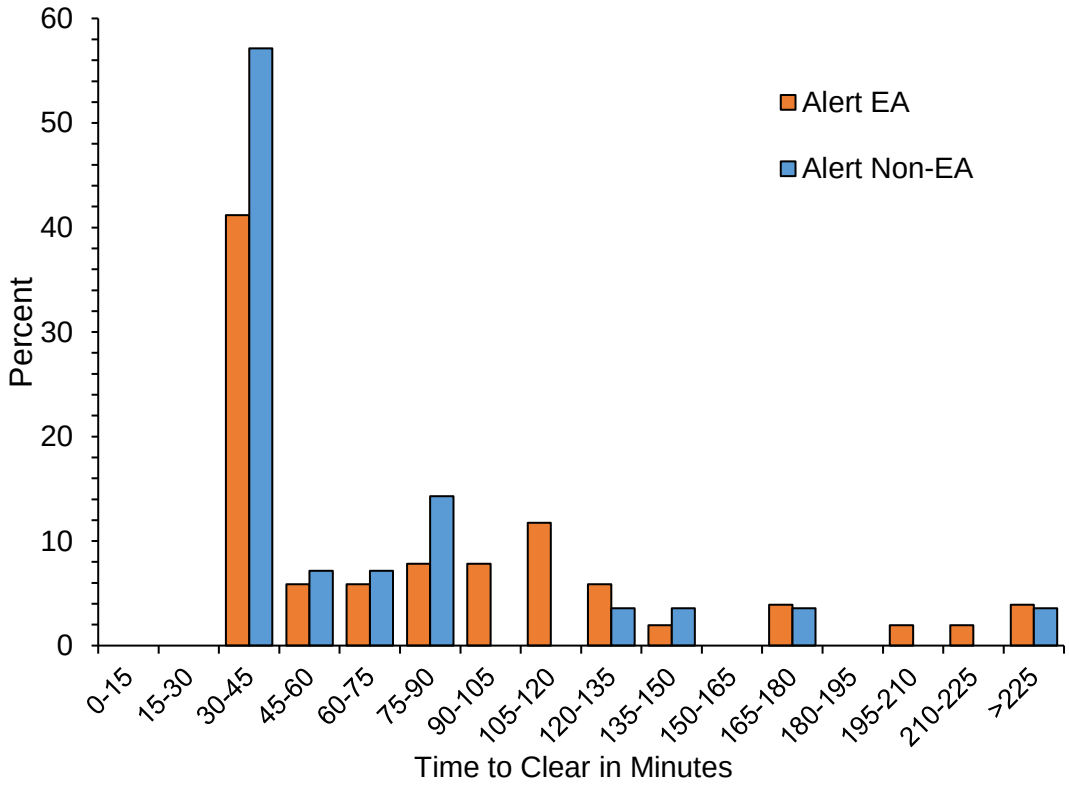

Figure 50: Distribution of TTC for alerts in minutes for effective and non-effective alarms.

The median and mean TTC for shutdowns for all 79 cases are 35.93 minutes and 42.44 minutes, respectively. Considering the different observed areas from 5 km to 15 km radius, the median and mean values each lie in a similar range. The medians and means for shutdown TTC considering the individual areas are shown in Table 15.

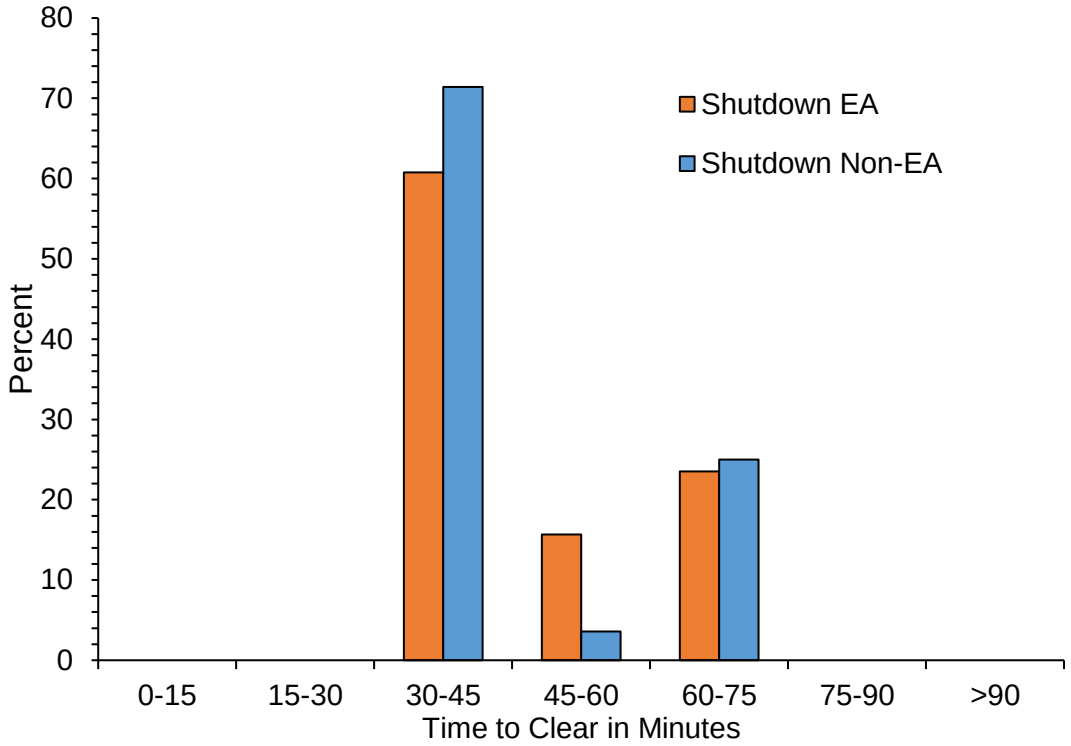

Figure 51: Distribution of TTC for shutdowns in minutes for effective and non-effective alarms.

Table 15: Median and mean TTC for Shutdowns (STC1) and different observed areas (radii) as well as for the total area and all analysed cases.

	Time to Clear for Shutdown				
	5 km	**8 km**	**10 km**	**15 km**	**Total Area**
	Minutes				
Median	35.67	38.80	36.87	35.80	35.93
Mean	42.44	43.16	42.67	42.18	41.99

8.4 Shutdown Termination Criterion 2

8.4.1 Lead Time Performance

The following Sections 8.4.1, 8.4.2 and 8.4.3, show additional results for shutdowns using the STC2 with a TTC of 10 minutes after the last IC discharge or CG lightning strike within 5 km radius or within the 5–8 km radius (see Section 7.3.2). Due to the short TTC, a total of 175 (compared to 79 shutdowns with STC1, see Section 8.3) shutdowns were triggered during the analysed thunderstorms. Again, all thunderstorms on which the algorithm triggered a shutdown were used for these analyses (79 thunderstorm cases on 65 thunderstorm days, see Section 5.4). A

distinction between different observed areas as in Section 8.3 was not carried out for this analysis. The alert periods remain the same and includes the shutdown periods in this analysis. The alerts are therefore not considered in more detail in the following analyses. Note that for 2022 data the earliest FM recordings started on 05 August 2022.

Table 16 shows a correlation between shutdown LTs and duration. For the LT range of 0–2 minutes, shutdowns have a median duration of 10 minutes and a mean of 14.16 minutes within an interval of 10.00 to 29.82 minutes. The optimal LT range of 2–30 minutes shows a median duration of 35.47 minutes and a mean of 40.71 minutes within an interval of 13.97 minutes and 109.55 minutes. For 30–60 minutes, there is only one shutdown with a duration of 71.75 minutes. The category of non-EAs has a median duration of 10.82 minutes and mean of 14.08 minutes in an interval between 2.37 minutes and 49.90 minutes. There are no shutdowns with a LT over 60 minutes. Furthermore, the table shows the 10th and 90th percentile of shutdown durations. Although the LT range of 0–2 minutes and the non-EAs category show a shutdown, the median duration is only around 30% of the duration of a shutdown in the optimum LT range.

Table 16: Statistical values for shutdown durations over lead time ranges and for non-effective alarms, the second column provides the count of shutdowns per lead time range.

Lead Time range	**Count**	**Shutdown Duration**					
		Min	**10th**	**Median**	**Mean**	**90th**	**Max**
Minutes		Minutes					
0–2	13	10.00	10.00	10.00	14.16	27.16	29.82
2–30	46	13.97	19.38	35.47	40.71	74.73	109.55
30–60	1			71.75			
>60	0						
Non-EA	115	2.37	9.47	10.82	14.08	22.51	49.90

Figure 52 depicts the distribution of shutdown LTs and for non-EA for the years 2022, 2023, 2024 and in total. For 2022, 30% are in the optimal range of 2–30 minutes, the rest of the shutdowns are non-EAs. For 2023, the optimal range holds 26.8%, while the rest is distributed over the 0–2 minutes and non-EA category. In 2024 24.7% are in the optimal range and 64.4% are non-EAs. 13 shutdowns had a LT of 0–2 minutes

and one shutdown had a LT of 30–60 minutes, which accounts for 9.6% and 1.4%, respectively. In total 26.3% are in the optimal range and 65.7% are non-EA, while 7.4% and 0.6% are in the range of 0–2 minutes and 30–60 minutes, respectively. None of the shutdowns has a LT of over 60 minutes.

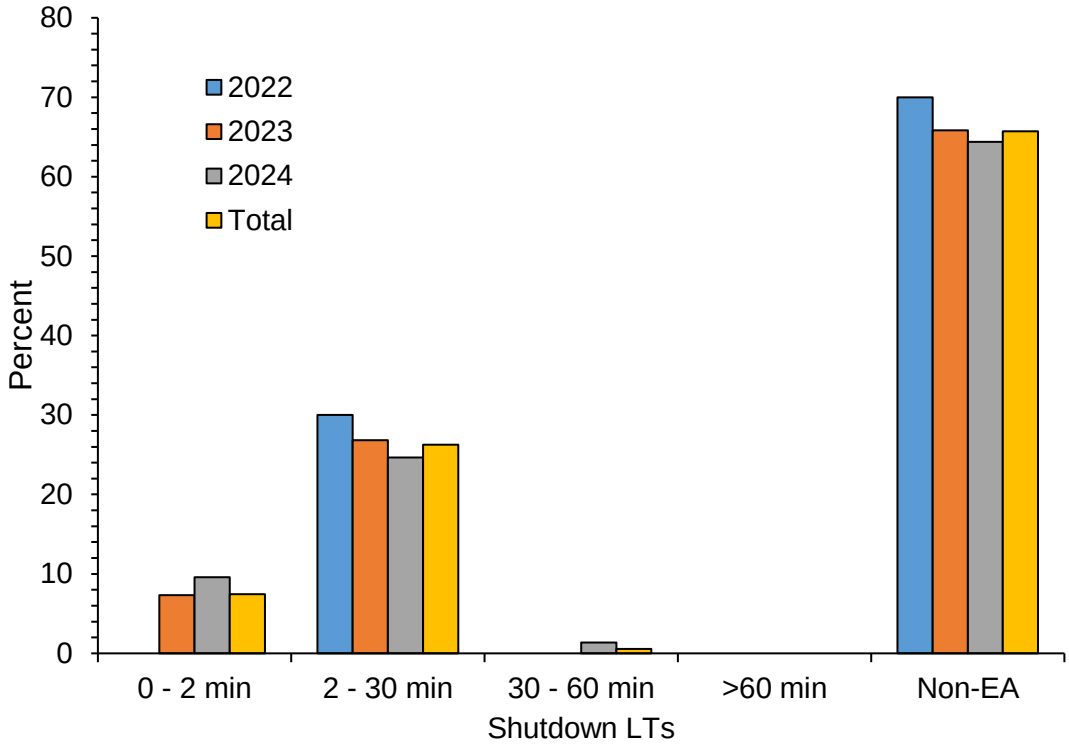

Figure 52: Distribution of shutdown LTs and non-effective alarms for 2022, 2023 and 2024.

Figure 53 shows the distribution of the shutdown criteria for 2022, 2023 and 2024. For 2022, the criteria for 20 shutdowns are almost equally distributed, with 20%, 25%, 25% and 30% for the SIC1, SIC2, SIC3 and SIC4, respectively. In 2023, the SIC3 leads the distribution for 82 shutdowns with 42%, followed by the SIC1 with 30.5%. The remaining share is distributed across the SIC2 (19.5%) and SIC4 (7.3%). A similar distribution is observed for the 73 shutdowns in 2024: the SIC3 accounts for 39.7%, the SIC1 for 37.0%, the SIC2 for 19.2% and the SIC4 for 4.1%.

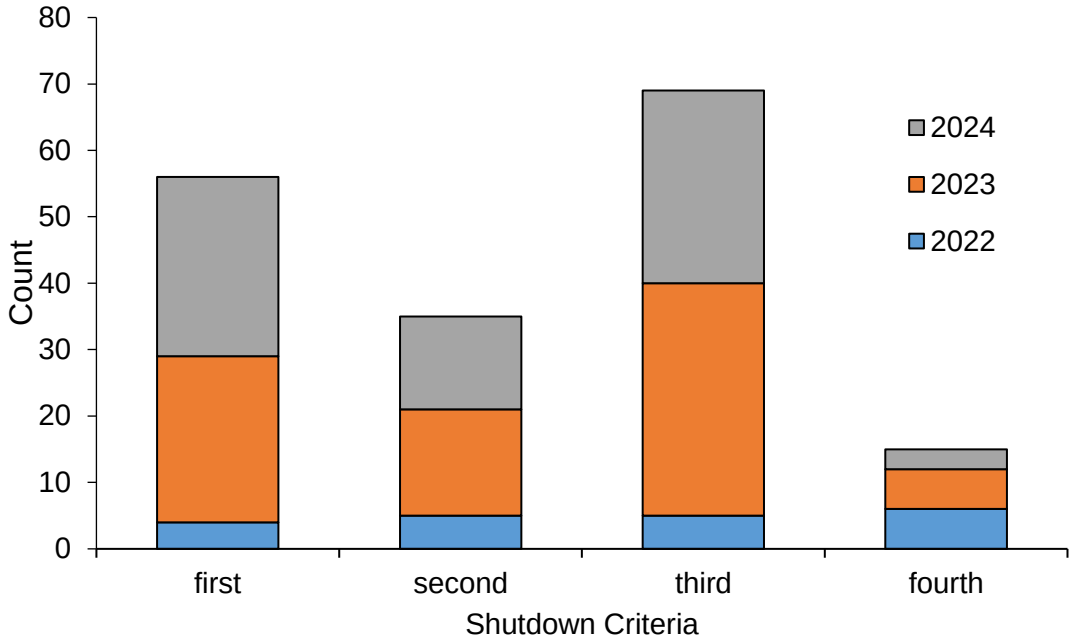

Figure 53: Distribution of shutdown criteria for the years 2022, 2023 and 2024.

8.4.2 Shutdown Duration for Effective and Non-Effective Alarms

This section compares the influence of EAs and non-EAs on shutdown duration for the three investigated years (2022 to 2024). For this purpose, a total of 60 EA and 115 non-EA shutdowns were analysed. Despite the lower number of 20 shutdowns in 2022 compared to 82 in 2023 and 73 in 2024, similar results are evident. No distinction was made between different observed areas; all days on which the algorithm triggered a shutdown were used (175 shutdowns on 65 thunderstorm days; see Sections 5.4 and 8.4.1).

Table 17 includes statistical values for the duration of EAs. These are for 2022, 2023 and 2024. Of the six shutdowns in 2022, the durations ranged from 24.9 to 109.6 minutes, with a median of 35.5 minutes. The 28 shutdowns in 2023 had durations ranging from 10.0 to 100.4 minutes, with a median of 27.7 minutes. The 26 shutdowns in 2024 had durations ranging from 10.0 to 78.0 minutes, with a median of 28.6 minutes. A median of 28.6 minutes and a mean of 35.5 minutes are obtained when considering all years. Additionally, the 10^{th} and 90^{th} percentiles are provided for all years.

Table 17: Statistical values for shutdown durations of effective alarms for 2022, 2023 and 2024 and in total.

Year	Shutdown Duration EA					
	Min	10th	Median	Mean	90th	Max
	Minutes					
2022	24.9	26.4	35.5	45.8	75.5	109.6
2023	10.0	14.8	27.7	34.3	65.7	100.4
2024	10.0	10.0	28.6	34.4	73.1	78.0
Total	10.0	10.0	28.6	35.5	72.3	109.6

Table 18 contains statistical values for the duration of non-EAs for shutdowns from 2022, 2023 and 2024. 14 shutdowns in 2022 have a duration between 2.8 minutes and 42.7 minutes, with a median of 12.0 minutes. For 54 shutdowns in 2023, the durations are between 3.4 minutes and 49.90 minutes, with a median of 13.4 minutes. The 47 shutdowns from 2024 have a duration between 2.37 minutes and 29.65 minutes and the median is 10.0 minutes. An overview of all years results in a median and mean of 10.8 minutes and 14.1 minutes, respectively. The 10th and 90th percentiles are also shown for all years additionally.

Table 18: Statistical values for shutdown durations of non-effective alarms for 2022, 2023 and 2024 and in total.

Year	Shutdown Duration Non-EA					
	Min	10th	Median	Mean	90th	Max
	Minutes					
2022	2.8	5.9	12.0	13.7	20.1	42.7
2023	3.4	10.0	13.4	16.2	28.9	49.9
2024	2.4	8.4	10.0	11.9	18.1	29.7
Total	2.4	9.5	10.8	14.1	22.5	49.9

Table 19 contains statistical values for the duration of the total number of alarms in 2022, 2023 and 2024. 20 shutdowns in 2022 have a duration of between 2.8 minutes and 109.6 minutes, with a median of 13.3 minutes. For 82 shutdowns in 2023, the durations are between 3.4 minutes and 100.4 minutes, with a median of 16.6 minutes. The 73 shutdowns from 2024 have a duration between 2.4 minutes and 78.0 minutes

and the median is 10.0 minutes. An overall view of all years also shows a median of 14.2 minutes and a mean of 21.4 minutes. The 10th and 90th percentiles are also shown for all years.

Table 19: Statistical values for shutdown durations of all shutdowns for 2022, 2023 and 2024 and in total.

Year	Shutdown Duration TNA					
	Min	10th	Median	Mean	90th	Max
	Minutes					
2022	2.8	9.4	13.3	23.3	41.6	109.6
2023	3.4	10.0	16.6	22.3	41.5	100.4
2024	2.4	10.0	10.1	19.9	40.2	78.0
Total	2.4	10.0	14.2	21.4	41.7	109.6

Figure 54 visualise these results as distribution showing the shutdown durations in 15-minute intervals. These intervals include the lower value and exclude the upper value, as described in Section 8.3.2. The left bar represents EAs, the middle bar shows non-EAs, and the right bar indicates the total number of alarms.

The shutdown EA cases exhibit a right-skewed distribution, with a concentration of 40% in the interval of 15–30 minutes. The second-highest proportion is found in the interval of 30–45 minutes, accounting for 25%. Beyond this point, the values gradually decline up to the interval of 105–120 minutes. In contrast, the non-EA cases show a decreasing distribution, with the highest share (70%) in the interval of 0–15 minutes, steadily decreasing up to the interval of 45–60 minutes. There are no non-EA cases with durations exceeding 60 minutes. The second-highest share of non-EA cases is in the interval of 15–30 minutes, at 25%. The TNA also follows a decreasing pattern, with a peak of 50% in the interval of 0–15 minutes. Another 25% are within the interval of 15–30 minutes, after which the distribution steadily declines up to the interval of 105–120 minutes. No shutdown exceeds 120 minutes in duration when applying STC2.

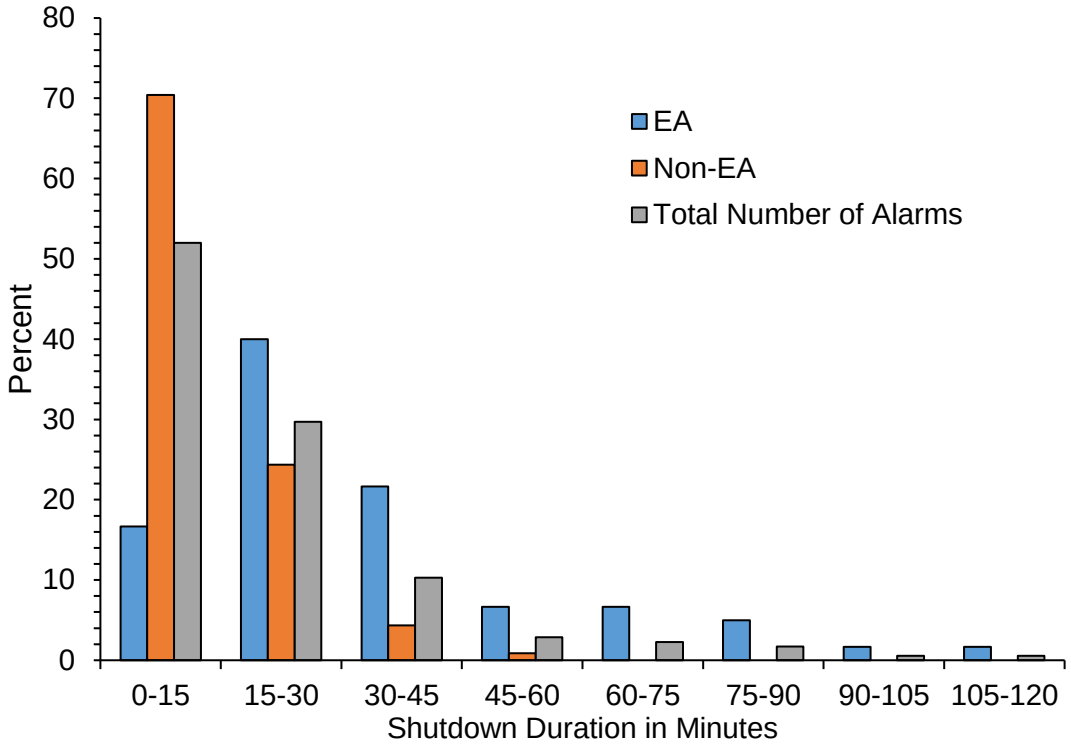

Figure 54: Distribution of shutdown durations for EA, Non-EA and TNA, all shutdowns are within these intervals.

8.4.3 Annual Shutdown Duration

An annual overview of the total shutdown durations, when using STC2 and a TTC of 10 minutes, is shown in Table 20. The year 2022 shows the lowest total duration with 467 minutes for the TNA of 20 shutdowns. Less than 33% compared to the years 2023 and 2024. The reason for this is the start of measurement in August 2022, whereby only part of the entire thunderstorm season could be recorded. The proportion of EAs in 2022 is 58.9% for shutdown durations. The entire thunderstorm season was recorded for 2023 and 2024, resulting in similar shutdown durations for both years. In 2023, 82 shutdowns have a total duration of 1831 minutes and in 2024, 73 shutdowns have a total duration of 1450 minutes. The percentage for shutdown durations in EAs is 52.5% and 61.58% for 2023 and 2024, respectively. All 175 shutdowns (see Section 8.4.1) in total lasted 3748 minutes. The share for shutdown durations by EAs is 56.8% overall.

Table 20: Shutdown duration per year for 2022, 2023, 2024 and in total; EA, non-EA and total number of alarms, durations in minutes; count of shutdowns in parenthesis.

Year	Shutdown duration per year		
	EA	Non-EA	TNA
	Minutes (Count)		
2022*	275 (6)	192 (14)	467 (20)
2023	961 (28)	871 (54)	1831 (82)
2024	893 (26)	557 (47)	1450 (73)
Total	2128 (60)	1620 (115)	3748 (175)

*The earliest FM recordings started in August 2022, for 2023 and 2024 the full thunderstorm season was recorded.

8.5 Influence of Different Thunderstorm Types on Shutdown Triggering

The influence of the thunderstorm type on the performance is presented in this section. Therefore 47 thunderstorms in 44 thunderstorm days were classified by the meteorologist Dr. Rudolf Kaltenböck as described in Section 6.2. The types are single cell, multi cell, super cell and squall line thunderstorms. The differentiation was performed using 2D MaxCappi weather radar data. In the years studied (2022, 2023, and 2024) and among the 47 thunderstorms, all four types of thunderstorms were observed. Eleven thunderstorms showed hybrid or transitional forms, in these cases, the predominant type was chosen as representative by the expert. The following analyses refer to thunderstorms within a radius of 5 km, which are shown in Section 8.2.2. Shutdowns were cleared using STC1 (see Section 7.3.1).

Table 21 shows the range of shutdown LTs and the median for the different thunderstorm types. Eight thunderstorms were of the single-cell type with LTs between 4.05 minutes and 24.98 minutes and with a median of 11.07 minutes. A total of 28 of the analysed thunderstorms have been categorised as multicell. Multicell thunderstorms show LTs between 0 minutes and 83.89 minutes, with a median of 16.48 minutes. The supercell type occurred in only three thunderstorms, which should be considered when making comparisons. The three supercell thunderstorms (e.g., Figure 55) show a minimum, median, and maximum LT of 0, 7.58, and 23.77 minutes, respectively.

For the supercell thunderstorms, it should be noted that none of the three thunderstorms passed directly over the airport, but only grazed it with the edge of the thunderstorm. The squall line type occurred in eight thunderstorms with a LT of 3.87 to 19.37 minutes and a median of 11.08 minutes.

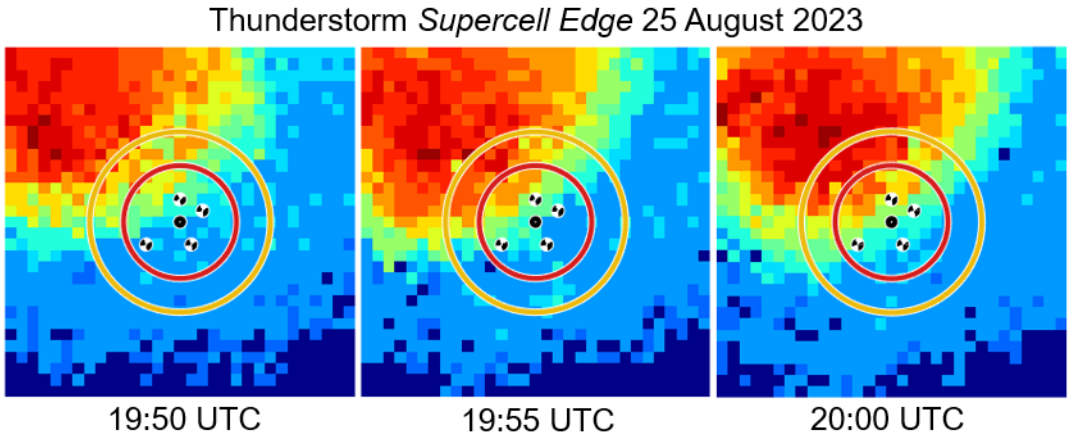

Figure 55: Radar images of a classified supercell thunderstorm on 28 August 2023 from 19:50 to 20:00 UTC passing the 5 km radius with its edge.

Table 21: Shutdown lead times (minimum, median and maximum) in minutes for different thunderstorm types, second column shows the number of thunderstorms per thunderstorm type.

Thunderstorm type	Number of Thunderstorms	Shutdown Lead Times in Minutes			
		Min	Median	Mean	Max
Single-cell	8	4.05	11.07	12.84	24.98
Multicell	28	0	16.48	24.99	83.98
Supercell	3	0	7.58	10.45	23.77
Squall line	8	3.87	11.08	10.81	19.37

Table 22 shows the range of shutdown durations and the median for the different thunderstorm types. Single-cell thunderstorms show the shortest shutdowns with a median duration of 72.27 minutes, 22.1% shorter than the median for multicell thunderstorms (92.74 minutes). All three supercell thunderstorms hit the 5 km radius and Graz Airport only at the edge, resulting in comparatively short shutdown durations for these long-lived thunderstorms, with a median of 91.02 minutes in the multicell range.

Table 22: Shutdown durations (minimum, median and maximum) in minutes for different thunderstorm types, second column shows the number of thunderstorms per thunderstorm type.

Thunderstorm type	Number of thunderstorms	Shutdown duration in Minutes			
		Min	Median	Mean	Max
Single-cell	8	48.28	72.27	77.71	124.47
Multicell	28	44.9	92.74	103.42	204.37
Supercell	3	33.48	91.02	77.64	108.43
Squall line	8	60.92	72.69	86.64	157.23

Table 23 shows how the shutdown criteria are distributed among the respective thunderstorm types. Here, similar to the analyses in Section 8.2.3, the SIC3 occurs most frequently for all thunderstorm types. Supercells have been excluded here due to the small sample size of 3 thunderstorms. The second most frequent criterion is the SIC1. It stands out that only multicell thunderstorms were triggered by the SIC2.

Table 23: Shutdown criteria distribution for different thunderstorm types.

Thunderstorm type	Number of Thunderstorms	Shutdown criteria			
		SIC1	SIC2	SIC3	SIC4
Single-cell	8	3	0	5	0
Multicell	28	8	6	11	3
Supercell	3	2	0	1	0
Squall line	8	3	0	4	1

8.6 CNN Supported Pre-Classification of LLS and Weather Radar Data

The following section provides an overview of the training of five different CNN models using LLS and weather radar data. For the analysis radar data from 2020, 2021 and 2022 to train CNN models have been used (Schwalt et al., 2024 [58]).

The success of the training was evaluated by comparing the accuracy and loss curves of classification for each training unit. Figure 56 shows an example of this evaluation, depicting the accuracy and loss curves for the pre-trained (PT True) SqueezeNet model without feature extraction (FE False) for the balanced dataset.

The close alignment of the training and validation accuracy suggests that the CNN model was effectively trained. The loss curves for training and validation of the models were also evaluated (see Figure 56). Once again, convergence of the validation and training loss curves can be observed. This underscores the capability of automatic flash detection in the analysed weather radar data using CNN models.

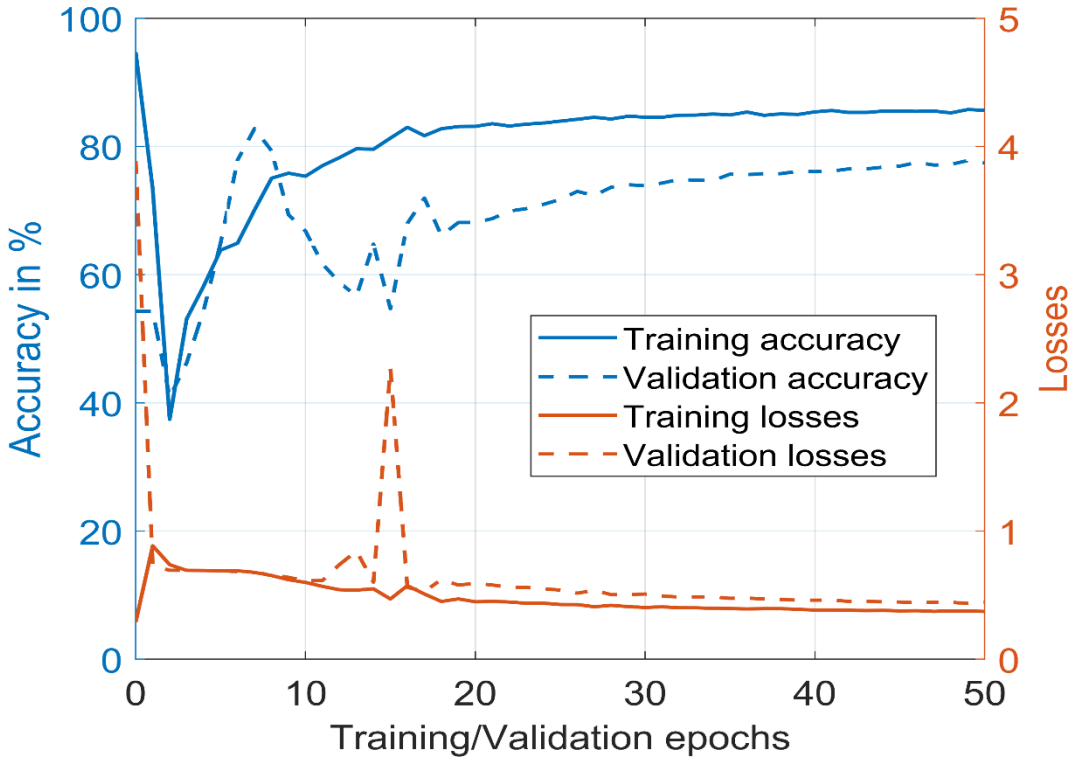

Figure 56: Accuracy and loss curves for the pre-trained SqueezeNet model without feature extraction for the balanced data set.

Figure 57 shows an example of radar image classification, along with the classification results for the balanced dataset and the AlexNet model for PT True and FE True (see Table 24).

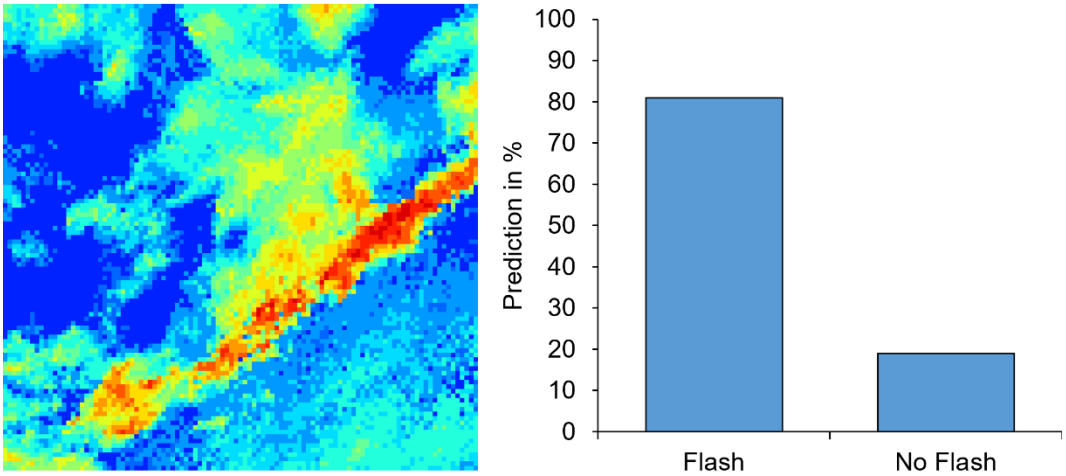

Figure 57: Classification of radar images of 100 km × 100 km and categorisation results for the balanced data set and the AlexNet model, PT True and FE True (80.96%).

Radar images from 2020 were used to test and analyse the trained CNN models. For this year, there were 2,700 images with at least one flash and 41,000 images without a flash (“No Flash” class) have been included. To improve comparability between the models, the prediction accuracy achieved is shown in Table 24.

Table 24: Prediction accuracy of the CNN models, Pre-Trained (PT) or not PT and with (True, T) or without (False, F) Feature Extraction (FE), for different distributions of the data sets.

Model	PT	FE	Unbalanced	<95% Blue	Balanced
			%	%	%
AlexNet	T	T	65.74	63.91	80.96
AlexNet	T	F	75.09	79.05	87.22
DenseNet	T	T	50.00	50,00	50.00
DenseNet	T	F	50.00	50.00	50.00
ResNet	T	F	50.72	51.46	51.92
ResNet	F	F	50.00	50.00	50.00
SqueezeNet	T	F	63.47	59.90	89.84
SqueezeNet	F	F	50.00	51.22	50.00
VGG	T	F	53.18	53.22	50.00
VGG	F	F	50.35	50.39	50.29

The highest accuracies were obtained using a balanced data set. Among the models, SqueezeNet achieved the top performance in the pre-trained case without feature extraction (FE), with a prediction accuracy of 89.84%. AlexNet followed with an accuracy of 87.22% in the same configuration, and 80.96% when feature extraction was included.

DenseNet, ResNet and VGG all failed to train on the dataset, consistently assigning all data to the “No Flash” class. Interestingly, the non-pretrained SqueezeNet model without feature extraction also failed to train successfully, despite the pretrained version achieving the highest accuracy. Of the CNN models that successfully completed training, all demonstrated improved accuracy corresponding to enhancements in data distribution.

9 Discussion

9.1 Assessment of Prediction Parameters

Despite the fact, that different approaches using mathematical models and deep learning for short-term forecasts of lightning have been published (e.g., Mansouri et al., 2023 [16]; Antonescu et al., 2013 [17]), they still do not provide an accurate prediction or localisation of lightning strikes. By analysing 44 thunderstorms from the 2022, 2023 and 2024 thunderstorm seasons, producing CG lightning strikes within the 5 km radius, universal predictive parameters for lightning onset in E-field, LLS and weather radar data in the surroundings of Graz Airport could be defined.

Due to the diversity of different thunderstorms, the analyses have shown that a single criterion, like an E-field threshold, is not sufficient for reliably triggering a shutdown. The box plots in Figure 37, Section 8.1 show that the use of single parameters lead to a large scattering regarding the time of initiation of an alert or shutdown. The extended analyses of FM, LLS and weather radar data of 79 thunderstorms with and without CG lightning strike in a surrounding area of 5 km radius around Graz Airport revealed predictive parameters to predict the onset of the first CG lightning strike. By logically linking these parameters, a shutdown was successfully initiated for 47 of 79 cases of 2022, 2023 and 2024. Due to this linking, a long LT of a single parameter (e.g., Zero Crossing E-field) won't negatively affect shutdown LTs or leads to non-EAs. The parameters appear to be universally applicable for future thunderstorms in the area. Looking at the results, the most important parameter for time optimisation is the shutdown LT.

Under the most important aspect of personal protection, shutdown LTs of less than 2 minutes are too short. Although in some cases, shutdown LTs did not meet this 2-minute limit, all alert LTs exceeded 2.42 minutes. Under this aspect, also short shutdown LTs may be acceptable under this condition. A shutdown LT of at least 2 minutes was defined to be sufficient to seek shelter, e.g., in a vehicle on the apron or indoors. The four Cases 1, 11, 46 and 47 with a zero-minute shutdown LT (i.e., FTW) had alert LTs over 46.5 minutes. For the extended analyses, the median shutdown LT of 12.83 (initial analyses: 12.35 minutes) minutes and the mean shutdown

LT of 19.10 minutes (initial analyses: 19.85 minutes, see Section 8.2.1 and Section 8.2.2) fits within the range of published mean LTs from 13 to 17 minutes, but the observed area of 5 km radius is smaller compared to the published observed areas, ranging from a 10 km radius up to an observed area of south Romania. This underlines the high performance of the presented prediction model for such a small observed area (Silva Ferro et al. [12]; Rodriguez et al. [14]; Antonescu et al., 2013 [17]).

9.2 Lead Time Analyses for Alerts and Shutdowns

Compared to the results from the initial analyses (see Section 8.2.1), six additional thunderstorm cases with at least one CG lightning strike within a 5 km radius of Graz Airport were included in the extended analyses (see 8.2.2). In some cases, multiple triggers of the same shutdown or shutdown LT occurred almost simultaneously as multiple shutdown criteria were met. For further analyses, only the chronologically first fulfilled criterion that triggered the shutdown was considered, regardless of its designation (i.e., SIC1, SIC2, SIC3, SIC4 and SIC5, see Section 7.2.2). To use the first shutdown initiation criterion, SIC1, the inclusion of additional radar and E-field conditions was necessary because, although the “IC in 5 km” parameter offered optimal shutdown LTs, it occasionally led to excessively long LTs, reducing its effectiveness as a one parameter override criterion. The SIC4 takes into account cases in which the first IC or CG lightning strike in the 5–8 km radius occurs immediately before the first CG within the 5 km radius. The SIC5 criterion was only used for the results of initial analyses shown in Section 8.2.1, but was excluded from extended analyses, as it results in a high number of non-EAs due to the low thresholds set for the E-field and weather radar parameters under this criterion.

For some cases the “First CG” were poorly located, showing low-quality LLS data and were therefore manually reclassified by Wolfgang Schulz (see Section 8.2.1). These “First CG” events were misclassified IC discharges. As a result, these cases would fall into the 5–8 km (or 8–10 km) categories. Due to the disproportionate effort required, but also the high performance of the Austrian LLS (Kohlmann et al. 2017 [95], see Section 4.4), a manual classification of all investigated cases was not performed. Furthermore, misclassifications in the opposite direction (i.e., CG lightning strikes classified as IC discharges or vice versa) may also occur. To avoid unbiased results,

the entire LLS dataset for the investigation period would need to be reclassified manually an effort not justified by the scope of this work. Therefore, the analyses and results are based solely on the original LLS classification, which also reflects the conditions of real-world application.

In addition to the fact that the choice of FM network sites and the developed algorithm were designed to predict CG lightning strikes within a surrounding area of 5 km radius, Section 8.2.3 analyses how extending this area affects the prediction as well as the alert and shutdown systems. The 28 Cases 52 to 79 had no CG lightning strikes within the 5 km radius or no CG lightning strikes at all and are therefore classified as cases with non-EA shutdowns. If the surrounding area were extended to include the 5–8 km radius, there would be six FTW (Cases 52–57) and twelve EAs (up to Case 69). Including the 8–10 km radius would add three FTW (Cases 70–72) and one additional EA (up to Case 73). Extending the surrounding area to 15 km would add three more EAs (Cases 74–76), all within the optimal LT range. Considering all cases in which the algorithm triggered a shutdown, the remaining three cases (Cases 77–79), where thunderstorms produced no CG lightning strikes are classified as non-EAs. This analysis shows, that Non-EA, EA and FTW depend as expected directly on the defined surrounding area. For a reliable prediction of CG lightning strikes in extended surrounding areas, both the algorithm and the FM network (i.e., additional FMs in the respective areas) would need to be adapted.

Comparison of Shutdown Lead Time Ranges

To make Shutdown LTs comparable, four areas were specified. As discussed, LTs of less than two minutes are considered insufficient for taking protective action. The optimal range is between two and 30 minutes, which aligns with real shutdown LTs by ACG. Lead Times over 30 minutes may unnecessarily disrupt airport operations, and those exceeding 60 minutes are considered inadequate outliers. The selected ranges are based on values from the literature (e.g., Silva Ferro et al. [12]; Rodriguez et al. [14]; Antonescu et al., 2013 [17]) and the standard (OVE, 2022 [5]), which provides examples such as of different LTs, but no fixed limits as well as actual shutdowns issued by ACG between 2018 and 2021 (see Appendix D).

A comparison of shutdown LT for lightning strikes based on results from the initial analyses in Section 8.2.1 and the extended analyses in Section 8.2.2 is given in Table 25. The LTs for the initial analyses include a 90-minute time limit (see Section 7.1) and the SIC5 (see Section 7.2), while the extended analyses exclude them. The 90-minute limit was excluded for extended analyses as it is not possible to define an onset time for thunderstorm during continuous monitoring of the data. When results are compared, it shall be noted that the percentages for the initial analyses and for the extended analyses were calculated from 45 and 51 cases, respectively. The extended analyses show 3.5 times higher percentage for shutdown LTs of less than 2 minutes, but still just 7.8%. The percentage of LTs in a range of 2–30 minutes dropped to 72.5%, while the percentage in a LTs range 30–60 minutes increased to 15.7%. When these two LT ranges are considered together, the difference is small (91.1% for initial analyses vs. 88.2% for extended analyses for shutdown LTs from 2 to 60 minutes). For LTs over 60 minutes, the percentage drops to 3.9% in the extended analyses, which can be considered an improvement.

Table 25: Comparison of shutdown LT ranges for lightning strikes within a 5 km radius based on results from the initial analyses (with 90-minute limit and SIC5) versus the extended analyses (without 90-minute limit and SIC5).

Lead Time Range	**Initial Analyses**	**Extended Analyses**
minutes	%	%
Less than 2	2.2	7.8
From 2 to 30	80.0	72.5
From 30 to 60	11.1	15.7
Over 60	6.7	3.9

The pre-season thunderstorm Cases 1 and 72 from 16.04.2024 and 23.04.2023 were recorded previously to the convective thunderstorm season (May–September) in Austria (see Sections 8.2.2 and 8.2.3). Case 1 showed features of a winter thunderstorm in Austria and its only CG lightning strike in 5 km radius was missed by the algorithm. No shutdown LT was provided for the first CG in 5 km and thus led to an FTW. Case 72 showed mild temperatures and a high lightning frequency. The nearest

CG lightning strike for this case was in 8–10 km radius. A detailed description of these thunderstorms can be found in Appendix C.

The alert LTs presented in Table 3 and Table 4 are not analysed or discussed in such detail but they are included in the statistical analyses for LTs and duration in Section 8.3. Alerts serve as an early warning preceding shutdowns, which is shown to be effective in Sections 8.2 and 8.3. Except for one case, the alert LTs were always ahead the corresponding shutdown LTs. However, the main focus of the evaluation lay on the shutdown LTs.

Borderline Cases

The limitations given by the quality of the LLS data for analysis with such strict constraints (surrounding area of 5 km) described in Section 4.4 also impose restrictions on the location accuracy, which lies at a median of approx. 100 m but up to 3.5 km for lightning strikes with low detection quality are possible (Schwalt et al., 2020 [56]). Further, Schwalt and Schulz, 2023 [57] revealed a median distance between two ground strike points of the same lightning strike of 1.4 km and a maximum distance of 6.9 km for CG lightning strikes in the alpine region. Therefore, and because LLS data are used not only for forecasting but also for verification, a buffer zone with a radius of 5 ± 0.5 km was defined. Cases with CG lightning strikes within this area were marked as borderline cases.

Among the 79 cases analysed, 20 were identified as borderline cases, 18 within the 5 km radius (Table 4, Section 8.2.2) and two in the 5–8 km radius (Table 5, Section 8.2.3). If CG lightning strikes within this buffer zone were used as the first CG, and they happened before the one currently used in the analysis, it would result in a shorter LT.

For 14 of the 20 borderline cases, the analysis shows no change in the shutdown LTs, as CG lightning strikes occurred simultaneously or shortly after the first CG lightning strike used. As shown in Sections 8.2.2 and 8.2.3, for the remaining six borderline cases, the shutdown LTs are shortened by 0.55 to 17.07 minutes. There is an improvement in two cases, which are shifted from the LT range of 30–60 minutes to

the optimal range of 2–30 minutes. This shows that extending the surrounding area by this buffer area does not bring a significant improvement.

Considering a wider buffer zone of up to 7.5 km radius (instead of 5 km) would further shorten the LTs in some cases (e.g., Cases 41 and 42) and thus improve them, in other cases it can also lead to additional FTW. More FTW can appear, when the algorithm may trigger a shutdown because of CG lightning strike outside of 5 km radius (which are used in the parameter “IC/CG in 8 km”, see Section 7.1) and there is therefore no LT. The shutdown criteria would have to be adjusted accordingly in order to avoid many FTWs in larger surrounding areas.

Since the algorithm is optimised for a shutdown radius of 5 km, its ability to predict CG lightning strikes beyond this range is limited. This is especially evident in Case 52 and Case 53 in Table 5, Section 8.2.3, both of them show negative shutdown LTs, meaning the nearest CG lightning strike for each case occurred before the algorithm was triggered and was therefore missed.

9.3 Shutdown Termination Criterion 1

The STC1 resolves the shutdowns for the analyses in Section 8.3. While the minimum shutdown TTC is set to 30 minutes, the actual TTC depends also on E-field values and weather radar parameters. Resolution occurs after 60 minutes at the latest, regardless of other parameters (see Section 7.3.1).

Lead Time Performance

For the alert distribution in Section 8.3.1, no alert LTs are below two minutes. Most alerts occur within the range of 2–30 minutes, then gradually decrease for all observed areas up to beyond 60 minutes. Within a 5 km radius, all alerts are classified as EAs, resulting in 100%. When the observed area is extended to 8 km radius, the proportion of non-EAs rises to 26.1%. When all 79 cases are considered, non-EAs increase further to 35.4%. Thus, the EA rates for the 8 km radius and for all cases are 73.9% and 64.6%, respectively.

The distribution of shutdowns follows a similar pattern. Fewer than 8% of shutdown LTs are under 2 minutes. The highest accumulation is again in the range of 2–30 minutes, gradually decreasing up to over 60 minutes across all observed areas. Within a 5 km radius, 72.5% of shutdowns are classified as EAs. When the observed area is extended to 8 km radius, the proportion of non-EA shutdowns rises to 26.1%, and to 35.4% when all 79 cases are included. This results in EA rates of 68.1% for the 8 km radius and 59.5% for the complete dataset.

Alert and Shutdown Duration

As expected, the results show that across all observed areas, alerts generally last longer than shutdowns, both in individual cases and in statistical measures. Alerts, with their lower thresholds, were developed to trigger before a shutdown and also include them. Therefore, they have to have a longer duration than shutdowns. For example, within the 5 km radius, the median alert duration is 1.92 times longer than the median shutdown duration. This difference decreases with larger observed areas and drops to 1.60 times when considering all cases. Likewise, the median shutdown duration decreases from 82.23% (relative to the total alert duration) in the 5 km radius to 73.88% across all cases. The distributions of alert and shutdown durations follow a similar pattern across all observed areas. Shutdown durations cluster around the intervals of 60–75 minutes and 75–90 minutes, aligning with the median duration. Alert durations, however, show peaks at intervals of 60–75 minutes, 180–195 minutes, and above 225 minutes, with no clear trend. The shortest shutdown durations fall within the interval of 0–15 minutes, one anomaly that can be explained by Case 52, a non-EA. The first CG lightning strike in the observed area of 5–8 km radius occurred 20.32 minutes before the shutdown was triggered. The last IC discharge in 5 km (indicator for STC1, starting point for TTC) occurred 27.10 minutes before the shutdown, so 6.78 minutes before the first CG lightning strike. The TTC in this case was 40.32 minutes. This led to a shutdown duration of 13.22 minutes, while the minimum TTC is 30 minutes.

A comparison of EA and non-EA durations shows that, for both alerts and shutdowns, non-EAs are consistently shorter than EAs. For shutdowns, non-EAs most frequently fall in the interval of 30–45 minutes, while EAs peak in 60–75 minutes. The longest

durations are in the interval of 105–120 minutes for non-EAs and 195–200 minutes for EAs.

Even though non-EAs have been triggered by the system, their durations are shorter than the one of EA. For future analyses one approach would be to find criteria to further reduce the total duration of non-EAs, as it is not expected that the proportion can be lowered to zero. This conclusion refers to the observed variability of the analysed thunderstorms which, for example, can have very high radar values or variability in the E-field even in the case of no CG lightning strikes in the radius of 5 km appearing. This emphasizes the limited suitability of using FMs as a standalone solution for TWS (see Appendix E).

An overview of total alert and shutdown durations per year shows similar values for 2023 and 2024, with a full thunderstorm seasons were recorded for those years. Due to the first FM recordings starting in August 2022 shows significantly lower alert and shutdown duration of about 30% of the durations for 2023 and 2024 for each alert and shutdown duration.

Overall, alerts last 1.7 times longer than shutdowns. Non-EA shutdowns account for about a quarter of the total annual shutdown duration triggered by the algorithm. Across all years, the total alert duration is 11,136 minutes (186 hours), while the total shutdown duration is 6,407 minutes (108 hours).

Time to Clear for Effective and Non-Effective Alarms

For alerts, most EAs (41.2%) and non-EAs (57.1%) have a TTC between 30–45 minutes. The rest are spread across longer durations, with 11.8% of EAs ending in 105–120 minutes and 14.3% of non-EAs in 75–90 minutes. Due to the condition that an alert cannot outlast a shutdown, the minimum TTC is 30 minutes. For shutdowns, TTC is limited to 30–75 minutes. The majority of EAs (60.8%) and non-EAs (71.4%) for shutdowns fall within the interval of 30–45 minutes. There is no significant difference in TTC between EA and non-EA shutdowns. The minimum duration is set by STC1, and the maximum is 60 minutes. The STC1 and the end of alert criterion are based on the fact that, during the dissipation stage of a thunderstorm, the cloud structure starts to degrade and so it breaks down and the electric charges gradually dissipate.

Additionally, as a thunderstorm moves away from the observed area (Figure 9, Phase 3, Section 3.1), the charge centre of the thunderstorm also shifts further from the measurement locations. As a result, radar reflectivity decreases for the observed area and falls below threshold values. Furthermore, the absolute values of the E-field decrease, and the rate of change in the E-field slows down, with zero crossings observed. Ultimately, the frequency of lightning strikes within the observed area also declines.

This comparison shows that parameter changes are associated with compromises. Increasing the observed area increases the number of EAs or the non-EAs while the surrounding area (5 km radius) remains the same. When considering only thunderstorm cases with CG lightning strikes within a 5 km radius, 72.5% of EA shutdowns are in the optimal lead range, and no non-EAs occur. However, when the observed area is expanded to a 30 km radius (total area) and all cases are included, the proportion of non-EA shutdowns increases to 35.4%. Consequently, the EA rate within the optimal lead time range drops to 59.5%.

9.4 Comparison of Shutdown Termination Criteria 1 and 2

Due to the short TTC of 10 minutes defined by STC2 (see Section 7.3.2), the frequency of shutdowns increases, despite the number of thunderstorm cases being the same as under STC1. Thus, even cases with CG lightning within a 5 km radius can lead to non-EA shutdowns over the duration of the thunderstorm. For a general performance analysis of the system under STC2, all 79 cases within the 30 km observed area were analysed. Unlike STC1, no breakdown by different observed areas was carried out. Since alerts remain identical under both STC1 and STC2, they are not discussed further.

Because of the shorter TTC (i.e., time to clear a shutdown) of STC2 and the continuously running algorithm with its four shutdown criteria (SIC5 was excluded for extended analysis, see Section 8.2.2), a new shutdown is initiated as soon as one or a combination of the shutdown criteria are met again. This results in 175 shutdowns (see Section and 8.4.1) under STC2: 47 EAs, 13 FTWs, and 115 non-EAs. In

comparison, STC1 led to 79 shutdowns with 47 EAs, 4 FTWs, and 28 non-EAs. While the proportion of non-EA shutdowns under STC2 is significantly higher (65.7% for STC2 vs. 35.4% for STC1), the total annual shutdown duration is relatively low compared to STC1.

The total duration of all STC2 shutdowns is 3,748 minutes (62 hours), with 2,128 minutes (35 hours) for EAs and 1,620 minutes (27 hours) for non-EAs. Compared to STC1 (6,407 minutes or 107 hours), this represents a reduction of 41.5% in total duration, 55.5% for EAs, and 0.3% for non-EAs. EA shutdown durations lasted longer overall, with a consistent median around 28.6 minutes across all years. Individual shutdowns ranged from around 10 to over 100 minutes. In contrast, non-EA shutdowns were significantly shorter, with medians ranging from 10.0 to 13.4 minutes and no shutdowns exceeding 60 minutes. The distribution of EA shutdown durations shows a right-skewed pattern, peaking in the interval of 15–30 minutes (40%) and gradually declining at higher intervals. Non-EA shutdown durations are concentrated in the interval of 0–15 minutes (70%), and no duration is longer than 60 minutes. The TNA of shutdown durations follow a similar trend to non-EA cases, with 50% lasting under 15 minutes and 25% in the interval of 15–30 minutes. No shutdowns exceeded a duration of 120 minutes. The distribution of shutdown durations shows significantly lower values than for STC1.

For STC2, the distribution and statistical parameters of the TTC for are not presented in detail, as it is always 10 minutes (see Section 7.3.2). This applies to all 175 related to STC2.

Reducing shutdown duration or TTC leads to an increase for both non-EAs and FTWs but can also significantly reduce the overall shutdown duration (107 hours for STC1 vs. 62 hours for STC2). The rise in non-EA cases occurs, for example, when a shutdown is terminated 10 minutes after a CG lightning strike, while the shutdown initiation criteria are still met. A new shutdown is then triggered, but no CG lightning strike occurs in the short interval that follows. Conversely, the increase in FTW cases happens because a shutdown is ended and immediately re-initiated with the next CG lightning strike within 5 km radius. These results reveal a trade-off between minimizing downtime and maintaining safety margins. Since no universally optimal setting exists,

the most effective approach depends on the specific operational context and risk tolerance.

9.5 Influence of Different Thunderstorm Types on Triggering Shutdowns

Due to the sample size of 47 thunderstorms analysed in Section 8.5, no definitive conclusions can be drawn regarding a correlation between shutdown triggering and thunderstorm types. However, a general trend is apparent: multicell thunderstorms are the most common ones in the observed area (59.6% multicells). This is expected, as multicells are the predominant thunderstorm type in Central Europe (mid-latitudes) (Markowski and Richardson, 2010 [37]). As noted in Section 6.2, hybrid or transitional thunderstorm forms were observed and the predominant type was selected for the analysis by the expert. Again, further subdivision of those hybrids was not carried out for the share of cases in the analysed data set (11 vs. 47 in total).

It was observed that LT performance varied by thunderstorm type. Single-cell storms (8 cases) had LTs ranging from 4.05 to 24.98 minutes, with a median of 11.07 minutes. Multicells were most common (28 cases), with a wider range of 0 to 83.89 minutes and a median of 16.48 minutes. Supercells (3 cases) had shorter LTs (0–23.77 minutes min–max, 7.58 minutes median), likely due to only affecting the area with their edge area (see Figure 55). Squall line thunderstorms (8 cases) showed a LT range of 3.87 to 19.37 minutes, with a median of 11.08 minutes. Shutdown durations also reflected thunderstorm characteristics. Single-cell storms had the shortest median duration (72.27 minutes), about 22% shorter than multicells (92.74 minutes). This is to be expected given the characteristic duration of the respective thunderstorm types (see Section 2.2). Shutdown durations shorter or longer than the characteristic thunderstorm duration could be explained by the hybrid cases (transitional forms between thunderstorm types) described in Section 6.2. Supercells, despite their long-lived nature, showed similar durations to multicells (median 91.02 minutes). This result could be related to the small size of the observed area of 5 km radius compared to the extent of supercells with a diameter of several 10 km. Note that thunderstorm durations depend not only on storm type but also on vertical wind shear (e.g., between 0–6 km

amsl). However, vertical shear was not considered in this analysis. (Markowski & Richardson, 2010 [37]). A comparison of the different thunderstorm types and the four shutdown initiation criteria (SIC1, SIC2, SIC3 and SIC4; see Section 7.2.2) shows that, there is no tendency for a criterion to be associated with a particular type of thunderstorm in the analysed data set. This underlines the general validity of the developed criteria. The SIC3 was most frequently triggered for all types (excluding the three supercell thunderstorms due to limited data), followed by the SIC1. The SIC2 appeared only in multicell cases.

9.6 CNN Supported Pre-Classification of LLS and Weather Radar Data

Training various CNN models with weather radar data from ACG for the years 2020, 2021, and 2022 demonstrated that radar images with lightning flashes can be distinguished from those without flashes by the models. The pre-trained SqueezeNet model without feature extraction achieved the best results for a “balanced” data set, with a prediction accuracy of 89.84%. These results demonstrate that weather radar data can be used to pre-classify lightning strikes in the area covered by the radar image (Schwalt et al., 2024 [58]). A further attempt using a “balanced” dataset, with blue background pixels converted to white, as described in Section 6.3, did not lead to improved CNN training performance in any of the models. Therefore, this data set is not included in the results presented in this thesis.

Most similar publications do not provide directly comparable results, as they focus, e.g., on forecasting rather than on the classification or identification of lightning in weather radar data. Other studies apply machine learning solely to lightning data (e.g., Mansouri et al., 2023 [16]) or to meteorological parameters (e.g., Mostajabi et al., 2019 [106]).

One recent study by Lu et al., 2025 [107] addresses lightning identification using radar images in a comparable way. They applied a dynamic window of 13 × 13 pixels centred on the lightning strike location to map lightning onto the radar data, whereas the present work used a fixed 100 × 100 pixels grid. Like this work, they also tested various CNN models. Their best result was a probability of detection of 81.12%, which is

comparable to the prediction accuracy in this work. Mostajabi et al., 2019 [106] showed a POD of 84% for an observed area of 30 km around Monte San Salvatore weather station, with LTs of 10–20 minutes. Their results show similar accuracies to those presented in this thesis.

9.7 Future Prospects and Application

Future Prospects

Based on the findings of this work, several avenues for future investigation are proposed:

- A more precise delineation and improved distinction of the observed areas (5 km, 5–8 km, 8–10 km, 10–15 km radius) could be achieved through a denser FM network extended to cover areas outside the considered 5 km radius. This could improve the accuracy of alert LTs and also help reduce the duration of shutdowns as well as non-EAs.
- Further measurements and validation using additional thunderstorm observations could help reduce the variance in the prediction parameters. This approach is motivated by the complex and dynamic nature of thunderstorms as a natural phenomenon.
- For a different region with different thunderstorm characteristics, it is assumed that the developed parameters may differ. In any case, the system should be revalidated over one year or even several measurement periods if the recorded data shows great variance to the presented one.
- Pattern recognition in the E-field, e.g., zero-crossing intervals, rise times, distances between zero-crossings and lightning strikes, or between threshold exceedances and lightning strikes could be implemented. Questions to answer would be, if there are differences between various thunderstorm types or if there are differences between lightning-producing thunderstorms and those without lightning.
- The relationship between low cloud base and E-fields was preliminarily investigated using laser data (ceilometer), maximum temperature, and dew point, but no clear correlation was found. However, only entire days were considered for the analyses. Restricting the analyses to shorter time windows (e.g., 1 hour or the duration of a thunderstorm) might yield better results. High E-fields may be linked to low cloud bases on days with colder days without lightning activity. The theoretical relationship between point charge, distance, and E-field is explained in Section 2.3.

- Additional radar products could be included in the analysis besides 2D MaxCAPPI, such as examination of individual radar data layers, 3D radar analyses, vertically integrated ice composite, etc.
- Estimating the charge distribution within thunderstorms from recorded FM data could give more insight on the actual status of the thunderstorm and so a possible derivation of the probability of CG lightning could improve the presented algorithm. Such an approach is presented by Yamashita et al., 2022 [48] and 2024 [19].
- CNN can serve as a foundation for further integration into multimodal forecasting strategies. Further weather radar datasets should be trained with selected models for different areas in Austria in future, to determine the extent to which model accuracy can be increased. Additionally, meteorological measurement data could be incorporated into the training process. This would enable the implementation of multimodal machine learning approaches in a subsequent step, combining image and time series data.

Application

A real-world application could support meteorologists in their decision-making, especially in the context of remote work (see Sections 1.1 and 3.1). In this context, the alert and shutdown LTs provided by the developed algorithm could be seen as guidance. The measurement campaign at Graz Airport in 2022, 2023, and 2024 demonstrated that no mutual interference between the FM network and the permanently installed instruments and sensors at the airport is to be expected. The criteria described in this thesis were developed with the most important aspect of personnel safety in mind.

To enable operational use, the system must be further developed to process real-time measurement data from the FM network, LLS, and weather radar. The analyses presented in this thesis were conducted using recorded data that were post-processed. The installation of the FM network should be carried out at the locations (FM 1 North, FM 2 South, FM 3 East, FM 4 West) described in Section 4.1.3, as these sites have already been validated and correction factors have been determined (see Appendix A). For the locations outside the airport area, long-term usage would need to be clarified.

For thunderstorms that produce CG lightning strikes within a 5 km radius of Graz Airport, bring the following LTs. The potential of the system, based on the findings of this thesis, is subsequently compared with the data from ACG. The mean and median LTs are 12.83 minutes and 19.10 minutes, respectively.

- LTs of less than 2 minutes: 7.8%
- LTs from 2 to 30 minutes: 72.5%
- LTs from 30 to 60 minutes: 15.7%
- LTs over 60 minutes: 3.9%

In the following, selected results of the present thesis applying STC2 (a fixed time to clear of 10 min after the last IC discharge or CG lightning strike, see Section 7.3.2) are compared with actual ACG shutdowns from the years 2018–2021. For the evaluation of the ACG shutdowns, also thunderstorms with CG lightning strikes within a 5 km radius of Graz Airport were considered (see Appendix D). The ACG median and mean LTs are 6.2 minutes and 9.2 minutes. The median shutdown duration is 14.2 minutes for the present thesis and 16.0 minutes for the ACG. The total shutdown duration per year is in a range of 24.17–30.52 hours for the present thesis and 8.67–18.78 hours for the ACG. Table 26 shows a comparison of the distribution of shutdown LT ranges and non-EAs for the present thesis applying STC2 and for real ACG shutdowns for 2018–2021.

Table 26: Comparison of the distribution of shutdown LT ranges and non-effective alarms (Non-EA) for the present thesis applying STC2 and for real Austro Control GmbH (ACG) shutdowns for 2018–2021.

Lead Time range	**Present Thesis STC2** Count	**ACG 2018–2021** Count
0–2 minutes (FTW)	13	95*
2–30 minutes	46	39
30–60 minutes	1	3
>60 minutes	0	1
Non-EA	115	72
Total Events	175	210

*For 78 of 95 CG lightning strikes in 5 km no shutdown was initiated.

It is noticeable that for ACG 45.2% of the total events (95 of 210) is in the LT range of 0–2 minutes, which is considered to be a failure to warn. For the results in the present

thesis 7.4% of the total events (13 of 175) are FTWs. The results of the present thesis show a higher share of non-EA shutdowns (65.7% for present thesis vs. 34.3% for ACG). Actual values for ACG may differ, as the documented shutdowns do not necessarily reflect the actual shutdowns issued at the airport.

10 Summary

This work was aimed at predicting the first and last Cloud-to-Ground (CG) lightning strikes of a thunderstorm within an observed area of 5 km radius and assessing the associated risks to personnel and infrastructure, as well as determining suitable parameters and criteria for reducing these risks. The resulting alert and shutdown durations triggered by the developed algorithm were intended to be as short as possible, without compromising the safety of personnel. For this purpose, an experimental system was developed that combined an electric Field Meter (FM) network, LLS and weather radar data. The FM network, consisting of four sensors installed within the observed area of 5 km and two additional sensors for reference outside this area, recorded E-field data continuously over the years 2022, 2023, and 2024 in the vicinity of Graz Airport.

Four FMs were installed on different strategically selected measurement sites to provide comprehensive coverage around Graz Airport, with installations to the north, south, east, and west. Site selection was based on technical requirements such as an environment showing minimal vegetation, correct sensor orientation, and a stable power supply, in accordance with the manufacturer's specifications. Accessibility and compatibility with existing infrastructure were also considered. The FMs installed in the two additional locations were used for testing and reference measurements to validate the system over the entire measurement period but were excluded from the main analysis. Correction factors were determined for all sites to account for their individual environmental conditions and structural influences.

The measurement period covered the convective thunderstorm seasons of 2022, 2023 and 2024. For this period E-field data from the FM network was continuously recorded, supported by LLS and weather radar data. The analysis comprised several observed areas around Graz Airport with radii of 5 km, 8 km, 10 km, 15 km and 30 km, with the 5 km radius serving as the primary area of interest. A sensitivity analyses of larger observed areas indicated the performance limitations of the system (intended for lightning prediction within 5 km radius) and suggested that expanding observed areas would benefit from an extension of the FM network and a readjustment of the algorithm. A ±0.5 km buffer zone around this core area was introduced to account for borderline

lightning strikes and potential inaccuracies in LLS data; events within this transitional zone were analysed in greater detail. Cases where the algorithm triggered a shutdown but without CG lightning were also included for a comprehensive assessment.

The core of this thesis was the development of a Thunderstorm Warning System (TWS) that combines data from the FM network, LLS, and weather radar. This integrated approach leveraged the strengths of each subsystem while increasing reliability through redundancy. Predictive parameters were identified for each subsystem and based on terminology used by the International Air Transport Association (IATA), alert and shutdown criteria were defined by combining these parameters. Alerts precede shutdown initiation and are terminated only after the shutdown has been cleared. Since single parameters were sometimes fulfilled long before the first CG lightning strike, leading to long shutdown Lead Times (LTs) or non-Effective Alarms (non-EAs), logical operators were used to link parameters from multiple data sources to avoid such decisions. In addition to the initiation logic, termination criteria were defined in the same way to clear alerts and shutdowns.

A total of 79 thunderstorm cases with 7 in 2022, 36 in 2023, 36 in 2024 (note that recording in 2022 started in August) on 65 days were analysed. There were 51 thunderstorm cases producing lightning strikes within the critical observed area of 5 km radius. The remaining 28 cases triggered a shutdown but either showed no CG lightning within 5 km or no CG lightning at all.

Five different shutdown initiation criteria were used to analyse the cases with lightning strikes within the 5 km radius. Using a 90-minute limit and including an additional fifth Shutdown Initiation Criterion (SIC5) (intended for low-reflectivity thunderstorms within 5 km radius, see Section 7.2.2) for the initial analyses, 80% of cases achieved shutdown LTs within the optimal range of 2–30 minutes, while 11.1% were within a shutdown LT range of 30–60 minutes. For the extended analyses the 90-minute limit was excluded as it is not possible to define an onset time for thunderstorm during continuous monitoring of the data. Also, the initially included SIC5 was excluded from the extended analysis because it proved to be too specific, triggered only a single shutdown, and is expected to lead to an increase in non-EAs. After excluding the time limit and the SIC5, 72.5% of the shutdown LTs remained within the optimal range (2–30 minutes) and 15.7% were within the range of 30–60 minutes window.

To clear shutdowns, two shutdown termination criteria were developed. The Shutdown Termination Criterion 1 (STC1) defines a Time to Clear (TTC) of 30 minutes after the last Intracloud (IC) discharge or CG lightning strike within a 5 km radius. The 30-minute TTC represents a minimum, as shutdowns may continue if other criteria, such as high reflectivity in weather radar data or elevated E-field values, are still met. After 60 minutes, any shutdown is cleared regardless of other criteria. STC2, in contrast, uses a shorter TTC of 10 minutes. If no further IC or CG lightning occurs within 5 km radius after the last lightning strike, the shutdown is cleared. Additionally, if the last lightning strike is detected in the 5–8 km radius and no further lightning activity occurs within 8 km, the shutdown is also cleared after 10 minutes (the additional areal condition is needed, because some shutdowns are initiated without any IC discharges or CG lightning strikes in 5 km).

Under STC2, the non-EA ratio increased significantly compared to STC1 (65.7% vs. 35.4%), due to the shorter TTC of 10 minutes. Despite the higher number of shutdowns (175 vs. 79) and the higher non-EA ratio, the total shutdown duration over the years was notably reduced under STC2. Overall, STC2 resulted in 62 hours of shutdowns, 41.5% less than under STC1. While STC2 introduces more frequent but shorter non-EA shutdowns, it improves system responsiveness and reduces overall operational disruption.

The influence of thunderstorm types on the system performance was also investigated. A total of 47 thunderstorms across 44 days from 2022 to 2024 were classified into single cell, multicell, supercell, and squall line type using 2D MaxCappi radar data. All four types were observed, with hybrid forms assigned to the predominant thunderstorm type. The analysis focused on thunderstorms within a 5 km radius and used STC1. No definitive correlation between thunderstorm type and shutdown triggering could be established, though multicell thunderstorms were the most frequently observed, consistent with the typical weather in Central Europe.

The training of various Convolutional Neural Network (CNN) models with Austro Control GmbH (ACG) radar data from 2020 to 2022 showed that radar images with lightning could be reliably distinguished from those without. The best result was achieved by a pre-trained SqueezeNet model without feature extraction, reaching an

accuracy of 89.84%. These findings demonstrated the potential of weather radar data for pre-classifying lightning strikes.

Overall, the results of this thesis demonstrate that a modular TWS based on multiple parameters from different data sources is technically feasible and could be operationally valuable. The approach allows for further adaptation to site-specific needs or evolving safety standards. Future work in the field of TWS will benefit from the insights gained, especially regarding the achieved alert and shutdown lead times and durations. The system represents a promising step toward more responsive lightning prediction in aviation and related sectors.

Abbreviations

ACG	Austro Control GmbH (Austrian air navigation service provider for civil aviation)
ALDIS	Austrian Lightning Detection and Information System
AMSL	Above Mean Sea Level
BLIDS	Blitz-Informationsdienst (Lightning Information Service)
CA	Classification Accuracy
CAPE	Convective Available Potential Energy
CAPPI	Constant Altitude Plan Position Indicator (weather-radar product on a fixed altitude plane)
CG	Cloud-to-Ground lightning flash
CNN	Convolutional Neural Network
E-field	Electric field (atmospheric electric-field strength)
EA	Effective Alarm
EAR	Effective Alarm Rate
EASA	European Union Aviation Safety Agency
ECMWF	European Centre for Medium-Range Weather Forecasts
EUCLID	European Cooperation for Lightning Detection
FA	False Alarm
FAR	False Alarm Rate
FM	(Electric) Field Meter
FTP	File Transfer Protocol
FTW	Failure to Warn
FTWR	Failure to Warn Rate

GB	Gigabyte (approx. 1 000 000 000 bytes of digital data)
GEC	Global Electric Circuit
GOES	Geostationary Operational Environmental Satellite
GPS	Global Positioning System
GSP	Ground Strike Point of a lightning strike
IATA	International Air Transport Association
IC	Intracloud discharge
ICAO	International Civil Aviation Organization
KSC	Kennedy Space Center
LLCC	Low-Level Cloud Cover
LLS	Lightning Location System
LOWG	ICAO airport code for Graz Airport, Austria
LT	Lead Time
MA	Monitored Area
MB	Megabyte (approx. 1 000 000 bytes of digital data)
MDF	Magnetic Direction Finding
MaxCappi	Maximum Constant Altitude Plan Position Indicator (radar composite showing the strongest reflectivity in a vertical column)
NASA	National Aeronautics and Space Administration
NL201	Campbell Scientific Network Link Interface
NLDN	National Lightning Detection Network (USA)
NLI	Network Link Interface
NaN	Not a Number (value of numeric data type which is undefined as a number)
Non-EA	Non-Effective Alarm

ODBC	Open Database Connectivity
PC	Personal Computer
PCTL	Percentile
POD	Probability of Detection
PT	Pre-Trained (an option for training of CNN models)
PTB	Physikalisch-Technische Bundesanstalt Braunschweig (German metrology institute)
RTLRA	Real-Time Lightning Risk Assessment
SA	Surrounding Area
SIC	Shutdown Initiation Criterion
STC	Shutdown Termination Criterion
TA	Total Alarm
TH	Threshold
TLM	Transmission Line Model
TNA	Total Number of Alarms
TOA	Time of Arrival
TTC	Time to Clear
TWS	Thunderstorm Warning System
UTC	Coordinated Universal Time
VLF/VHF	Very Low/High Frequency
WXR	Weather Radar
WXR3D	Three-Dimensional Weather Radar composite
YYYYMMDD	Year Month Day date format (e.g., 20220812 equals 12 August 2022)
hhmmss	Hour Minute Second time format (e.g., 235959 equals 23:59:59)

References

[1] International Air Transport Association (IATA), “Airport Handling Manual: Airside Management and Safety”, 26th Edition, 2006.

[2] European Union Aviation Safety Agency, “Guidance Material on remote aerodrome air traffic services”, iss. 3, Annex to ED Decision 2023/005/R, 2023.

[3] T. Long and I. Miller, “Impact of Lightning Strikes on Airport Facility and Ground Operations”, Collegiate Aviation Review International, vol. 40, pp. 143–167, 2022.

[4] F. Liebold, J. Schmitz, and J. Hinkelbein, “Lightning accidents worldwide: regional analysis and medical therapy”, Flugmedizin · Tropenmedizin · Reisemedizin, vol. 28, pp. 237–243, 2021.

[5] OVE Österreichischer Verband für Elektrotechnik, “OVE EN IEC 62793:2022-11-01 Gewitterwarnsysteme – Blitzschutz”, 2022.

[6] E. A. Jacobson and E. P. Krider, “Electrostatic field changes produced by Florida lightning”, Institute of Atmospheric Physics, The University of Arizona, vol. 33, pp. 103–117, 1976.

[7] G. M. Lucas, J. P. Thayer, and W. Deierling, “Statistical analysis of spatial and temporal variations in atmospheric electric fields from a regional array of fieldmills”, Journal of Geophysical Research: Atmospheres, vol. 122, pp. 1158–1174, 2017.

[8] M. J. Murphy, R. L. Holle, and N. W. S. Demetriades, “Cloud-to-ground lightning warnings using electric field mill and lightning observation”, 20th International Lightning Detection Conference & 2nd International Lightning Meteorology Conference, p. 9. 2008.

[9] J. G. Wilson and K. L. Cummins, “Thunderstorm and fair-weather quasi static electric fields over land and ocean”, Atmos. Res., vol. 257, p. 105618, 2021.

[10] K. Michimoto, “A study of the charge distribution in winter thunderclouds by means of network recording of surface electric fields and radar observation of

clouds structure in the Hokuriku district", Journal of Atmospheric Electricity, vol. 13, no. 1, 1993.

[11] W. H. Beasley, D. E. Williams, and P. T. Hyland, "Analysis of surface electric-field contours in relation to cloud-to-ground lightning flashes in air-mass thunderstorms at the Kennedy Space Center", 20th International Lightning Detection Conference & 2nd International Lightning Meteorology Conference, p. 6. 2008.

[12] M. A. da Silva Ferro, J. Yamasaki, D. R. M. Pimentel, K. P. Naccarato, and M. M. F. Saba, "Lightning risk warnings based on atmospheric electric field measurements in Brazil", Journal of Aerospace Technology and Management, vol. 3, no. 3, pp. 301–310, 2011.

[13] K. N. Pustovalov and P. M. Nagorskiy, "Response in the surface atmospheric electric field to the passage of isolated air mass cumulonimbus clouds", J. Atmos. Sol. Terr. Phys., vol. 172, pp. 33–39, 2018.

[14] F. Rodrigues and M. Lacerda, "Warning of lightning risk for the first lightning produced by a thunderstorm using electric field mill network records", 36th International Conference on Lightning Protection (ICLP), pp. 720–723. 2022.

[15] J. Montanyà, D. Aranguren, N. Pineda, G. Solà, D. Romero, and V. March, "Total Lightning, Electrostatic Field and Meteorological Radar Applied to Lightning Hazard Warning", 20th International Lightning Detection Conference & 2nd International Lightning Meteorology Conference, Tucson, Arizona, USA, 2008.

[16] E. Mansouri, A. Mostajabi, C. Tong, M. Rubinstein, and F. Rachidi, "Lightning Nowcasting Using Solely Lightning Data", Atmosphere 2023, vol. 14, Page 1713, vol. 14, no. 12, p. 1713, 2023.

[17] B. Antonescu, S. Burcea, and A. Tanase, "Forecasting the onset of cloud-to-ground lightning using radar and upper air data in Romania", International Journal of Climatology, vol. 33, no. 6, pp. 1579–1584, 2013.

[18] A. Antunes, R. A. Marshall, A. P. Sousa, A. Viets, and W. Deierling, "An Array of Low-Cost, High-Speed, Autonomous Electric Field Mills for Thunderstorm Research", Advancing Earth and Space Science, vol. 7, 2020.

[19] K. Yamashita et al., “A new electric field mill array with each of the mill’s rotor controlled precisely by a GPS module: Equipment and initial results”, Earth and Planetary Physics, vol. 8, 2024.

[20] O. Povcshenko and V. Bazhenov, “Analysis of modern atmospheric electrostatic field measuring instruments and methods”, Technology audit and production reserves, no. 4, 2023.

[21] B. Franklin, “XCV. A letter of Benjamin Franklin, Esq; to Mr. Peter Collinson, F. R. S. concerning an electrical kite”, Philos. Trans. R. Soc. Lond., vol. 47, pp. 565–567, 1752.

[22] A. McAdie, “The date of Franklin’s kite experiment”, The Proceedings of the American Antiquarian Society, vol 34, no. 2, 1924.

[23] J. Canton “XCIII. A letter to the Right Honourable the Earl of Macclesfield, President of the Royal Society, concerning some new electrical experiments, by John Canton, M. A. and F. R. S”, Philos. Trans. R. Soc. Lond., vol. 48, pp. 780–785, 1753.

[24] J. Parsons and W. Mazeas, “Observations upon the electricity of the air, made at the Chateau de Maintenon, during the months of June, July, and October 1753; Being Part of a Letter from the Abbé Mazeas, F.R.S. to the Rev. Stephen Hales, D. D. F.R.S. Translated from the French by James Parsons, M. D. F. R. S.”, JSTOR Philosophical Transactions (1683-1775), vol.48, pp. 377–384, 1753.

[25] W. Thomson, “XVI. On a self-acting apparatus for multiplying and maintaining electric charges, with applications to illustrate the voltaic theory”, Proceedings of the Royal Society of London, vol. 16, pp. 67–72, 1868.

[26] R. G. Harrison, “The Carnegie Curve”, Surv. Geophys., vol. 34, no. 2, pp. 209–232, 2013.

[27] C. T. R. Wilson, “On the measurement of the earth-air current and on the origin of atmospheric electricity”, Proc. Camb. Philos. Soc., vol. 13, no. 6, 1906.

[28] K. L. Aplin, R. G. Harrison, and M. J. Rycroft, “Investigating earth’s atmospheric electricity: A role model for planetary studies”, Space Sci. Rev., vol. 137, no. 1–4, pp. 11–27, 2008.

[29] M. J. Rycroft, S. Israelsson, and C. Price, “The global atmospheric electric circuit, solar activity and climate change”, J. Atmos. Sol. Terr. Phys., vol. 62, no. 17–18, pp. 1563–1576, 2000.

[30] G. B. Burns, M. H. Hesse, S. K. Parcell, S. Malachowski, and K. D. Cole, “The geoelectric field at Davis station, Antarctica”, Journal of Atmospheric and Terrestrial Physics, vol. 57, no. 14, pp. 1783–1797, 1995.

[31] Y. Minamoto and A. Kadokura, “Extracting fair-weather data from atmospheric electric-field observations at Syowa Station, Antarctica”, Polar Sci., vol. 5, no. 3, pp. 313–318, 2011.

[32] V. A. Rakov and M. A. Uman, *Lightning: Physics and Effects*, Cambridge University Press, 2003.

[33] C. T. R. Wilson, “Some Thundercloud Problems”, J. Franklin Inst., vol. 208, no. 1, pp. 1–12, 1929.

[34] H. K. Burke and A. A. Few, “Direct measurements of the atmospheric conduction current”, J. Geophys. Res. Oceans, vol. 83, iss. C6, pp. 3093–3098, 1978.

[35] R. Yaniv, Y. Yair, C. Price, and S. Katz, “Local and global impacts on the fair-weather electric field in Israel”, Atmos. Res., vol. 172–173, pp. 119–125, 2016.

[36] J. M. Wallace and P. V. Hobbs, Atmospheric Science: *An Introductory Survey, Second Edition*, Elsevier, Academic Press, 2006.

[37] P. Markowski and R. Yvette, *Mesoscale Meteorology in Midlatitudes*, Wiley-Blackwell, 2010.

[38] C. A. Doswell, “The Distinction between Large-Scale and Mesoscale Contribution to Severe Convection: A Case Study Example”, Weather Forecast, vol. 2, no. 1, pp. 3–16, 1987.

[39] N. Kitagawa and K. Michimoto, “Meteorological and electrical aspects of winter thunderclouds”, J. Geophys. Res., vol. 99, no. D5, pp. 10713–10721, 1994.

[40] V. Cooray, *The Lightning Flash 2nd Edition*, The Institution of Engineering and Technology, London, United Kingdom, 2014.

[41] E. R. Jayaratne, C. P. R. Saunders, and J. Hallett, “Laboratory studies of the charging of soft-hail during ice crystal interactions”, Quarterly Journal of the Royal Meteorological Society, vol. 109, no. 461, pp. 609–630, 1983.

[42] E. R. Jayaratne and C. P. R. Saunders, “The “rain gush”, lightning, and the lower positive charge center in thunderstorms.”, J. Geophys. Res., vol. 89, iss. D7, pp. 11816–11818, 1984.

[43] P. R. Krehbiel and M. Brook, “The electrical structure of thunderstorms”, The Earth’s electrical environment, National Academy Press, pp. 90–113, 1986.

[44] M. G. Bateman, T. C. Marshall, M. Stolzenburg, and W. D. Rust, “Precipitation charge and size measurements inside a New Mexico mountain thunderstorm”, Journal of Geophysical Research Atmospheres, vol. 104, no. D8, pp. 9643–9653, 1999.

[45] S. Schatz, L. Schwalt, S. Pack, H. Kohlmann, and H. Pichler, “Lightning Risk Assessment – Electric Field Meter, Lightning Location System and Weather Radar Data”, CIGRE International Colloquium on Lightning and Power Systems & XVII International Symposium on Lightning Protection, Suzhou, China, IEEE, 2023.

[46] I. M. Imyanitov, Y. V. Chubarina, and Shvarts Y. M., “Electricity of Cloud”, Hydrometeorological Press, Leningrad, Gidrometeoizdat (NASA Technical Translation from Russian, NASA TT-F-718 1972), p. 92, 1971.

[47] V. A. Rakov, “Lightning flashes transporting both negative and positive charges to ground”, Research Signpost, vol. 661, no. 2, pp. 9–21, 2005.

[48] K. Yamashita, H. Fujisaka, H. Iwasaki, K. Kanno, and M. Hayakawa, “A New Electric Field Mill Network to Estimate Temporal Variation of Simplified Charge Model in an Isolated Thundercloud”, Sensors 2022, vol. 22, no. 5, p. 1884, 2022.

[49] J. R. Dwyer and M. A. Uman, “The physics of lightning”, Phys. Rep., vol. 534, no. 4, pp. 147–241, 2014.

[50] V. A. Rakov, “The Physics of Lightning”, Surv. Geophys., vol. 34, no. 6, pp. 701–729, 2013.

[51] W. Schulz, K. Cummins, G. Diendorfer, and M. Dorninger, “Cloud-to-ground lightning in Austria: A 10-year study using data from a lightning location system”, Journal of Geophysical Research: Atmospheres, vol. 110, no. 9, pp. 1–20, 2005.

[52] W. Schulz and G. Diendorfer, “EUCLID network performance and data analysis”, 17th International Lightning Detection Conference, Vaisala, Inc., Tucson, Arizona, USA, 2002.

[53] K. Cehak, “Zur Gewitter- und Hagelklimatologie von Österreich”, Tagungsbericht der 15. Internationalen Tagung für alpine Meteorologie in Grindelwald, Ver. Schweizer. Meteorol. Anstalt, vol. 40, pp. 316–319, 1980.

[54] C. Frei and C. Schär, “A precipitation climatology of the Alps from high-resolution rain-gauge observations”, International Journal of Climatology, vol. 18, no. 8, pp. 873–900, 1998.

[55] C. Vergeiner, W. Schulz, and S. Pack, “On the Performance of the Austrian Lightning Detection and Information System (ALDIS)”, 11. Höfler’s Days, Portorož, Slovenia, 2013.

[56] L. Schwalt, S. Pack, and W. Schulz, “Ground truth data of atmospheric discharges in correlation with LLS detections”, Electric Power Systems Research, vol. 180, no. 106065, 2020.

[57] L. Schwalt and W. Schulz, “Analyses of negative cloud-to-ground flashes and their ground strike points in Austria”, Electric Power Systems Research, vol. 217, no. 109140, 2023.

[58] L. Schwalt, S. Schatz, F. Obenaus, and S. Pack, “Application of Convolutional Neural Networks for the Detection of Lightning in Weather Radar Data”, 37th International Conference on Lightning Protection, Dresden, Germany, IEEE, 2024.

[59] W. Schulz, H. Pichler, G. Diendorfer, C. Vergeiner, and S. Pack, “Validation of detection of positive flashes by the Austrian lightning location system ALDIS”, XII International Symposium on Lightning Protection, pp. 47–51, 2013.

[60] W. Qian, *Temporal Climatology and Anomalous Weather Analysis*. Springer Atmospheric Science, 2017.

[61] P. Meischner, *Weather Radar: Principles and Advanced Applications*. Physics of Earth and Space Environments. Berlin, Heidelberg: Springer Berlin Heidelberg, 2004.

[62] R. J. Doviak and D. S. Zrnic, *Doppler Radar and Weather Observations*. 1st Edition. Academic Press, 1984.

[63] J. S. Marshall and W. M. K. Palmer, “The Distribution of Raindrops with Size”, J. Atmos. Sci. vol. 5, no. 4, pp. 165–166, 1948.

[64] R. R. Rogers and M. K. Yau, *A Short Course in Cloud Physics*, 3rd Edition. International Series in Physical Philosophy. Butterworth Heinemann Publications, 1989.

[65] F. P. Ostby, “Use of CSIS in severe weather forecasting”, Proceedings of SPIE, International Society for Optical Engineering, vol. 481, pp. 78–85, 1985.

[66] W. L. Smith et al., “The meteorological satellite: Overview of 25 years of operation”, Science, vol. 231, no. 4737, pp. 455–462, 1986.

[67] R. L. Holle, N. W. S. Demetriades, and A. Nag, “Lightning Warnings with NLDN Cloud and Cloud-to-ground Lightning Data”, 23rd International Lightning Detection Conference and 5th International Lightning Meteorology Conference, Tucson, Arizona, USA, 2014.

[68] S. Schmitt, “Thunderstorm Warning Systems: Why Lightning Detection Networks should be considered as the most relevant solution in Western Europe Thunderstorm warning systems: why lightning detection networks should be considered as one of the most relevant solution in Western Europe?”, 24th International Lightning Detection Conference & 6th International Lightning Meteorology Conference, San Diego, California, USA, 2016.

[69] S. Schmitt, “Thunderstorm warning systems in developing countries”, ICLEASM, Kathmandu, Nepal, 2023.

[70] F. J. Merceret et al., “A History of the Lightning Launch Commit Criteria and the Lightning Advisory Panel for America’s Space Program”, NASA/SP—2010–216283, 2010.

[71] D. Aranguren, J. Montanya, G. Sola, V. March, D. Romero, H. Torres, “On the lightning hazard warning using electrostatic field: Analysis of summer thunderstorms in Spain”, Atmos. Res., 2009.

[72] A. Küchler, *Hochspannungstechnik, 2nd Edition*. Springer, 2005.

[73] W. Plaßmann and D. Schulz, *Handbuch Elektrotechnik*. Vieweg+Teubner, 2009.

[74] S. C. Handel, K. L. Cummins, and E. P. Krider, “Surface Potential Gradients and NEXRAD Radar Reflectivities Before the Onset of Lightning at the KSC-ER”, Journal of Geophysical Research: Atmospheres, vol. 127, no. 18, 2022.

[75] G. Diendorfer, “A Review of 25 Years of Lightning Research in Austria from 1991-2015”, World Meeting on Lightning, Cartagena, Colombia, 2016.

[76] S. Schatz, L. Schwalt, J. Maier, S. Pack, H. Kohlmann, and H. Pichler, “Successful Short-Term Prediction of First Cloud-to-Ground Lightning Strikes in Thunderstorm Events,” 37th International Conference on Lightning Protection, Dresden, Germany, IEEE, 2024.

[77] S. Schatz, S. Pack, H. Kohlmann, H. Pichler, L. Schwalt, and J. Maier, “Enhanced short-term prediction of first cloud-to-ground lightning strikes in convective season thunderstorms”, Electric Power Systems Research, vol. 247, no. 111810, 2025.

[78] G. Diendorfer, “LIGHTNING LOCATION SYSTEMS (LLS)”, IX International Symposium on Lightning Protection, Brazil, 2007.

[79] G. Diendorfer, “LLS performance validation using lightning to towers”, 21st International Lightning Detection Conference and 3rd International Lightning Meteorology Conference, Orlando, USA, 2010.

[80] A. Nag, M. J. Murphy, W. Schulz, and K. L. Cummins, “Lightning locating systems: Insights on characteristics and validation techniques”, Earth and Space Science, vol. 2, no. 4, pp. 65–93, 2015.

[81] V. Cooray, “Effects of propagation on the return stroke radiation fields”, Radio Sci., vol. 22, no. 5, pp. 757–768, 1987.

[82] K. L. Cummins and M. J. Murphy, “An Overview of Lightning Locating Systems: History, Techniques, and Data Uses, With an In-Depth Look at the U.S. NLDN”, IEEE Trans. Electromagn. Compat., vol. 51, no. 3, p. 499, 2009.

[83] K. L. Cummins, W. L. Hiscox, A. E. Pifer, and R. O. Burnett, “Line reliability and fault analysis using the National Lightning Detection Network”, Precise Measurements in Power Conference, National Science Foundation and Center for Power Engineering at Virginia Tech, Arlington, VA, USA, 1993.

[84] K. L. Cummins, M. J. Murphy, E. A. Bardo, W. L. Hiscox, R. B. Pyle, and A. E. Pifer, “A combined TOA/MDF technology upgrade of the US National Lightning Detection Network”, Journal of Geophysical Research Atmospheres, vol. 103, iss. D8, pp. 9035–9044, 1998.

[85] M. A. Uman, K. D. McLain, and Krider E. Philip, “The Electromagnetic Radiation from a Finit Antenna”, American Journal of Physics, vol. 43, iss. 1, pp. 33-38, 1975.

[86] G. Diendorfer et al., “Review of CIGRE Report Cloud-to-Ground Lightning Parameters Derived from Lightning Location Systems – The Effects of System Performance”, CIGRE SC C4 2009 Kushiro Colloquium, 2009.

[87] R. Kaltenböck, “New generation of dual polarized weather radars in Austria”, ERAD 2012 – European Conference on Radar in Meteorology and Hydrology, France, 2012.

[88] R. Kaltenböck, „Wetterradar (WXR): Konvektion im Remote/AUTOMETAR“, ÖGM-DMG Fortbildungstag/Flugmeteorologie, Austria, 2016.

[89] J. Maier, S. Schatz, L. Schwalt, S. Pack, and H. Kohlmann, “Environmental Influences on Measurements with Electric Field Meters for Lightning Observation”, 37th International Conference on Lightning Protection, Dresden, Germany, IEEE, 2024.

[90] E. P. Krider, R. C. Noggle, A. E. Pifer, and D. L. Vance, “Lightning Direction-Finding Systems for Forest Fire Detection”, Bull. Am. Meteorol. Soc., vol. 61, no. 9, pp. 980–986, 1980.

[91] G. Diendorfer, W. Schulz, and V. A. Rakov, “Lightning characteristics based on data from the Austrian lightning locating system”, IEEE Trans. Electromagn. Compat., vol. 40, no. 4, part 2, pp. 452–464, 1998.

[92] K. L. Cummins et al., “THE U.S. NATIONAL LIGHTNING DETECTION NETWORK: POST-UPGRADE STATUS”, Second Conference on Meteorological Applications of Lightning Data, Atlanta, GA, USA, 2006.

[93] M. J. Murphy, J. A. Cramer, and R. K. Said, “Recent History of Upgrades to the U.S. National Lightning Detection Network”, J. Atmos. Ocean. Technol., vol. 38, no. 3, pp. 573–585, 2021.

[94] C. J. Biagi, K. L. Cummins, K. E. Kehoe, and E. P. Krider, “National Lightning Detection Network (NLDN) performance in southern Arizona, Texas, and Oklahoma in 2003-2004”, Journal of Geophysical Research Atmospheres, vol. 112, no. 5, p. 5208, 2007.

[95] H. Kohlmann, W. Schulz, and S. Pedeboy, “Evaluation of EUCLID IC/CG classification performance based on ground-truth data”, XIV International Symposium on Lightning Protection, pp. 35–41, Natal, Brazil, 2017.

[96] G. Diendorfer, W. Hadrian, F. Hofbauer, M. Mair, and W. Schulz, “Evaluation of lightning location data employing measurements of direct strikes to a radio tower”, e & i Elektrotechnik und Informationstechnik, vol. 119, no. 12, pp. 422–427, 2002.

[97] Doswell and Markowski, “Is Buoyancy a Relative Quantity?”, Monthly Weather Review, vol 132, iss. 4, pp. 853-863, 2004.

[98] Craven J. P. and Brook H. E., “Baseline Climatology of Sounding Derived Parameters Associated with Deep Moist Convection”, National Weather Digest, vol. 28, pp. 13–24, 2004.

[99] I. Goodfellow, Y. Bengio, and A. Courville, *Deep learning*. MIT Press Cambridge, 2016.

[100] A. Krizhevsky, I. Sutskever, and G. E. Hinton, “Imagenet classification with deep convolutional neural networks”, Commun. ACM, vol. 60, no. 6, pp. 84–90, 2017.

[101] G. Huang, Z. Liu, L. van der Maaten, and K. Q. Weinberger, “Densely Connected Convolutional Networks”, Proceedings of the IEEE Conference on Computer Vision and Pattern Recognition, Honolulu, USA, 2017, pp. 2261–2269.

[102] K. He, X. Zhang, S. Ren, and J. Sun, “Deep Residual Learning for Image Recognition”, Proceedings of the IEEE Conference on Computer Vision and Pattern Recognition, Las Vegas, USA, pp. 770–778. 2016.

[103] F. N. Iandola, M. W. Moskewicz, K. Ashraf, S. Han, W. J. Dally, and K. Keutzer, “SqueezeNet: AlexNet-level accuracy with 50x fewer parameters and <0.5 MB model size”, arXiv preprint arXiv:1602.07360, 2016.

[104] K. Simonyan and A. Zisserman, “Very Deep Convolutional Networks for Large-Scale Image Recognition”, 3rd International Conference on Learning Representations, San Diego, USA, 2015.

[105] A. Paszke et al., “PyTorch: An Imperative Style, High-Performance Deep Learning Library”, Advances in Neural Information Processing Systems, 2019, pp. 8024–8035.

[106] A. Mostajabi, D. L. Finney, M. Rubinstein, and F. Rachidi, “Nowcasting lightning occurrence from commonly available meteorological parameters using machine learning techniques”, NPJ Clim. Atmos. Sci., vol. 2, no. 1, pp. 1–15, 2019.

[107] M. Lu et al., “Lightning identification based on multiple weather radar product data”, J. Digit. Earth, vol. 18, no. 1, p. 2498604, 2025.

[108] C. P. R. Saunders, “A Review of thunderstorm electrification processes”, Journal of Applied Meteorology, vol. 32, no. 4, 1992.

[109] G. Diendorfer, R. Kaltenböck, M. Mair, and H. Pichler, “Characteristics of Tower Lightning Flashes in a Winter Thunderstorm and related Meteorological Observations”, ILDC/ILMC Vaisala, 2006.

List of Figures

List of Tables

Publications by the Author

Publications with Scientific Relation to this Thesis

S. Schatz, L. Schwalt, S. Pack, H. Kohlmann, H. Pichler, “Enhanced Short-Term Prediction of First Cloud-to-Ground Lightning Strikes in Convective Season Thunderstorms”, Electric Power System Research, vol. 247, spec. iss., 2025.

S. Schatz, L. Schwalt, S. Pack, H. Kohlmann, H. Pichler, „Erfolgreiche Kurzzeitvorhersage der ersten Wolke-Erde-Blitze während Gewitterereignissen“ Elektrotechnik und Informationstechnik, vol. 141, iss. 7, pp. 431-439, 2024.

S. Schatz, L. Schwalt, S. Pack, H. Kohlmann, H. Pichler, “Successful Short-Term Prediction of First Cloud-to-Ground Lightning Strikes in Thunderstorm Events”, 37th International Conference on Lightning Protection, Dresden, Germany, IEEE, 2024. – *awarded with the ICLP Young Scientist Award 2024*

L. Schwalt, S. Schatz, F. Obenaus, S. Pack, “Application of Convolutional Neural Networks for the Detection of Lightning in Weather Radar Data”, 37th International Conference on Lightning Protection, Dresden, Germany, IEEE, 2024.

J. Maier, S. Schatz, L. Schwalt, S. Pack, H. Kohlmann, “Environmental Influences on Measurements with Electric Field Meters for Lightning Observation”, 37th International Conference on Lightning Protection, Dresden, Germany, IEEE, 2024.

S. Schatz, L. Schwalt, S. Pack, H. Kohlmann, H. Pichler, “Lightning Risk Assessment - Electric Field Meter, Lightning Location System and Weather Radar Data”, CIGRE International Colloquium on Lightning and Power Systems & XVII International Symposium on Lightning Protection, Suzhou, China, IEEE, 2023.

L. Schwalt, S. Schatz, S. Pack, “Lightning Risk Assessment in Real-Time in the Vicinity of Power Systems”, CIGRE CAIRNS 2023 International Symposium, Cairns, Australia, 2023.

Other Publications by the Author

L. Schwalt, S. Schatz, S. Pack, W. Schulz, “A five-year analysis of ground truth data for positive flashes”, Electric Power Systems Research. vol. 231, 110307, 2024.

S. Schatz, L. Schwalt, S. Pack, W. Schulz, “Analysis of Two Bipolar Flashes Recorded in Austria”, CIGRE International Colloquium on Lightning and Power Systems & XVII International Symposium on Lightning Protection, Suzhou, China, IEEE, 2023.

Appendix

A Correction Factors from Fair-Weather E-field

The correction factors were determined to account for site-specific influences at the FM measurement locations and to ensure comparability between the recordings of the six FMs. These correction factors, which were applied to the E-field recordings of all six FMs, were calculated using data from 14 February 2023 between 00:00 and 15:00 UTC. On that day, weather conditions were fair, with clear blue skies. The values were derived from a section of the mean E-field data with minimal fluctuations (Figure 58). The relative correction factors were referenced to FM 2 South, as this site was identified as having the least external influence on the E-field measurements.

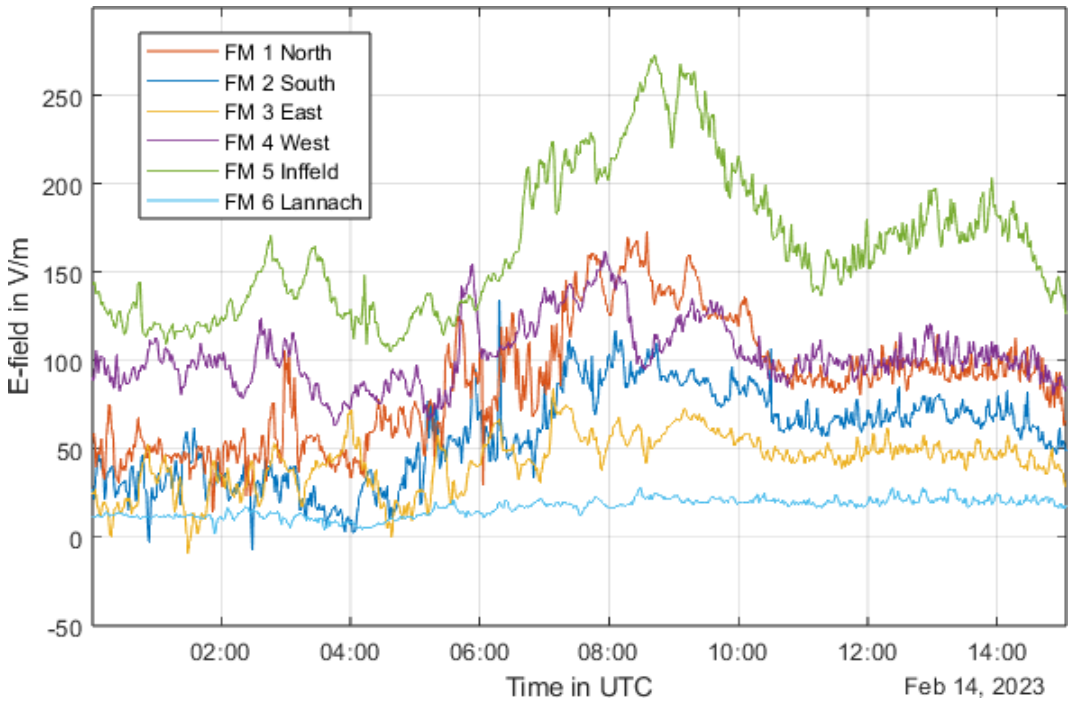

Figure 58: E-field records for fair-weather conditions and cloudless sky on 14 February 2023 from 00:00 to 15:00 UTC for the determination of correction factors for different FM sites.

Based on the online, real-time visualisation of E-field data in Grafana, as shown in Section 5.1, Figure 15, it was observed on additional fair-weather days that FM 1 North appeared to report values that were too low. Consequently, the correction factor for this station was adjusted to $C_{FM1} = 1.00$, which provides a reliable correction. The other

FMs showed consistent and accurate results when applying the previously calculated correction factors.

The following correction factors could be derived:

- FM 1 North $C_{FM1} = 1.00, initially\ C_{FM1}\ was\ 0.73$
- FM 2 South $C_{FM2} = 1.00$
- FM 3 East $C_{FM3} = 1.44$
- FM 4 West $C_{FM4} = 0.68$
- FM 5 Inffeld $C_{FM5} = 0.41$
- FM 6 Lannach $C_{FM6} = 3.30$

Figure 59 shows the same E-field recordings from 14 February 2023 between 00:00 and 15:00 UTC with the correction factors applied.

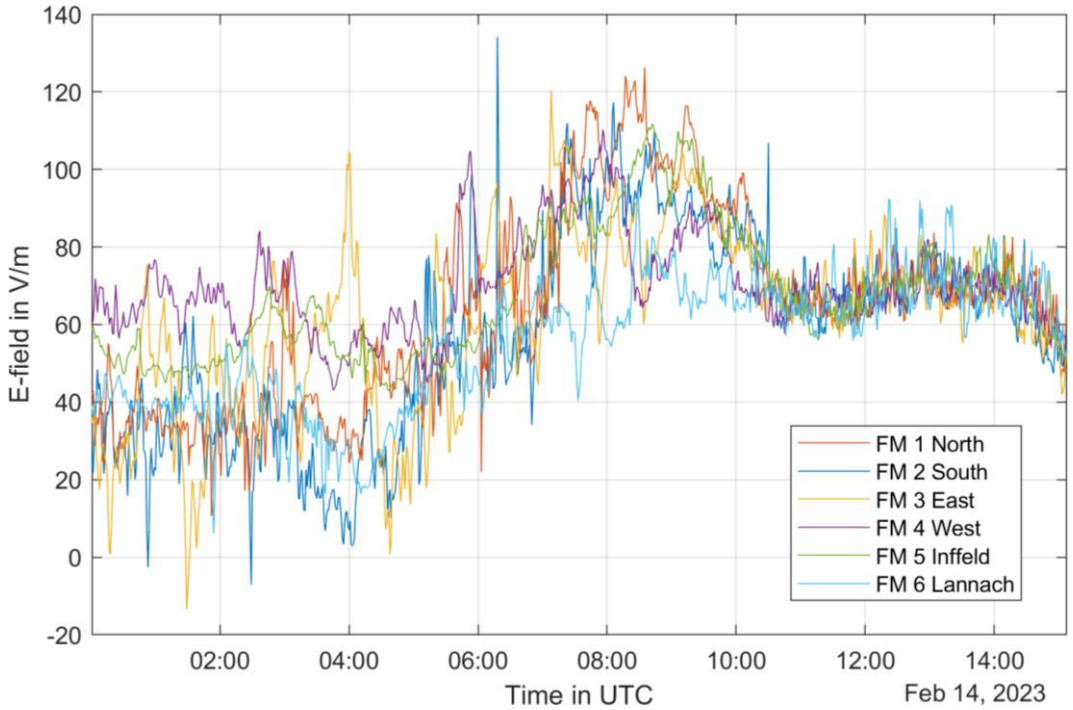

Figure 59: E-field records, with correction factors applied, for fair-weather conditions and cloudless sky on 14 February 2023 from 00:00 to 15:00 UTC.

B Thunderstorm Cases with CG Lightning Strikes in 5 km Radius

The Appendix provides the visualisation of the combined data sets for thunderstorm cases with CG lightning strikes within the 5 km radius around Graz Airport for the investigated years 2022, 2023, and 2024. The top diagram shows the respective weather radar variables (reflectivity values in dBZ) over time in UTC as described in Section 6.1. The bottom diagram shows the E-field in V/m for the four FM 1 North, FM 2 South, FM 3 East, FM 4 West and the LLS located distance of CG lightning strikes over time in UTC. For the LLS data IC discharges are represented by yellow crosses, while positive and negative CG lightning strikes are displayed as red and blue crosses, respectively.

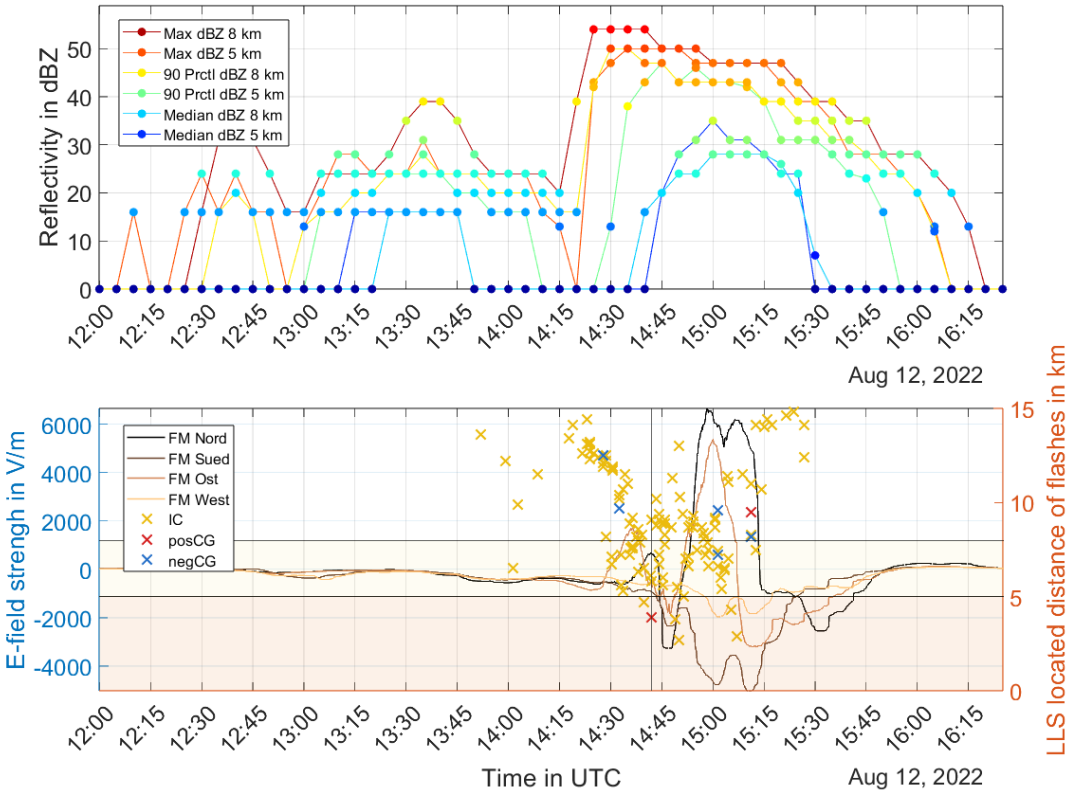

Figure 60: Combined data set of weather radar data (top) and LLS and FM network data (bottom), for a thunderstorm on 12 August 2022 from 12:00 to 16:15 UTC.

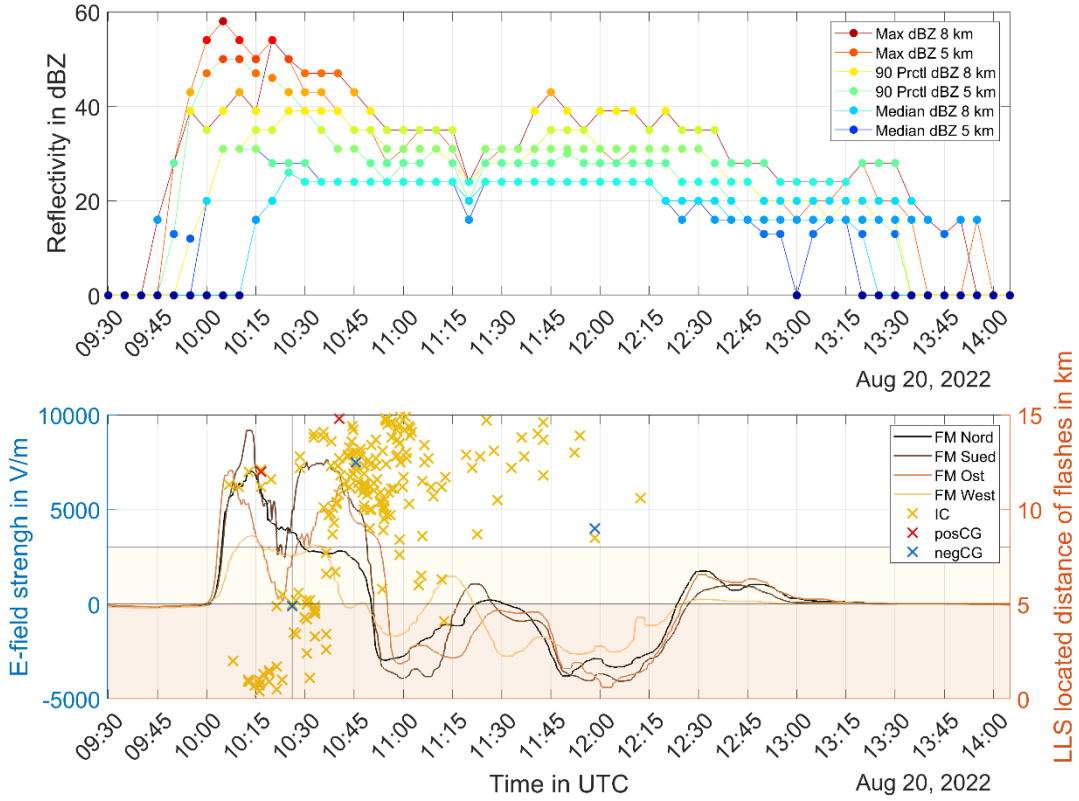

Figure 61: Combined data set of weather radar data (top) and LLS and FM network data (bottom), for a thunderstorm on 20 August 2022 from 09:30 to 14:00 UTC.

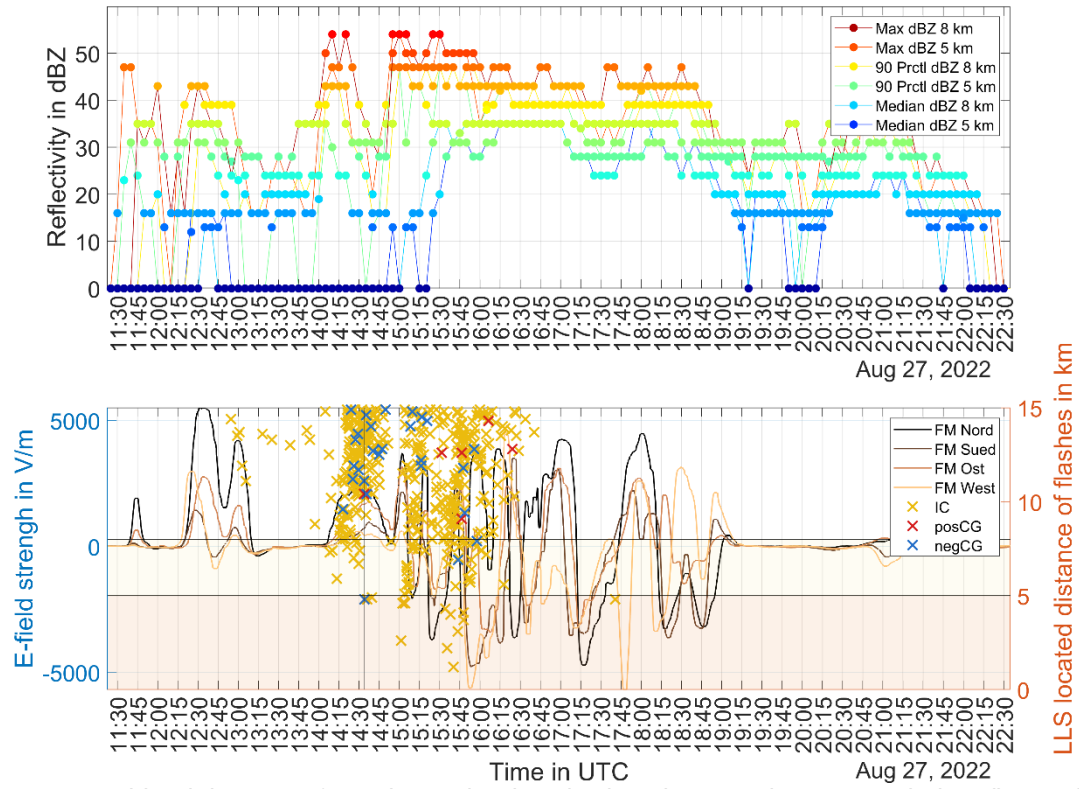

Figure 62: Combined data set of weather radar data (top) and LLS and FM network data (bottom), for a thunderstorm on 27 August 2022 from 11:30 to 22:30 UTC.

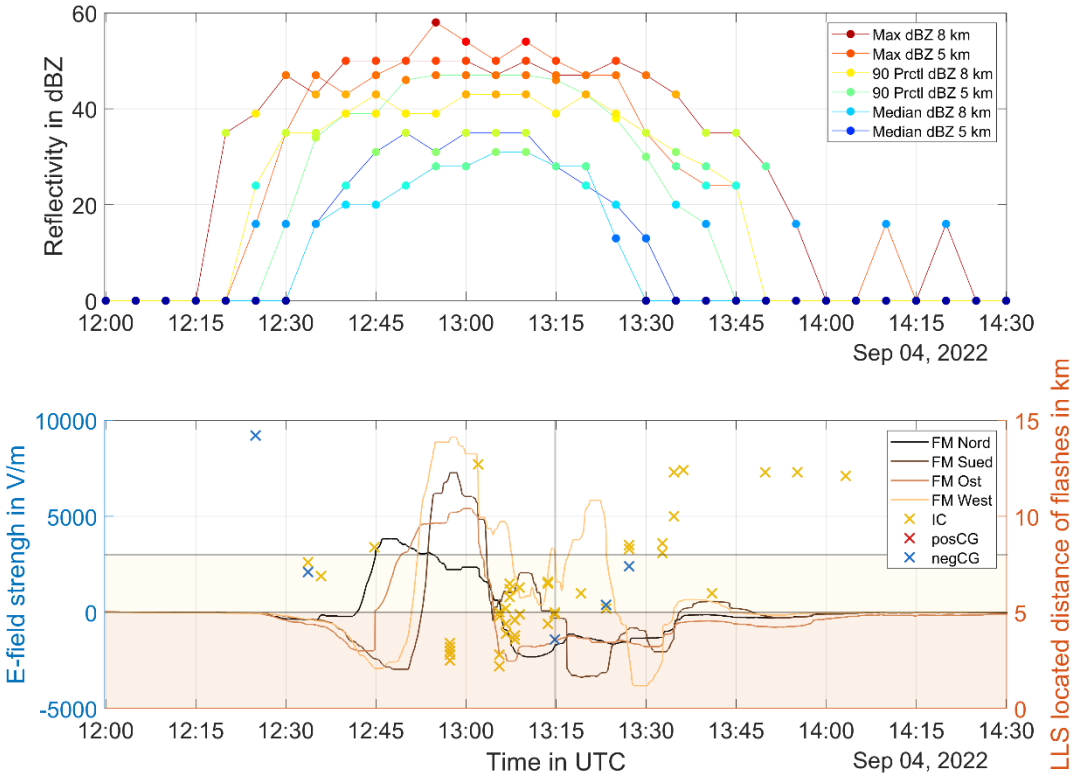

Figure 63: Combined data set of weather radar data (top) and LLS and FM network data (bottom), for a thunderstorm on 04 September 2022 from 12:00 to 14:30 UTC.

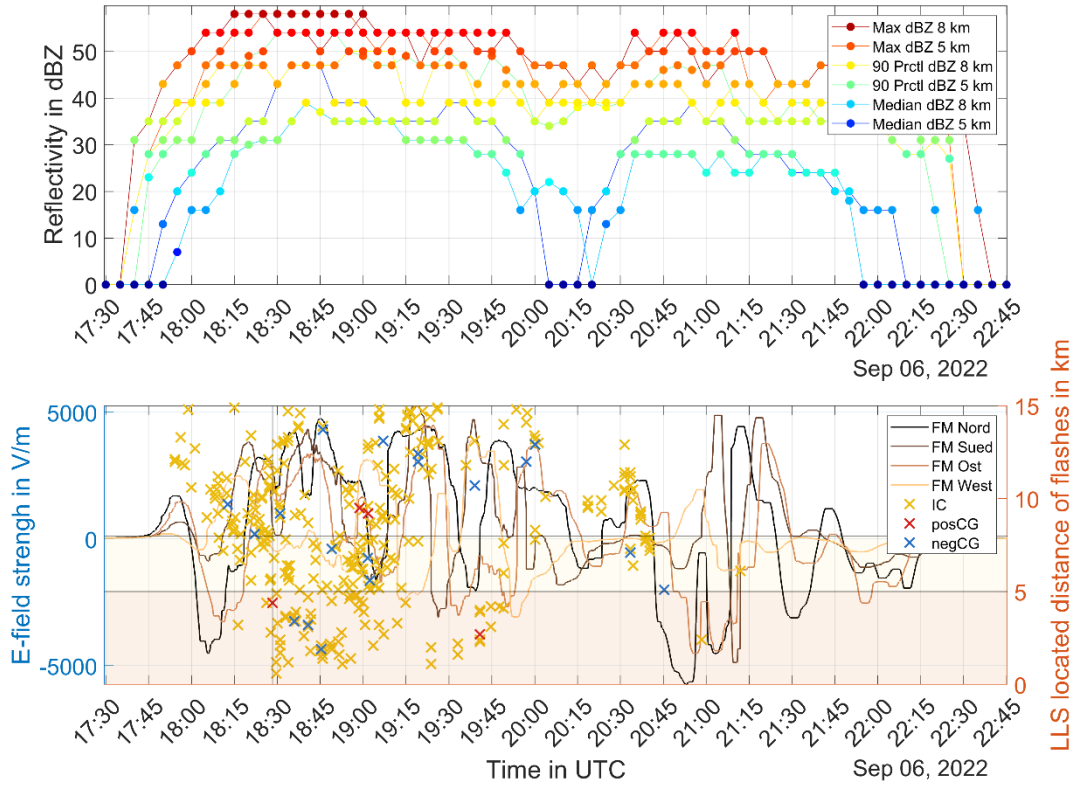

Figure 64: Combined data set of weather radar data (top) and LLS and FM network data (bottom), for a thunderstorm on 06 September 2022 from 17:30 to 22:45 UTC.

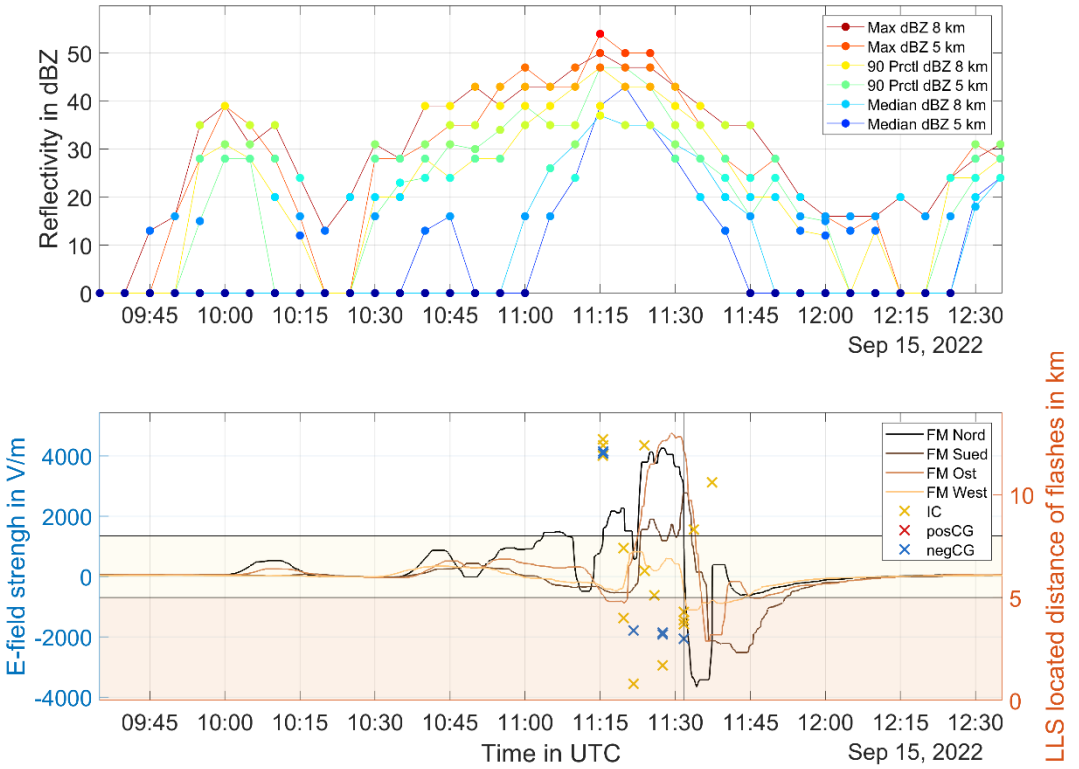

Figure 65: Combined data set of weather radar data (top) and LLS and FM network data (bottom), for a thunderstorm on 15 September 2022 from 09:30 to 12:30 UTC.

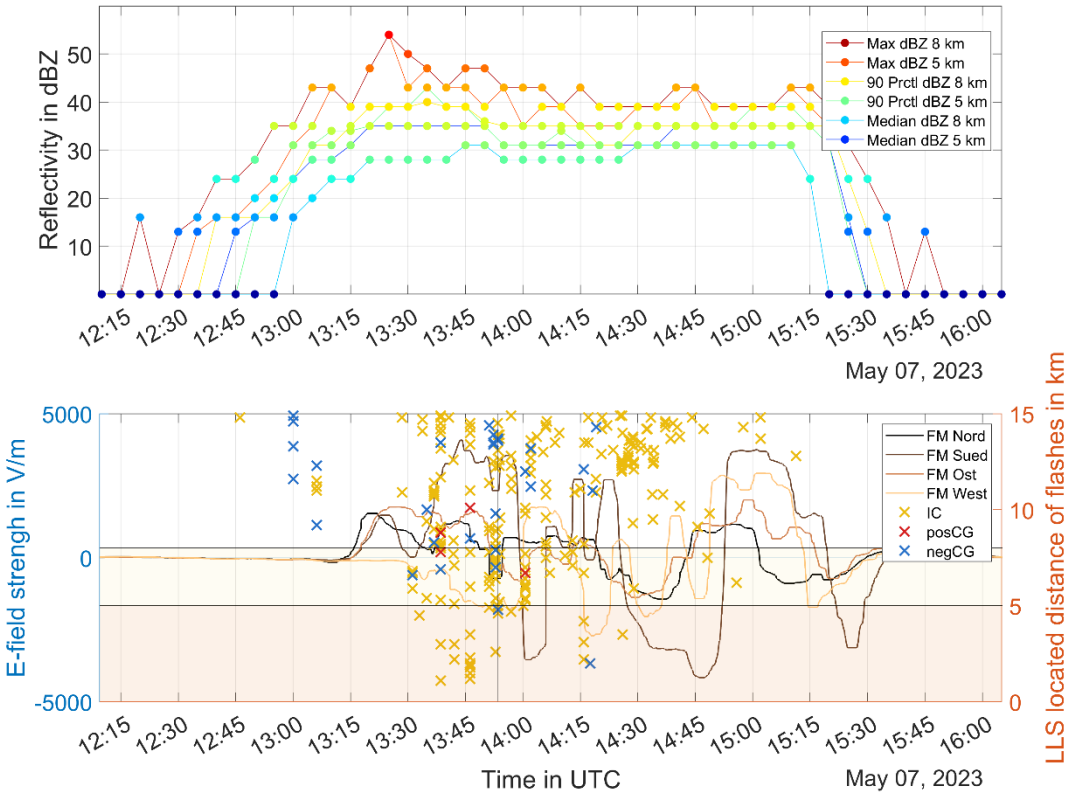

Figure 66: Combined data set of weather radar data (top) and LLS and FM network data (bottom), for a thunderstorm on 07 May 2023 from 12:15 to 15:45 UTC.

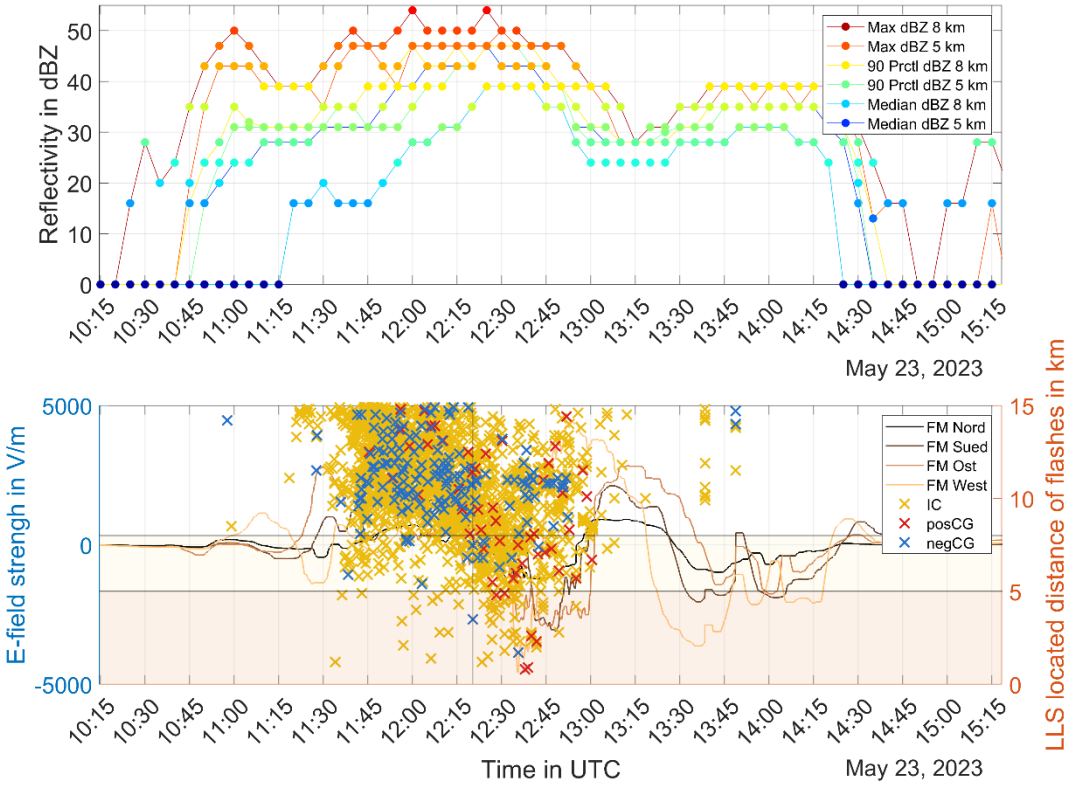

Figure 67: Combined data set of weather radar data (top) and LLS and FM network data (bottom), for a thunderstorm on 23 May 2023 from 10:15 to 15:15 UTC.

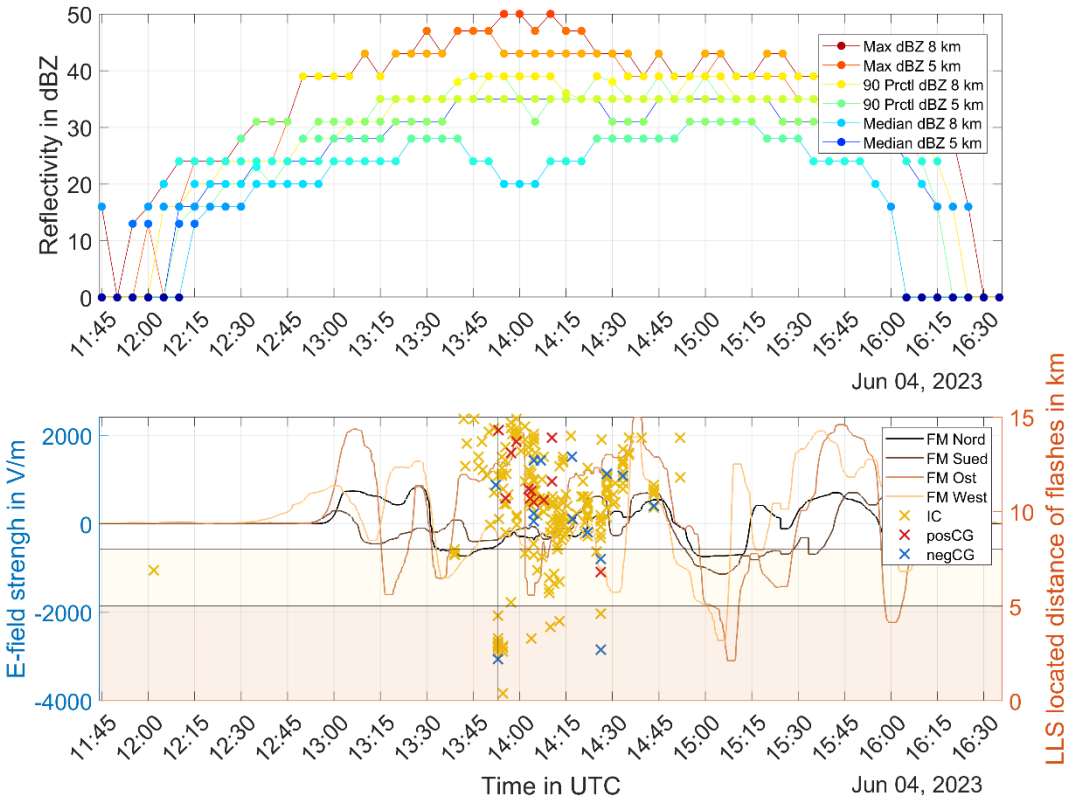

Figure 68: Combined data set of weather radar data (top) and LLS and FM network data (bottom), for a thunderstorm on 04 June 2023 from 11:45 to 16:30 UTC.

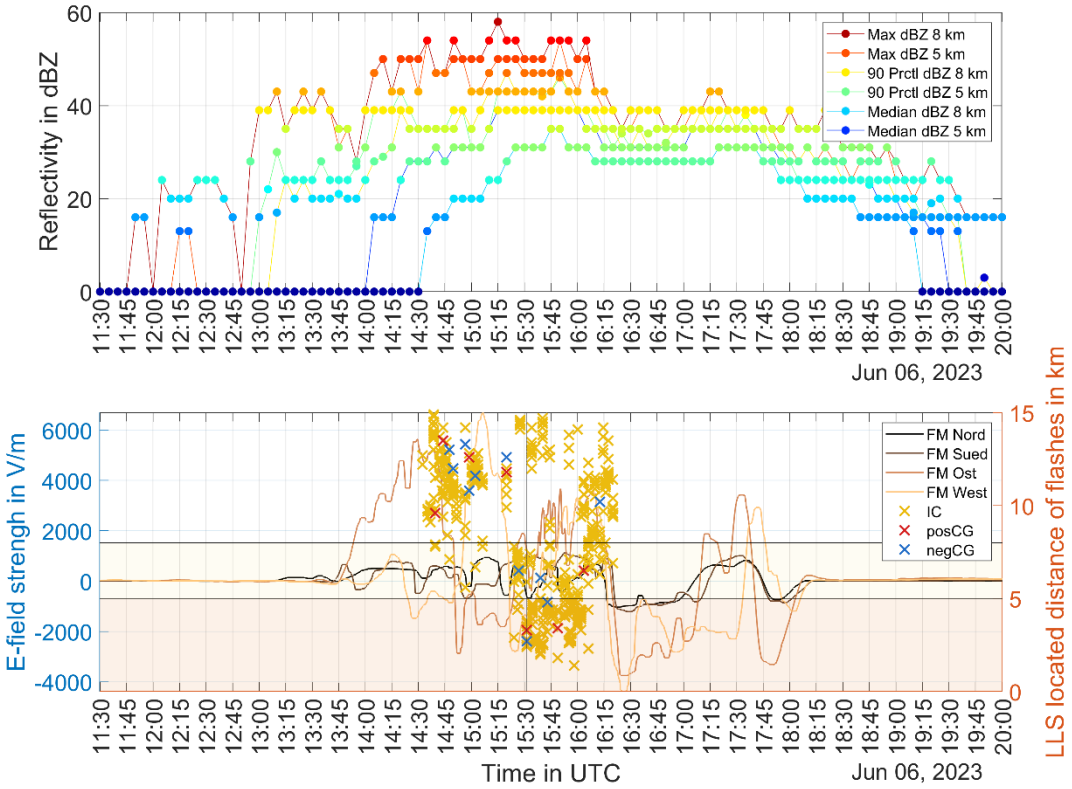

Figure 69: Combined data set of weather radar data (top) and LLS and FM network data (bottom), for a thunderstorm on 06 June 2023 from 11:30 to 20:00 UTC.

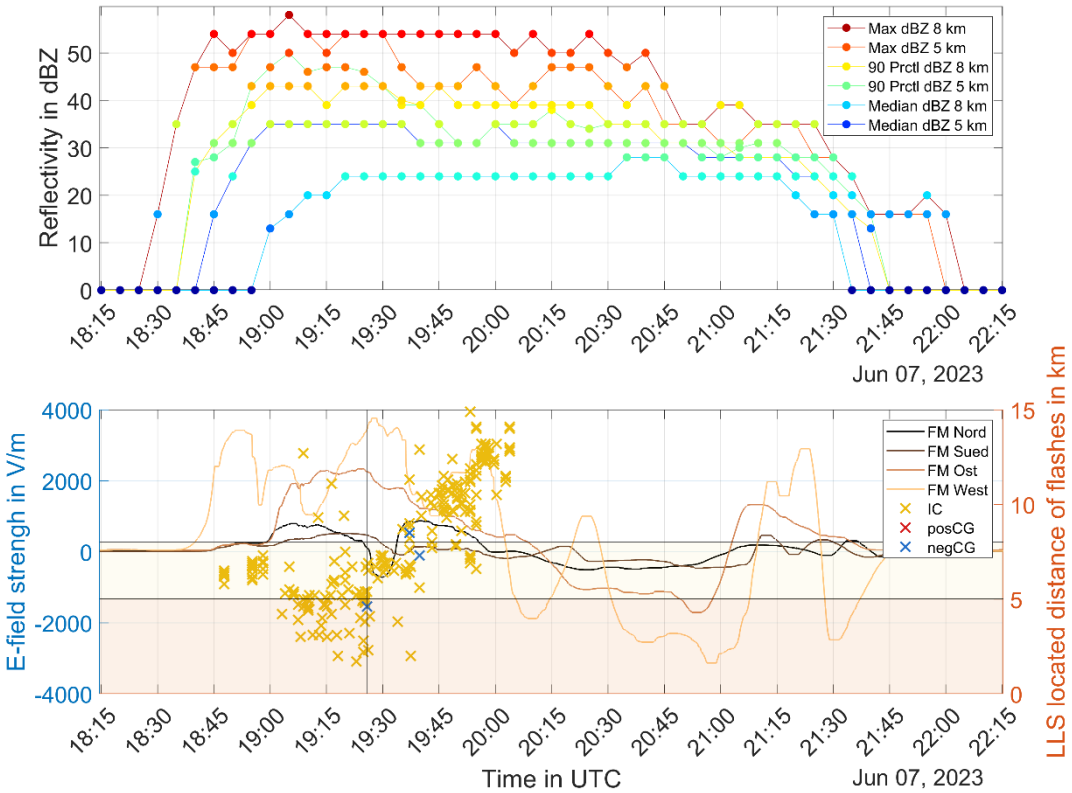

Figure 70: Combined data set of weather radar data (top) and LLS and FM network data (bottom), for a thunderstorm on 07 June 2023 from 18:15 to 22:15 UTC.

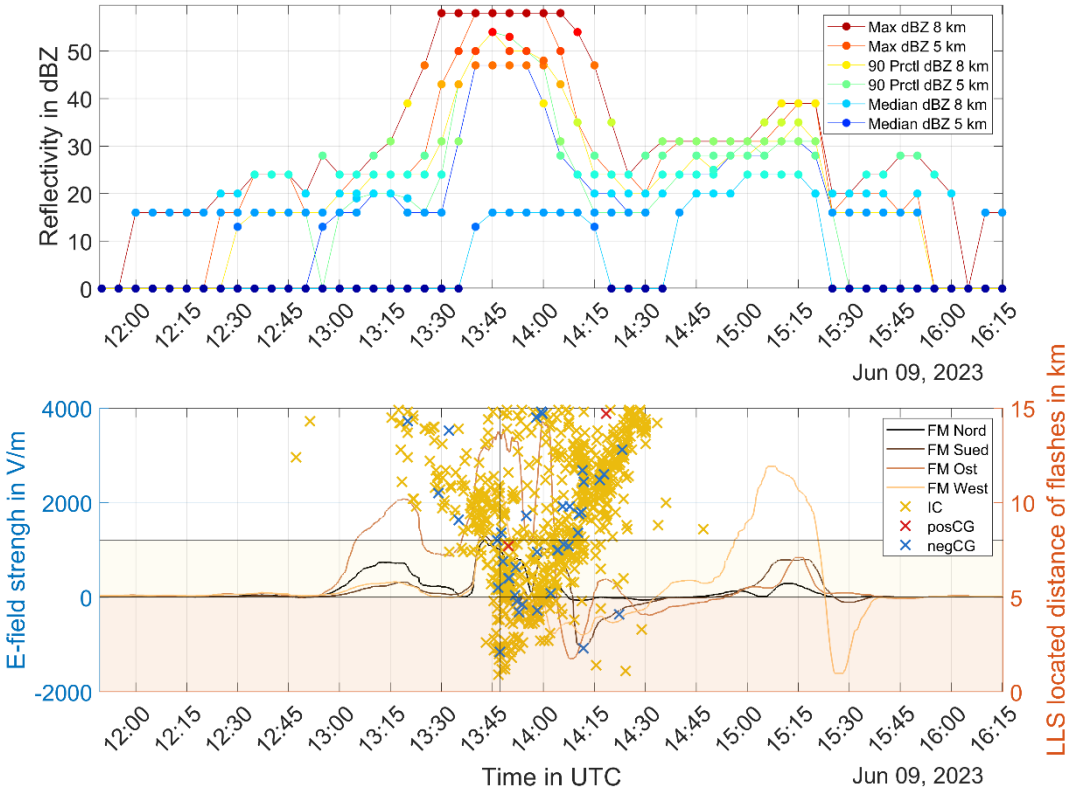

Figure 71: Combined data set of weather radar data (top) and LLS and FM network data (bottom), for a thunderstorm on 09 June 2023 from 12:00 to 16:15 UTC.

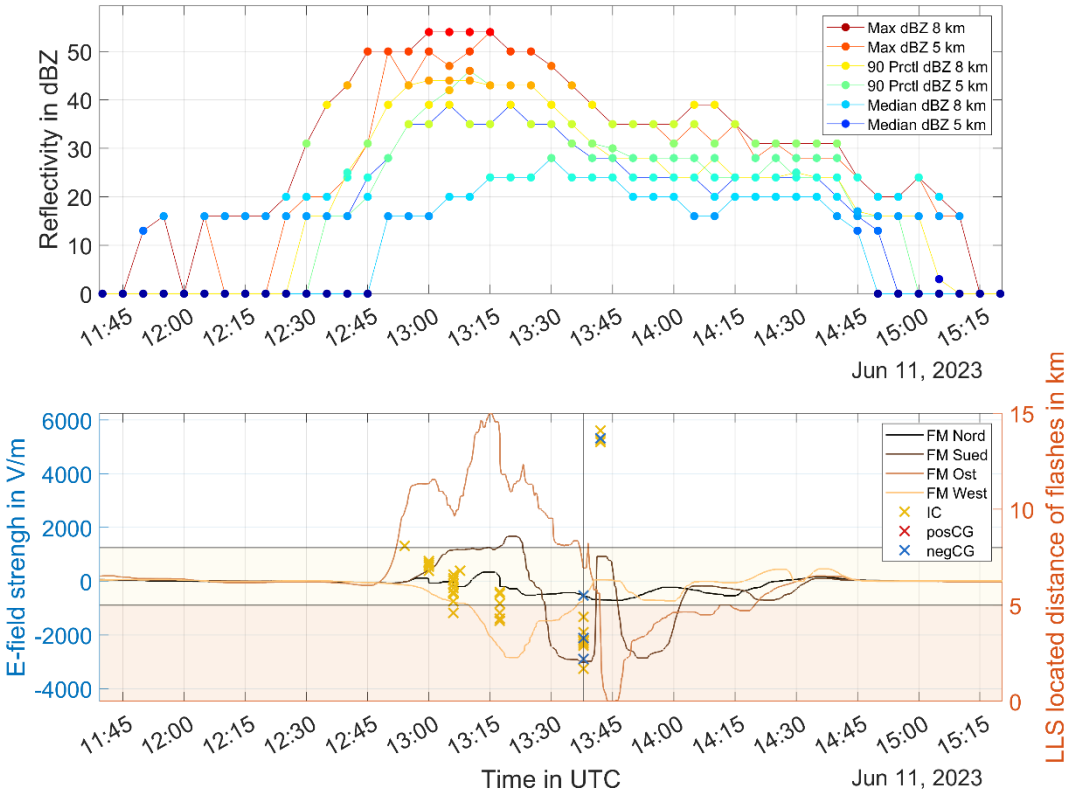

Figure 72: Combined data set of weather radar data (top) and LLS and FM network data (bottom), for a thunderstorm on 11 June 2023 from 11:45 to 15:15 UTC.

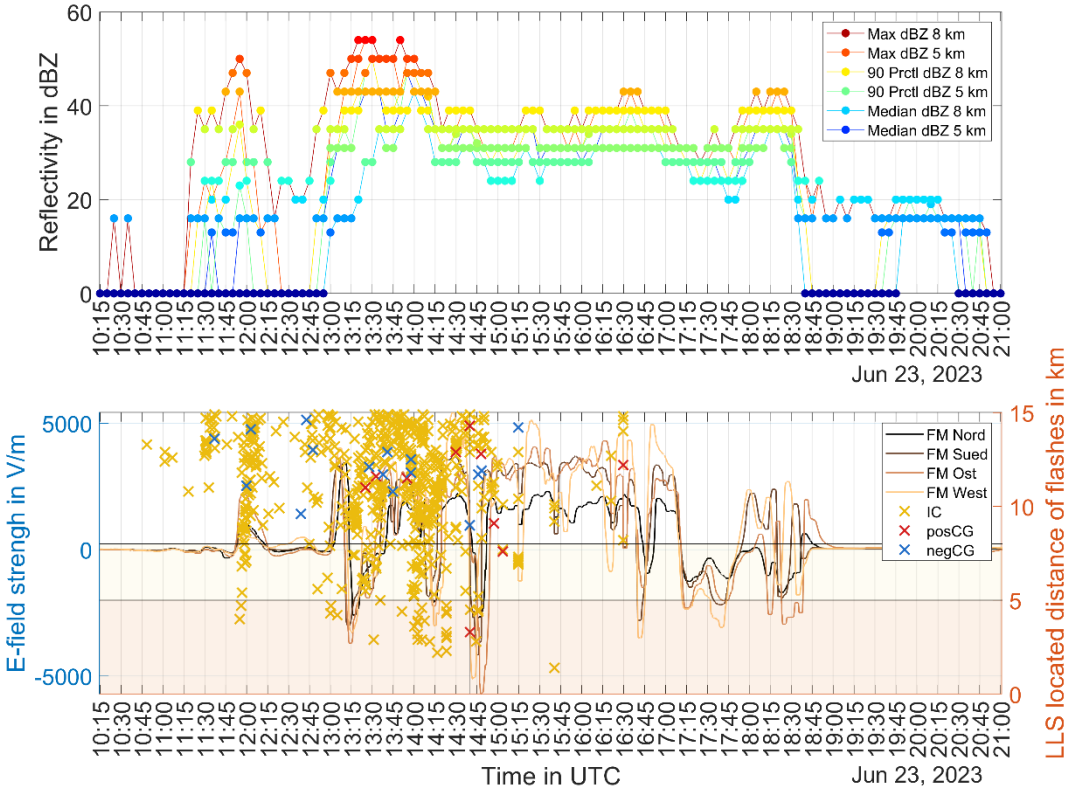

Figure 73: Combined data set of weather radar data (top) and LLS and FM network data (bottom), for a thunderstorm on 23 June 2023 from 10:15 to 21:00 UTC.

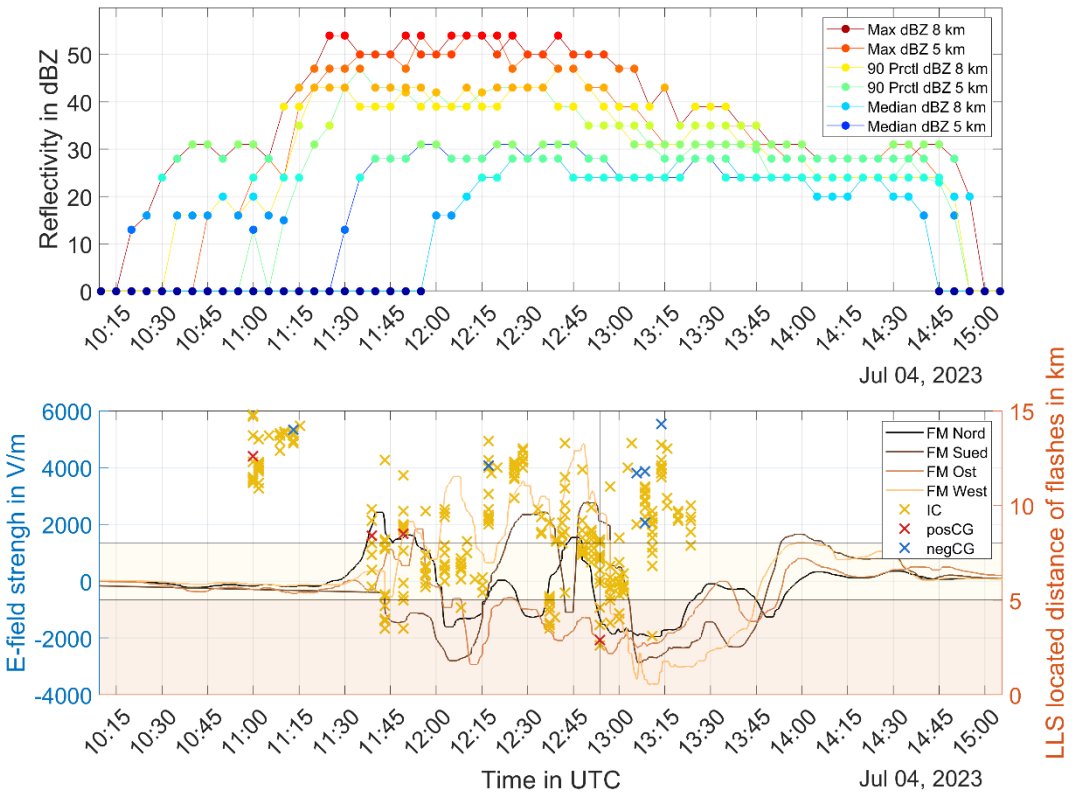

Figure 74: Combined data set of weather radar data (top) and LLS and FM network data (bottom), for a thunderstorm on 04 July 2023 from 10:15 to 15:00 UTC.

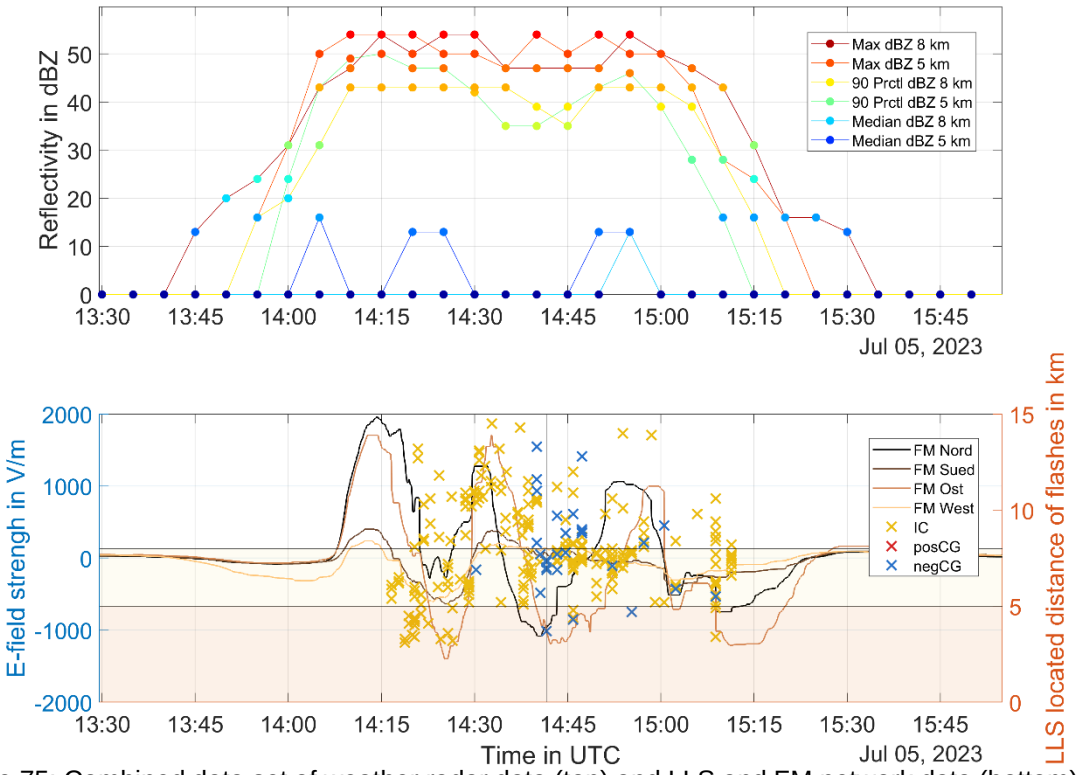

Figure 75: Combined data set of weather radar data (top) and LLS and FM network data (bottom), for a thunderstorm on 05 July 2023 from 13:30 to 15:50 UTC.

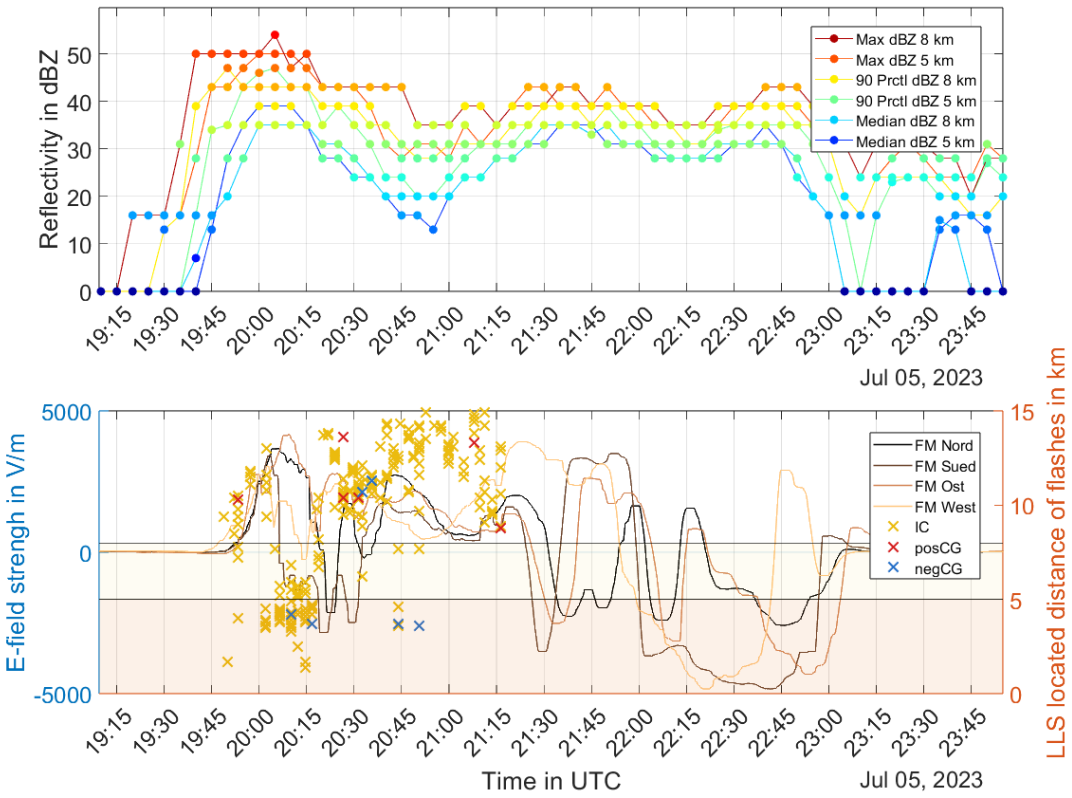

Figure 76: Combined data set of weather radar data (top) and LLS and FM network data (bottom), for a thunderstorm on 05 July 2023 from 19:15 to 23:45 UTC.

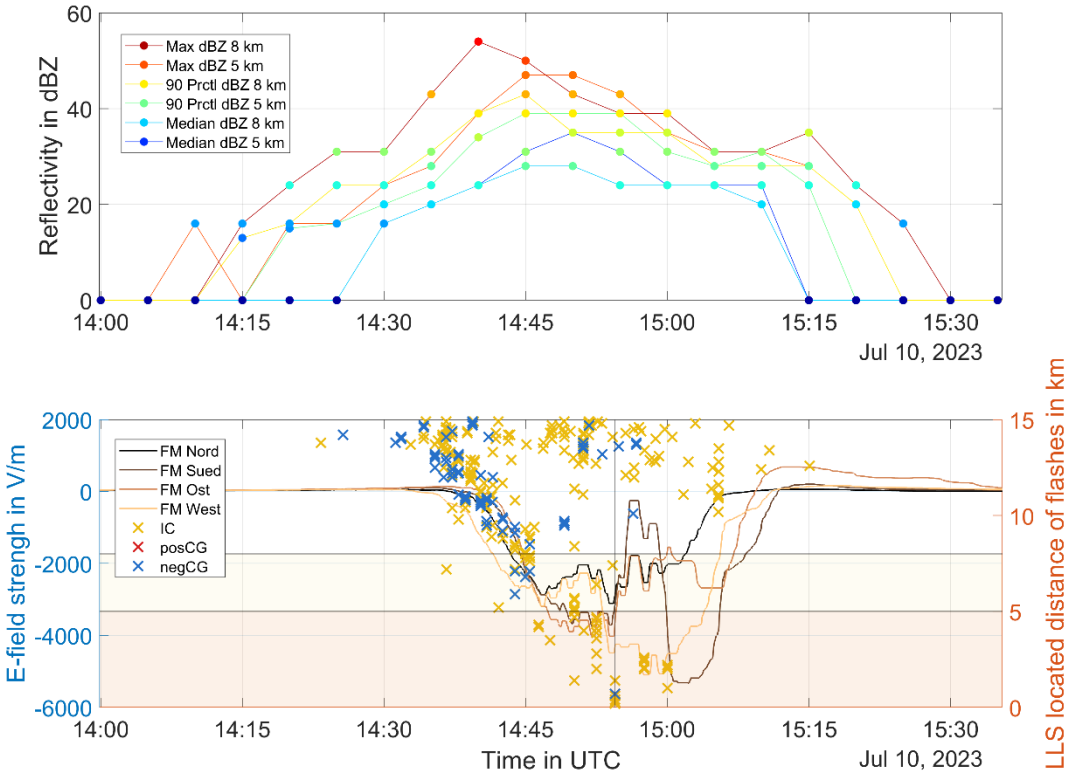

Figure 77: Combined data set of weather radar data (top) and LLS and FM network data (bottom), for a thunderstorm on 10 July 2023 from 14:00 to 15:35 UTC.

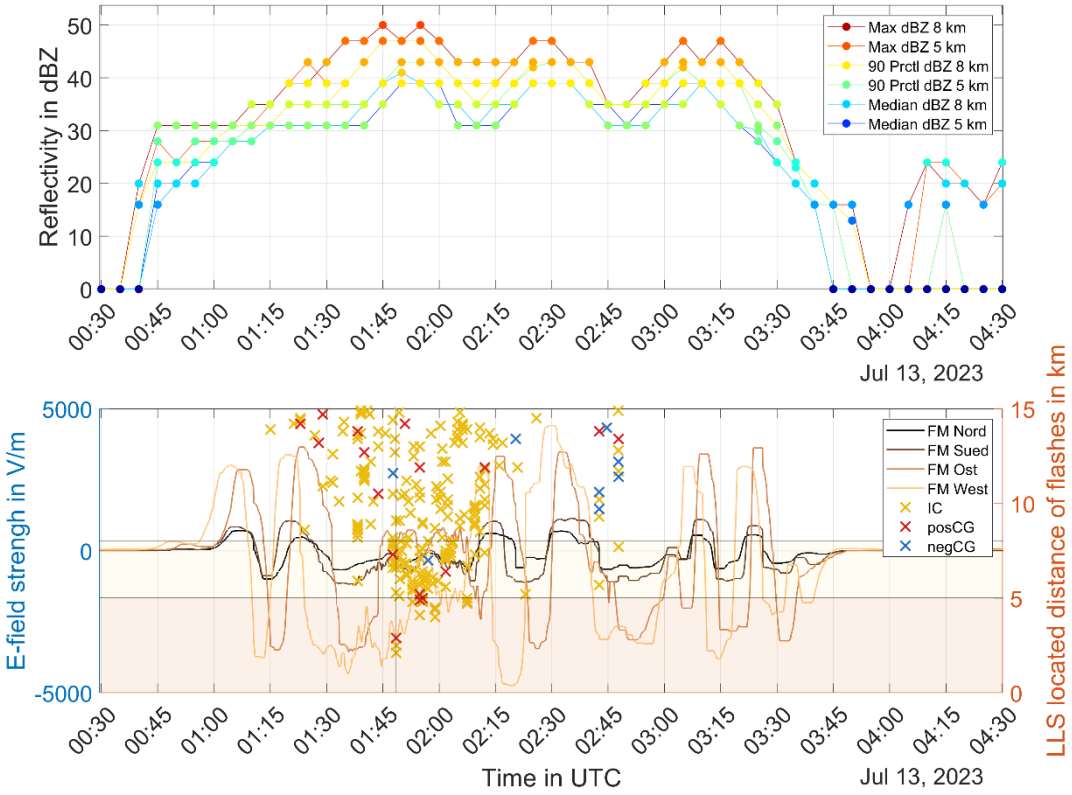

Figure 78: Combined data set of weather radar data (top) and LLS and FM network data (bottom), for a thunderstorm on 13 July 2023 from 00:30 to 04:30 UTC.

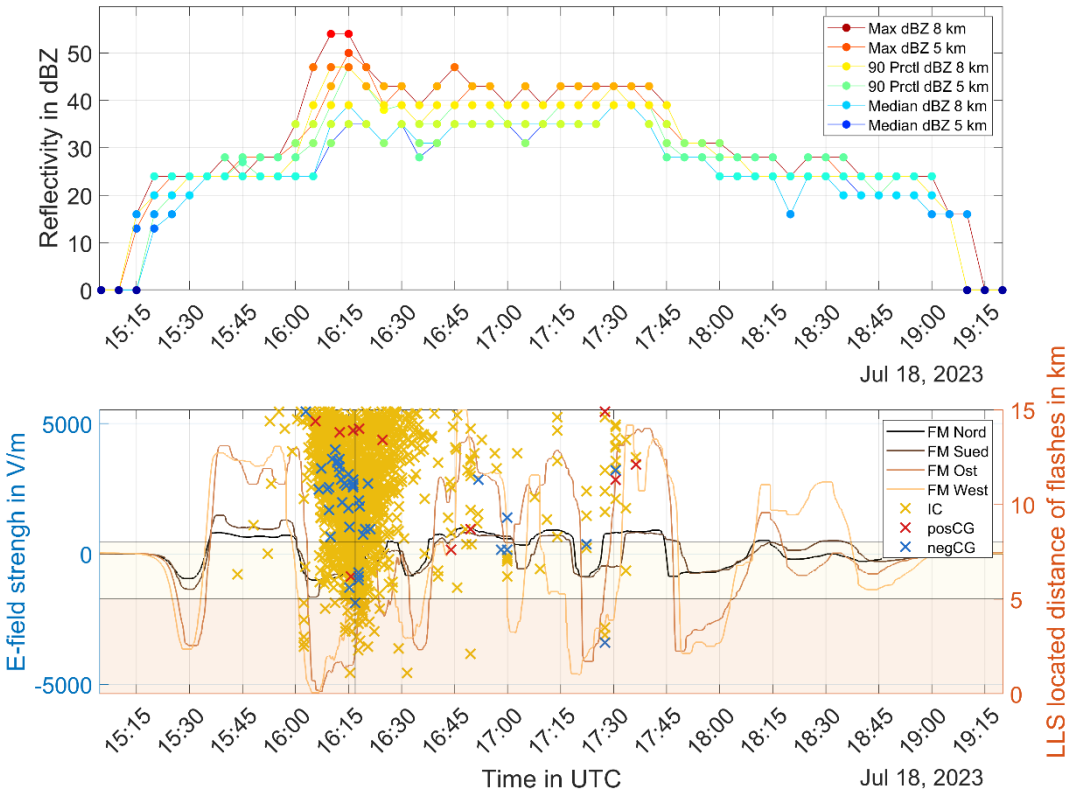

Figure 79: Combined data set of weather radar data (top) and LLS and FM network data (bottom), for a thunderstorm on 18 July 2023 from 15:10 to 19:15 UTC.

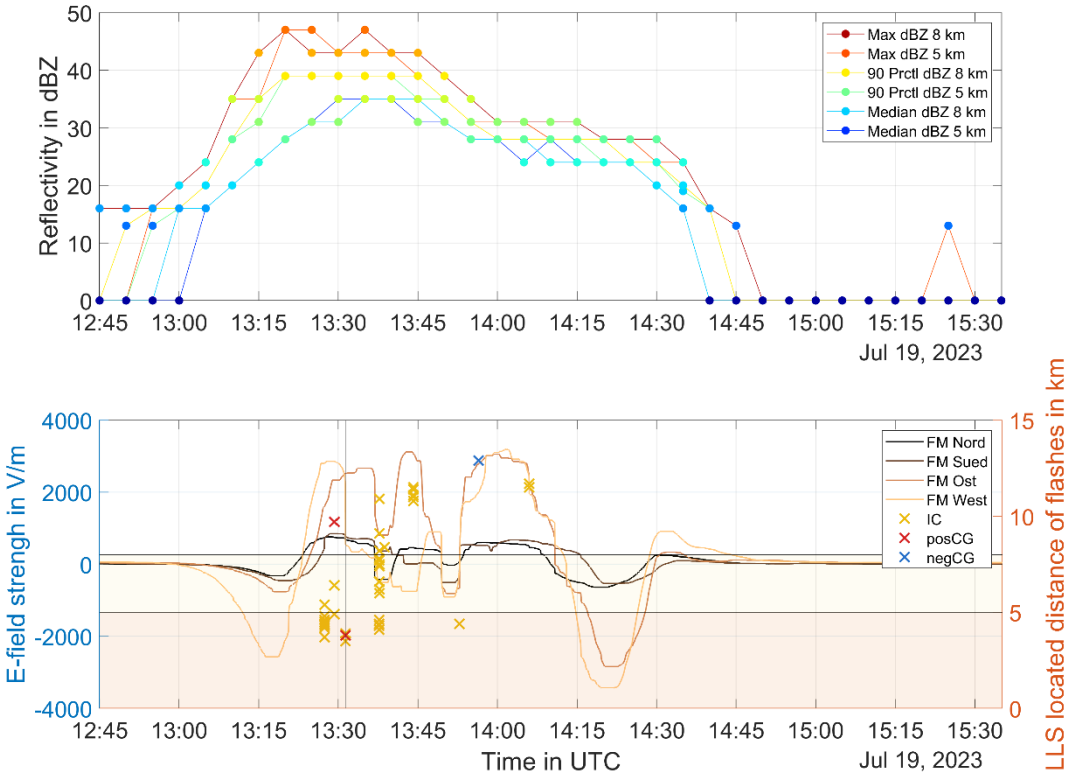

Figure 80: Combined data set of weather radar data (top) and LLS and FM network data (bottom), for a thunderstorm on 19 July 2023 from 12:45 to 15:30 UTC.

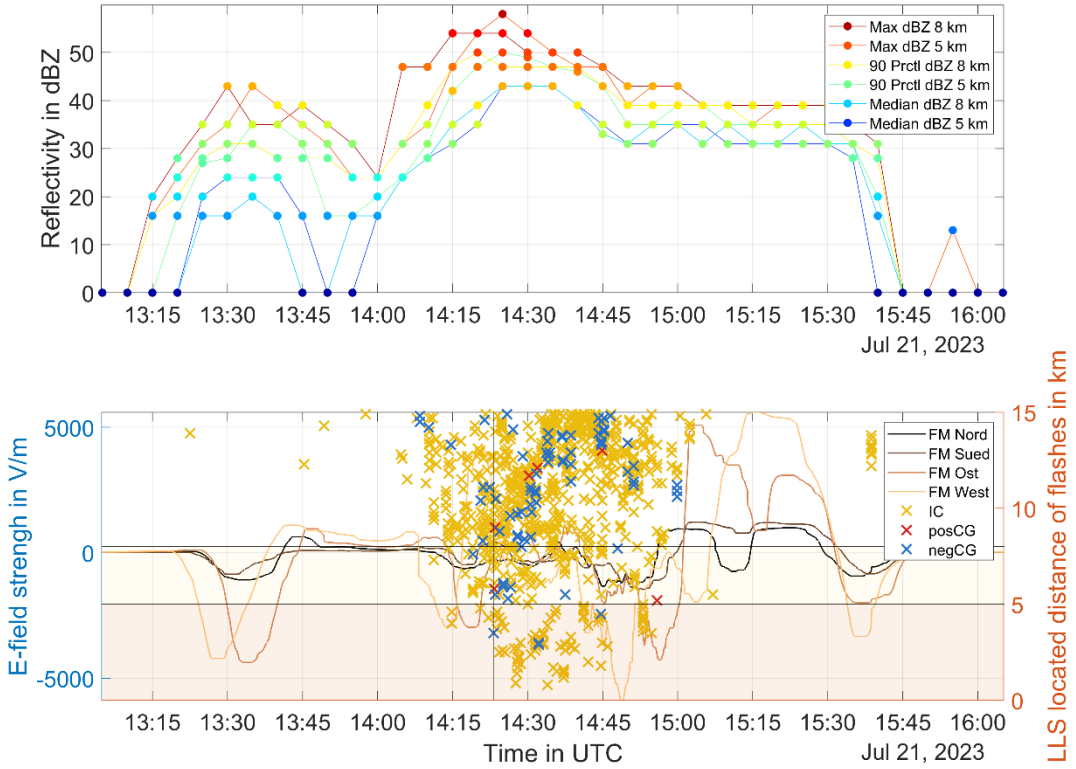

Figure 81: Combined data set of weather radar data (top) and LLS and FM network data (bottom), for a thunderstorm on 21 July 2023 from 13:05 to 16:05 UTC.

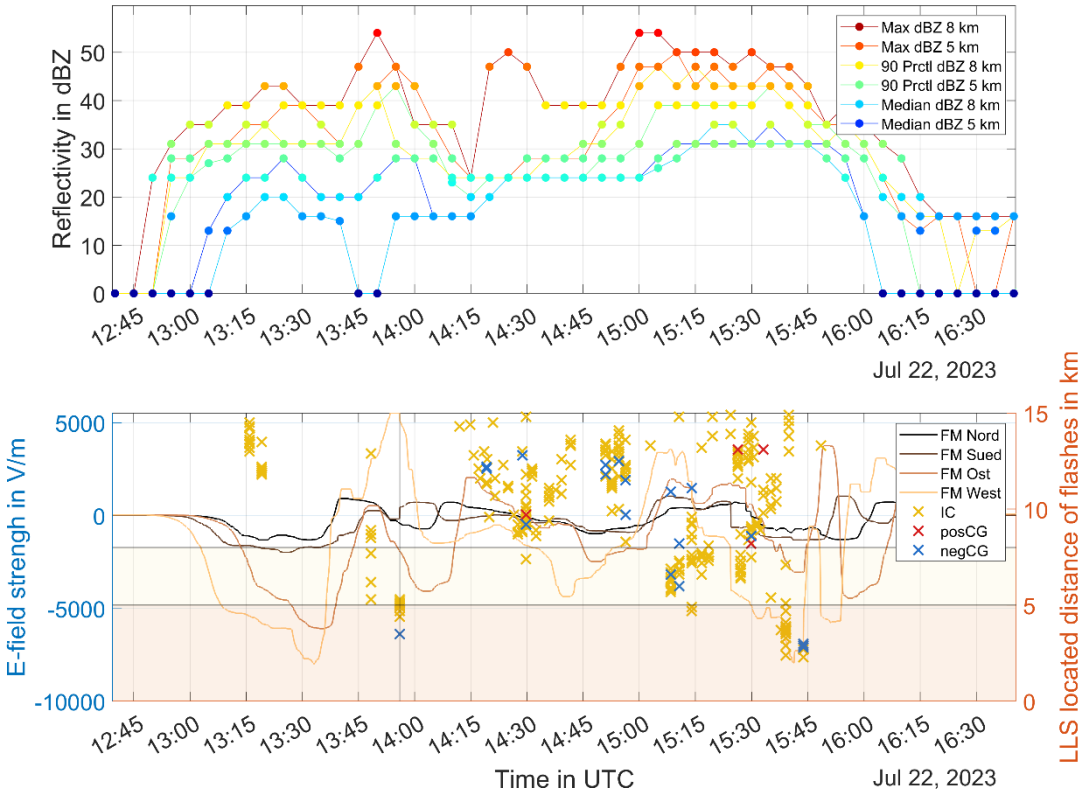

Figure 82: Combined data set of weather radar data (top) and LLS and FM network data (bottom), for a thunderstorm on 22 July 2023 from 12:45 to 16:30 UTC.

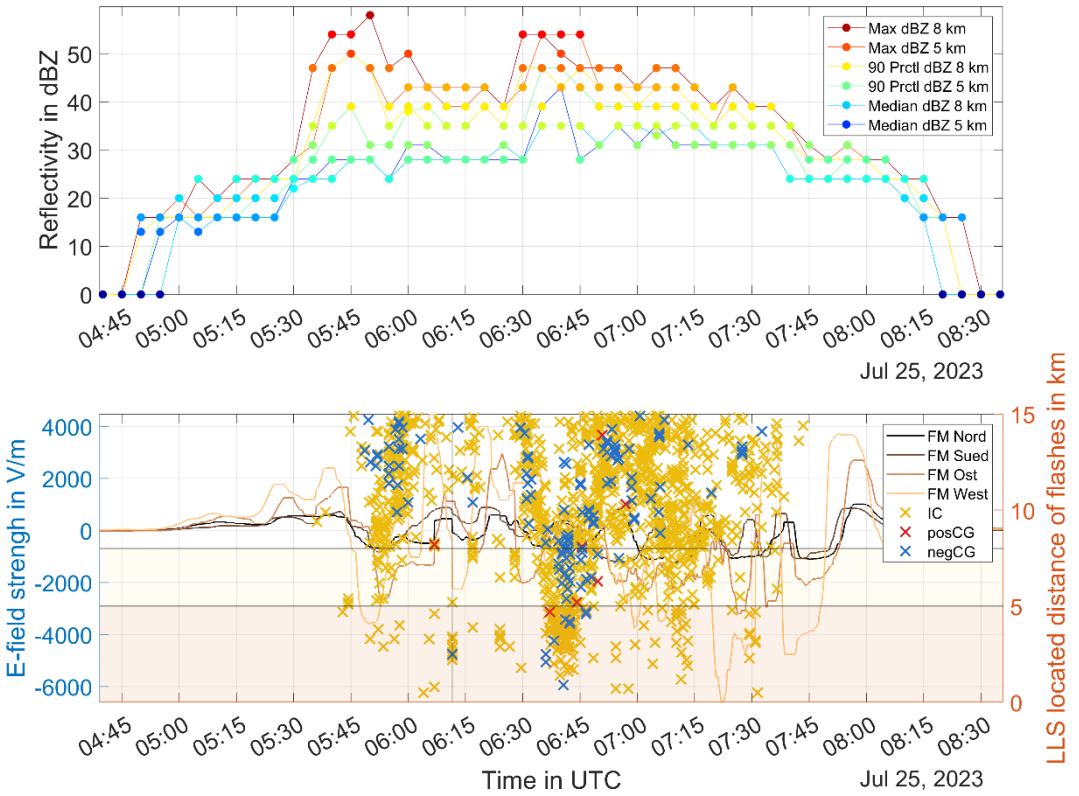

Figure 83: Combined data set of weather radar data (top) and LLS and FM network data (bottom), for a thunderstorm on 25 July 2023 from 04:45 to 08:30 UTC.

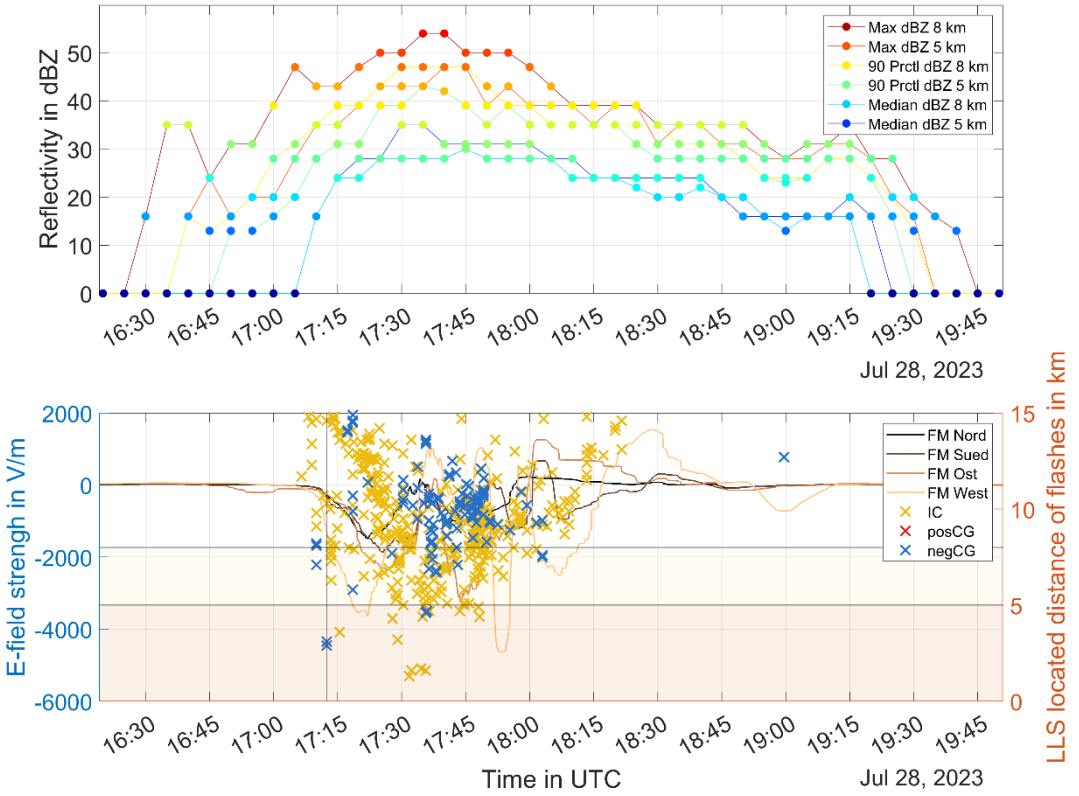

Figure 84: Combined data set of weather radar data (top) and LLS and FM network data (bottom), for a thunderstorm on 28 July 2023 from 16:30 to 19:45 UTC.

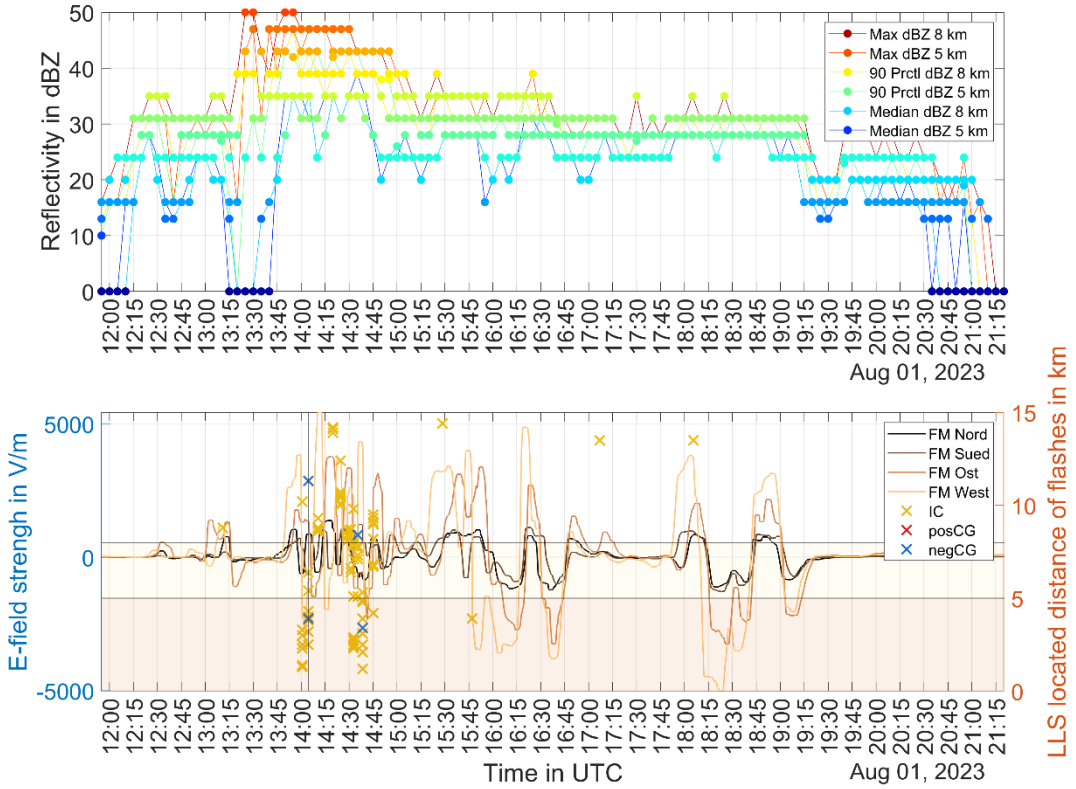

Figure 85: Combined data set of weather radar data (top) and LLS and FM network data (bottom), for a thunderstorm on 01 August 2023 from 12:00 to 21:15 UTC.

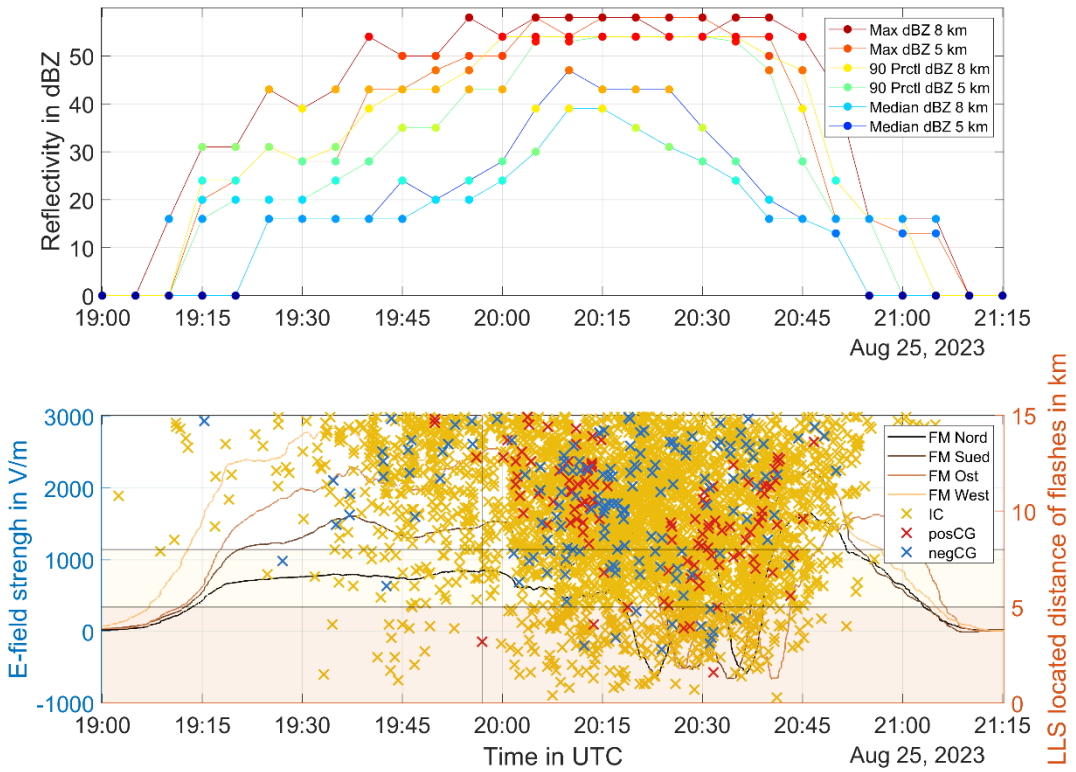

Figure 86: Combined data set of weather radar data (top) and LLS and FM network data (bottom), for a thunderstorm on 25 August 2023 from 19:00 to 21:15 UTC.

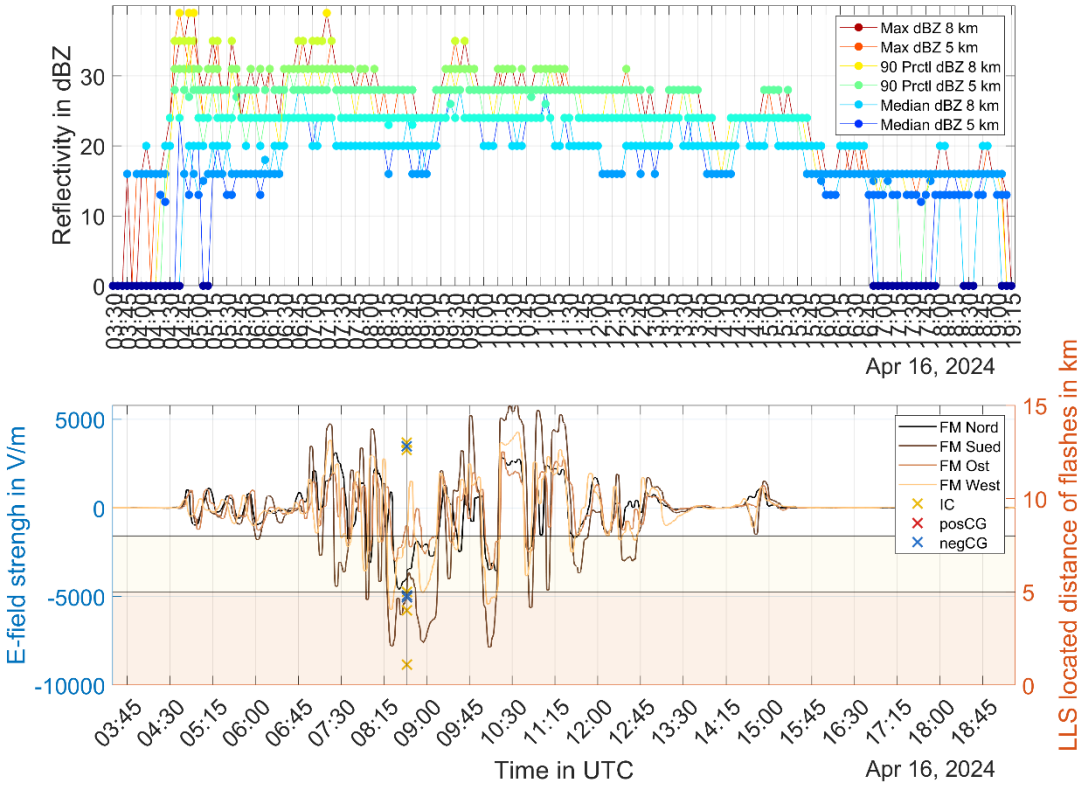

Figure 87: Combined data set of weather radar data (top) and LLS and FM network data (bottom), for a thunderstorm on 16 April 2024 from 03:45 to 18:45 UTC.

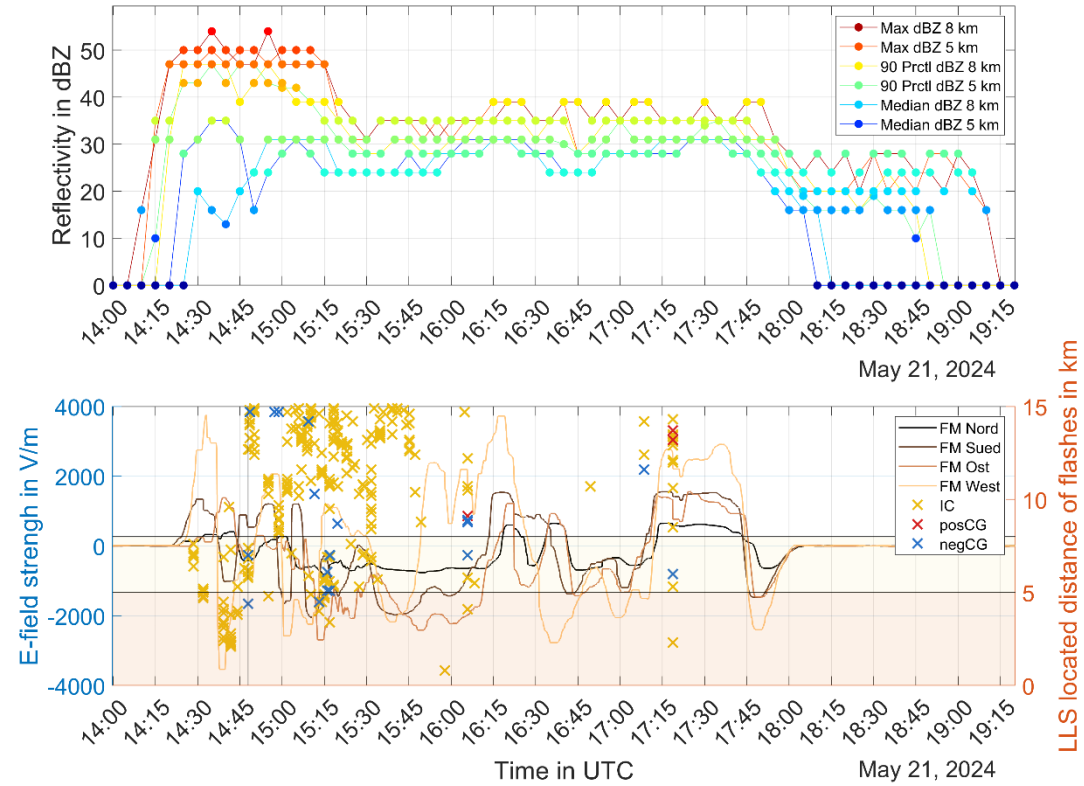

Figure 88: Combined data set of weather radar data (top) and LLS and FM network data (bottom), for a thunderstorm on 21 May 2024 from 14:00 to 19:15 UTC.

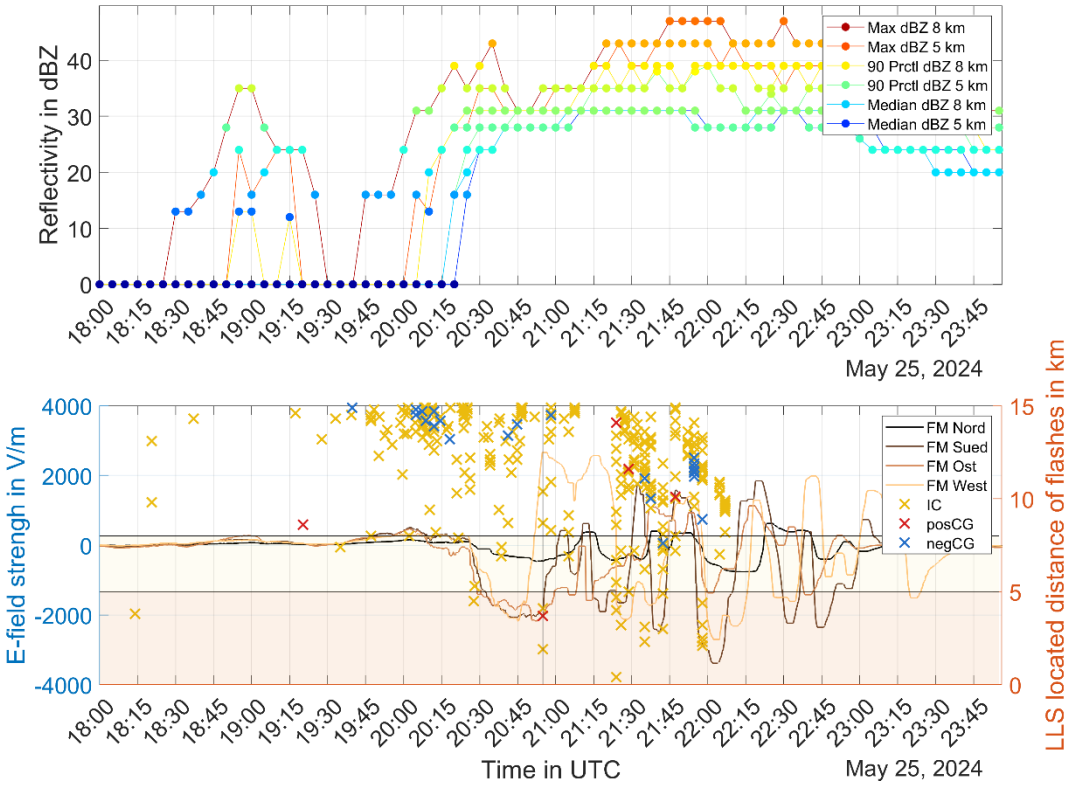

Figure 89: Combined data set of weather radar data (top) and LLS and FM network data (bottom), for a thunderstorm on 25 May 2024 from 18:00 to 23:45 UTC.

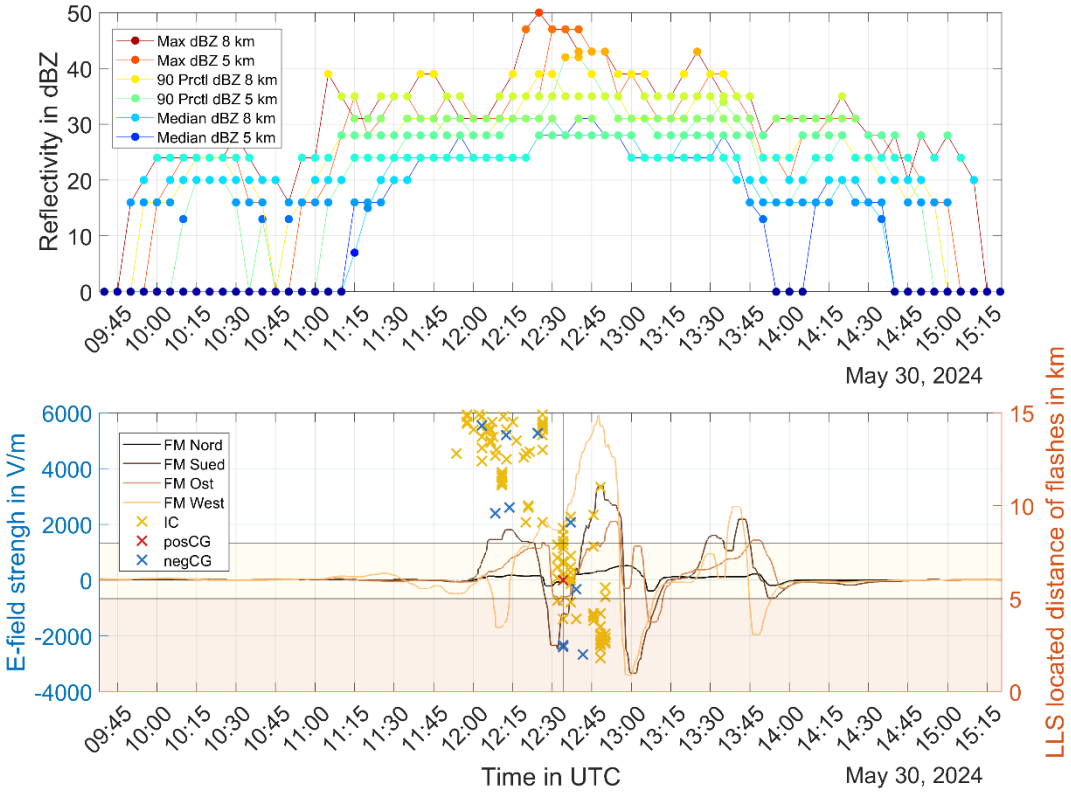

Figure 90: Combined data set of weather radar data (top) and LLS and FM network data (bottom), for a thunderstorm on 30 May 2024 from 09:45 to 15:15 UTC.

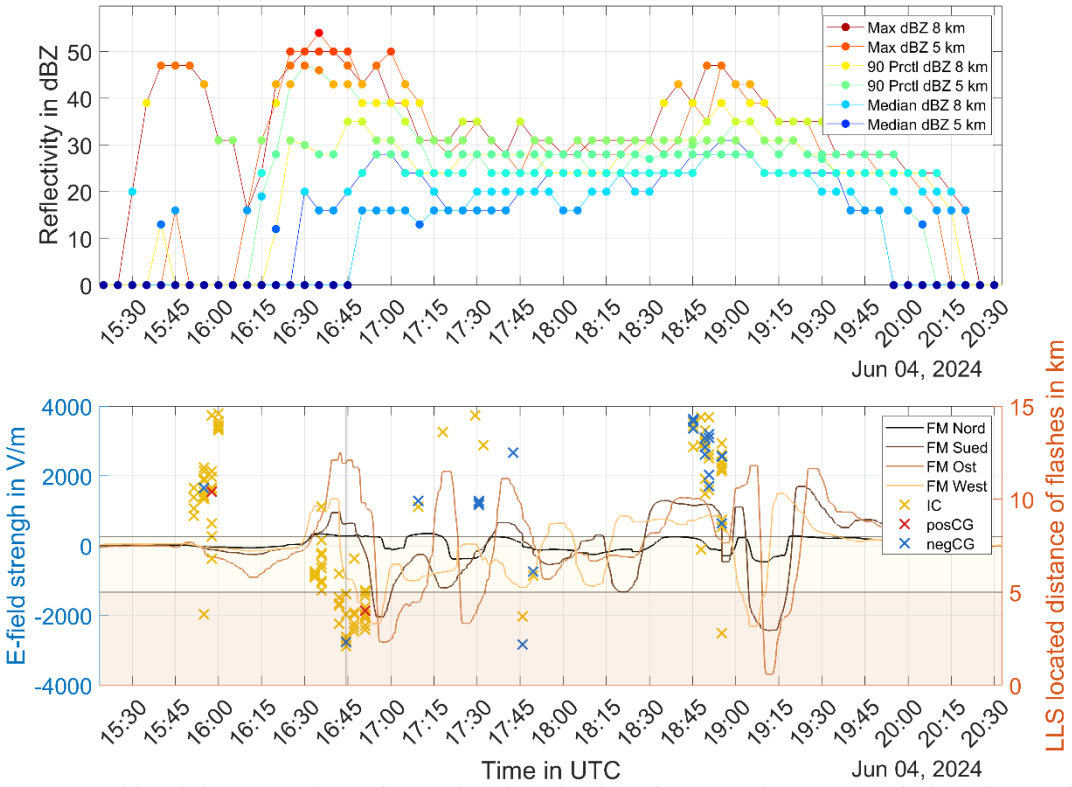

Figure 91: Combined data set of weather radar data (top) and LLS and FM network data (bottom), for a thunderstorm on 04 June 2024 from 15:30 to 20:30 UTC.

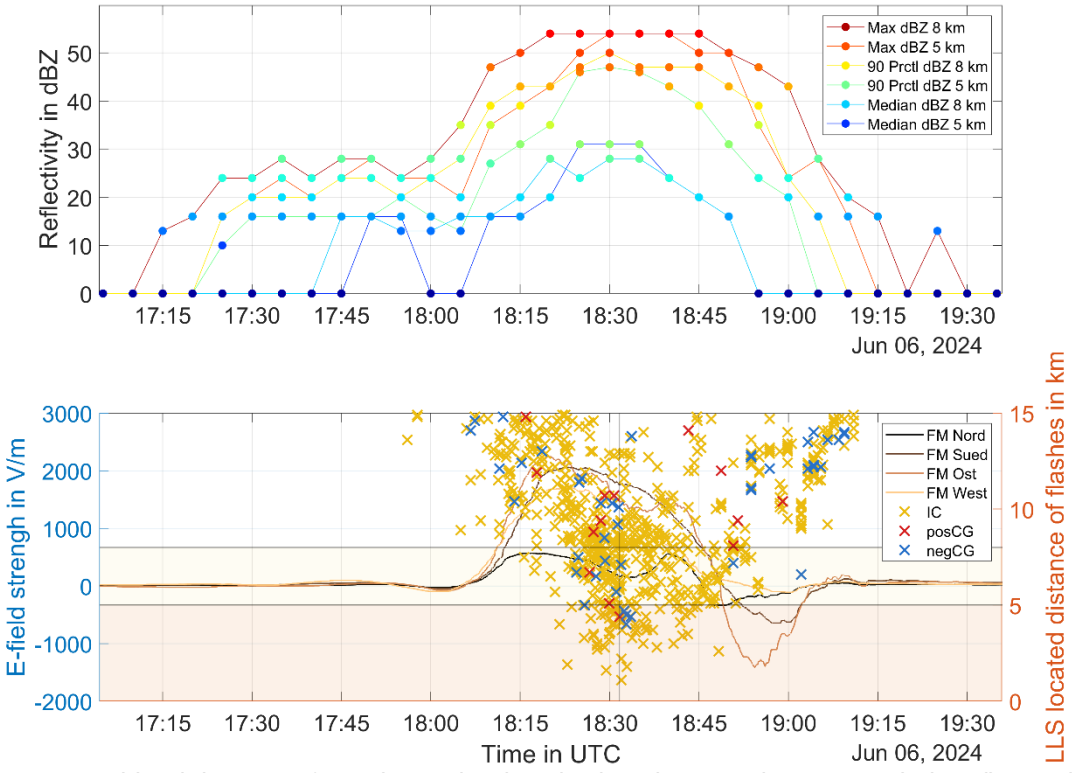

Figure 92: Combined data set of weather radar data (top) and LLS and FM network data (bottom), for a thunderstorm on 06 June 2024 from 17:05 to 19:35 UTC.

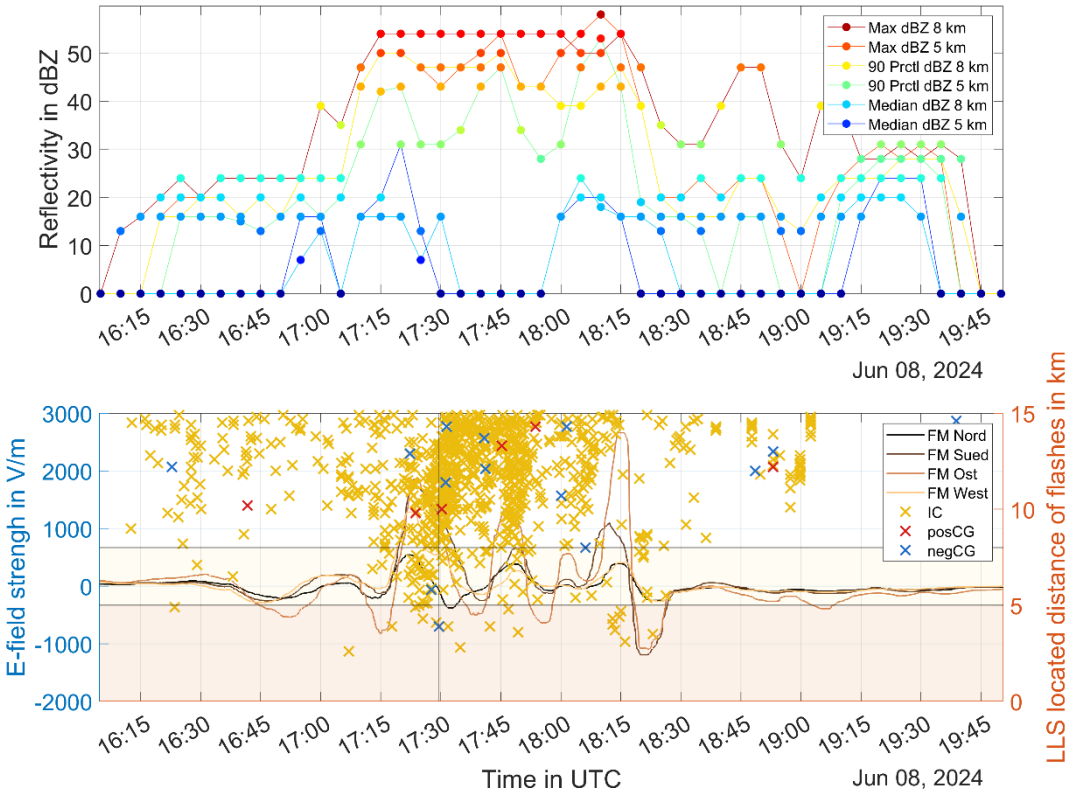

Figure 93: Combined data set of weather radar data (top) and LLS and FM network data (bottom), for a thunderstorm on 08 June 2024 from 16:15 to 19:45 UTC.

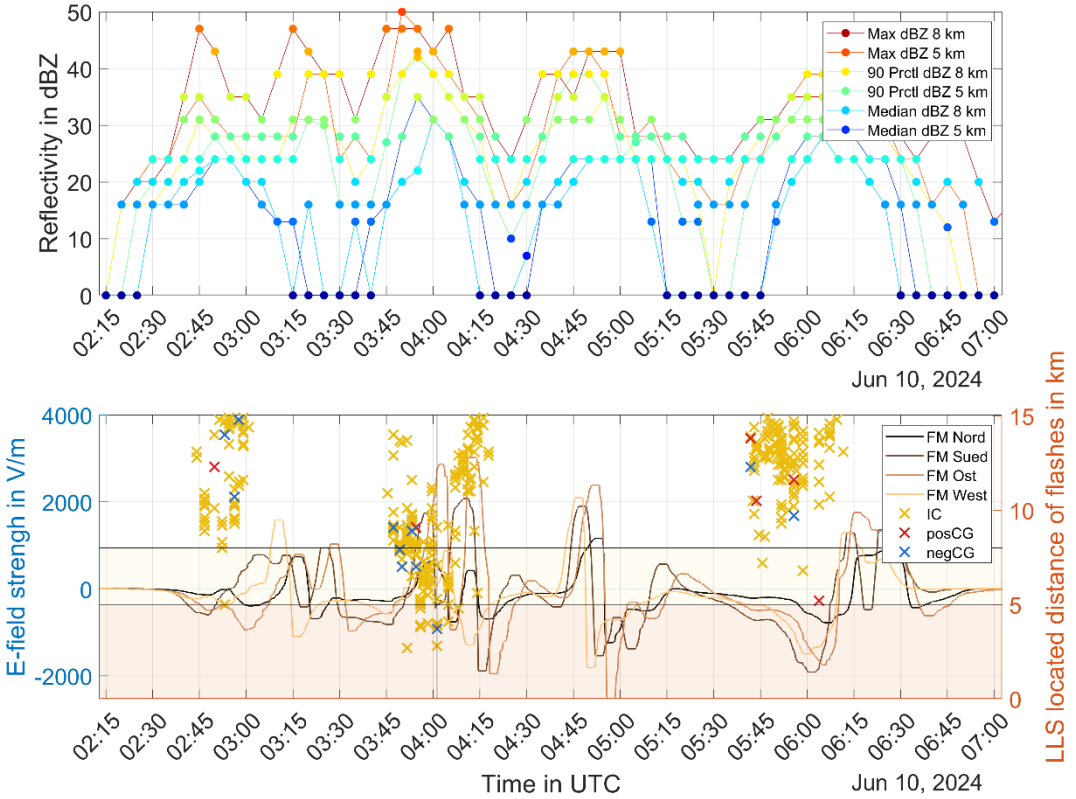

Figure 94: Combined data set of weather radar data (top) and LLS and FM network data (bottom), for a thunderstorm on 10 June 2024 from 02:15 to 07:00 UTC.

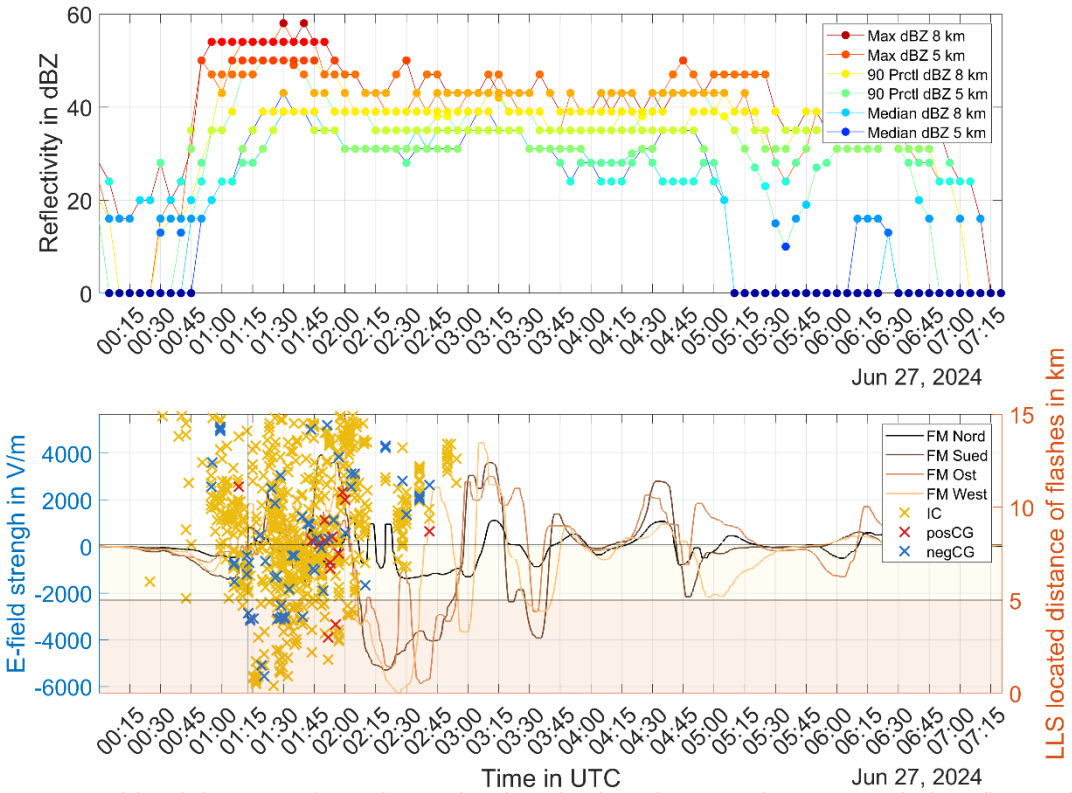

Figure 95: Combined data set of weather radar data (top) and LLS and FM network data (bottom), for a thunderstorm on 27 June 2024 from 00:15 to 07:15 UTC.

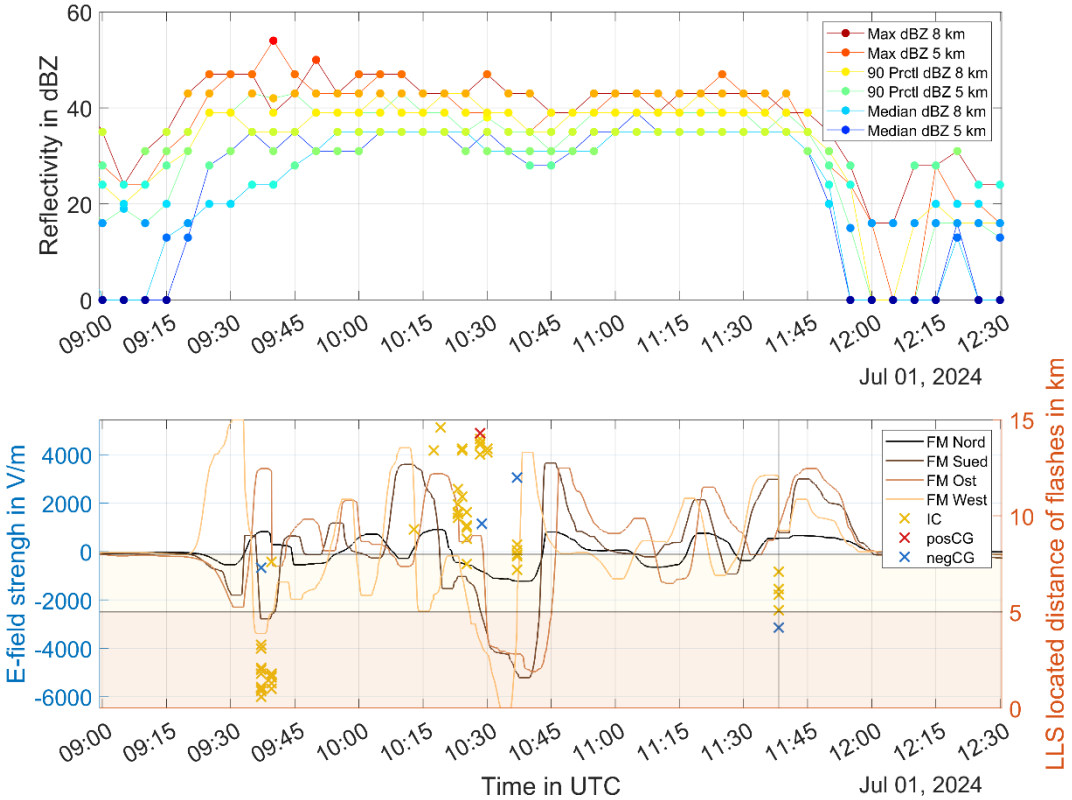

Figure 96: Combined data set of weather radar data (top) and LLS and FM network data (bottom), for a thunderstorm on 01 July 2024 from 09:00 to 12:30 UTC.

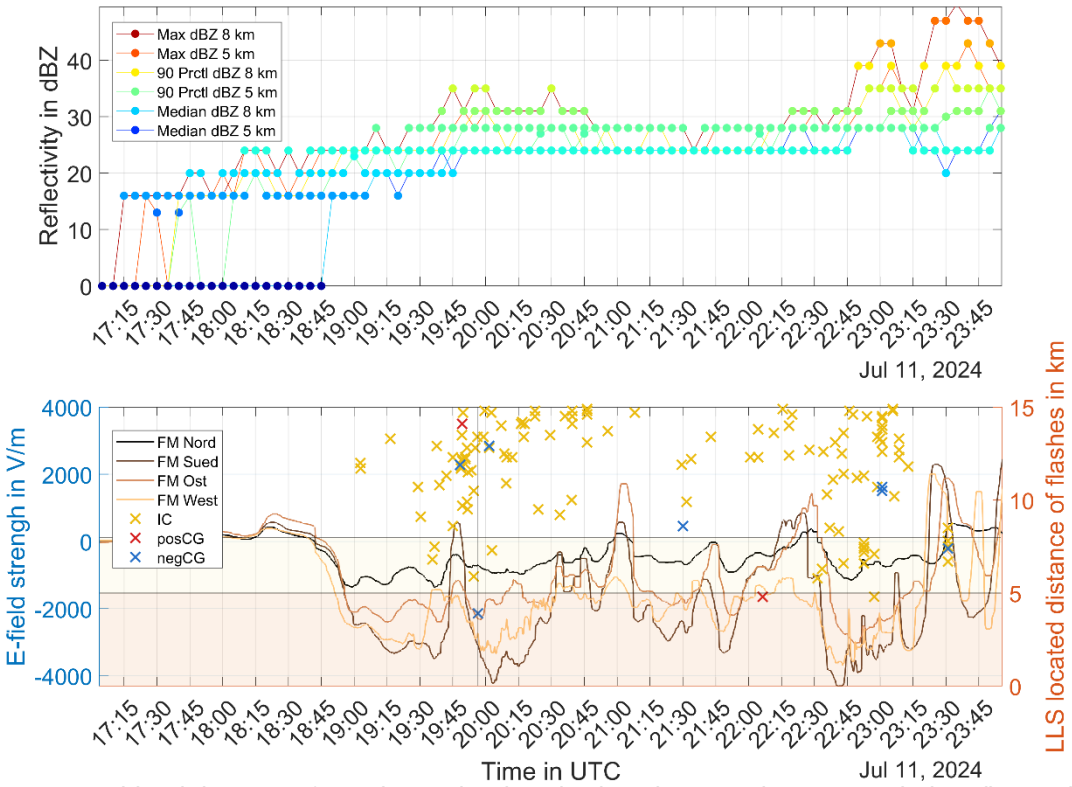

Figure 97: Combined data set of weather radar data (top) and LLS and FM network data (bottom), for a thunderstorm on 11 July 2024 from 17:15 to 23:45 UTC.

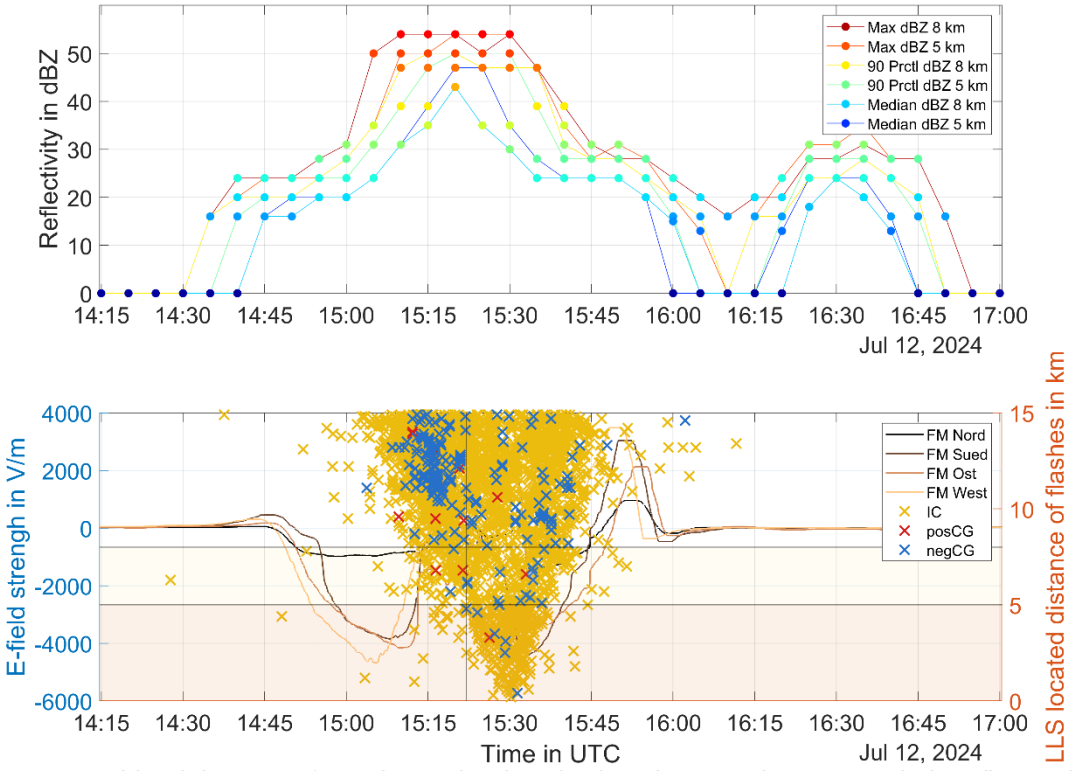

Figure 98: Combined data set of weather radar data (top) and LLS and FM network data (bottom), for a thunderstorm on 12 July 2024 from 14:15 to 17:00 UTC.

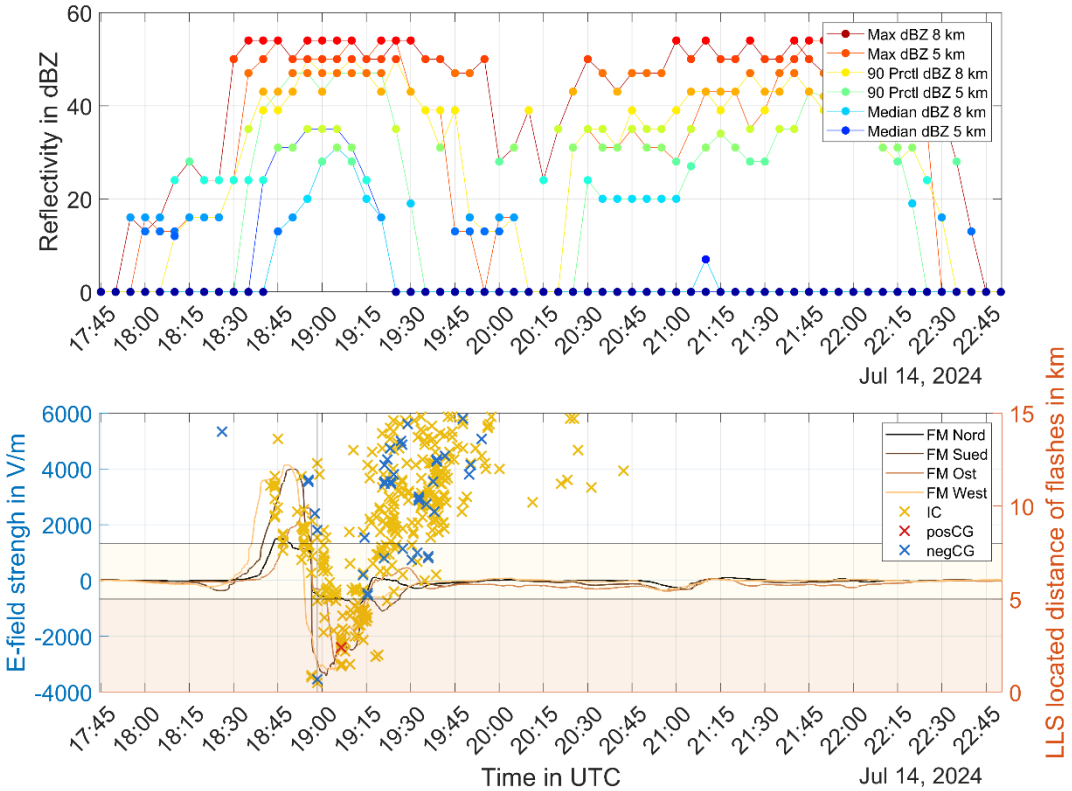

Figure 99: Combined data set of weather radar data (top) and LLS and FM network data (bottom), for a thunderstorm on 14 July 2024 from 17:45 to 22:45 UTC.

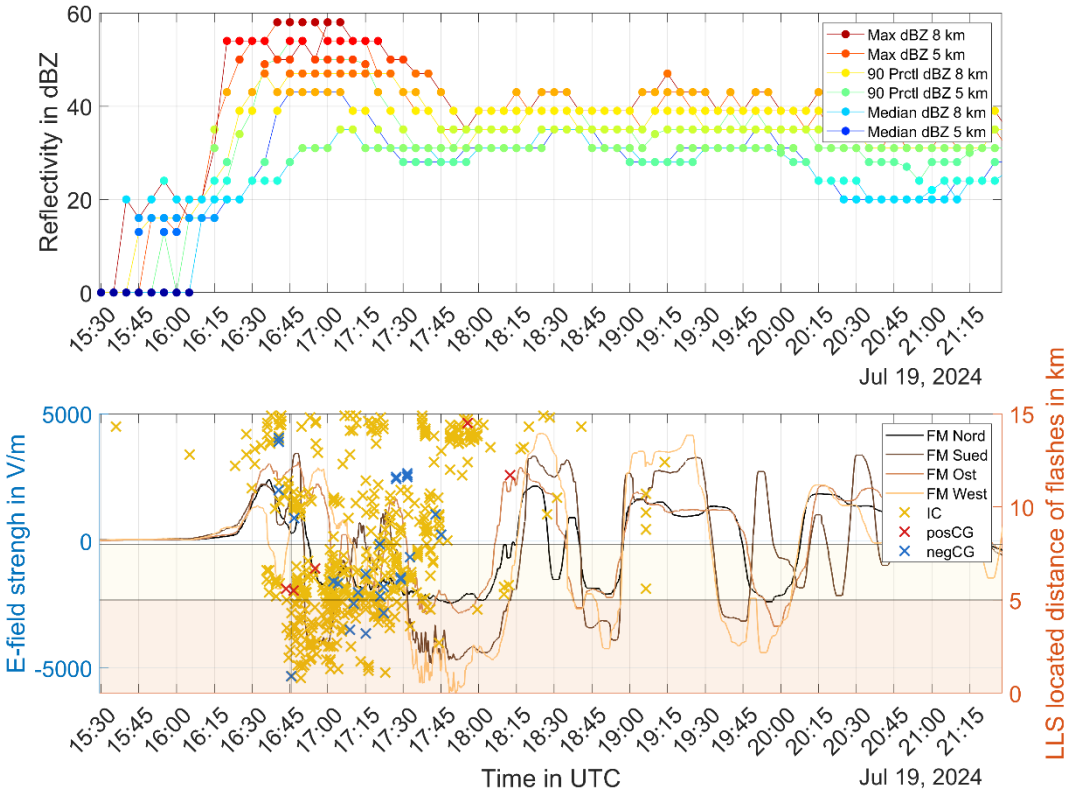

Figure 100: Combined data set of weather radar data (top) and LLS and FM network data (bottom), for a thunderstorm on 19 July 2024 from 15:30 to 21:15 UTC.

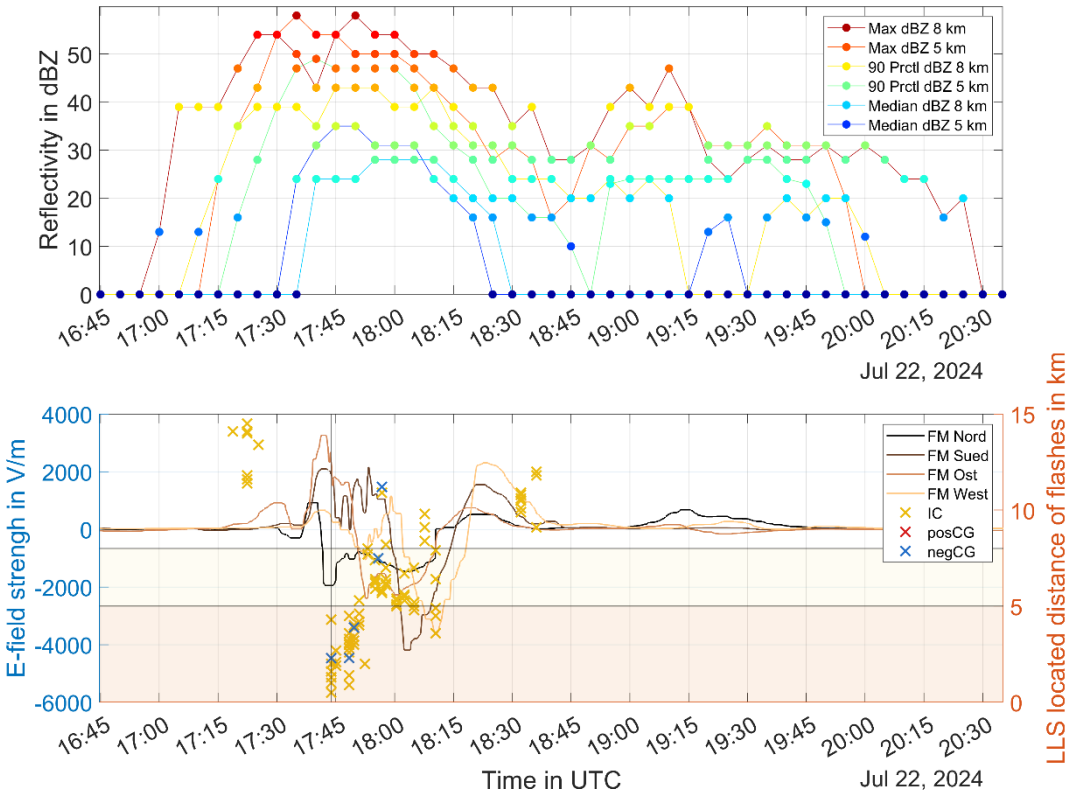

Figure 101: Combined data set of weather radar data (top) and LLS and FM network data (bottom), for a thunderstorm on 22 July 2024 from 16:45 to 20:30 UTC.

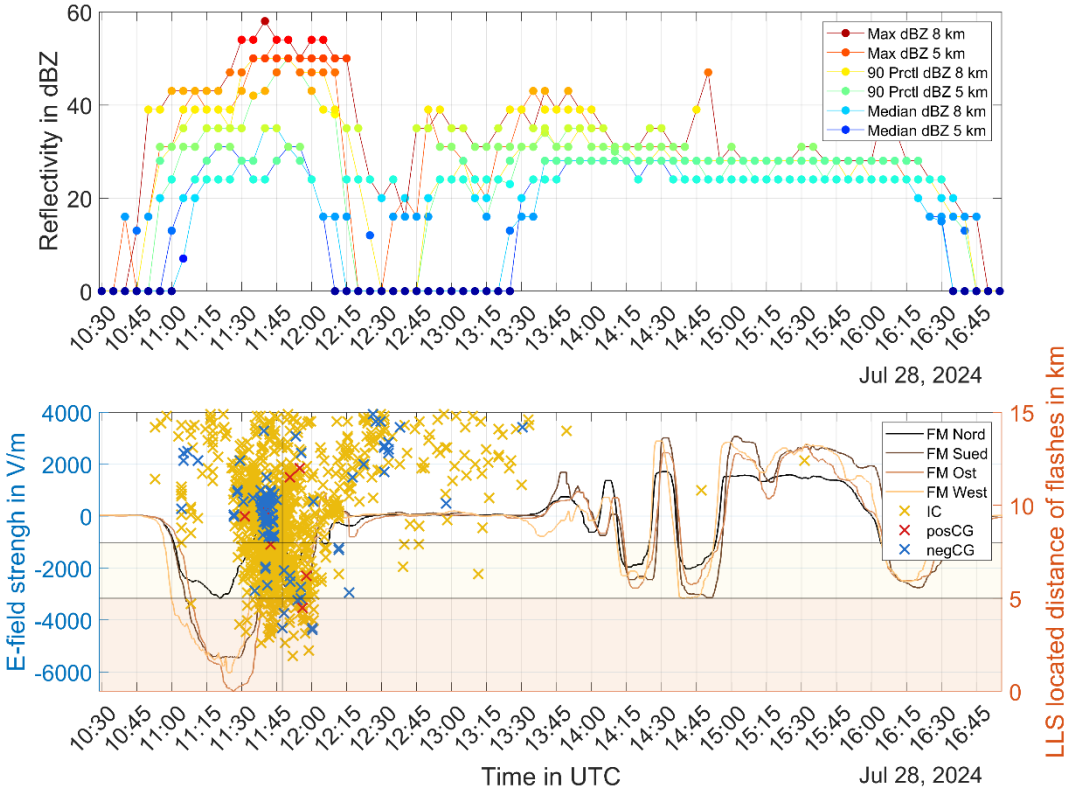

Figure 102: Combined data set of weather radar data (top) and LLS and FM network data (bottom), for a thunderstorm on 28 July 2024 from 10:30 to 16:45 UTC.

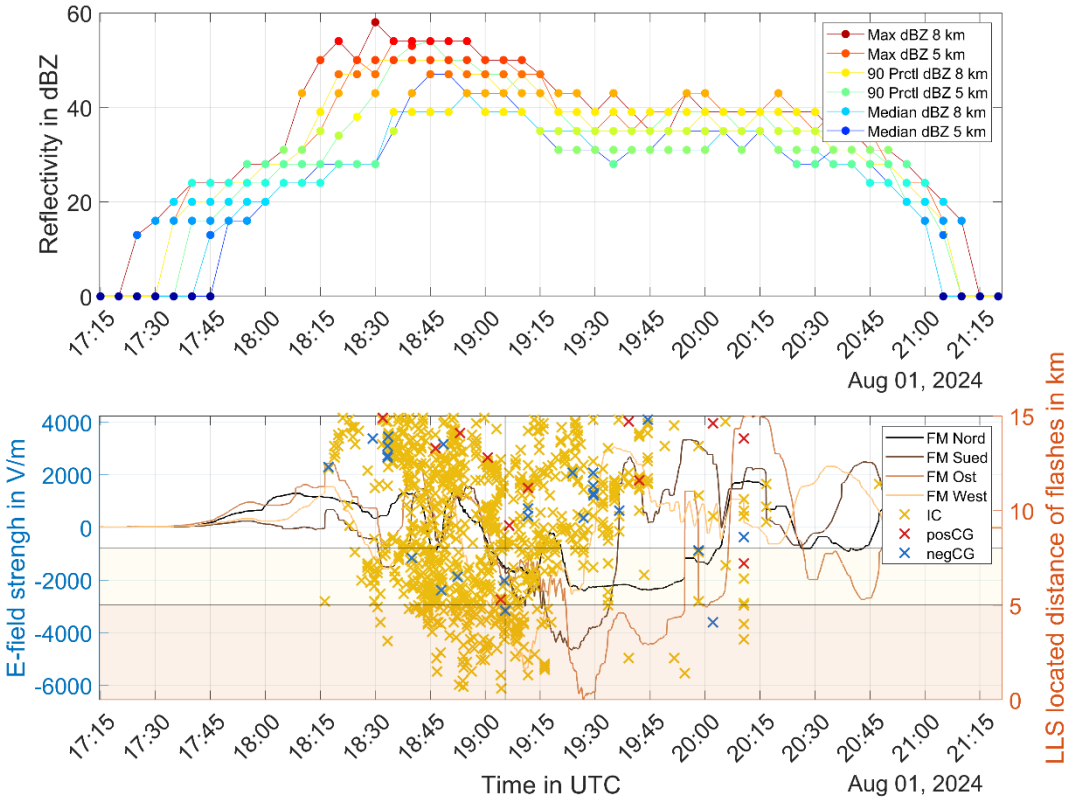

Figure 103: Combined data set of weather radar data (top) and LLS and FM network data (bottom), for a thunderstorm on 01 August 2024 from 17:15 to 21:15 UTC.

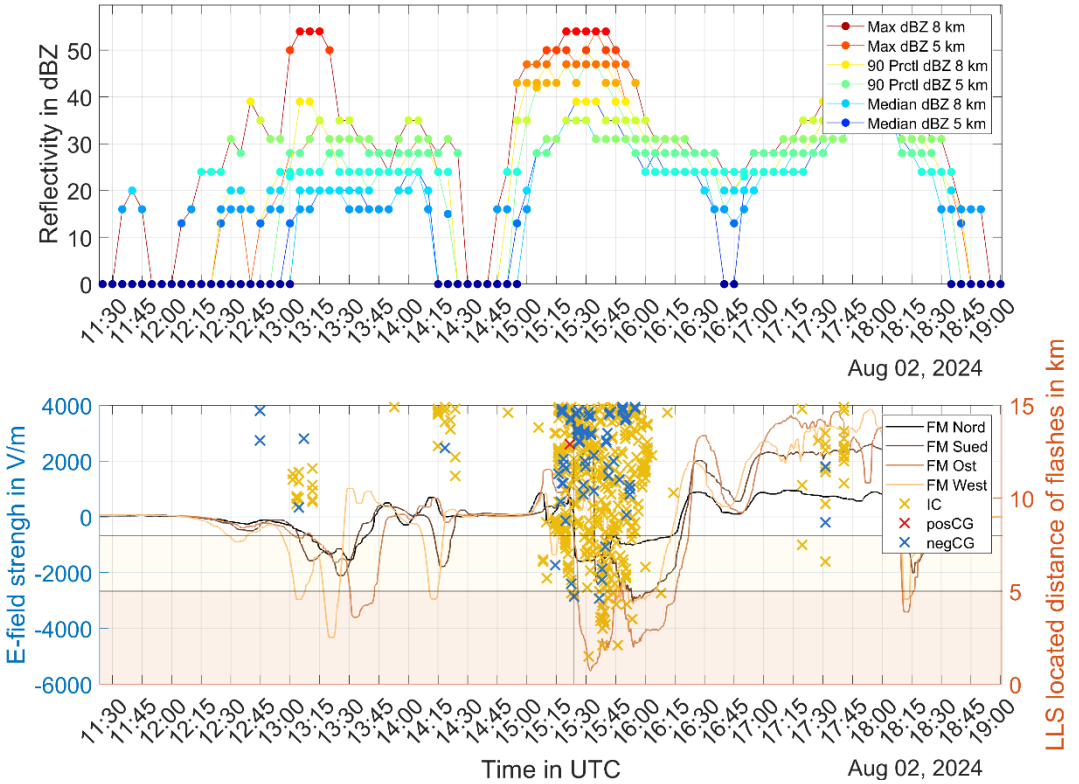

Figure 104: Combined data set of weather radar data (top) and LLS and FM network data (bottom), for a thunderstorm on 02 August 2024 from 11:30 to 19:00 UTC.

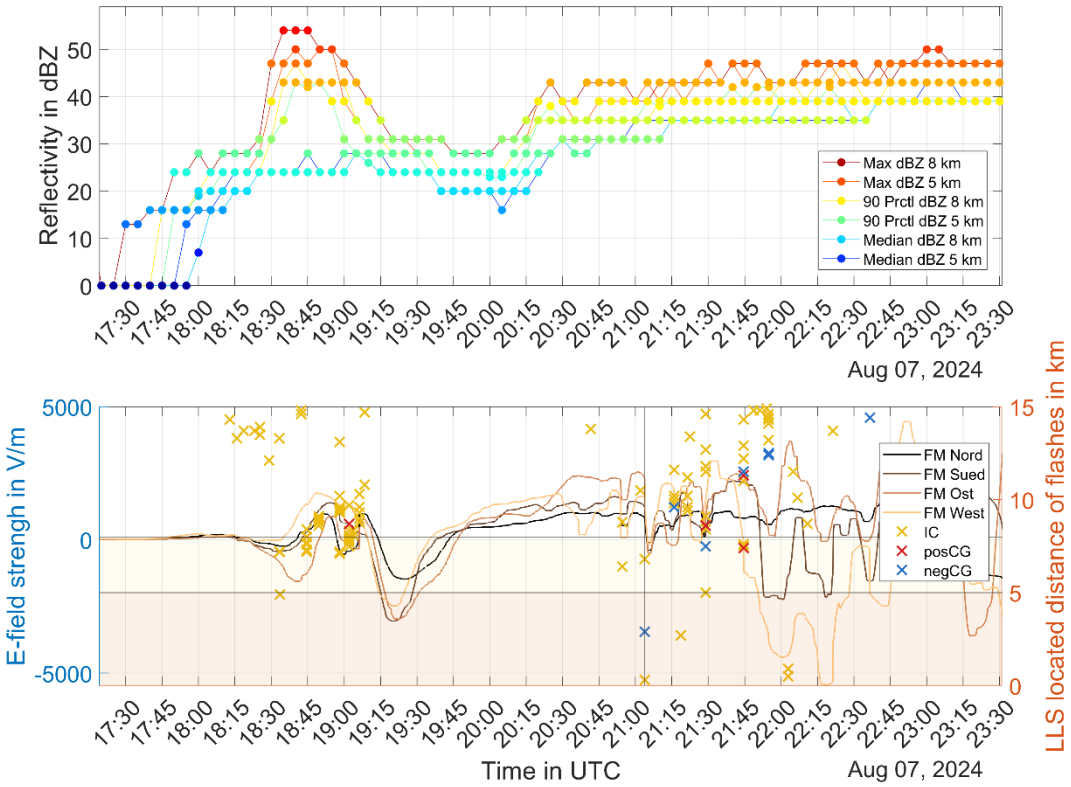

Figure 105: Combined data set of weather radar data (top) and LLS and FM network data (bottom), for a thunderstorm on 07 August 2024 from 17:30 to 23:30 UTC.

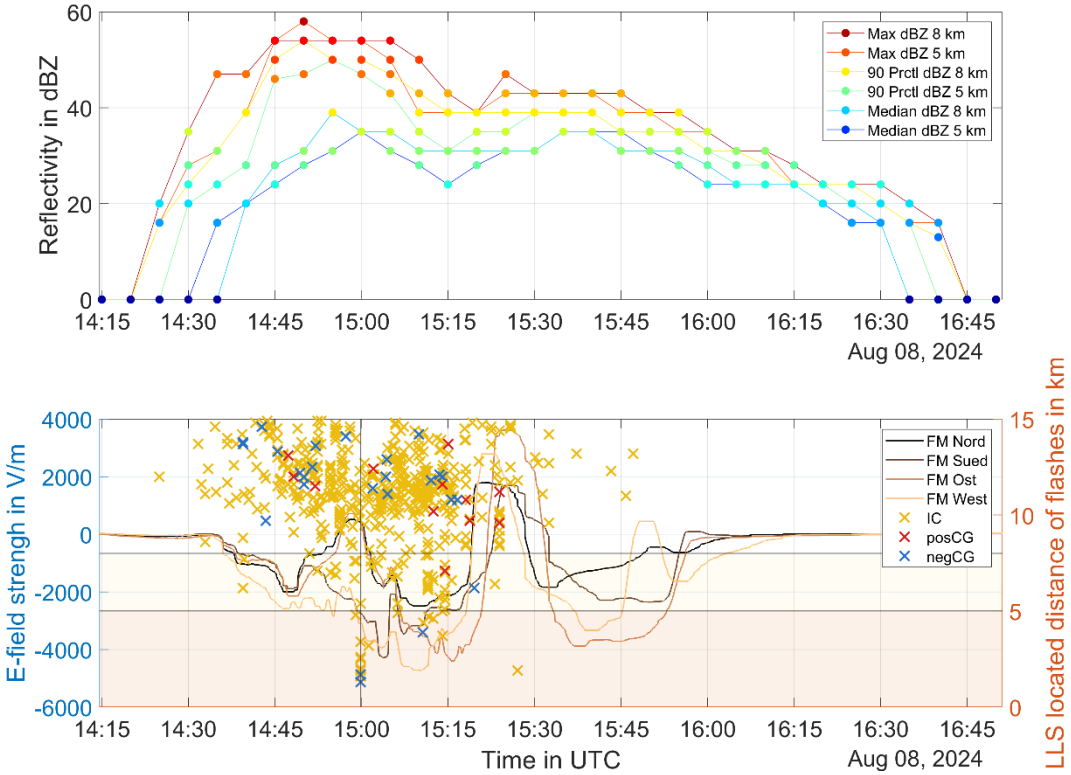

Figure 106: Combined data set of weather radar data (top) and LLS and FM network data (bottom), for a thunderstorm on 08 August 2024 from 14:15 to 16:45 UTC.

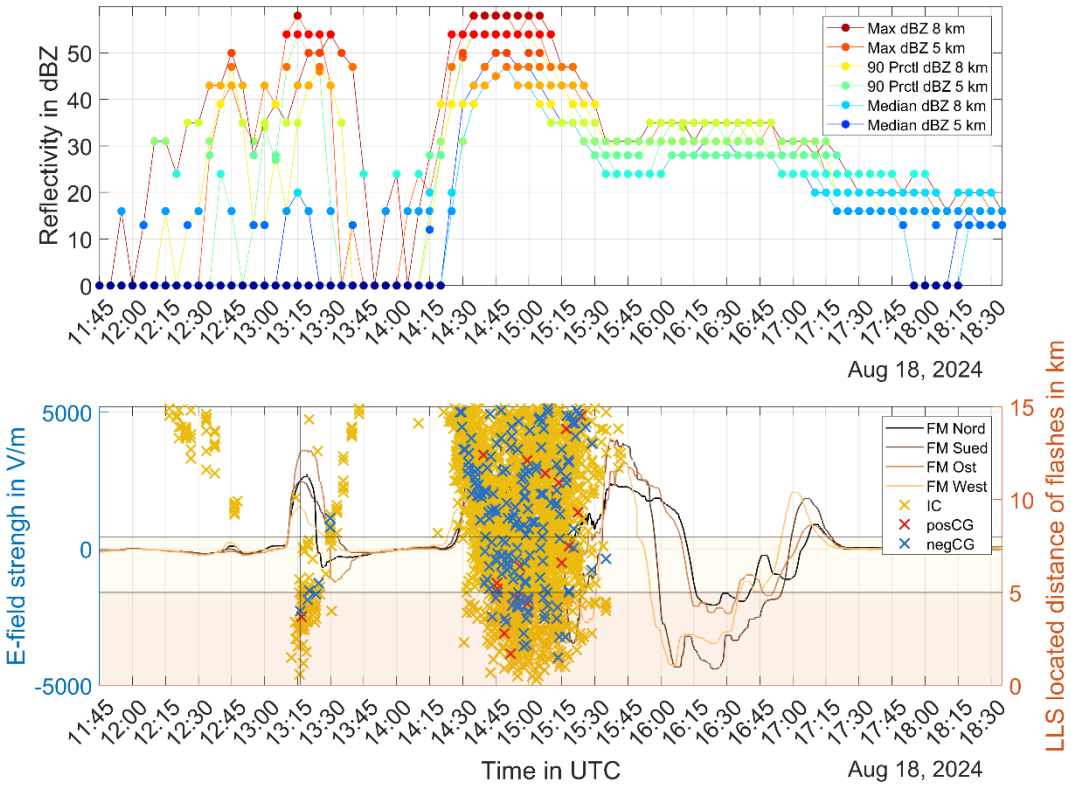

Figure 107: Combined data set of weather radar data (top) and LLS and FM network data (bottom), for a thunderstorm on 18 August 2024 from 11:45 to 18:30 UTC.

C Pre-Season Cases 16 April 2024 and 23 April 2023

This Appendix shall highlight the features of the two pre-season thunderstorm cases from 16 April 2024 (Case 1) and 23 April 2023 (Case 72). The two thunderstorms are described according to the findings by Schatz et al., 2025 [77].

Thunderstorm Case 1 – 16 April 2024

Among the 51 thunderstorms with CG lightning strikes in 5 km radius around Graz Airport, the event on 16 April 2024 was the only case which occurred before the convective thunderstorm season from May to September. For this case, the first and only CG lightning strike (no other IC discharges either) within the 5 km radius was not predicted by the algorithm. Weather data indicated a cold front approaching from the WNW, ground fog, and no convective available potential energy (CAPE = 0 J/kg), based on radiosonde data from Graz Airport (03:00 UTC). The low maximum temperature and dew point on this day were 13.2 °C and 10.6 °C, respectively. The freezing level was at approximately 2000 amsl, and the cloud base around 700 amsl. Radar, LLS, and E-field time series for this event are shown in Appendix B, Figure 87.

The storm passed over the area between 05:05 and 06:40 UTC, with low radar reflectivity (median <20 dBZ; max approx. 30 dBZ) and weak, stable E-field values fluctuating between –1800 V/m and 1200 V/m. Zero-crossings occurred roughly every 15 minutes. Reflectivity and E-field activity increased from 06:45 UTC, with FM South recording a local maximum of 4760 V/m by 07:18 UTC. Zero-crossing frequency also rose to about one every 9 minutes.

From 08:16 UTC, E-field values at all FMs dropped to negative values, reaching local minima approx. 5 minutes after the respective zero-crossing. At 08:39 UTC, two negative CG lightning strikes occurred at 4.7 km and 4.8 km, accompanied by IC discharges. These were the only lightning events detected within the examined area. E-field strengths at that moment ranged from –1025 V/m to –4732 V/m across the FMs.

Radar reflectivity peaked at 39 dBZ that day but generally remained low throughout. Additional weak E-field activity and moderate reflectivity (up to 35 dBZ) were observed

until 10:00 UTC. From 15:20 UTC onwards, fair-weather field conditions were restored. Reflectivity values gradually decreased and fell to 0 dBZ by 19:10 UTC.

This case shows that the algorithm, developed primarily for convective summer thunderstorms, failed to detect the first and only nearby CG lightning strike of this colder pre-season storm. Future improvements should consider adjusted parameter sets for such cases. Indicators may include a lower freezing level, as it influences thunderstorm structure. Previous studies (e.g., Saunders, 1992 [108]; Diendorfer et al., [109]) confirm that lightning can occur in environments with sub-zero temperatures and radar reflectivity exceeding 30 dBZ, conditions met during this event (Schatz et al., 2025 [77]).

Thunderstorm Case 72 – 23 April 2023

The thunderstorm Case 72 thunderstorms with first CG lightning strikes in 8–10 km radius around Graz Airport, was the second thunderstorm case in the extended analyses which occurred previously to the convective thunderstorm season. For this case, the first CG lightning strike in 8.5 km radius and the algorithm triggered a shutdown 1.90 minutes in advance. Weather data indicated a weak front approaching from the NW, and no convective available potential energy (CAPE = 0 J/kg), based on radiosonde data from Graz Airport (03:00 UTC). The freezing level was at approximately 2700 amsl. Compared to the 16.04.2024, for this day mild temperatures were recorded with a max of 21.2 °C, the dew point on this day was 10.8 °C. The combined data set is shown in Figure 108.

The thunderstorm passed during 14:45 and 18:00 UTC. From 14:45 UTC, the radar reflectivity began to rise in the 8 km radius and from 15:00 UTC in 5 km radius. At 15:33 UTC, an IC discharge was located in 8 km distance and at 15:35 UTC the maximum radar reflectivity 8 km already reached 50 dBZ (<40 dBZ in 5 km radius). The reflectivity then decreases. From 16:25 UTC the reflectivity increases for all radar values, up to 50 dBZ for the max value in 5 km radius. At 16:47 UTC the E-field exceeds 1 kV/m for the first time, at this time also the alert was triggered. At 16:49 UTC the shutdown was triggered. The E-field was over 2 kV/m at this time.

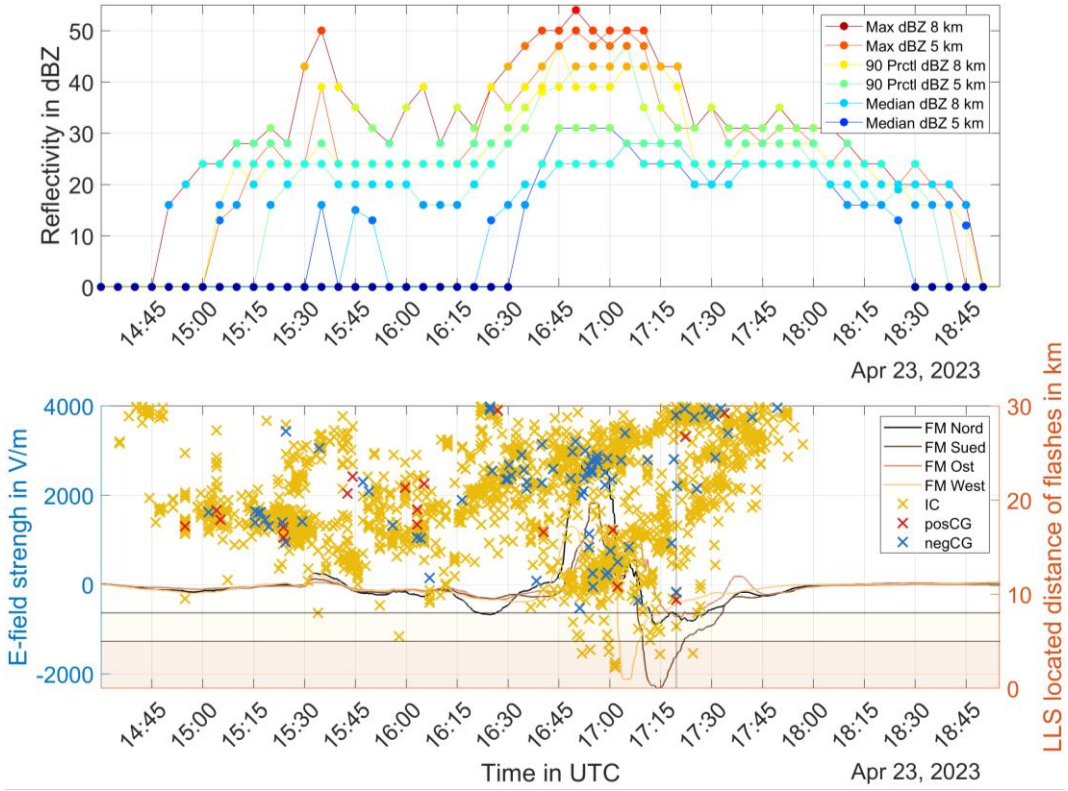

Figure 108: Combined data set of weather radar data (top) and LLS and FM network data (bottom), for a thunderstorm on 23 April 2023 from 14:30 to 18:45 UTC.

The reflectivity then decreases. From 16:25 UTC the reflectivity increases for all radar values, up to 50 dBZ for the maximum value in 5 km radius. At 16:47 UTC the E-field exceeds 1 kV/m for the first time, at this time also the alert was triggered. At 16:49 UTC the shutdown was triggered. The E-field was over 2 kV/m at this time. At 16:51 UTC the CG in 8.5 km is located. Another CG in the 8–10 km radius was located at 17:08 UTC. At this point radar reflectivity already starts to decrease monotonically and the E-field changed polarity. At 17:28 UTC all abs(E-field) values decreased below 1 kV/m, the maximum reflectivity in 5 km and 8 km is 35 dBZ. At 18:30 UTC, the electric field returns to fair-weather values, and by 18:50 UTC, all reflectivity values have dropped back to 0 dBZ.

D Results ACG Shutdowns 2018–2021

The following tables present the results for real ACG shutdowns from 2018–2021. The ACG shutdown values were compared with LLS data in a similar way as performed for the analyses and the results from Section 8.4. As critical surrounding area, the 5 km radius around Graz Airport was applied. A direct comparison for the shutdown lead times and durations is carried out in Section 9.7, Application.

Table 27: Lead times for ACG Shutdowns for 2018-2021 for a surrounding area of 5 km; minimum, 10th percentil, median, mean, 90th percentil and maximum in minutes.

Lead Time in Minutes					
Min	**10th**	**Median**	**Mean**	**90th**	**Max**
0.08	0.62	6.18	9.23	24.27	66.00

Table 28: Shutdown duration for ACG Shutdowns for 2018-2021 for a surrounding area of 5 km; minimum, 10th percentil, median, mean, 90th percentil and maximum in minutes.

	Shutdown Duration in minutes					
	Min	**10th**	**Median**	**Mean**	**90th**	**Max**
EA	5.00	13.00	32.00	34.88	55.10	165.00
Non-EA	0.00	4.10	11.00	12.13	20.80	46.00
TNA	0.00	7.00	16.00	22.47	47.80	165.00

Table 29: Shutdown duration per year for ACG Shutdowns for 2018-2021 for a surrounding area of 5 km; effective alarms, non-effective alarms and total number of alarms in minutes.

Year	Shutdown Duration per Year in Minutes		
	EA	**Non-EA**	**TNA**
2018	886	241	1127
2019	248	270	520
2020	649	107	756
2021	310	255	565

Table 30: Shutdown duration per year for ACG Shutdowns for 2018-2021 for a surrounding area of 5 km; effective alarms, non-effective alarms and total number of alarms in hours.

Year	Shutdown Duration per Year in Hours		
	EA	**Non-EA**	**TNA**
2018	14.77	4.02	18.78
2019	4.13	4.50	8.67
2020	10.82	1.78	12.60
2021	5.17	4.25	9.42

Table 31 shows the lead time performance for ACG shutdowns for the years 2018-2021 for a surrounding area of 5 km radius around Graz Airport. According to the TWS standard (see Section 3.3.1) the time range of 0–2 minutes refers to as FTW, the ranges of 2–30 minutes, 30–60 minutes and >60 minutes refer to as EA.

Table 31: LT performance for ACG Shutdowns for 2018-2021 for a surrounding area of 5 km.

Lead Time Ranges	Count
0–2 minutes*	95
2–30 minutes	39
30–60 minutes	3
>60 minutes	1
Non-EA	72
TNA	115

*For 78 of 95 CG lightning strikes in 5 km no shutdown was initiated

E High Electric Fields in the Absence of Lightning

This appendix examines the distribution of days with elevated E-field values. A comparison was made between days with lightning activity (Figure 109) and days without lightning (Figure 110), based on LLS data. The analysis focused on how many days per month exceeded absolute E-field thresholds of 1 kV/m, 2 kV/m, and 3 kV/m. Only days on which the respective threshold was exceeded for at least 100 seconds were considered. The E-field records were used in their raw form (unfiltered), with a recording rate of 1 Hz.

Figure 109 shows distribution of days with lightning from January to December, three different abs(E-field) thresholds 1 kV/m, 2 kV/m, 3 kV/m are compared. In total (per year) there are 132 days with thresholds over 1 kV/m, 121 days over 2 kV/m and 104 days over 3 kV/m.

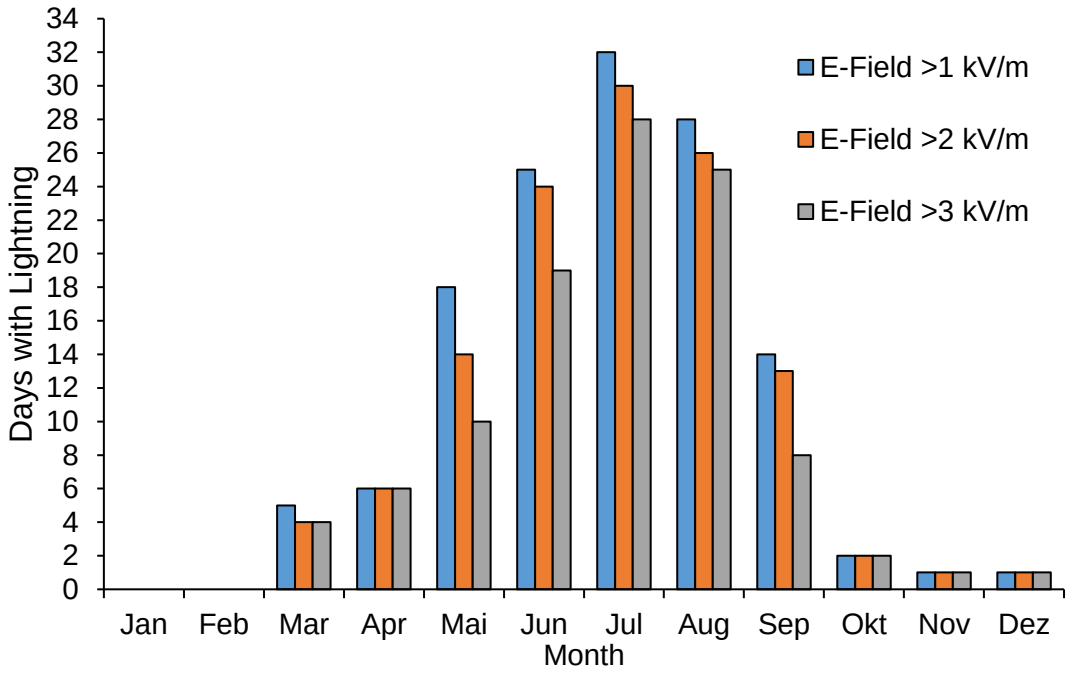

Figure 109: Distribution of days with lightning per month from January to December, three different abs(E-field) thresholds 1 kV/m, 2 kV/m, 3 kV/m are compared.

Figure 110 shows Distribution of days without lightning from January to December, three different abs(E-field) thresholds 1 kV/m, 2 kV/m, 3 kV/m are compared. In total (per year) there are 132 days with thresholds over 1 kV/m, 101 days over 2 kV/m and 42 days over 3 kV/m.

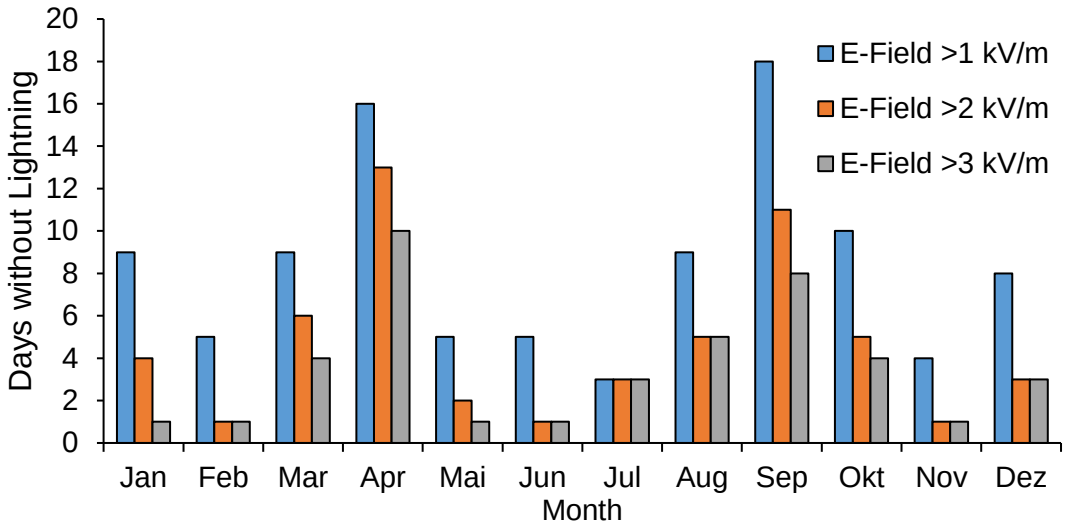

Figure 110: Distribution of days without lightning per month from January to December, three different abs(E-field) thresholds 1 kV/m, 2 kV/m, 3 kV/m are compared.